

Charles University
Second Faculty of Medicine

Doctoral study programme: Immunology



Mgr. Marina Bakardjieva

Immunophenotypic and functional characteristics of lymphocytes of patients with
primary immunodeficiency

Imunofenotypové a funkční charakteristiky lymfocytů pacientů s primární
imunodeficiencí

Dissertation Thesis

Supervisor: prof. Tomáš Kalina, Ph.D.

Prague, 2024

Declaration

Prohlášení

Prohlašuji, že jsem disertační práci zpracovala samostatně a že jsem řádně uvedla a citovala všechny použité prameny a literaturu. Současně prohlašuji, že práce nebyla využita k získání jiného nebo stejného titulu.

Souhlasím s trvalým uložením elektronické verze mé práce v databázi systému meziuniverzitního projektu Theses.cz za účelem soustavné kontroly podobnosti kvalifikačních prací.

V Praze, 29. 2. 2024

Marina Bakardjieva

.....

Acknowledgement

First of all, I would like to thank my supervisor prof. Tomáš Kalina, Ph.D. for giving me the opportunity to participate in so many significant projects, for his support, guidance and valuable advice and feedback throughout my studies. I would also like to thank RNDr. Veronika Kanderová, Ph.D. for her practical support, suggestions and experience shared, which contributed significantly to the successful completion of my projects. Many thanks belong to my colleagues Mgr. Jitka Stančíková, Ph.D. and Mgr. Daniela Kužílková Ph.D. for their help and advice regarding my experimental work, Mgr. Jan Stuchlý, Ph.D. for his bioinformatics contribution, Mgr. Petra Hadlová for her help in improving this thesis, Mgr. Nad'a Brdičková, PhD., Ing. Adéla Vávrová and Mgr. Tereza Podolská for creating a motivating working environment. I would like to also thank Daniel Thürner, Mgr. Kateřina Rejlová, Ph.D., Pavla Luknárová and Pavel Semerák for their great technical assistance. I would like to thank prof. Ondřej Hrušák, Ph.D. and prof. Jan Trka, Ph.D. for providing superb working facilities in the CLIP laboratories.

My thanks also belong to our abroad colleagues prof. Marta Rizzi, Ph.D. and Julian Staniek, Ph.D. from the University of Freiburg for the fruitful ongoing collaboration and great welcome in their lab.

I would like to acknowledge the patients and healthy donors who consented to provide samples for this work and made our research possible.

My deepest thanks belong to my family, without their patience and support, these achievements would not have been possible.

Abstrakt (CZ)

Primární imunodeficiencie (PID) jsou heterogenní skupinou více než 480 geneticky podmíněných poruch imunitního systému, které vznikají v důsledku bloku ve vývoji leukocytů nebo funkčních defektů v imunitní odpovědi. PID mají širokou škálu příznaků, včetně zvýšené náchylnosti k infekcím, ale také k autoimunitě nebo malignitám. Podrobné znalosti o PID jsou nezbytné nejen v klinické/diagnostické oblasti, ale také v základním výzkumu, protože mohou sloužit jako modelové systémy pro studium imunitního systému.

První část práce se zabývá využitím cytometrického testu SCID-RTE, který jsme vyvinuli v rámci EuroFlow konsorcia, jako diagnostického nástroje pro včasnou detekci pacientů s podezřením na závažný PID. Na základě studovaných parametrů (hladiny naivních $CD4^+$ a $CD8^+$ T buněk, tzv. recent thymic emigrant (RTE) buněk a aktivačního stavu) jsme prokázali, že SCID-RTE je senzitivním testem vhodným pro pacienty s klinickým podezřením, detekované v rámci širšího EuroFlow PID diagnostického algoritmu nebo novorozeneckého screeningového programu. Dále jsme v rámci EuroFlow poskytli detailní imunofenotypizaci alterací B buněčných subsetů pacientů s primárními protilátkovými imunodeficiencemi, včetně exprese různých imunoglobulinových subtypů na paměťových B buňkách a plazmatických buňkách. Rozčlenění podskupin identifikovalo odlišné imunitní profily, které korelovaly s diagnostickým podtypem a klinickým obrazem. S cílem vytvořit nástroj pro podrobné porozumění B buněčných imunodeficitů jsme vyvinuli protokol pro hmotnostní cytometrii a nový analytický výpočetní nástroj, který je schopný podrobně zkoumat B buněčné vývojové dráhy s potenciálem odhalit alternativní dráhy, které mohou být přítomny u PID, navrhnout lepší diagnostické testy nebo terapeutické cíle.

Ve druhé části práce jsme zkoumali dosud nepopsanou roli neapoptotické signalizace přes Fas receptor a její funkci v diferenciaci B buněk s využitím autoimunitního lymfoproliferativního syndromu (ALPS) jako modelového onemocnění. Konkrétně se tato signalizace podílí na rozhodování diferenciaci B buněk na extrafolikulární nebo B buňky germinálního centra tím, že moduluje aktivitu mTOR. Dále jsme identifikovali a funkčně charakterizovali novou mutaci v genu *TLR8*, která vedla k autoimunitnímu a autoinflamatornímu onemocnění u jednovaječných dvojčat. Výsledná částečná ztráta TLR8 proteinu vedla k dysregulaci mezi TLR8 a TLR7 odpověďmi na základě zkřížené reaktivity TLR8 receptoru na ligandy TLR7 a zvýšené signalizace TLR7 receptoru.

Klíčová slova

primární imunodeficiencie, imunofenotypizace, průtoková cytometrie, hmotnostní cytometrie, diagnostika, standardizace, EuroFlow, B buněčný vývoj, vývojové trajektorie, funkční testování, SCID, ALPS, TLR8

Abstract (ENG)

Primary immunodeficiencies (PIDs) are a heterogeneous group of over 480 genetically inherited disorders of the immune system that result from a block in leukocyte development or functional defects in the immune response. PIDs have a wide range of symptoms including increased susceptibility to infections but also autoimmunity or malignancy. Detailed knowledge of PIDs is essential not only in the clinical/diagnostic field, but also in basic research, as they can serve as model systems for the study of the immune system.

The first part of the thesis focuses on the use of the SCID-RTE cytometric test, which we developed within the EuroFlow consortium, as a diagnostic tool for detection of patients suspected of severe PID. Based on the parameters studied (levels of naive CD4⁺ and CD8⁺ T cells, recent thymic emigrants and the activation status), we have demonstrated that the SCID-RTE tube is a sensitive test suitable for patients clinically suspected of PID, identified within the broader EuroFlow diagnostic algorithm, or the national newborn screening program. Next, within EuroFlow, we provided a sensitive immunophenotypic evaluation of B cell subset alterations in patients with predominantly antibody deficiencies (PADs), including the expression of distinct immunoglobulin subclasses on memory B cells and plasma cells. Subset dissection identified distinct immune profiles that correlated with diagnostic subtype and clinical presentation. In order to create a tool for detailed understanding to B cell immunodeficiency, we developed a mass cytometry protocol and a novel computational framework capable of detailed interrogation of human B cell developmental pathways, with the potential to reveal alternative pathways possibly present in PIDs, to suggest improved diagnostic tests or therapeutic targets.

In the second part of the thesis we investigated previously unreported role of non-apoptotic Fas signaling and its function in B cell differentiation using autoimmune lymphoproliferative syndrome (ALPS) as a model disease. Specifically, it contributes to the extrafollicular versus germinal center fate decision by modulating the activity of mTOR. Next, we identified and functionally characterized a novel mutation in the *TLR8* gene that caused an autoimmune and autoinflammatory disease in monozygotic twins. The resulting partial loss of TLR8 protein led to dysregulation between the TLR8 and TLR7 responses, based on cross-reactivity of the TLR8 receptor to TLR7 ligands and enhanced signaling of the TLR7 receptor.

Keywords

primary immunodeficiency, immunophenotyping, flow cytometry, mass cytometry, diagnosis, standardization, EuroFlow, B cell development, trajectory inference, functional testing, SCID, ALPS, TLR8

List of abbreviations

ADA	adenosine deaminase
AID	activation-induced cytidine deaminase
AK2	adenylate kinase 2
ALPS	Autoimmune lymphoproliferative syndrome
APC	antigen presenting cell
APDS	Activated PI3K δ syndrome
BAFFR	B-cell activating factor
BCR	B cell receptor
BLNK	B-cell linker
BTK	Bruton tyrosine kinase
CID	Combined immunodeficiency
CLP	common lymphoid progenitors
CSR	class switch recombination
CTL	cytotoxic T cell
CVID	common variable immunodeficiency
DGC	DiGeorge syndrome
DNT	double negative α/β T cells
EF	extrafollicular
ESID	European Society for Immunodeficiencies
FDC	follicular dendritic cell
FO	follicular
GALT	gut associated lymphoid tissue
GC	germinal center
GvHD	graft-versus-host disease
HSC	hematopoietic stem cell
HIGM	Hyper-IgM syndrome
HSCT	hematopoietic stem cell transplantation
IFN	interferon

IGHM	Ig μ heavy chain
IGLL1 λ 5	molecule encoding the surrogate light chain
IL	interleukin
IPEX	Immune dysregulation, polyendocrinopathy, enteropathy X-linked
IUIS	International Union of Immunological Societies
KREC	kappa-deleting recombination excision circles
MHC	major histocompatibility complex
MPP	multipotent progenitor cells
MZ	marginal zone
NBS	newborn screening
NGS	next generation sequencing
PAD	predominantly antibody deficiencies
PI3K	phosphatidylinositol-3-kinase
PID	primary immunodeficiency
RAG	recombination-activating gene
RTE	recent thymic emigrant
SCID	Severe combined immunodeficiency
SHM	somatic hypermutation
TACI	transmembrane activator and calcium modulator and cyclophilin ligand interactor
Tcm	central memory T cell
TCR	T cell receptor
TEC	thymic epithelial cell
Tem	effector memory T cell
TFH	follicular helper T cell
Th	helper cell T cell
TLR	Toll like receptor
TNF	tumor necrosis factor
TREC	TCR excision circle
Treg	regulatory T cell
Tscm	stem-cell memory T cell

UNG	uracil N-glycosylase
WAS	Wiskott-Aldrich syndrome
WES	whole exome sequencing
WGS	whole genome sequencing
XLA	X-linked agammaglobulinemia
XLP	X-linked lymphoproliferative disease
Zap-70	ζ chain-associated protein of 70 kDa
γc	common gamma chain

Table of contents

1.	Introduction	13
1.1.	General aim of the thesis	13
1.2.	Development of the adaptive immune system.....	15
1.2.1.	Development of T cells.....	15
1.2.2.	Development of B cells	21
1.3.	Primary immunodeficiencies	27
1.3.1.	Severe combined immunodeficiencies (SCIDs).....	28
1.3.2.	Combined immunodeficiencies (CIDs).....	31
1.3.3.	Diseases of immune dysregulation	35
1.3.4.	Predominantly antibody deficiencies.....	36
1.3.5.	Defects in innate immunity.....	37
1.4.	Diagnostic approaches in PIDs	39
1.4.1.	T cell and B cell receptor excision circles	39
1.4.2.	Genetic testing	40
1.4.3.	Flow cytometry immunophenotyping and functional testing	41
1.4.4.	Mass cytometry functional immunophenotyping.....	43
1.5.	Treatment and management of PIDs.....	44
1.5.1.	Hematopoietic stem cell transplantation	44
1.5.2.	Gene therapy	44
1.5.3.	Targeted therapies.....	45
1.5.4.	Immunoglobulin replacement therapy.....	46
2.	Specific aims of the thesis.....	47
3.	Methods.....	48
4.	Results.....	49
4.1.	EuroFlow Standardized Approach to Diagnostic Immunophenotyping of Severe PID in Newborns and Young Children	49
4.2.	Defects in memory B-cell and plasma cell subsets expressing different immunoglobulin-subclasses in patients with CVID and immunoglobulin subclass deficiencies	52
4.3.	<i>Tviblin</i> di algorithm identifies branching developmental trajectories of human B cell development.....	54

4.4.	Non-apoptotic FAS signaling controls mTOR activation and extrafollicular maturation in human B cells	56
4.5.	TLR8/TLR7 dysregulation due to a novel TLR8 mutation causes severe autoimmune hemolytic anemia and autoinflammation in identical twins	59
5.	Discussion.....	61
6.	Summary	67
7.	List of publications	69
8.	Literature references	72
9.	Appendix - attached manuscripts	83

1. Introduction

1.1. General aim of the thesis

The beginning of primary immunodeficiency (PID) research dates back to the early 1950s when clinical cases of infants who suffered from recurrent life-threatening infections were first reported. The first one described was X-linked agammaglobulinemia, or Bruton's agammaglobulinemia named after the American pediatrician O. Bruton in 1952¹. Subsequently, more severe cases that presented not only with lack of serum γ -globulins but also with absent lymphocytes were reported from Switzerland. Originally, they were described to be suffering from Swiss-type agammaglobulinemia², however, later on the condition was defined as severe combined immunodeficiency (SCID). In an effort to find other similar cases, patients with defects of the innate immunity were reported as well by C. Janeway in 1954³ and A. Good in 1957⁴.

Such clinical reports provided the base for proposing a model of separate lymphocyte lineages and for the discovery of T and B lymphocytes in the following years. Considering the monogenic nature of PIDs, they represent the perfect model system to investigate different aspects of the immune system. Indeed, the forthcoming identification of underlying mutations causing PIDs led to the discovery of many crucial mechanisms of the development and differentiation within the immune system.

Back in the day, only supportive forms of treatment, such as prevention, antibody replacement or infection treatment, were available. The groundbreaking discovery of stem cells and the first application of hematopoietic stem cell transplantation (HSCT) provided definitive cure for an XR-SCID patient in 1968⁵. In the WHO's recommended classification of PIDs from 1970⁶ are only 14 different types of PID with suggested cellular defect. However, advances in molecular biology and genetics have allowed for a rapid increase in the number of known genes associated with specific PIDs. With the completion of The Human Genome project in 2003⁷ and the application of next-generation sequencing (NGS) to PIDs a few years later, the number of identified PIDs began to grow exponentially (Figure 5), with the current number of over 480 disorders according to the latest 2022 IUIS report ⁸.

Notably, defining newly found PIDs has brought previously unknown aspects to this already heterogeneous group of disorders. For example, it has been acknowledged that autoimmunity, allergy or malignancy represent other manifestations of PID. The definition of “one gene-one disease” has been challenged by the observation that one phenotype can be caused by different affected genes, and many phenotypes can be caused by one affected gene. In these settings, flow and mass cytometry play an important role as they allow for investigating multiple parameters simultaneously.

The detailed characterization of PIDs at the cellular and molecular level has enabled more accurate diagnostic methods to be developed, allowing prompt and reliable identification of patients suspected of having PID. Consequently, more accurate diagnosis leads to better management of the disease, including improved survival after HSCT. It has also led to the development of new treatment approaches in the form of gene and targeted therapy.

The overall aim of this work is to contribute to a better understanding of selected PIDs with the objective of more sensitive and reliable identification of patients suspected of having PID (using standardized flow cytometric tests) and subsequent characterization of a novel PID-causing mutation (using personalized functional tests), and possibly to future more effective treatment approaches. In addition, to gain novel insights into specific (dys)regulatory mechanisms of the human immune system (using multiparameter mass cytometry), while using selected PIDs as model systems. In addition, to introduce novel analytical tools for dealing with multidimensional data.

1.2. Development of the adaptive immune system

Lymphocytes develop from hematopoietic stem cells (HSCs) in the bone marrow which give rise to multipotent progenitor cells (MPPs) that differentiate into common lymphoid progenitors (CLPs). Next, they mature either in the bone marrow (B cells) or in the thymus (T cells) and migrate to the periphery where they circulate through blood and secondary lymphoid organs.

1.2.1. Development of T cells

DEVELOPMENT IN THE THYMUS

T cells develop in the thymus from CLPs originating in the bone marrow. The T cell program is initiated after receiving signals from molecules such as Notch ligands and cytokines coming from the thymic microenvironment. Next, they undergo a selection process and subsequently they migrate to the periphery⁹.

CLPs commit to the T cell lineage as they migrate to the thymus, where the earliest committed T cell progenitors are called pro-T cells. Impaired differentiation of CLP into pro-T cells can be caused by mutations in *IL2RG*, which encodes the common γ chain (γ c) of the receptors for the cytokines IL-2, IL-4, IL-7, IL-9, IL-15 and IL-21. The resulting defective signaling leads to a complete or partial disruption of T cell generation, depending on the type of mutation (null or hypomorphic), but has no effect on the B cell development. Such patients are diagnosed with X-SCID and represent one of the most severe forms of PID with a T⁻B⁺NK⁻ phenotype¹⁰. The same phenotype resulting from arrested cells developing into pro-T cells, but inherited as an autosomal recessive trait, is caused by mutations in *JAK3*, which encodes Jak3 kinase signaling downstream of γ c-dependent cytokine receptors¹¹. Other forms of autosomal recessive SCID due to impaired transition of CLP into T cell progenitors are caused by mutations in *i. IL7R* gene encoding the α chain of the IL-7 receptor¹², suppressing the T cell development but not affecting the B cell and NK cell development *ii. adenosine deaminase (ADA)*^{13,14} and *iii. adenylylase kinase 2 (AK2)*¹⁵ both causing premature apoptosis of progenitors with effect on all the immune cells (Figure 1).

In the next pre-T cell stage, the cells already express recombination-activating genes RAG1 and RAG2 which mediate the cleavage step during V(D)J recombination allowing for TCR β rearrangement. Successful V(D)J rearrangement enables expression of pre-TCR (TCR β with invariant pre-TCR α). Impaired transition to pre-T cells can be caused by defects in RAG1/RAG2¹⁶,

ARTEMIS¹⁷, DNA-dependent protein kinase catalytic subunit (DNA-PKcs)¹⁸ and DNA ligase 4¹⁹ leading to defective V(D)J recombination and a phenotype of T⁻B⁻ SCID, or in CD3 δ , CD3 ϵ and CD3-associated ζ chain which result in defective pre-TCR signaling²⁰, block in $\alpha\beta$ T cell development and causes T⁻B⁺ SCID (Figure 1). At this point, the cells that are able to signal through the pre-TCR and make the transition into the DP T cell stage. The cells express both CD4 and CD8 coreceptors and undergo TCR α gene rearrangement which forms a complete $\alpha\beta$ TCR⁹. The transition to DP stage can be blocked by deficiency in CD45²¹ (Figure 1). The DP cells expressing functional TCR $\alpha\beta$ receptor go through the process of positive selection in the cortex as they interact with self-antigens presented on MHC-I or MHC-II molecules by the cortical thymic epithelial cells (TECs). Depending on the affinity, the cells either undergo death by neglect (too weak signaling) or continue the maturation and migrate into the medulla where they undergo negative selection, i.e. cells which encounter self-antigens with strong affinity presented on APCs undergo apoptosis. Next, they migrate to the periphery as single positive (SP) naive T cells and differentiate into CD4⁺ T helper cells, having TCR that binds peptide-MHC-II complexes, or CD8⁺ cytotoxic T cells, having TCR that binds peptide-MHC-I class complexes⁹. The cells can be arrested in the DP stage in cases of MHC-II deficiency, also known as bare lymphocyte syndrome, resulting in defective positive selection in the thymus and reduced mature CD4⁺ T cells, or transporters associated with antigen processing *TAP1*, *TAP2*, or tapasin genes essential for peptide transport and loading for proper MHC-I presentation, which is characteristic with low levels of CD8⁺ T cells²². Also, mutations in the ζ chain-associated protein of 70 kDa (Zap-70 protein) tyrosine kinase affect positive selection of CD8⁺ T cells and cause peripheral CD8⁺ deficiency^{23,24} (Figure 1).

As described above, the positive selection process for self-MHC recognition depends on the interactions with thymic epithelial cells (TECs) and the negative selection is based on the interactions with thymic DCs in order to remove self-reactive clones. However, this concept may be challenged by evidence from studies of thymic transplantation, i.e. the procedure performed in cases of athymia either associated with complete DiGeorge syndrome or SCID due to FOXP1 LOF mutations (nude-SCID). Transplanted patients are able to generate a functional repertoire of naive T cells that respond to self-APCs and have the ability to clear and resist infections, regardless of the fact that the TECs are of donor origin. They are also tolerant of “self” and the thymus graft without the need for immunosuppression²⁵.

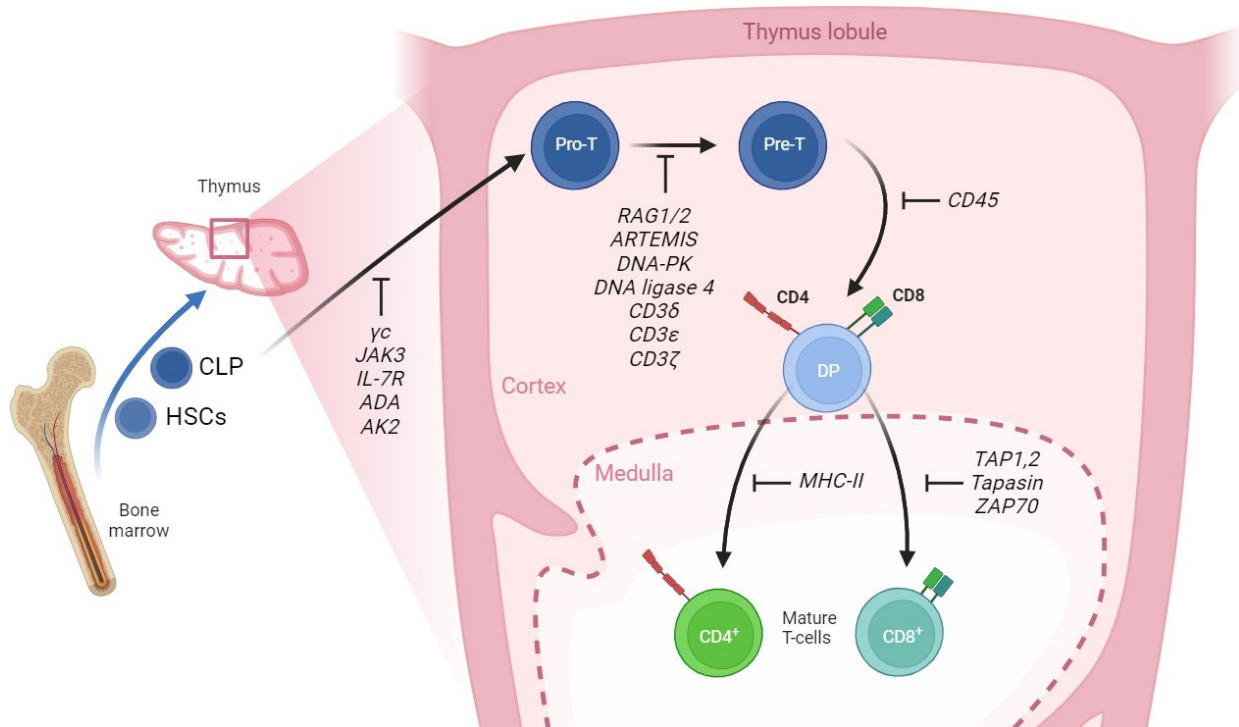


Figure 1. **T cell development with gene and protein defects associated with PIDs.** Hematopoietic stem cell (HSCs) develop into common lymphoid progenitors (CLPs) which migrate from bone marrow to the thymus. There they develop into pro-T, pre-T, double positive (DP) and finally single positive (SP) CD4⁺ or CD8⁺ T cells which migrate to the periphery. Examples of mutated genes known to cause blocks in the developmental stages are indicated. γ c, common cytokine-receptor γ -chain; JAK3, Janus kinase 3; IL-7R α , interleukin-7 receptor α -chain; ADA, adenosine deaminase; AK2, adenylate kinase 2; RAG, recombination-activating gene; DNA-PKcs; DNA-dependent protein kinase catalytic subunit; TAP, transporter associated with antigen processing; ζ -chain-associated protein kinase of 70 kDa. Created in BioRender. Adapted from Cunningham-Rundles and Ponda 2005²⁶, and Notarangelo 2010²⁴.

THYMIC EGRESS

SP thymocytes in the medulla undergo negative selection. Also, they interact with various types of cells such as thymic medullary epithelial cells, dendritic cells and macrophages. They provide the thymocytes the necessary stimuli for their final maturation and competence to egress from the thymus via the circulation. It has been shown that SP thymocytes are developmentally heterogeneous. They can be distinguished on the basis of phenotypic markers CCR4, CCR7, CCR9, where more mature cells are CCR4⁻CCR7⁺CCR9⁻. Genes controlling the thymic egress include sphingosine-1-phosphate receptor 1 (S1PR1). This G protein-coupled receptor enables

S1PR1⁺ thymocytes to migrate toward a S1P gradient provided by thymic DCs and to enter the perivascular space (PVS). Finally, mature SP thymocytes exit from the PVS and enter the bloodstream²⁷. Thymic egress can be blocked by mutations in Coronin 1A (CORO1) and mammalian sterile 20-like protein kinase 1 (MST1)²⁸.

With age the thymus undergoes changes such as loss of epithelial cells and replacement of the tissue with fat leading to decrease in thymopoiesis. The thymic function can be examined by detecting the presence of the most naive cells freshly emigrated from the thymus called RTEs which are CD4⁺ T cells characteristic with expression of the marker CD31. Another way of tracking the thymic output is examination of TCR excision circles (TRECs) which are the products of the TCR α rearrangement. Generally, RTEs and TRECs are highest in infants and decline with age²⁹ (Figure 2).

T CELLS IN THE PERIPHERY

Humans maintain the level of naive T cells thanks to peripheral homeostatic proliferation and long lifespan of the cells up to several years while retaining their naive phenotype. This explains replenishment of naive T cells with aging regardless of the lowering thymic output³⁰. The homeostatic proliferation takes place within secondary lymphoid tissues (predominantly LNs) under the influence of survival cytokine IL-7 produced by a specialized stromal cell population³¹ and self-peptide MHC complexes. Also, expansion of potentially autoreactive naive T cell clones might be generated considering the fact that the peripheral proliferation is driven by self-peptide MHC complexes. Especially in cases of lymphopenia, a hallmark of primary immunodeficiencies, the reduced T cell population undergoes compensatory exaggerated IL-7 driven proliferation which together with lowering the TCR activation threshold might lead to the initiation of autoreactivity (or dysregulation)³².

Considering that RTEs and naive CD4⁺ T cells with proliferative history are of the same naive phenotype CD45A⁺CD27⁺CD62L⁺, distinguishing them phenotypically became possible only after introducing the molecule CD31 (PECAM-1) as a marker specific for RTEs³³. CD31 is a transmembrane glycoprotein of the Ig superfamily expressed on various cell types. Besides T cells it is present on endothelial cells, platelets, monocytes and polymorphonuclear cells. Also, it engages in a variety of interactions including homophilic and heterophilic bindings. Thus, in dependence of the cell type and the ligand, CD31 engagement leads to adhesive contacts, migration

or can play a role in down-regulating proliferation of T cells. Hence, there could be a role of CD31 in the process of homeostatic proliferation itself³⁴. Another way of discrimination between the two is based on the content of TCR excision circles (TRECs) which are the products of TCR α rearrangement. Since TRECs are not replicated during mitosis their number lowers as cells divide. Indeed, CD31⁺ RTEs were shown to have significantly higher TRECs content in comparison to CD31⁻ naive CD4⁺ T cells. Thus, high content of TRECs in RTEs indicates no proliferative history while CD31⁻ naive CD4⁺ T cells are characteristic with diminished TRECs content implying undergone proliferation³⁵. RTEs exit the blood and enter secondary lymphoid organs thanks to the expression of the molecule CD62L which functions as a lymph node homing receptor. Here, they mature into naive T cells over the period of 2-3 weeks. Among the requirements for maturation of RTEs to naive T cells are successful exit from the thymus, access to secondary lymphoid organs and the function of APCs³⁶ (Figure 2).

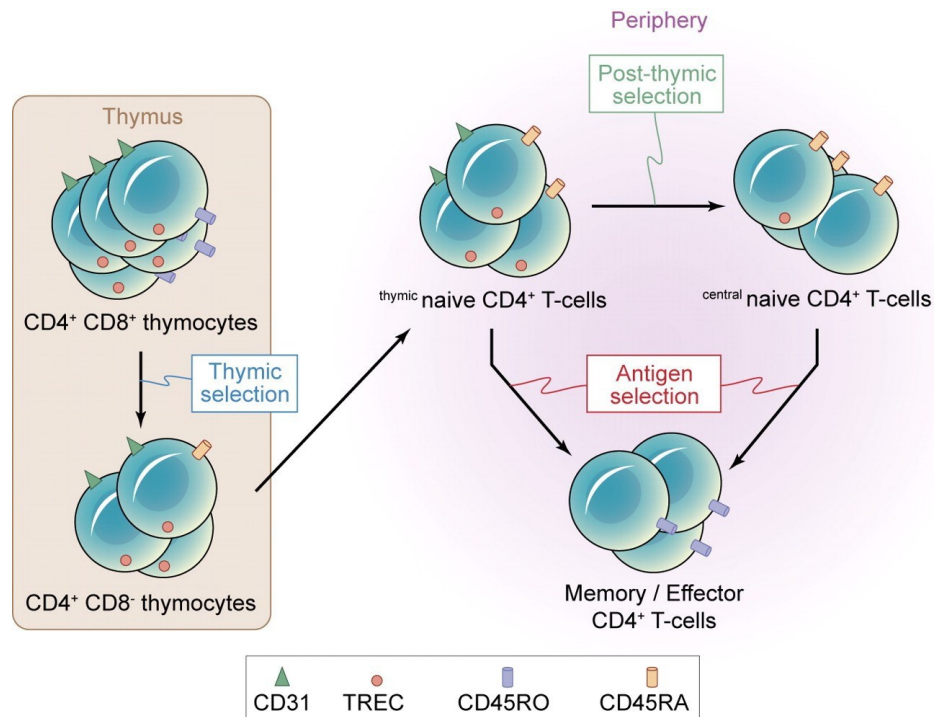


Figure 2. **Proliferation of naive CD4⁺ T cells.** Recent thymic emigrants (RTEs) emigrate from the thymus having high content of T-cell receptor excision circles (TRECs) and expressing CD31. Some of them differentiate into central naive CD4⁺ T cells contributing to the naive CD4⁺ T cell pool. Both of the subsets can differentiate into memory/effector T cells after encountering antigen. Taken from Kohler et al., 2009²⁹.

After encountering antigen on DCs in lymphoid organs, naive T cells undergo activation. Complete activation of T cells occurs only after recognition of peptide-MHC complex on the surface of APCs together with ligation of CD28 on T cells by CD80 or CD86 on APCs (co-stimulation). In the absence of co-stimulation, T cells undergo apoptosis or become anergic. Within hours of activation, T cells express CD69, which reduces the expression of S1RP1, which is responsible for T cell egress from lymphoid tissues. This allows T cells to remain in the lymphoid organ in order to receive proliferation and differentiation signals, mainly driven by IL-2. At this point, T cells begin to express CD25, the alpha chain of IL-2 receptor. Later, T cells express CD40L, which provides the necessary help signal to macrophages and B cells and a positive feedback signal to APCs. Deficiency of the CD40L causes X-linked Hyper IgM syndrome and affects both the cellular (impaired T cell proliferation) and humoral immunity (lowered IgG, IgA and IgE with normal or elevated IgM)³⁷. Another marker of activation present on T cells is the molecule HLA-DR which was shown to be acquired by allogeneic transfer from APCs³⁸. Migration of activated cells to the peripheral tissue is enabled by a reduction in the expression of CD62L and CCR7, both of which are responsible for homing to lymphoid organs.

IL-2 driven proliferation results in clonal expansion of antigen-specific cells and subsequent differentiation of naive T cells into CD4⁺ helper effector cells (Th1, Th2 or Th17) and CD8⁺ cytotoxic T lymphocytes (CTLs). Part of the activated cells differentiate into memory T cells which forms a heterogeneous group of cells maintaining long-term immunity. They can be divided according to their phenotype and function into i. central memory (T_{cm}, CD45RA⁻CCR7⁺), effector memory (T_{em}, CD45RA⁻CCR7⁻) and stem-cell memory (T_{scm}, CD45RA⁺CCR7⁺CD95⁺CD122⁺) T cells. Upon antigenic stimulation, T_{cm} express lymph-node homing receptors (CCR7, L-selectin), exhibit high proliferative capacity and generate many effector cells, whereas T_{em} migrate to peripheral sites and display immediate effector functions such as INF- γ production and cytotoxicity, thus responding rapidly to repeated exposure to pathogens. T_{scm} form a small long-lived population with enhanced proliferative and self-renewal capacity. They have no effector functions but can give rise to central memory, effector memory and effector T cells^{39,40}. A population of terminal effector cells (TEMRA) re-expressing CD45RA (CD45RA⁺CCR7⁻) can also be found in the circulation. These are mostly CD8⁺ T cells with a low proliferation rate but a high capacity for INF- γ production and are correlated with persistent viral infection such as CMV⁴¹.

After eliminating the antigen, there are several regulatory mechanisms responsible for decline of the T cell response which maintains homeostasis of the immune system. In particular, the level of IL-2 and costimulatory signals decreases which leads to apoptosis of activated cells and lowered production of newly activated cells. The regulatory mechanisms involved in the process are provided by the inhibitory receptors CTLA-4 and PD-1, regulatory T cells and Fas mediated apoptosis. Disruption of these mechanisms are connected to various types of PIDs characteristic with immune dysregulation, such as CTLA-4⁴² and PD-1⁴³ deficiency, and immune dysregulation, polyendocrinopathy, enteropathy X-linked (IPEX)⁴⁴ or autoimmune lymphoproliferative syndrome (ALPS)⁴⁵.

1.2.2. Development of B cells

DEVELOPMENT IN THE BONE MARROW

B cells develop in the bone marrow from CLPs. Stable commitment to the B-lineage is dependent on the transcription factor (TF) PAX5, as together with the TF EBF1 (induced by the TF E2A=E12 and E47) prevent alternative cell fates and induce B-lineage transcriptional program⁴⁶. In mice, the induction of these critical TFs is regulated by IL-7, a crucial cytokine in the process of murine early B cell development⁴⁷. Interestingly, the requirements of IL-7 in human B cell development are different. Patients with X-linked SCID, IL-7R deficiency or Jak3 deficiency present with normal or increased numbers of circulating B cells⁴⁸. It has led to the assumption that B cell lymphopoiesis is independent of the IL-7 signaling. Recently it was shown that IL-7 plays an important role in driving proliferation and expansion of the early B cell progenitors and also promotes the expression of PAX5, EBF1 and BACH2 TFs, revealing previously unknown effect of this cytokine on the human B cell development⁴⁹. As the B-lineage committed progenitors differentiate, they express CD19 and become pro-B cells. This early phase of development can be disrupted by E47 deficiency, causing autosomal recessive agammaglobulinemia⁵⁰, AK2¹⁵ and ADA¹⁴ deficiencies (Figure 3). pro-B cells do not produce immunoglobulin molecules and can be phenotypically defined as CD34⁺CD10⁺CD19⁺ cells. At this stage, RAG proteins are expressed, the VH(D)JH rearrangements of the heavy chain is initiated and its successful completion and expression of μ HC marks the transition to pre-B cells⁵¹. The transition is blocked in cases of RAG1 or RAG2 mutations causing absence or deficiency of B cells (and T cells, as described above in

1.2.1.) causing T-B-SCID¹⁶. Transmembrane μ HC assembles with the surrogate light chains ($\lambda 5$ and VpreB), Ig α and Ig β to form the pre-BCR. Expression of the pre-BCR is a key checkpoint regulator in the B cell development as it is responsible for further differentiation, allelic exclusion and clonal expansion. Mutations in the genes encoding both downstream signaling transduction, i.e. Bruton tyrosine kinase (BTK)⁵² and B-cell linker (BLNK)⁵³, as well as additional components of the pre-BCR, i.e. Ig μ heavy chain (IGHM)⁵⁴, signal transduction molecules Ig α and Ig β (CD79A⁵⁵ and CD79B⁵⁶), $\lambda 5$ molecule encoding the surrogate light chain (IGLL1)⁵⁷ arrest B cells in the early stage of development leading to primary immunodeficiencies caused by absence of peripheral B cells and antibodies. Also, loss of function (LOF) mutations in PI3KCD (encoding the p110 δ catalytic subunit of PI3K δ kinase) and PIK3R1 (encoding the p85 α regulatory subunit of PI3K δ kinase) result in early B cell developmental block⁵⁸ (Figure 3). Cells with productive heavy chains undergo clonal expansion and are named large pre-BI cells. As the proliferation decreases, they become small pre-BII cells arrested in G1, which undergo rearrangements of the κ or λ light chain. Productive rearrangement will produce κ or λ light chain protein which associates with the μ HC forming a complete IgM BCR. Expression of the complete BCR on the surface represents the entry into the immature B cells as well as the first tolerance checkpoint. Cells with high affinity to self-antigens undergo secondary gene rearrangement of the light chains called receptor editing or are deleted from the repertoire by apoptosis. Immature cells then give rise to transitional cells which are found in the periphery⁵¹.

B cell development

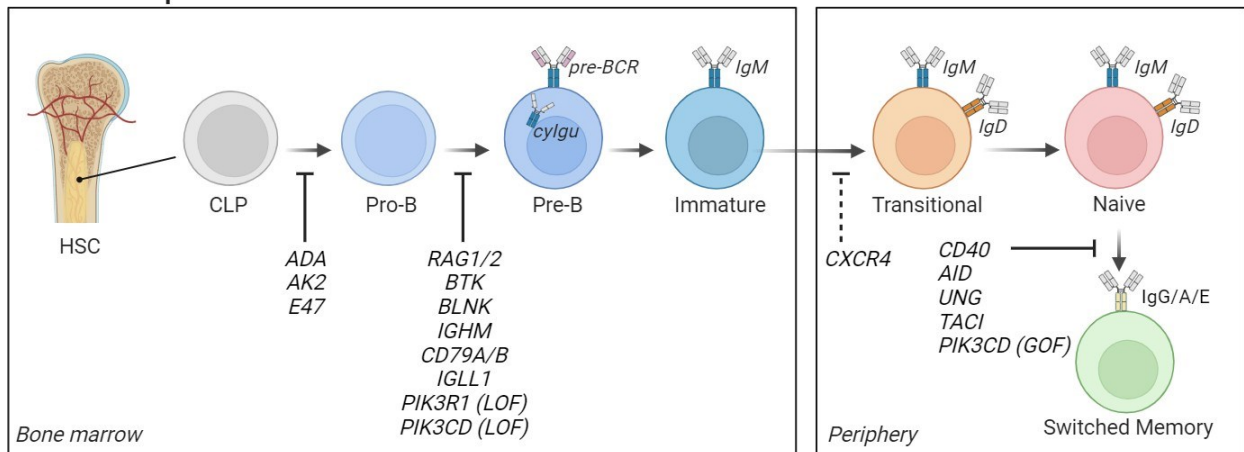


Figure 3. **B cell development with gene and protein defects associated with PIDs.** Hematopoietic stem cells (HSCs) develop into common lymphoid progenitors (CLPs) which give rise to pro-B cells, pre-B cells and Immature cells with complete B-cell receptor (BCR IgM). Transitional B cells then emerge from the bone marrow to the periphery and develop into mature Naive cells which differentiate into Switched Memory B cells. Indicated are examples of mutated genes known to cause blocks in the developmental stages. ADA, adenosine deaminase; AK2, adenylate kinase; RAG, recombination-activating gene; BTK, Bruton's tyrosine kinase; BLNK, B-cell linker; IGHM, Igμ heavy chain; IGLL1, λ5 molecule encoding the surrogate light chain; PIK3R1, p85α regulatory subunit of PI3Kδ kinase; PIK3CD, p110δ catalytic subunit of PI3Kδ kinase; AID, activation-induced cytidine deaminase; UNG, uracil N-glycosylase; TAC1, transmembrane activator and calcium modulator and cyclophilin ligand interactor. Created in BioRender. Adapted from Notarangelo 2010²⁴ and Smith et al. 2019⁵⁹.

BONE MARROW EGRESS

The bone marrow egress is predominantly controlled by attenuation of CXCR4 signaling⁶⁰. Mutations in CXCR4 are associated with WHIM syndrome, a combined immunodeficiency characteristic with peripheral B lymphopenia due to impaired emigration of cells from the bone marrow⁶¹. Emigrated transitional B cells form a heterogeneous population of cells which express IgD alongside IgM and can be detected as IgD⁺CD10⁺CD38⁺CD24⁺ cells (Figure 3). Initially, the human transitional B cells have been divided into two stages named T1 and T2 transitional B cells based on the expression of markers CD10, CD24, CD38 and IgM which are gradually lost as B cells mature. Next, another stage named T3 Transitional B cells was discovered as the third consecutive population. It is a population of cells phenotypically similar to mature naive B cells

but lacking the expression of the ABCB1 transporter, a protein present on mature naive B cells but absent on transitional cells⁶².

Expansion of circulating transitional B cells are associated with immunodeficiencies APDS, also known as activated PI3K δ syndrome caused by gain-of-function (GOF) mutations in the PI3K genes PIK3CD and PIK3R1⁵⁸, X-linked lymphoproliferative disease (XLP) or common variable immunodeficiency (CVID) which /are also characteristic with reduction of circulating class-switched memory B cells⁶³.

B CELLS IN THE PERIPHERY

The spleen plays an important role in the process of further survival and differentiation of the transitional cells into mature naive B cells, where self-reactive cells are inactivated or eliminated⁶². However, transitional cells are also found in the GALT⁶⁴ or lymph nodes⁶⁵ suggesting they can mature at other sites as well. Mature naive B cells are then transported by peripheral blood to the secondary lymphoid tissues and organs.

In the secondary lymphoid organs, mature naive B cells locate to *i.* marginal zones (splenic regions between the red pulp and the white pulp) where they differentiate into natural effector B cells (also known as marginal zone (MZ)-like B cells, *ii.* B-cell follicles (follicular (FO) B cells) where they differentiate into germinal center (GC) B cells and then to long-lived plasma cells or memory B cells. B cells located in the peritoneal and pleural cavities are known as B1 cells⁶⁶.

Natural effector B cells produce natural IgM antibodies and antibodies against T-independent antigens (blood-borne pathogens) and are important in the early phases of infection as they differentiate into short-lived IgM secreting plasma cells. At this stage, the spleen microenvironment plays a crucial role in generating such cells. Patients with dysfunctional or absent spleen have reduced/absent natural effector B cells and are at risk of infections caused by encapsulated bacteria possibly due to the combination of the filtering capabilities of the spleen and the absence of generating natural effector B cells. Apart from the spleen, natural effector B cells can be found in the peripheral blood, PP, tonsils and activated LN of humans⁶⁷. Long-lived plasma cells and memory B cells are canonically generated from naive B cells in the secondary lymphoid organs in B cell follicles and in germinal centers. In the primary response, antigen stimulation of the BCR induces naive B cells to differentiate into extrafollicular (EF) short-lived plasma cells,

providing a rapid response to the pathogen, with some of them developing into EF-memory B cells, and to FO B cells in the B cell follicles⁶⁸. Subsequently, FO B cells form GCs around day 4-6 after encountering the antigen, undergo proliferation and somatic hypermutation in the dark zone and enter the light zone where antigen-affinity based selection takes place. Here they recognize antigen on follicular dendritic cells (FDC) and interact with T follicular helper (TFH) cells. Next, they encounter three main fate decisions, development into *i.* memory B cells, which are present within SLOs, *ii.* long-lived plasma cells which reside in the bone marrow or *iii.* re-entry to the GC dark zone to undergo additional SHM and selection. In the secondary response after re-encountering antigen, memory B cells differentiate into long-lived plasma cells or re-enter the GC reactions⁶⁹ (Figure 4).

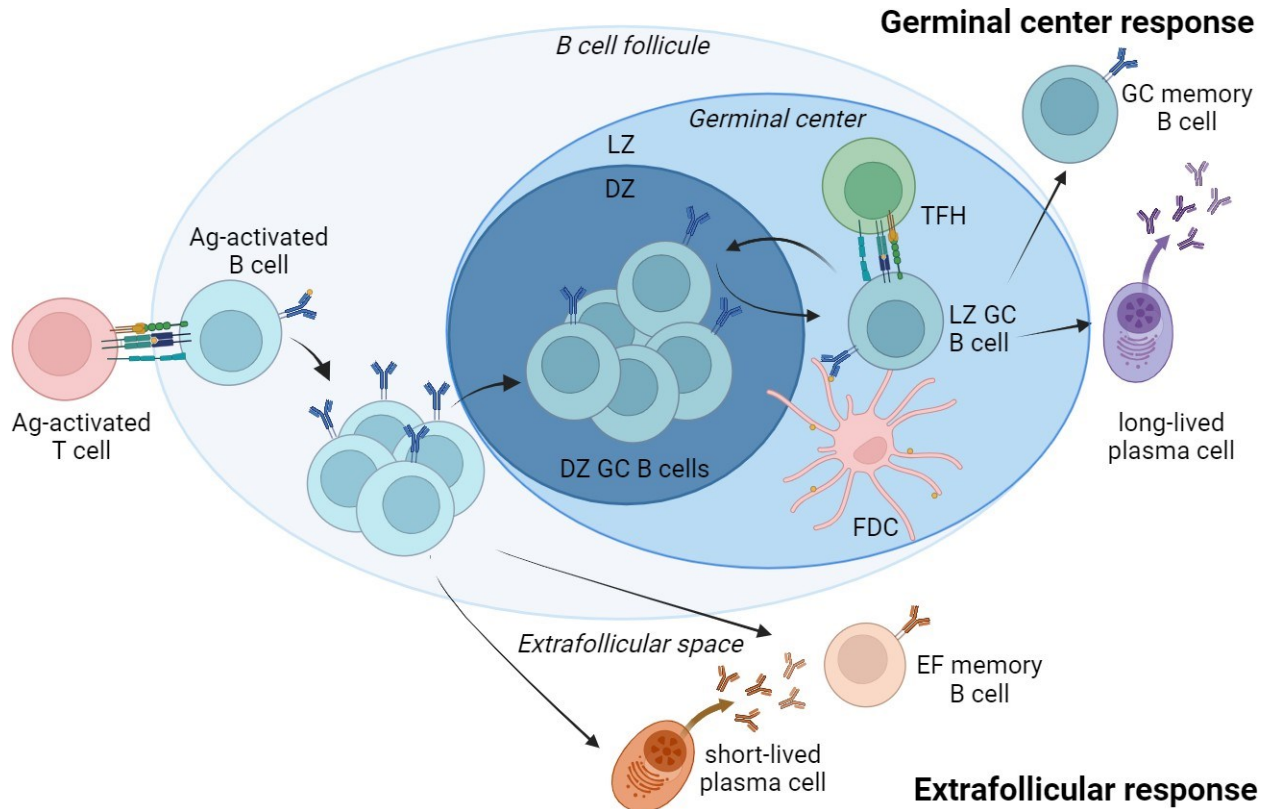


Figure 4. **B cell differentiation.** Antigen activated B cells receive helper signal from cognate CD4⁺ T cells. Activated B cells undergo proliferation, part of the cells differentiate into short-lived plasma cells at the extrafollicular space, and some of them differentiate into EF memory B cells. Alternatively, part of the B cells proliferates to form germinal center and differentiate into long-lived plasma cells or GC memory B cells. TFH: T follicular helper cell; FDC: follicular dendritic cell. Created in BioRender. Adapted from Kurosaki et al. 2015⁶⁶ and Elsner et al. 2020⁷⁰.

The commitment of B cells to EF differentiation or formation of GC is dependent on various factors, one of them is type of infection. Bacterial infections such as *Salmonella enterica*⁷¹ promote dominant formation of EF responses while human influenza A virus promotes predominantly GC formation⁷². Next, the type of TLR engaged. The formation of GCs was described to be diminished by TLR9⁷³ signaling via blocking B cells to present antigen and to activate TFH cells *in vitro*. Moreover, in a human clinical trial the TLR9 agonist CpG failed to promote affinity maturation and induced extrafollicular differentiation towards short-lived plasma cells. In contrast to that, TLR7⁷⁴ signaling was shown to promote the GC formations. Cytokines indirectly influence the EF or GC responses by affecting the differentiation of TFH cells. For example, IL-6 drives TFH differentiation, thereby GC responses, while IL-12, IFN- γ , TNF- α or IL-2 repress TFH cells, thereby repress the GC formation⁷⁰. It is also influenced by properties of the BCR and the affinity and avidity of the antigen, where high affinity multimeric antigens were favored for GC reaction completion^{75,76}. However, there are still unanswered questions about the factors driving the switch between EF and GC responses in the B cell differentiation.

Notably, despite the appreciation that CSR and SHM can take place only in the GC, both the EF and GC responses are characteristic with somatic V region hypermutation, affinity maturation and isotype switching. They were shown to take place at EF sites after encountering pathogens (*Salmonella typhimurium*)⁷⁷, hyper IgM syndrome caused by CD40L deficiency⁷⁸ and also in autoimmune pathologies, which are connected to dysregulated EF vs. GC responses^{79,80}.

The terminal differentiation of B cells can be disrupted due to mutations in the activation-induced cytidine deaminase (AID) or uracil N-glycosylase (UNG) which result in defect of class switch recombination (CSR) and absent IgG, IgA and IgE with normal or increased levels of IgM (hyper IgM phenotype). CSR is also disrupted in cases of CD40L-CD40 interaction defects due to deficiency of either CD40L (expressed by activated CD4⁺T cells) or CD40 (expressed by B cells, monocytes or dendritic cells)²⁴. Also, mutations in *TNFRSF13C* (coding for transmembrane activator and calcium modulator and cyclophilin ligand interactor, TACI) and its ligands *TNFRSF13B* (coding for B-cell activating factor, BAFFR) and a proliferation-inducing ligand (APRIL), or GOF mutations in PIK3CD are associated with CVID-like phenotype⁸¹ (Figure 3).

1.3. Primary immunodeficiencies

Primary immunodeficiencies (PIDs) are genetically inherited heterogeneous disorders of the immune system initially characterized as defects in responding to infection. The first several PIDs of the adaptive (Bruton's agammaglobulinemia¹ and Swiss-type agammaglobulinemia², currently known as SCID) and the innate immunity (congenital neutropenia⁸² and chronic granulomatous disease⁴) are dated back to the 1950s. However, the field of PIDs has expanded to such an extent that they now comprise a much more heterogeneous spectrum of phenotypes. Indeed, the 2022 update of the International Union of Immunological Societies (IUIS) reports over 480 single-gene PIDs⁸ (Figure 5).

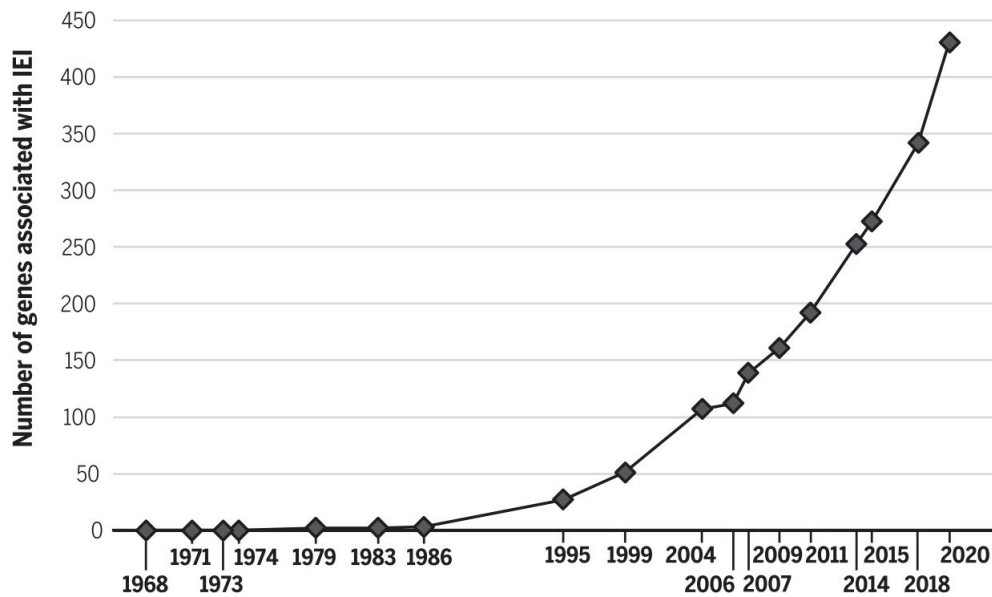


Figure 5. **Growth of newly discovered primary immunodeficiencies (PIDs).** The number of genetic defects associated with PIDs as reported by the WHO/IUIS from 1968 to 2020. Taken from Notarangelo et al. 2020⁸³.

Mutations within these genes may impair their function or cause complete absence of essential protein affecting the development and/or function of the immune system. They can result in loss or gain of function of the encoded protein, can be dominant or recessive, autosomal or X-linked and present with complete or incomplete penetrance. The clinical manifestations of PIDs are therefore diverse, ranging from mild to life-threatening complications. Patients diagnosed with PID present with increased susceptibility to infections, often to opportunistic pathogens and failure to thrive, but also depending on the specific PID, with autoimmune, autoinflammatory, atopic and

malignant phenotypes. Treatment varies according to the severity of the PID. It ranges from immunoglobulin replacement therapy, immunomodulating or immunosuppressive therapy to hematopoietic stem cell transplantation (HSCT), gene therapy and precision medicine⁸⁴.

The worldwide prevalence of PID has been reported to be 1:8 500 to 1:100 000 depending on the selected population and the type of PID. The rate is higher within populations with high consanguinity as well as among isolated populations. However, these numbers are thought to be underestimated since PIDs are generally underdiagnosed and underreported in many countries. The estimation for the PID prevalence in Europe as a whole is 5:100 000, for the Czech Republic it is 1:100 000, with the most common one being IgA deficiency⁸⁵.

1.3.1. Severe combined immunodeficiencies (SCIDs)

Severe Combined Immunodeficiencies (SCIDs) are rare (1:58 000 according to NBS for SCID in the US⁸⁶, 1:130 903 according to NBS in Europe⁸⁷) monogenic disorders causing block in the development and differentiation of T cells. SCIDs are characterized by impairment of both the cellular and the humoral immunity since the absence of T cells prevents B cells from functioning properly, i.e. producing antigen specific antibodies. Complete lack of the adaptive immunity makes patients diagnosed with SCID highly susceptible to pathogens, including opportunistic ones. Without prompt treatment (in most cases in the form of HSCT) these patients succumb to infection within the first year of life. Another presentation of SCID can be proliferation and skin/organ infiltration of maternally engrafted T cells⁸⁴.

To date, there are 22 known genes⁸ in which mutations that cause SCID can occur. SCIDs can be classified *i.* phenotypically based on the absence/presence of B cells as T⁻B⁻ SCID or T⁻B⁺ SCID with further subclass division based on the presence/absence of NK cells, *ii.* based on the impaired mechanisms, *iii.* depending on the inheritance as either X-linked or autosomal recessive.

The following part describes the five different groups of typical SCIDs based on the impaired mechanisms.

Defective survival of hematopoietic precursors

This rare (up to 2% of all cases) type of SCID, also known as reticular dysgenesis, is caused by mutations in the gene *AK2* coding for adenylate kinase 2. It is involved in transporting ADP into the matrix of mitochondria and in ATP synthesis. Deficiency of AK2 causes progenitor cells to be prone to apoptosis since they are deprived of ATP. It is associated with impairment of both innate and adaptive immunity leading to life-threatening conditions shortly after birth and is one of the most serious forms of SCID⁸⁸.

Defective V(D)J recombination

Approximately 30% of SCID patients have mutations in the genes involved in the process of V(D)J recombination resulting in impaired generation of T cell and B cell receptors. Consequently, individuals with this type of autosomal recessive form of SCID present with absent T and B cells but have NK cells (T⁻B⁻NK⁺ SCID). Mutations occur in the genes involved in the *i.* initiation of V(D)J recombination (null mutations in the *RAG1* and *RAG2* genes), *ii.* DNA repair pathway (*DCLRE1C* encoding Artemis nuclease¹⁷ and *PRKDC* encoding DNA dependent protein kinase catalytic subunit⁸⁹), *iii.* end-joining of double-stranded DNA breaks (*LIG4* encoding DNA ligase IV¹⁹ and *NHEJ1*⁹⁰ encoding a DNA repair member) which can lead to additional manifestations such as microcephaly and facial dysmorphism.

Toxic metabolite accumulation

The first SCIDs described at the molecular level are adenosine deaminase (ADA) and purine nucleoside phosphorylase (PNP) deficiencies. In particular, ADA deficiency causes premature apoptosis of lymphocyte progenitors (T cells, B cells, NK cells) by the accumulation of deoxy-ATP which disables the synthesis of other deoxynucleotides. It occurs in 10-20% of all SCID patients and is autosomal recessive. Besides early HSCT patients are treated with enzyme replacement and/or gene therapy. PNP deficiency also leads to abnormalities in purine metabolism causing T cell lymphopenia and is more uncommon than ADA deficiency^{91, 92}.

Defective pre-TCR and TCR signaling

Individuals with SCID due to mutations in the subunits of the (pre)TCR complex (CD3 δ , CD3 ϵ and CD3 ζ) found on T cells and T cell progenitors and in CD45, a tyrosine phosphatase expressed on all hematopoietic cells, account for about 2% of all cases. The TCR-CD3 complex is critical for antigen recognition during the process of thymic development of T cell progenitors and for adaptive immunity whereas CD45 is crucial for the regulation of kinases involved in the TCR signaling. It causes a selective T cell deficiency due to impairment of T cell development and differentiation steps, i.e. DN T cell proliferation and antigen recognition, and is inherited as an autosomal recessive trait (see below for CD3 γ deficiency causing CID)²⁰.

Defective cytokine signaling

The most frequently occurring type of SCIDs comprises three disorders caused by abnormalities in cytokine signaling in T cells and NK progenitor cells. The most common type of SCID is caused by a deficiency of the common γ chain (γ c) encoded by *IL2RG* gene. It is inherited as an X-linked recessive trait and is also known as XR-SCID. It is characterized by the absence of both T cells and NK cells and normal or increased number of circulating B cells⁹³. It was originally thought that *IL2RG* encodes only for the γ c of interleukin-2 (IL-2) receptor, but shortly after it was discovered that it is shared by five other cytokine receptors (for IL-4, IL-7, IL-9, IL-15 and IL-21)⁹⁴.

The next type of SCID is Jak3 deficiency (with autosomal recessive inheritance) which is clinically and immunologically indistinguishable from XR-SCID (T⁻B⁺NK⁻ SCID). Jak3 is a tyrosine kinase associated with the common γ c and is responsible for the activation of downstream kinases and STATs. It is essential for proper signaling of all γ c-containing cytokine receptors, which explains the similarities between Jak3 deficiency and XR-SCID. It is observed in 5-10% of SCID patients⁹⁵.

The third subtype is also autosomal recessive and is caused by mutations in *IL7RA* coding IL7 receptor α (CD127). It results in a phenotype with T cell deficiency (T⁻B⁺NK⁺ SCID) which reveals the importance of IL-7 signaling in the early steps of T cell development⁹⁶. The effect on human B development has been thought to be negligible, but a recent study shows its important role in the proliferation and expansion of the early B cell progenitors as well⁴⁹.

1.3.1.1. Atypical SCIDs

Atypical or leaky are considered the forms of SCID with different clinical and immunological presentation, generally due to hypomorphic mutations of SCID-associated genes. Consequently, these mutations result in residual protein expression and function and lead to different clinical phenotypes. Commonly, they present with immune dysregulation and less severe susceptibility to infections than typical SCIDs.

For example, several phenotypes caused by hypomorphic mutations in the *RAG* genes have been described. The spectrum depends on the level of residual V(D)J activity caused by distinct variants and ranges from *i.* newborns with Omenn syndrome, characterized by the expansion of oligoclonal, activated T cells of autologous origin, due to the severely impacted/residual V(D)J recombination activity, which infiltrate skin or other tissues, *ii.* patients with atypical SCID and expansion of $\gamma\delta$ T cells with persistent CMV infection *iii.* or patients with delayed onset immunodeficiency with granulomas and autoimmunity usually with less severely impacted enzymatic function⁹⁷. Also, an identical mutation in the *RAG2* gene found in siblings can lead to either a typical SCID phenotype or Omenn syndrome. This may be due to exposure to an infectious agent, demonstrating the possible effects of environmental factors on the clinical phenotype of such PIDs¹⁶. Alternatively, atypical X-SCID cases caused by hypomorphic mutations in the *IL2RG* gene have been described to present as a less severe form of SCID immunodeficiency. Among other examples are atypical SCIDs caused by hypomorphic mutations in the genes *JAK3*, MHC II deficiency, *Cernunnos*, *LIG4* or *DCLRE1C*⁹⁸.

1.3.2. Combined immunodeficiencies (CIDs)

1.3.2.1. CIDs less profound than SCIDs

As opposed to SCIDs, CIDs are caused by gene defects reported in more than 40 genes which allow partial survival of T cells but impair their function. The hallmark of CIDs is immune dysregulation usually in the form of severe eczema, autoimmune disease, autoimmune cytopenias, lymphoproliferation or inflammatory bowel disease. This phenotype is often combined with infectious events such as invasive bacterial or severe acute viral infections. Of note, dysregulation of the immune system leading to autoimmunity and inflammation may be present in some forms

of SCIDs (i.e. Atypical SCIDs) and is also commonly associated with other forms of PIDs (i.e. Diseases of immune dysregulation)⁹⁹.

Defective T cell survival/ Coronin A deficiency

Deficiency of Coronin 1A is associated with nearly absent naive T cells, oligoclonal peripheral TCR repertoire and impaired NK cells. Coronin 1A is encoded by CORO1A gene and functions as an important regulator of actin cytoskeleton which affects T cell survival and migration. Despite this, patients present with normal percentages of total CD3⁺ T cells and normal thymus size. Patients are also at high risk of developing EBV lymphoproliferative disease¹⁰⁰.

Defective TCR signaling

Defective TCR signaling associated with CID is connected to *i.* deficiency in CD3 γ (as opposed to other CD3 deficiencies responsible for typical SCIDs) which leads to impaired but not entirely blocked development of T cells and is associated with different levels of susceptibility to infection and common occurrence of autoimmunity. Defects in T cells manifest mainly in the population of Tregs which show reduced diversity and suppressive function as well as self-reactivity characteristics¹⁰¹, *ii.* deficiency of IL-2-inducible T cell kinase (ITK), a TEC family member which functions as non-receptor protein-tyrosine kinase in the development and signaling in the lymphoid lineage, which is in most patients connected to massive EBV B-cell lymphoproliferation and autoimmune cytopenias¹⁰², *iii.* deficiency in the zeta-associated protein of 70kDa (ZAP70), a member of the Syk family (non-receptor protein tyrosine kinase family) regulating motility, adhesion and cytokine expression, causing a variety of clinical manifestations including recurrent respiratory infections, lymphoproliferation and autoimmunity, immunologically the patients present with low CD8⁺ T cell counts and defective CD4⁺ T cell function²³, *iv.* MST1 (*STK4* gene) deficiency immunologically characteristic with CD4⁺ T cell lymphopenia and clinically presenting with bacterial and viral infections and mucocutaneous candidiasis. Lack of MST1 protein leads to abnormalities in adhesion and cellular migration affecting thymocyte trafficking and thymic egress¹⁰³, *v.* T lymphocyte-specific protein tyrosine kinase (Lck) deficiency causing recurrent respiratory infections accompanied by inflammatory and autoimmune manifestations, characteristic is CD4⁺ T cell lymphopenia where the residual cells exhibit TCR signaling defect and oligoclonal repertoire¹⁰⁴.

DOCK proteins deficiency

DOCK proteins are guanine nucleotide exchange factors which regulate reorganization of the actin cytoskeleton in lymphocytes. DOCK8 deficiency is associated with autoimmunity and malignancy as well as eczema and elevated IgE levels. It was found to be the underlying cause in most of the patients with autosomal recessive hyper IgE syndrome (AR-HIES). (AD-HIES is caused by mutations in STAT3). DOCK2 deficiency is characteristic with early-onset severe viral infections, T cell lymphopenia and functional defects of T, B and NK cells. Additionally, it causes impaired neutrophil function. Similar to Coronin 1A deficiency, DOCK2 deficient patients have detectable thymus. Clinically, patients can fulfill diagnostic criteria for leaky SCID or Omenn syndrome^{105, 106}.

MHC class II deficiency

The MHC class II deficiency, also called bare lymphocyte syndrome, is mostly caused by mutations in the TFs required for the expression of MHC class II genes. Autosomal recessive mutations of these genes impair the expression of MHC class II genes (patients express low or no levels of HLA-DP, HLA-DQ or HLA-DR on B cells, macrophages and DCs) and affect the positive selection of T cells in the thymus leading to lowered number of mature CD4⁺ T cells. It also leads to defective antigen presentation by all immune cells and activation of cells in the periphery. Patients present with early onset severe and recurrent infections in combination with autoimmune cytopenias with the only curative option of HSCT¹⁰⁷.

1.3.2.2. CIDs with associated or syndromic features

The following group of CIDs includes diseases with associated or syndromic features, i.e. in which mutations cause clinical symptoms additional to the problems connected to the immune system.

Wiskott-Aldrich syndrome (WAS)

Wiskott-Aldrich syndrome (WAS) is an X-linked PID associated with recurrent infections accompanied by an increased incidence of autoimmunity and malignancies, thrombocytopenia and eczema, in cases of complete absence of the WAS protein. However, different mutations of the *WAS* gene causing only decreased WAS protein expression lead to various clinical manifestations. One of them is X-linked thrombocytopenia (XLT), mainly characterized by thrombocytopenia and milder immunodeficiency, and the second is X-linked neutropenia (XLN) causing neutropenia and myelodysplasia because of activating mutations in the GTPase-binding domain of WAS protein¹⁰⁸.

Ataxia telangiectasia

Ataxia Telangiectasia is an autosomal recessive disorder characteristic with progressive neurodegeneration due to the absence of ATM (Ataxia Telangiectasia, Mutated) protein which is responsible for cellular signaling in response to double strand breaks and oxidative stress. Immunodeficiency, in the form of reduced numbers of lymphocytes and impaired antibody production, is a consequence of inability in repairing double strand breaks generated in the process of lymphocyte development and class switch recombination¹⁰⁹.

DiGeorge syndrome

DiGeorge syndrome (DGS) is caused by abnormal development of the third and fourth pharyngeal arches and genetically most commonly connected to microdeletion at chromosome 22q11. In majority of the cases the deletion includes over 30 different genes leading to a wide spectrum of clinical features including neurodevelopmental defects, cardiac malformations and hypoparathyroidism. Thymic hypoplasia or complete absence of the thymus leads to varying degrees of immunodeficiency, ranging from partial (pDGS) to complete (cDGS). In pDGS, patients manifest with increased susceptibility to infection which can be accompanied by autoimmunity (cytopenias, arthritis). The cDGS associated with athymia results in SCID which needs to be treated by HSCT or thymus transplantation²⁵.

1.3.3. Diseases of immune dysregulation

The term immune dysregulation describes a range of autoimmune and inflammatory conditions. In addition to increased susceptibility to infection, PIDs within this group are often associated with immune dysregulation of varying degrees (i.e. CIDs, Atypical SCIDs), or with a risk of developing it. In some cases, e.g. Autoimmune lymphoproliferative syndrome (ALPS) or Immune dysregulation, polyendocrinopathy, enteropathy X-linked (IPEX) syndrome, autoimmunity and autoinflammation are the primary clinical manifestations of such PIDs¹¹⁰.

ALPS

ALPS is caused by mutations in the genes involved in the apoptotic pathway, most commonly in the FAS gene but also in the *FASL*, *CASP8*, *CASP10* and *FADD* genes. It leads to defective Fas-mediated apoptosis and consequently to disturbed lymphocyte homeostasis (in response to pathogenic antigens) and to accumulation of autoreactive T and B cells. Clinically, ALPS patients present with autoimmunity, lymphadenopathy and splenomegaly and are usually treated with immunosuppressive agents and antibiotics, in minority of cases with HSCT. Phenotypically, it is characterized by elevated double negative α/β T cells (DNT)¹¹¹.

IPEX

IPEX is immune dysregulation syndrome characteristic with severe inflammation and systemic autoimmunity due to lack of Tregs, which are essential for self-tolerance and homeostasis of the immune system. The underlying cause is mutations in the Forkhead box protein 3 (FOXP3) which is TF crucial for the development of Tregs. Clinical manifestations most commonly involve enteropathy and skin manifestations. The severity of the overall clinical phenotype depends on the mutated region of FOXP3 where milder forms are treated with immunosuppressive treatment and severe cases with HSCT¹¹².

1.3.4. Predominantly antibody deficiencies

Predominantly antibody deficiencies (PADs) result from molecular defects intrinsic to B cells, impaired interaction between B cells and T cells and defects of immune regulation. It can lead to loss of B cells, complete absence of immunoglobulins or their reduction with or without loss of function. They represent the most prevalent PIDs and result in a wide spectrum of disorders. However, many of them have not been described on molecular and genetic level (mainly isotype or light chain deficiencies). As opposed to other PIDs, PADs have a variable and often later age of onset. Moreover, patients with antibody deficiencies typically suffer from recurrent infections caused by encapsulated bacteria contrary to patients with combined immunodeficiencies, who mostly present with opportunistic or severe viral or bacterial infections. They can be divided into four different categories¹¹³.

Agammaglobulinemia

Agammaglobulinemia is characterized by severe reduction in all immunoglobulin isotypes and very low levels or absence of B cells. It includes *i.* X-linked agammaglobulinemia (XLA), caused by mutations in the gene *BTK* encoding Bruton's tyrosine kinase leading to a block in development of B cells with only pro-B and pre-B cells present and *ii.* autosomal recessive agammaglobulinemia mainly caused by mutations in the components of the pre-BCR complex or downstream signaling pathways, and also agammaglobulinemia caused by *iii.* PIK3R1 and PIK3CD LOF mutations, *iv.* E47 TF deficiency¹¹⁴.

Hyper IgM syndromes

Hyper-IgM syndromes (HIGM) are characteristic with normal or even elevated IgM levels and severe reduction in IgG and IgA isotypes. They can be caused by defects in the class-switch recombination process, i.e. mutations in activation-induced cytidine deaminase (AID) and uracil-DNA glycosylase (UNG), or in the process of interaction between B cells and T cells, i.e. CD40L and more rarely CD40 deficiencies, which also makes a form of combined immunodeficiency (CID¹¹⁵).

Common variable immune deficiency (CVID) phenotype

CVID phenotype typically presents with severe reduction in at least 2 immunoglobulin isotypes but normal or low levels of B cells which either fail in becoming fully activated, proliferating normally or completing successful differentiation into memory and plasma cells. The cause lies in blocks in various steps during B cell development. In the majority of CVID cases the genetic basis has not been found even though it represents one of the most common symptomatic PIDs (1:25 000-1:50 000¹¹⁶). The CVID phenotype can arise as a result of deficiencies in i. TACI¹¹⁷ that has been linked to CSR and plasma cell differentiation, ii. NFκB1/2 deficiencies¹¹⁸, LRBA and CTLA4¹¹⁰ deficiencies, PIK3CD GOF⁵⁸ mutations, which all contribute to defects connected to dysregulation of the immune system.

Isotype, light chain or functional deficiencies

This group generally presents with normal levels of B cells and may include functional defects. The most common primary antibody deficiency, i.e. selective IgA deficiency belongs to this category. The incidence is 1:143 to 1:18 500 and the majority of patients (about two thirds) are clinically asymptomatic¹¹⁹. Other examples are kappa chain deficiency¹²⁰ where all immunoglobulins have the lambda light chain, IgH chain mutations and deletions, isolated IgG or IgG with associated IgA subclass deficiencies. The clinical presentations vary from asymptomatic to increased susceptibility to bacterial infection or associated with conditions such as atopic disorders or allergy¹¹³.

1.3.5. Defects in innate immunity

Most defects of innate immunity lead to disrupted development or function of immune cells other than T and B cells. They are linked to infectious diseases and susceptibility to different pathogens depending on the affected innate immunity mechanism.

Examples of defects of the innate immunity involve Chronic granulomatous disease (CGD) caused by mutations in the phagocyte oxidase (phox) enzyme complex, leukocyte adhesion deficiencies, which are result of mutations in the endothelial adhesion molecules of neutrophils, defective NK cells and phagocytes causing Chédiak-Higashi syndrome and defects in the IL-12/INF-γ pathway causing Mendelian susceptibility to mycobacterial disease (MSMD)¹²¹.

This category also involves Toll-like receptor (TLR) signaling pathway deficiencies. TLRs are pattern recognition receptors mediating recognition of pathogen-associated molecular patterns (PAMPs) and danger associated molecular patterns (DAMPs) and are located on the plasmatic membrane (TLR1, TLR2, TLR4, TLR5 and TLR6), detecting extracellular pathogens and also the endosome membrane (TLR3, TLR7, TLR8 and TLR9), detecting viral nucleic acids, intracellular bacteria antigens and endogenous particles¹²². Among the proteins, which are commonly affected are IRAK4 and MyD88, which are involved in the signaling pathway of most TLRs and their cooperative function results in the induction of NF- κ B signaling pathway and production of pro-inflammatory cytokines. They can be also linked to susceptibility to viral infections, such as TLR7 or TLR3 deficiencies¹²³.

1.4. Diagnostic approaches in PIDs

Diagnosis of PID follows well-established guidelines which are updated on a regular basis. They are defined by the International Union of Immunological Societies (IUIS⁸), providing classification catalog of PID, and the European Society for Immunodeficiencies (ESID¹²⁴) with the working definitions for clinical diagnosis. Diagnosis is completed upon a combination of clinical manifestation definitions, a variety of laboratory tests and genetic testing. The laboratory testing starts from basic full blood count test and serology (evaluating total immunoglobulins, followed by subclass and specific antibody determination) to more advanced flow cytometric immunophenotyping tests which are able to characterize and quantify subpopulations of immune cells. It plays an important role in the further guidance of functional and genetic testing decisions. Next, definitive diagnosis is made using Sanger or next generation sequencing (NGS) which localizes the genetic defect(s) in the DNA ¹²⁵.

Early diagnosis of PID is crucial for early initiation of appropriate therapy in order to reduce patient mortality in the most severe cases of PID and morbidity such as organ damage in other PIDs. Correct diagnosis needs to be done before the potential occurrence of infection, as SCID patients with early diagnosis and infection-free state at treatment have higher (95%) survival than patients with late diagnosis and active infection (81%)¹²⁶. Similarly, early and precise diagnosis of PAD patients can avert infectious complications and organ damage associated with lower quality of life and survival rate¹²⁷. However, PIDs could be susceptible to diagnostic delay for a number of reasons, including overlapping symptoms of immune dysregulation, newly assigned phenotypes of previously known genetic defects or different genetic defects presenting with a similar phenotype, hypomorphic mutations, maternal engraftment and others. This overall variability, only emphasizes the importance of reliable, sensitive and rapid diagnostic tools and creates the necessary motivation to develop new, more efficient ones.

1.4.1. T cell and B cell receptor excision circles

T cell receptor excision circles (TRECs) are products of the T cell receptor rearrangement during the development of T cells in the thymus. Analogous to TRECs are kappa-deleting recombination excision circles (KRECs) which are products of BCR rearrangement analogous to TCR. They can be detected in a DNA extracted from newborn dried blood spots utilizing a real-time quantitative

polymerase chain reaction (RTqPCR). Quantification of TRECs/KRECs reflects the relative number of naive cells in the periphery and are correlated with the thymic/bone marrow output¹²⁸. Because of the life-threatening consequences in the case of late diagnosis and data showing that infants undergoing hematopoietic stem cell transplantation (HSCT) within the first months of life and without the onset of infection prior to transplantation have higher survival rate and superior thymic output¹²⁹, SCID was proposed as the first PID in newborn screening (NBS) program. NBS for SCID was initially implemented in Wisconsin, United States (US) in 2008¹³⁰. Since then, it was established all over the US and subsequently worldwide including several European countries. Since 2022 monitoring of TRECs and KRECs has been included in the NBS program in the Czech Republic¹³¹ (Klocperk et al., manuscript in preparation). In the case of abnormally low TRECs/KRECs, flow cytometric immunophenotypic test focused on the naive T/B subsets is followed by consequent NGS testing for definitive diagnosis. Nonetheless, a considerable number of countries have not implemented NBS for SCID mainly because of challenges associated with logistics, optimizing for accuracy and cost.

Of note, some cases of CIDs (e.g. ZAP70 or MHC II deficiencies) or SCIDs caused by hypomorphic mutations, where the thymic output is not significantly affected, may not be detected by the NBS program. In such cases, other tools such as immunophenotyping are needed for early detection of SCID and CID patients¹³².

1.4.2. Genetic testing

Genetic testing in the form of sequencing, including NGS methods such as targeted gene panels, whole exome sequencing (WES) and finally whole genome sequencing (WGS) provide definitive molecular diagnosis of PID. As these methods are becoming more accurate, affordable and routinely available, they allow to identify new entities which allows for expanding the field of PID. However, analyzing and interpreting a variant requires time and expertise, which can be a disadvantage. Moreover, new variants need to be functionally validated which represents one of the main challenges. Contrary to that, fast and reliable results in the early diagnosis of patients suspected of PID (either due to clinical manifestations, family history or low or absent TRECs in cases of severe immunodeficiency) as well as the functional impact of new gene variants can be provided by cytometry immunophenotyping. On top of that, functional tests describing the affected

signaling pathways complete the newly found variants and open the door for possible targeted treatment. Notably, all of these methods are complementary to each other and only their combination can lead to a successful description of known and yet unknown PIDs¹³³.

1.4.3. Flow cytometry immunophenotyping and functional testing

Flow cytometry is a single cell method enabling measurement of multiple parameters at once thanks to light scattering and fluorescence emitted by fluorochrome-conjugated antibodies. It is able to detect the expression of surface and intracellular markers, including cellular functional responses in a form of activated phosphorylated kinases using phospho-flow. It is used for identification, quantification and characterization of specific cell populations in research and diagnostic applications with capability to provide results in brief period of time (typically few hours)¹³⁴.

Flow cytometry based basic T, B and NK population enumeration is standardly used screening test in cases of suspected PID. The results usually form a base for eventual application of following, more specific immunophenotyping tests which include markers of maturation or activation of T and B cell subsets. When complete lack of T cell counts is detected, the interpretation of the T-B-NK test is straightforward and leads to an elevated suspicion of SCID. However, T cells can be present in subtypes of SCID patients such as leaky SCIDs⁹⁷ or Omenn syndrome¹³⁵, also in cases of maternal T cell engraftment¹³⁶. Such patients cannot be detected by the T-B-NK- test as it fails to provide the needed phenotypic information about the subsets, such as maturation stage. The detectable T cells are of memory phenotype (either autologous or of maternal origin) confirming the defect in the production of T cells¹³⁷. In cases of reduced T cell counts determined by the T-B-NK- test, there is lack of information on the following direction of testing, which also confirms the need to develop new screening tools.

Similarly, cases of absent/strongly decreased peripheral blood B cells suggest agammaglobulinemia (due to mutations in BTK or related genes in the BCR signaling pathway), but further phenotyping of the B cell precursor subsets in the bone marrow can provide the information about the position of arrest in the early development. If B cell counts are reduced, additional analysis focused on the identification of the transitional and naive B cells or memory B cells, plasmablasts and plasma cells, in combination with the isotype and subclass classification,

needs to be performed, to differentiate between different diagnoses, e.g. hyper IgM syndrome, CVID or IgH isotype defects.

To overcome the limitations of the T-B-NK- test and previously published protocols^{138,139}, our group, as part of the EuroFlow consortium, developed standardized flow cytometric tools and strategies to reliably diagnose and classify PIDs of the lymphoid system. In particular, it consists of a screening PID Orientation tube (8-color and 12 markers, already informative about the maturation stages) and seven specialized classification tubes. According to the proposed PID algorithm, the PID Orientation tube is applied alone or in combination with the classification tubes, which are focused on detailed dissection of T cell or B cell defects. Besides the optimized and validated antibody panels, the EuroFlow approach includes standardized protocols for sample preparation, acquisition, and analysis^{140,141,142}.

It is important to note that to achieve a complete and optimal diagnosis of PID, specialized or functional assays may be needed to complement the above. For instance, assessing specific surface or intracellular proteins on different cell populations, e.g. CD40L on activated T cells in X-linked hyper IgM syndrome or CTLA-4 in CD4 Treg cells in CTLA-4 haploinsufficiency and LRBA deficiency¹⁴³, or implementing functional assays using flow cytometry to evaluate leukocyte responses to stimulatory, proliferative and apoptotic stimuli, or to various pharmacological and biologically active molecules when monitoring targeted therapy. For example, evaluating the phosphorylation state of STAT1 can differentiate between gain-of-function (GOF) and loss-of-function (LOF) STAT1 variants responsible for different clinical manifestations, i.e. chronic mucocutaneous candidiasis (CMCD) caused by GOF and Mendelian susceptibility to mycobacterial disease (MSMD) caused by LOF STAT1 mutations¹⁴³. Moreover, STAT1 phosphorylation state can report the effect of JAK/STAT inhibitors and describe the immune and clinical state of patients treated with targeted therapy¹⁴⁴. As another example of functional assay by flow, T cells from patients with ALPS characterized by impaired FAS/CD95-mediated cell death of lymphocytes, can be delineated by not undergoing apoptosis following stimulation with anti-Fas antibody, as opposed to control T cells¹⁴³.

1.4.4. Mass cytometry functional immunophenotyping

Measuring a higher number of parameters using conventional flow cytometry has limitations mainly due to similarities and overlaps in the emission spectra causing spillovers, spillover-spreading errors occurring after compensation leading to decreased resolution, but also autofluorescence and the number of lasers and detectors available. On the other hand, mass cytometry allows for the measurement of over 40 parameters¹⁴⁵ simultaneously, as it uses monoclonal antibodies coupled to metal isotope tags which overcomes the above-mentioned pitfalls of flow cytometry. The stained cells are nebulized into single cell droplets, pass through argon plasma which converts the cells into ion clouds. The ions are filtered through quadrupole which passes only the ions corresponding to the metal isotope probes. Then they are analyzed in the time-of-flight chamber by mass-to-charge ratio. The number of parameters that could be studied simultaneously is mainly limited by the availability of isotopes and antibody conjugation chemistry¹⁴⁵.

Mass cytometry gives the possibility to combine phenotypic markers together with molecules involved in signaling pathways, e.g. phospho-kinases or other proteins involved in proliferation, apoptosis, senescence or others and to obtain a full picture of the biological mechanism of interest. However, the acquisition of multidimensional data has brought with it challenges in analyzing such data and the need for appropriate tools to truly understand and interpret them. First, for data visualization, dimensionality reduction techniques were introduced to the analysis of mass cytometry data, one of the initially used was a linear method PCA¹⁴⁶. Better preservation of the relationships in space is achieved by non-linear reduction techniques, such as t-SNE¹⁴⁷ or UMAP¹⁴⁸. However, further development of methods is highly demanded to interpret large datasets in the most truthful way. Most recently, methods using unsupervised machine learning have been introduced¹⁴⁹.

Given the complexity of PIDs described above, mass cytometry can be extremely beneficial, especially when describing novel mechanisms due to selected gene defects and for subsequent guidance in developing new diagnostic or monitoring tools¹⁵⁰. Considering the longer time required for sample preparation, acquisition and analysis, as well as as the need for a larger sample volume, mass cytometry is primarily used for exploratory research-based questions rather than for diagnostics.

1.5. Treatment and management of PIDs

Thanks to the advances in the characterization of PIDs it has been possible to shift from supportive care consisting mainly of treatment of infections or inflammation to definitive treatment such as hematopoietic stem cell transplantation (HSCT) or gene therapy as well as to targeted medicine comprising monoclonal antibodies and small molecules.

1.5.1. Hematopoietic stem cell transplantation

Hematopoietic stem cell transplantation (HSCT) is based on the replacement of the diseased bone marrow cells by healthy cells from a related HLA-matched or unrelated HLA-matched donor and provides a definitive cure for the disease. For the procedure, it is necessary for the patients to undergo chemotherapy or irradiation in order to eradicate their bone marrow stem cells. Notably, in patients with SCID reduced-intensity conditioning (less intensive chemotherapy/radiotherapy used lowering the complications associated with conventional conditioning regimen) can be applied due to low risk of graft rejection. Other factors influencing the overall outcome include the degree of HLA compatibility between the recipient and the donor which is responsible for the graft-versus-host disease (GvHD). Next, the function of the thymus and history of infectious diseases. Hence, the earlier the patients are diagnosed the better prognosis they have thanks to the high rate of newly generated T cells and shorter exposure to infectious agents. HSCT is the only definitive treatment for SCIDs (exception can be made if gene therapy is available) who are characteristic with complete lack of T cells and is indicated shortly after birth. However, in cases of low to intermediate levels of T cells (in CID patients) the indication of HSCT is less straightforward in the context of future prognosis and risks of HSCT and is evaluated individually based on the clinical condition of the patient¹⁵¹.

1.5.2. Gene therapy

Gene therapy is a treatment method based on the autologous application of genetically modified hematopoietic stem and progenitor cells (and possibly T cells). The cells are infused after *in vitro* correction of the molecular defect by introduction of a viral vector carrying the wild-type gene. The initial trials began in the early 1990s and targeted ADA-SCID¹⁵² and X-SCID¹⁵³ and resulted

in a successful correction of the defective gene as well as with beneficial clinical outcome. However, the use of first-generation γ -retroviral vectors in the clinic was approved only for ADA-SCID since in the case of X-SCID and later in WAS it was connected to oncogene transactivation events¹⁵⁴. Development of next-generation self-inactivating γ -retroviral and lentiviral vectors later enabled safe and efficient gene delivery for correction of other IEIs, such as XR-SCID or WAS. Also, lentiviral vector-based gene therapy protocol for RAG1-deficient SCID is currently in preclinical phase¹⁵⁵. Recently, gene editing has been investigated as another promising curative therapy, especially in the form of CRISPR/Cas9. It enables precise insertion of the gene coding sequence after the natural promotor thus maintaining physiological expression and regulation of the cells. Of great benefit is also the potential of this method to correct dominant-negative and GOF mutations. Currently gene editing is in (pre)clinical trials for a number of IEIs, such as X-SCID, hyper IgM syndrome or X-agammaglobulinemia. Another way of gene editing is in the form of a single nucleotide exchange. However, it is in the preclinical stage in the field of IEIs¹⁵⁶.

1.5.3. Targeted therapies

Molecular diagnosis of PIDs has allowed identification of critical targets which can be specifically modulated or replaced by monoclonal antibodies or small molecules. One of the first targeted treatments used in the clinic is replacement of the ADA enzyme in patients with ADA-SCID with polyethylene glycol conjugated bovine ADA. Thanks to the advances in molecular tools being used to diagnose PIDs, many other targets have been identified with new molecules being developed and tested. Commonly used targeted therapies include kinase inhibitors, such as mTOR inhibitors (sirolimus, used in various PIDs with immune dysregulation manifestation), PI3K inhibitors (leniolisib, used in patients with APDS) or JAK/STAT inhibitors (ruxolitinib, used in patients STAT1 GOF and STAT3 GOF mutations). Another form of targeted therapies are CTLA4-IgG fusion proteins (abatacept, used in patients with CTLA-4 haploinsufficiency or LRBA deficiency) or IL-1 antagonists (anakira, used in patients with inflammasome pathologies). Targeted therapeutic molecules can be used in combination with immunosuppressive treatment or on their own¹³³.

1.5.4. Immunoglobulin replacement therapy

Immunoglobulin replacement therapy is mostly used in patients diagnosed with common variable immune deficiency (CVID). It is also choice of treatment in other diagnoses including agammaglobulinemia, IgG subclass deficiency and hyper IgM syndromes. Immunoglobulins, in the form of natural IgG prepared from pooled plasma from healthy donors, are administered intravenously or subcutaneously and aim to reduce infections¹⁵⁷.

2. Specific aims of the thesis

The first part of the thesis aims to investigate the immunophenotype of severe and predominantly antibody PIDs and to contribute to improved diagnosis of patients suspected of having such PIDs. Subsequently, it aims to provide a comprehensive approach to allow for a detailed study of B cell development to potentially discover alternative developmental pathways, improved diagnostic tests or novel therapeutic targets.

Specifically, we focused on the following points:

- 1) To develop and to report the clinical performance of a standardized diagnostic test for the identification and immunophenotypic description of T cells from newborns suspected of having severe PID (SCID and CID).
- 2) To provide a detailed immunophenotypic description of B cell subsets of potential diagnostic relevance in patients with predominantly antibody deficiencies (CVID, IgAdef, IgG/Adef).
- 3) To develop a mass cytometry protocol in combination with a novel computational framework for visualization of multidimensional data and detailed interrogation of human B cell developmental pathways.

The second part of the thesis focuses on elucidating the mechanism behind the dysregulated B cell differentiation in ALPS patients caused by mutated *FAS* (ALPS-Fas). It also aims to functionally describe the character of a newly identified mutation causing a novel type of PID.

In particular, we focused on the following points:

- 4) To describe the role of Fas signaling in ALPS-Fas patients in the extrafollicular vs. germinal center fate decision.
- 5) To functionally characterize a novel mutation in the *TLR8* gene found in monozygotic twins clinically leading to severe autoimmunity and autoinflammation.

3. Methods

The laboratory methods are described in detail in the attached manuscripts of this thesis. They include flow cytometry, cell sorting and mass cytometry measurements and sample preparation as the main methods used to gain the presented results.

All human material was collected after informed consent according to the Declaration of Helsinki and with the approval of the respective ethics committees. The samples were processed following standardized EuroFlow approaches or specifically designed protocols, which are described in the respective manuscripts. Data acquisition was performed on flow cytometers equipped with 405, 488 and 633/640 nm lasers (BD Biosciences) or cell sorter FACS Aria II (BD Biosciences) or mass cytometer CyTOF2/Helios (Fluidigm).

For data analysis, FlowJo or Infinicyt software was used. Statistical analyses were performed using GraphPad and StatView programs. Computational methods were developed in our group by Mgr. Jan Stuchlý, Ph.D., used R-project language and are reported in detail elsewhere.

4. Results

4.1. EuroFlow Standardized Approach to Diagnostic Immunophenotyping of Severe PID in Newborns and Young Children

*Tomas Kalina**, *Marina Bakardjieva**, *Maartje Blom*, *Martin Perez-Andres*, *Barbara Barendregt*, *Veronika Kanderová*, *Carolien Bonroy*, *Jan Philippé*, *Elena Blanco*, *Ingrid Pico-Knijnenburg*, *Jitse H. M. P. Paping*, *Beata Wolska-Kúsnierz*, *Malgorzata Pac*, *Jakub Tkaczyk*, *Filomeen Haerynck*, *Himmet Haluk Akar*, *Renata Formánková*, *Tomáš Freiberger*, *Michael Svatoň*, *Anna Šedivá*, *Sonia Arriba-Méndez*, *Alberto Orfao*, *Jacques J. M. van Dongen* and *Mirjam van der Burg*

Front Immunol. 2020 Mar 19;11:371. doi: 10.3389/fimmu.2020.00371

** contributed equally*

Severe forms of PID include Severe combined primary immunodeficiency (SCID) and Combined immunodeficiency (CID), both of which are rare disorders with an incidence of 1:58 000 - 1:130 903 newborns^{78,159}. For the Czech Republic it means 1-3 new patients per year¹³¹. Patients with SCID or CID are usually born asymptomatic, but the resulting complications caused by the lack of the adaptive immunity lead to life-threatening conditions before the age of one year. Therefore, prompt diagnosis followed by appropriate treatment, most commonly HSCT, is critical to their well-being and survival. Typically, patients completely fail to develop T cells. Paradoxically, some patients have T cells present, due to hypomorphic mutations or maternal engraftment. These patients are at diagnostic risk because the conventionally used T-B-NK screening test may not be sufficient to detect them.

In this study, we set out to develop a sensitive cytometric diagnostic test to reliably detect all patients suspected of having SCID/CID (including the ones with presence of T cells) as early as possible in an effort to avoid diagnostic delay. Considering the incidence of SCID/CID, this is a multicenter study and we sought a standardized approach within the EuroFlow consortium.

We have developed a diagnostic test called SCID-RTE, which is an 8-color flow cytometry test assessing the presence of the naive forms of CD4⁺ and CD8⁺ T cells defined as cells expressing the naive T cell marker L-selectin (CD62L) and lacking the memory T cell marker (CD45RO) as well as the activation marker (HLA-DR). Within the population of naive CD4⁺ T cells, the tube identifies the most naive T cells released from the thymus to the periphery called recent thymic

emigrants (RTE) using the marker CD31. By evaluating the expression of the molecules CD62L and CD45RO, other T cell maturation stages can be defined, i.e. central memory and effector memory T cells. The activation status of the cells can be determined by the expression of the HLA-DR molecule.

In collaboration with four other EuroFlow laboratories we collected 26 peripheral blood samples of patients diagnosed between birth and 2 years of age with molecularly defined defects causing SCID (n = 15, two of them presented with Omenn syndrome and three of them with maternal engraftment) or other form of PID (n = 11). Our control group consisted of 44 healthy donor samples in the same age range.

Using the SCID-RTE tube we were able to identify all SCID patients by detecting complete absence of RTE. Importantly, it included patients with normal absolute counts of CD3⁺ T cells due to maternal engraftment (n = 2) or oligoclonally expanded cells characteristic for Omenn syndrome (n = 1). This demonstrated the ability of the SCID-RTE tube to overcome the limitations of the routinely used TBNK assay, as it examines the origin of the T cells, i.e. CD4⁺CD31⁺ RTE cells. Other naive forms of T cells were also absent (CD4⁺/CD8⁺) or present at low detectable levels (CD8⁺).

Patients diagnosed with other forms of PID presented with varying degrees of abnormality in different cell subsets. In the majority of the patients (n = 7) we found detectable levels of RTE but significantly lower than in controls (lower than 5th percentile of healthy). The remaining patients (n = 2) had complete absence of RTE. An exception was patient diagnosed with ALPS who presented with above normal levels of RTE. Other forms of naive CD4⁺ and CD8⁺ cells were also abnormally low in the majority of the patients with the exception for the ALPS patient.

Another important parameter characteristic of patients with PID was an increased level of activated cells, as determined by the expression of HLA-DR. This finding was particularly important in SCID patients with detectable levels of T cells, i.e. Omenn syndrome or maternally engrafted cells. These cells showed massive signs of activation and were of memory phenotype (CD45RO⁺), demonstrating their oligoclonality and maternal origin, respectively. In patients with other forms of PID the activation status varied, but in the majority we found higher levels of HLA-DR⁺ cells than in the control group.

CONCLUSION

We have developed and demonstrated that the EuroFlow SCID-RTE tube is a powerful sensitive diagnostic test for the identification of patients suspected of having SCID/CID which is based on the immunophenotypic description of different T cell subpopulations, including the most naive RTE population correlating with thymic output, by standardized flow cytometry. It can be used in cases of clinical suspicion of SCID/CID, abnormal TRECs levels and subsequently to the PID Orientation tube (PIDOT) for more detailed analysis including RTE counts and the HLA-DR parameter.

4.2. Defects in memory B-cell and plasma cell subsets expressing different immunoglobulin-subclasses in patients with CVID and immunoglobulin subclass deficiencies

Elena Blanco, Martín Pérez-Andrés, Sonia Arriba-Méndez, Cristina Serrano, Ignacio Criado, Lucía Del Pino-Molina, Susana Silva, Ignacio Madruga, Marina Bakardjieva, Catarina Martins, Ana Serra-Caetano, Alfonso Romero, Teresa Contreras-Sanfeliciano, Carolien Bonroy, Francisco Sala, Alejandro Martín, José María Bastida, Félix Lorente, Carlos Prieto, Ignacio Dávila, Miguel Marcos, Tomas Kalina, Marcela Vlkova, Zita Chovancova, Ana Isabel Cordeiro, Jan Philippé, Filomeen Haerynck, Eduardo López-Granados, Ana E Sousa, Mirjam van der Burg, Jacques J M van Dongen, Alberto Orfao; EuroFlow PID group

J Allergy Clin Immunol. 2019 Sep;144(3):809-824. doi: 10.1016/j.jaci.2019.02.017

Predominantly antibody deficiencies (PADs) form a heterogeneous group of PIDs with high prevalence (50-70 % of all PIDs) but largely unknown genetic background. They are characteristic with aberrant production of one or more Ig isotypes or subclasses and include selective IgA deficiency (IgA-def), IgG deficiency with IgA deficiency (IgG/A def) and CVID with reduced total IgG, IgA and IgA and/or IgM serum levels. Their diagnosis and classification rely on the antibody serum levels, response to vaccination and clinical manifestations^{8,160}. However, B cell subset alterations and distribution of memory B cells (MBCs) and plasma cells (PCs) expressing different immunoglobulin subclass has not been widely studied in PAD patients, but can provide valuable information that can contribute to improved diagnosis and classification.

In this study, conducted within the EuroFlow consortium, we aimed to investigate the distribution of B cell subsets in more than 100 patients with PAD in comparison to more than 200 age-matched healthy controls, including IgG1 to IgG4 and IgA1 and IgA2 subclass distribution analysis within the PC and MBC compartments.

Most patients with IgA-def and IgG/A def had normal total B cell counts. Almost half of the IgA def patients and majority of the IgG/IgA def patients presented with decreased PC levels. IgA def patients could be divided into two subgroups based on the severity of the IgA⁺ MBC defects and different expression profile of the IgA subclasses. These two groups differed in the extent of autoimmunity manifestation and affected family members. IgG/A def patients also showed decreased IgG2⁺ MBCs. Around half of the CVID patients had decreased total B cell numbers

(with lowered immature/transitional and naive B cells subsets) and majority of them showed decreased switched IgG⁺ PC levels (98%). They were further divided into 6 subgroups based on differential expression of Ig isotype/subclass of the MBCs. These CVID subgroups did not differ in age or serum Ig levels, but did differ significantly in the frequency of autoimmunity, autoimmune cytopenia, and hepatomegaly.

CONCLUSION

In conclusion, this study provided a comprehensive evaluation of the B cell subsets alterations including the expression of distinct immunoglobulin subclasses on MBCs and PCs. Different subsets correlated with immune profiles, diagnostic subtypes and clinical presentations. This contributed to the classification of these PIDs and has a potential use in diagnostic.

4.3. *Tviblindi* algorithm identifies branching developmental trajectories of human B cell development

Marina Bakardjieva, Jan Stuchlý, Ondřej Pelák, Marjolein Wentink, Hana Glier, David Novák, Jitka Stančíková, Daniela Kužílková, Iga Janowska, Marta Rizzi, Mirjam van der Burg, Tomáš Kalina.

Under revision at European Journal of Immunology, January 2024

Preprint at bioRxiv, DOI: <https://doi.org/10.1101/2024.01.11.575178>

B cells develop from hematopoietic stem cells in the bone marrow. They then migrate to the peripheral blood and secondary lymphoid organs to differentiate into their final stages. Finally, they migrate back to the bone marrow as long-lived antibody-secreting cells. Blocks and regulatory defects in the B cell development lead to severe forms of PIDs or result in immune dysregulation, respectively, making this an area of intense research. The major developmental stages and their progression are well known. However, we lack detailed insight into the dynamics of expression of (non)canonical markers, potential intermediate stages, and suitable tools to discover possible alternative developmental pathways.

In this study, we aimed to develop *i.* a mass cytometry panel for detailed description of B cell developmental stages in healthy human bone marrow and peripheral blood samples and *ii.* a computational framework called *tviblindi* – trajectory inference algorithm and dimensionality reduction tool (*vaevictis*) that would allow us to analyze developmental trajectories in a user-friendly/interactive graphical user interface (GUI).

The dimensionality reduction tool *vaevictis* projected the B cell progenitor and mature B cell subsets progressing through the bone marrow and peripheral blood as a continuum, in a logical way preserving the local and global relationships between stages, along with the expression of canonical markers (CD34, TdT, CD10, surface IgM (sIgM), IgD and CD27) and the light chains indicating the κ and λ developmental branches. Therefore, it provided us reliable projection for interpretation of trajectories constructed by the *tviblindi* algorithm.

The *tviblindi* algorithm operates independently in the original multidimensional space and constructs random walks away from the defined starting point (CD34⁺ stem cells), directed by calculated pseudotime. The found developmental endpoints were located in clusters corresponding

to mature naive, natural effector and switched memory B cells. Next, we expertly selected the random walks that formed meaningful trajectories through biologically relevant subsets. We observed consistency between the manually analyzed and the pseudotime calculated expression of the canonical markers (TdT peak in pro-B/pre-BI stage, CD10 in pre-BI and sIgM in transitional B cells), and further analyzed the expression changes through and within the stages of all markers. They included nuclear factors (PAX-5, Ki-67, TdT or Bcl-2), phenotypic markers (CD34, CD10, CD20, sIgM, IgD, CD27) and cytokine and chemokine receptors (IL-7R α , CXCR4, CXCR5). Another layer of detail was provided when we compared the subpopulations (transitional, naive and natural effector) that were present in both the bone marrow and peripheral blood simultaneously. Even though they were projected in the same clusters we found a shift in the pseudotime and differential expression of the CXCR4 and CXCR5 markers.

Finally, *tvislindi* allowed for identification of branching points in the development of B cells. First, at the expected point of κ versus λ differentiation, and second, at the point of upregulation of the switched memory B cell marker CD73 which indicated the natural effector versus switched memory differentiation.

CONCLUSION

In conclusion, we have developed and validated a multiparametric mass cytometry protocol in combination with a computational framework that allows detailed analysis of B cell developmental trajectories. Of note, the presented algorithm is capable of analyzing multiple endpoints and finding multiple branching points in the dataset. This could provide a platform to study developmental/dysregulatory defects in PID patients with the potential to find alternative non-canonical pathways or endpoint populations. Finally, this knowledge could contribute to novel therapeutic targets or improved diagnostic tests.

4.4. Non-apoptotic FAS signaling controls mTOR activation and extrafollicular maturation in human B cells

Julian Staniek, Tomas Kalina, Geoffroy Andrieux, Melanie Boerries, Iga Janowska, Manuel Fuentes, Paula Díez García, Marina Bakardjieva, Jan Raabe, Julika Neumann, Jan Stuchly, Vladimir Benes, Rodrigo García Valiente, Jonatan Fernández García, Rita Carsetti, Eva Piano Mortari, Albert Catala Temprano, Bénédicte Neven, Frédéric Rieux-Laucat, Aude Magerus-Chatinet, Olaf Neth, Peter Olbrich, Reinhard E. Voll, Laia Alsina, Luis M. Allende, Luis I. Gonzales-Granado, Chiara Böhler, Jens Thiel, Nils Venhoff, Raquel Lorenzetti, Klaus Warnatz, Susanne Unger, Maximilian Seidl, Dirk Mielenz, Pascal Schneider, Stephan Ehl, Anne Rensing-Ehl, Cristian Roberto Smulski, and Marta Rizzi

Sci Immunol. 2024 Jan 12;9(91):eadj5948. doi: 10.1126/sciimmunol.adj5948

Autoimmune lymphoproliferative syndrome (ALPS) is a primary immunodeficiency classified as a disease of immune dysregulation, most commonly caused by mutations in the *FAS* gene (ALPS-Fas). It presents with lymphoproliferation, accompanied by autoimmunity with autoantibodies. The production of autoantibodies is attributed to impaired negative selection and removal of autoreactive B cells due to mutant Fas^{161,162}. ALPS-Fas patients are also characterized by disturbed peripheral B cell differentiation¹⁶³.

In this study, we aimed to investigate the role of mutant Fas in the disturbed B cell differentiation present in ALPS-Fas patients. We were interested in whether there is an additional signaling outcome after Fas engagement besides apoptosis, its role in the extrafollicular versus follicular B cell differentiation, and the regulatory mechanism behind it.

First, we focused on the immunophenotypic analysis of the B cell compartment and the effect of mutant Fas on the composition of B cell subsets. Of note, we used ALPS-Fas and healthy donor (HD) secondary lymphoid organ (SLO) cells (from the spleen, tonsils and lymph nodes) and found that ALPS-Fas patients had increased EF differentiation (spleen) and reduced GC B cell maturation (lymph node).

To combine immunophenotypic markers together with functional characterization of the skewed B cell differentiation in ALPS-Fas patients, we developed a high-dimensional mass cytometry panel including selected phospho-markers downstream of key signaling pathways. The data were

first visualized as a UMAP projection of all CD19⁺ cells (spleen) calculated using all phospho-markers and showed only partial overlap between ALPS patients and healthy controls. In particular, the ALPS-Fas samples showed increased pS6, pAkt as well as increased pBTK, pLyn and pPLC γ 2, suggesting increased mTOR signaling and increased BCR signaling, respectively. These results indicated that the EF response is associated with increased mTOR and BCR signaling. Further analysis of ALPS-Fas B cell subpopulations in two SLOs (spleen and LNs) revealed consistently and significantly increased mTOR signaling, as detected by pS6, leading to the hypothesis that the control of mTOR signaling is potentially affected by Fas.

To test this hypothesis, an *in vitro* system was developed to study non-apoptotic signaling after Fas engagement with FasL. Healthy naive B cells were activated with CD40L (to model initial activation and induce Fas expression) and transiently cultured with FasL. The signaling of non-apoptotic cells (cPARP⁻) was then studied. Activation with CD40L induced phosphorylation of the molecules S6, Akt, NF- κ B p65 and p38 MAPK. However, additional stimulation with FasL specifically reduced the pS6 and pAkt levels, thereby downregulating mTOR signaling. Importantly, the same experimental setup performed on ALPS-Fas cells showed an inability to downregulate the mTOR signaling (through CD40 in response to FasL), demonstrating that Fas provides the modulatory signal. This observation suggested that Fas triggering affects the PI3K/Akt/mTOR pathway in CD40L-activated B cells.

Further proteomic studies supported the data and helped to establish a mechanistic model in which Fas triggering causes intracellular protein relocalization (PTEN nuclear exclusion) that counteracts the activity of the CD40-induced PI3K/Akt/mTOR pathway. At the transcriptional level, Fas engagement induced the expression of CXCR4, c-MYC and BCL-6, which have been linked to GC formation and polarization.

CONCLUSION

This project used ALPS-Fas as a model system to elucidate a novel physiological role of non-apoptotic Fas signaling in the peripheral differentiation decisions in healthy B cells and the impaired signaling modulation caused by mutations in *FAS*. Taken together, the data show that healthy non-apoptotic Fas signaling contributes to GC versus EF developmental decisions, via downmodulation of mTOR signaling and transcriptomic changes, favoring GC formation, in CD40L-activated human B cells. In ALPS-Fas patients, this modulatory mechanism is impaired

due to defective Fas signaling, which results in upregulated mTOR signaling, reduced GC B cell maturation and increased extrafollicular responses, contributing to the immune dysregulation characteristic of these patients.

4.5. TLR8/TLR7 dysregulation due to a novel TLR8 mutation causes severe autoimmune hemolytic anemia and autoinflammation in identical twins

Martina Fejtkova, Martina Sukova, Katerina Hlozkova, Karolina Skvarova Kramarzova, Marketa Rackova, David Jakubec, Marina Bakardjieva, Marketa Bloomfield, Adam Klocperk, Zuzana Parackova, Anna Sediva, Jahnavi Aluri, Michaela Novakova, Tomas Kalina, Eva Fronkova, Ondrej Hrusak, Hana Malcova, Petr Sedlacek, Zuzana Liba, Martin Kudr, Jan Stary, Megan A Cooper, Michael Svaton, Veronika Kanderova

Am J Hematol. 2022 Mar 1;97(3):338-351. doi: 10.1002/ajh.26452

Both Toll-like receptor 8 (TLR8) and Toll-like receptor 7 (TLR7) are pattern recognition receptors (PRRs) found in the endosomes of immune cells. They are phylogenetically related and detect single-stranded (ss)RNA of viral and bacterial pathogens as well as endogenous ssRNA. Their stimulation promotes NF- κ B, MAPK and IFN signaling leading to the expression of inflammatory cytokines, chemokines and costimulatory molecules. Importantly, it has been shown that by triggering different signaling pathways, TLR8 and TLR7 negatively regulate each other and their interaction has an effect on balancing their inflammatory responses¹²¹.

In this study we presented a novel c.1715G>T (p. G572V) mutation in the gene encoding TLR8, located near the first ligand binding site, clinically leading to autoimmune and autoinflammatory disorder in two monozygotic male twins. In particular, severe autoimmune hemolytic anemia (AIHA) and autoinflammation presenting as fevers, arthritis, enteritis, and CNS vasculitis. We set out to functionally describe the character of the mutation and its effect on the mutant cells.

Based on the location of the mutation, we hypothesized altered activity of the TLR8 receptor upon ligand binding and a possible effect on the TLR8/TLR7 regulation. Indeed, we observed that the mutant TLR8 protein showed cross-reactivity to TLR7 ligands and also decreased inhibition of TLR7 signaling, as assessed by NF- κ B activity in human HEK-Blue cell lines.

The patient cells (monocytes) had half the amount of TLR8 protein compared to controls, but the mRNA levels were not significantly different from the healthy controls. Therefore, we compared the degradation rate of both TLR8^{WT} and TLR8^{G572V} proteins transiently transfected into the HEK293 cell line (treated with cycloheximide in order to inhibit proteosynthesis). This showed a

faster degradation of the mutant TLR8^{G572V} protein compared to the TLR8^{WT} protein, demonstrating a partial deficiency of the mutant TLR8 protein, possibly causing the mutant TLR8 to inhibit TLR7 less effectively and shifting the signaling balance towards TLR7.

Next, patient cells (monocytes) showed hyperactive NF-κB signaling and increased production of proinflammatory cytokines (IL-1β, IL-6, TNFα) when stimulated with TLR7 ligands compared to healthy controls, suggesting the disturbed TLR8^{G572V}/TLR7 balance towards TLR7.

In addition, we suggest that apart from the imbalance between TLR8 and TLR7 signaling towards TLR7, the pathological responses to microbes and the autoimmune/autoinflammatory phenotype in the patients are also caused by oligoclonality and expanded clonotypes within their effector T cell subsets which we found using T-cell receptor β repertoire sequencing across different FACS sorted T cell subsets.

CONCLUSION

This study reports a novel mutation in the *TLR8* that causes partial deficiency of TLR8 protein leading to a dysregulation between TLR8/TLR7 and imbalance towards TLR7. The mutation results in autoinflammatory and autoimmune clinical presentation. TLR8 partial deficiency has been proposed for inclusion in the classification of PIDs.

5. Discussion

Studying PIDs brings opportunities to understand and contribute to the elucidation of principles of different mechanisms of the immune system, which in turn contributes to the development of more efficient diagnostic approaches. This thesis aimed to contribute to the field of PIDs using several approaches, including the use of flow cytometry immunophenotyping (in a form of standardized tests for diagnostic evaluation of SCID/CID and classification of PAD), mass cytometry immunophenotyping with intracellular markers (for characterization of ALPS-Fas samples including key signaling proteins), functional testing (for functional characterization of a new mutation in the *TLR8* gene) and novel analytical approach (for analysis of B cell developmental mass cytometric multidimensional data and interrogation of developmental pathways).

Specifically, part of the thesis reports the potential diagnostic use and performance of a flow cytometric diagnostic test called SCID-RTE tube. This tube was designed to detect naive T cells, the most naive forms of CD4⁺ T cells, RTEs, together with the activation status, as HLA-DR⁺ cells, and the differentiation state of the T cells. All of the SCID patients in our cohort showed absence of naive T cells and RTEs and could be clearly detected. Notably, even the cases that had normal absolute counts of total CD3⁺ T cells. These patients had either maternally engrafted T cells¹³⁶ or oligoclonally expanded cells known in Omenn syndrome¹³⁵ and the SCID-RTE test also revealed, that the detected cells are characteristic with activated and memory phenotype. These patients pose a diagnostic challenge, because they may be missed if conventional T-B-NK- test is used, because this test does not consider the origin of the cells detected. It is known that maternal cells can pass through the placenta¹⁶⁵ and are eradicated in a healthy individual by the immune system. However, SCID patients fail to reject the cells, which can result in clinical symptoms of GvHD. Specifically, erythema with skin T-cell infiltration, but also organ involvement (liver, gastrointestinal tract). These maternal engraftment related symptoms are surprisingly present at a large proportion of SCID patients, up to 40% of the patients¹³⁶. SCID patients with Omenn syndrome have T cells present due to mono- or oligo-clonally expanded autologous T cells, as a result of hypomorphic mutations in various genes including *RAG1/2*, *IL2RG*, *DCLRE1C*, *DNA ligase 4*, *ADA* or *IL7RA*, leading to residual protein activity. T cell repertoire assessment of various V β families showed overrepresentation of a few T cell clones and underrepresentation or complete absence of most other V β families¹⁶⁶. The clinical symptoms are hardly distinguishable from the ones of patients

with maternal engraftment present. Although the SCID-RTE tube is not sufficient for disclosing final diagnosis, it plays a role in the early detection of the patients and direction of further diagnostic procedure (genetic testing).

According to ESID¹²⁴, at least 2 of the 4 laboratory criteria need to be fulfilled in cases of suspicion for SCID/CID. These are low or absent CD3⁺ or CD4⁺ or CD8⁺ T cells, reduced naive CD4⁺ and/or CD8⁺ T cells, elevated TCR $\gamma\delta$ ⁺ T cells, reduced/absent proliferation to mitogen or TCR stimulation. Using the SCID-RTE tube, already three of the criteria are covered, with the additional value of RTE cells which are also considered to reflect the thymic output¹⁶⁷ and correlate with TREC¹⁶⁸ levels. Majority of other PID patients in our cohort were clearly detected by the SCID-RTE tube as having decreased naive T cells and RTEs and activated phenotype. These included patients with PIDs primarily not caused by defects in the production of T cells but are defined according to IUIS⁸ as CID (mutation in *ZAP*), CID with associated or syndromic features (WAS), or diseases of immune dysregulation (IPEX) with dysregulation of the immune system as a hallmark present in all of them. As challenging for detection by the SCID-RTE tube was a patient with mutation in *FAS* who presented only with higher activation status and elevated TCR $\gamma\delta$ ⁺ T cell counts. However, we detected abnormally high counts of total CD3⁺ T cells and CD4⁺CD8⁻TCR $\gamma\delta$ ⁻ DN cells which fulfills one of the criteria for ALPS diagnosis defined by ESID¹²⁴. Another potential limitation of the study is seemingly low number of patients in our cohort (n=26). However, the prevalence of SCID/CID in Europe is around 1:130 000 (1-2 newborns per year in the Czech Republic). In order to tackle this issue, patient samples were collected in collaboration with three other laboratories to reach as high number as possible.

In such studies, where interlaboratory measurements are performed, standardization of laboratory techniques is more than desirable. The presented SCID-RTE tube is part of a more complex set of tools¹³⁷ applied in the diagnosis of PIDs developed by the EuroFlow consortium which aims for standardization and reproducibility in flow cytometric measurements¹⁶⁹. As opposed to other approaches^{170,171,172,139}, it provides a flexible system developed for PID, when a more general, diagnostic screening tube (PIDOT) covering the T, B (already with the information of naive subsets), and NK cell subsets is applied in combination with T cell or B cell specialized tubes following a proposed PID algorithm. It takes into consideration the cost-efficiency and availability of the sample volume. EuroFlow also provides automated gating procedures and age-related reference values¹⁴¹. Application of the SCID-RTE tube is therefore recommended in combination

with the PIDOT tube (a priori or after abnormal findings), in cases of clinical suspicion of SCID/CID or abnormal levels of TRECs measured in NBS programs.

Among the EuroFlow B cell specialized tubes is the IgH-isotype tube, which examines isotype and subclass expression within the memory B cells and plasma cells. The results of using this tube for better classification of PADs forms another part of this thesis. Diagnosis of PADs is challenging because of the variable clinical presentations and also the fact that they can presents from infancy to adulthood. The clinical hallmark of PADs is recurrent bacterial infections of the respiratory tract resulting from impaired antibody response. However, non-infectious complications such as autoimmunity or malignancy can be present as well^{173,120}. The diagnostic criteria are based upon a combination of clinical manifestations and laboratory parameters (based on Ig serum levels) but deeper insight is desirable, especially for patients with nonspecific clinical features. Studies of B cell alterations proved to be more useful for the classification and diagnosis of CVID patients but the associations between the B cell alterations and clinical manifestations are not completely uniform within them^{175,176,177,178}. Therefore, the detailed dissection based on the expression of immunoglobulin subclasses together with the standardized approach, large cohort of patients and age-matched controls presented a promising approach that can contribute to a improved diagnosis and insight into the underlying mechanisms of PADs.

As stated in the introduction to the thesis, PIDs serve as an excellent model for discovering general immune mechanisms. Subsequently, effective diagnostic testing depends on a comprehensive general understanding of the immune system. Therefore, there is a general attempt to study as many markers as possible simultaneously. Conventional clinical flow cytometry typically uses 4 to 12-color panels¹⁷⁹, spectral flow cytometry enables the measurement of 40-parameter panels¹⁸⁰ and mass cytometry allows for the analysis of over 40 parameters per panel¹⁸¹. For our B cell developmental project, we used the previously published 10-color EuroFlow tube exploring the B cell precursor development in bone marrow from healthy controls and PID patients as a benchmark to develop a 30-marker (plus 5 barcodes) mass cytometry panel. We designed and validated this panel to provide a detailed description of human B cell development in both the bone marrow and peripheral blood. We aimed to provide an innovative user-friendly interactive approach for interrogation and detailed analysis of developmental trajectories using a novel algorithm *tviblin* together with intuitive visualization of the data by an integrated dimensionality reduction technique *vaevictis*. Overall, we were able to describe B cell developmental trajectories from bone

marrow to peripheral blood, including the dynamic changes of marker expression (surface and nuclear) along the selected trajectory and in relation to developmental branching points. In the context of PIDs, the presented mass panel in combination with the computational tool can be used to discover any alternative trajectories and unknown branching points in affected patients and to elucidate new mechanisms or find therapeutic targets. In addition, it can provide insight into marker definition to address different cell fates in human B cell differentiation. Unlike other dimensionality reduction techniques such as UMAP¹⁸², t-SNE¹⁸³ or EmbedSOM¹⁸⁴, *vaevictis* visualizes the data while avoiding overrepresentation of large populations, creating a more continuous and intuitive representation of developmental data. Of great benefit is also the fact that once the projection is calculated, it can be applied to new data (if the same panel is used), allowing a clear comparison of patient samples with the healthy reference and among themselves over time. On top of that, *vaevictis* performs well at preserving both local and global structure (unlike for example t-SNE). Trajectory inference (TI) algorithms have been originally developed for single-cell RNA sequencing datasets and they form the majority, however some of the tools have been developed specifically for mass cytometry data¹⁸⁵. For example, Wanderlust¹⁸⁶ is a pseudotime algorithm that was presented for trajectory detection in B cell development, however it can only detect linear trajectories. Other algorithms, such as Monocle2¹⁸⁷ can detect branching points of trajectories, but it includes initialization of a dimensionality reduction in the iteration. The TI algorithm *tviblin* presented in our B cell development study is able to capture multiple branching points in trajectories and it analyzes the data in the original high-dimensional space, providing an unbiased approach. Importantly, the analysis process is interactive, allowing the user to expertly evaluate the biological significance of the selected trajectory and avoid possible shortcuts and artifacts in the dataset. Although our study represents a comprehensive approach to studying B cell development, in future investigations we could aim to complete the picture by measuring secondary lymphoid organ tissues, as they are crucial for B cell maturation.

Having acquired promising results using mass cytometry method, we designed another highly specific 30-parameter (plus 5 barcodes) panel to help reveal previously unrecognized non-apoptotic function of Fas signaling. This was possible thanks to using the ALPS-Fas PID as a model system. Importantly, the experiments were conducted on healthy and patient human samples from the spleen, lymph nodes, and tonsils, covering physiological conditions to study the complex signaling effects. As expected, the GC B cells were enhanced in tonsils and absent in spleen. In

contrast to that, EF B cell responses were present in the spleen but lowered in tonsils. These initial findings highlight the uniqueness of each tissue and the importance of studying such mechanisms at their natural sites. At the same time, the access to primary human tissues is rather limited, which only emphasizes the need for suitable and reliable methods capable of analyzing multiple parameters per cell to make the most of these valuable samples.

This extensive study demonstrated that the non-apoptotic Fas signaling affects EF versus GC fate decisions through mTOR activity. During B cell differentiation, signals from the BCR and CD40 are integrated, which activate PI3K and its downstream target Akt leading to activation of mTOR¹⁸⁸. In this study we showed that healthy CD40L-activated B cells have decreased mTOR axis upon transient Fas ligation. Mechanistically, through recruitment of DAXX to the activated Fas complex and nuclear exclusion of PTEN, leading to the expression of genes essential for GC formation. This axis is disrupted in ALPS-Fas patients, leading to increased mTOR signaling and impaired B cell differentiation - increased EF responses, while GC B cell maturation is reduced. The dysregulation towards EF responses that we observed in ALPS-Fas patients may be a contributor to the often-present autoimmunity¹¹¹. Further supporting this hypothesis, the enhanced EF responses have been connected to human autoimmunity disorders such as systemic lupus erythematosus (SLE), rheumatoid arthritis or Sjögren's syndrome⁷⁹. In ALPS, treatment with rapamycin (mTOR inhibitor) is efficient in reducing both lymphoproliferation and autoimmunity¹⁸⁹. The presented dysregulation of non-apoptotic Fas signaling contributes to the understanding of the efficacy of this treatment.

The next result of the thesis provided functional characterization of a novel mutation c.1715G>T (p.G572V) in the gene coding for TLR8 in a family with monozygotic twins suffering from autoimmune and autoinflammatory complications. The mutation led to a partial deficiency of the TLR8 protein and its pathogenic mechanism was discovered through personalized functional assays. The mutant TLR8 failed to efficiently inhibit TLR7 which caused an imbalance, resulting in a bias towards TLR7 signaling. The imbalance between TLR8 and TLR7 was described in mice models where deficiency of TLR8 resulted in increased activation of TLR7 and production of autoantibodies¹⁹⁰. Also, association between TLRs and autoimmunity development has been evidenced, for example in the pathogenesis of SLE¹⁹¹. According to IUIS⁸, the only known PID as a result of TLR8 mutation is TLR8 GOF variant described as a phenocopy of PID. Therefore, we

propose the presented partial TLR8 protein deficiency with TLR8/TLR7 dysregulation to be listed in the classification of PIDs.

Interestingly, although the twins had an identical mutation, the severity of the disease manifestation differed significantly. In particular, the twin A's worsening condition led to HSCT whereas twin B showed clinical improvement in response to hydroxychloroquine¹⁹³. This reflects the notion that exposure to infectious agents and other environmental factors influence the clinical phenotype of disease. In this particular case, exposure to pathogens or inflammation may have revealed various cryptic antigens, leading to varying degrees of autoimmune manifestation. In addition to this, we suggest that among the factors contributing to the autoimmune/autoinflammatory phenotype is oligoclonality and expanded clonotypes found in their T cell subpopulations. Taken together, to prove the causality of newly identified genetic variants in the pathogenesis can be challenging due to overlapping clinical presentations with other disorders, and requires careful experimental design (based on extensive literature review), considering potential problems with the *ex vivo* quality of patient samples due to treatment regimens, as well as close collaboration with clinicians.

6. Summary

This dissertation thesis focused on immunophenotypic and functional characterization of lymphocytes of patients with selected PIDs. It utilized several approaches, namely diagnostic immunophenotyping using conventional flow cytometry, deep immunophenotyping using multiparameter mass cytometry, functional testing and lastly and importantly novel computational tools for detailed analysis of multidimensional data.

The dissertation thesis fulfilled its objectives and obtained the following results:

- 1) We presented a standardized flow cytometric test called SCID-RTE (in the scope of EuroFlow) to be a suitable tool for evaluation and immunophenotypic description of T cells of newborns with suspicion of having a severe form of PID (SCID, CID). It showed high sensitivity for the monitored parameters (levels of naive CD4⁺ and CD8⁺ T cells, recent thymic emigrants (RTE), activation status) and presents a complete diagnostic test in combination with previously reported PID Orientation tube.
- 2) We provided a detailed immunophenotypic characterization of B cell and plasma cell subsets of patients with PAD (in the scope of EuroFlow) which included definitions based on the expression of different IgH subclasses. This provided a novel sensitive approach for defining B-cell alterations in PAD patients which were correlated with clinical manifestations, with potential for future diagnostic use.
- 3) We developed new mass cytometry panel focused on B cell development and computational tools that enabled us to visualize the multidimensional data and interrogate B cell developmental pathways. We demonstrated its utility in intuitively projecting B cell developmental stages in human bone marrow and peripheral blood and in describing pathways leading to multiple developmental endpoints, including detailed analysis of the dynamics of marker expression, also in relation to developmental branching points.
- 4) We contributed to the investigation of the role of Fas signaling in B cell differentiation by using ALPS-Fas as a model system. In particular, Fas provides non-apoptotic signaling which showed a regulatory role in the extrafollicular (EF) versus germinal center (GC) fate decision by modulating CD40-induced mTOR activity. This process is defective in Fas

deficient ALPS patients, explaining the skewed differentiation towards EF response and reduced GC B cells, which contributes to the immune dysregulation present in ALPS.

- 5) We reported a novel mutation in the gene coding for TLR8, which caused an autoimmune and autoinflammatory disorder in monozygotic twins. The mutation resulted in a partial deficiency of the TLR8 protein, leading to imbalance between TLR8 and TLR7 signaling. Specifically, the mutated TLR8 did not efficiently inhibit the activity of TLR7 and also showed cross-reactivity to TLR7 ligands, causing enhanced downstream signaling of TLR7 (NF- κ B and proinflammatory cytokine production).

7. List of publications

Publications supporting the thesis

1. Kalina T*, **Bakardjieva M***, Blom M, Perez-Andres M, Barendregt B, Kanderová V, Bonroy C, Philippé J, Blanco E, Pico-Knijnenburg I, Paping JHMP, Wolska-Kuśnierz B, Pac M, Tkaczyk J, Haerynck F, Akar HH, Formánková R, Freiburger T, Svatoň M, Šedivá A, Arriba-Méndez S, Orfao A, van Dongen JJM, van der Burg M. **EuroFlow Standardized Approach to Diagnostic Immunophenotyping of Severe PID in Newborns and Young Children.** *Front Immunol.* 2020 Mar 19;11:371. doi: 10.3389/fimmu.2020.00371.

*Authors contributed equally

IF = 7.3

I contributed to this study by analysis of all patient and control samples, sample preparation and measurement of healthy control samples, preparation of figures and writing of the draft of the manuscript together with T.Kalina.

2. Blanco E, Pérez-Andrés M, Arriba-Méndez S, Serrano C, Criado I, Del Pino-Molina L, Silva S, Madruga I, **Bakardjieva M**, Martins C, Serra-Caetano A, Romero A, Contreras-Sanfeliciano T, Bonroy C, Sala F, Martín A, Bastida JM, Lorente F, Prieto C, Dávila I, Marcos M, Kalina T, Vlkova M, Chovancova Z, Cordeiro AI, Philippé J, Haerynck F, López-Granados E, Sousa AE, van der Burg M, van Dongen JJM, Orfao A; EuroFlow PID group. **Defects in memory B-cell and plasma cell subsets expressing different immunoglobulin-subclasses in patients with CVID and immunoglobulin subclass deficiencies.** *J Allergy Clin Immunol.* 2019 Sep;144(3):809-824. doi: 10.1016/j.jaci.2019.02.017.

IF = 14.2

I contributed to this study by sample preparation, measurement and basic analysis of healthy control samples.

3. **Bakardjieva M**, Stuchlý M, Pelák M, Wentink M, Glier M, Novák D, Stančíková J, Kužílková D, Janowska D, Rizzi M, van der Burg M, Kalina T. **Tviblindi algorithm identifies branching developmental trajectories of human B cell development.**

Under revision at European Journal of Immunology, January 2024, ID: eji.202451004

Preprint at bioRxiv, DOI: doi.org/10.1101/2024.01.11.575178

I contributed to this study by experimental design, mass cytometry panel antibody validation, experimental setup and sample preparation, analysis of the data, preparation of the figures and writing of the draft of the manuscript. Currently, I am involved in the revision of the manuscript.

4. Staniek J, Kalina T, Andrieux G, Boerries M, Janowska I, Fuentes M, Díez P, **Bakardjieva M**, Stancikova J, Raabe J, Neumann J, Schwenk S, Arpesella L, Stuchly J, Benes V, García Valiente R, Fernández García J, Carsetti R, Piano Mortari E, Catala A, de la Calle O, Sogkas G, Neven B, Rieux-Laucat F, Magerus A, Neth O, Olbrich P, Voll RE, Alsina L, Allende LM, Gonzalez-Granado LI, Böhler C, Thiel J, Venhoff N, Lorenzetti R, Warnatz K, Unger S, Seidl M, Mielenz D, Schneider P, Ehl S, Rensing-Ehl A, Smulski CR, Rizzi M. **Non-apoptotic FAS signaling controls mTOR activation and extrafollicular maturation in human B cells.** *Sci Immunol.* 2024 Jan 12;9(91):eadj5948. doi: 10.1126/sciimmunol.adj5948

IF = 24.8

I contributed to this study by mass cytometry panel antibody preparation and validation, mass cytometry experimental setup and sample preparation and primary analysis of the mass cytometry data.

5. Fejtkova M, Sukova M, Hlozkova K, Skvarova Kramarzova K, Rackova M, Jakubec D, **Bakardjieva M**, Bloomfield M, Klocperk A, Parackova Z, Sediva A, Aluri J, Novakova M, Kalina T, Fronkova E, Hrusak O, Malcova H, Sedlacek P, Liba Z, Kudr M, Stary J, Cooper MA, Svaton M, Kanderova V. **TLR8/TLR7 dysregulation due to a novel TLR8 mutation causes severe autoimmune hemolytic anemia and autoinflammation in identical twins.** *Am J Hematol.* 2022 Mar 1;97(3):338-351. doi: 10.1002/ajh.26452.

IF = 12.8

I contributed to this study by performing *ex vivo* experiments on patient and healthy donor cells.

Other publications

1. Curik N, Polivkova V, Burda P, Koblihova J, Laznicka A, Kalina T, Kanderova V, Brezinova J, Ransdorfova S, Karasova D, Rejllova K, **Bakardjieva M**, Kuzilkova D, Kundrat D, Linhartova J, Klamova H, Salek C, Klener P, Hrusak O, Machova Polakova K. **Somatic Mutations in Oncogenes Are in Chronic Myeloid Leukemia Acquired De Novo via Deregulated Base-Excision Repair and Alternative Non-Homologous End Joining.** *Front Oncol.* 2021 Sep 20;11:744373. doi: 10.3389/fonc.2021.744373

IF = 4.7

8. Literature references

1. BRUTON OC. Agammaglobulinemia. *Pediatrics*. 1952;9(6):722-728.
2. Hitzig WH, Barandun S, Cottier H. The Swiss type of agammaglobulinemia. *Ergeb Inn Med Kinderheilkd*. 1968;27:79-154.
3. Janeway C, Craig J, Davidson M, Downey W, Gitlin D. Hypergammaglobulinemia associated with severe recurrent and chronic nonspecific infection. *AMA Am J Dis Child*. 1954;88(3):388-392.
4. Berendes H, Bridges RA, Good RA. A fatal granulomatosis of childhood: the clinical study of a new syndrome. *Minn Med*. 1957;40(5):309-312.
5. Gatti RA, Meuwissen HJ, Allen HD, Hong R, Good RA. Immunological reconstitution of sex-linked lymphopenic immunological deficiency. *Lancet*. 1968;2(7583):1366-1369. doi:10.1016/s0140-6736(68)92673-1
6. Fudenberg HH, Good RA, Hitzig W, et al. Classification of the primary immune deficiencies: WHO recommendation. *N Engl J Med*. 1970;283(12):656-657. doi:10.1056/NEJM197009172831211
7. National Human Genome Research Institute. <https://www.genome.gov/human-genome-project/timeline>
8. Bousfiha A, Moundir A, Tangye SG, et al. The 2022 Update of IUIS Phenotypical Classification for Human Inborn Errors of Immunity. *J Clin Immunol*. 2022;42(7):1508-1520. doi:10.1007/s10875-022-01352-z
9. Kumar B V., Connors TJ, Farber DL. Human T Cell Development, Localization, and Function throughout Life. *Immunity*. 2018;48(2):202-213. doi:10.1016/j.immuni.2018.01.007
10. Noguchi M, Yi H, Rosenblatt HM, et al. Interleukin-2 receptor γ chain mutation results in X-linked severe combined immunodeficiency in humans. *Cell*. 1993;73(1):147-157.
11. Liu A. MUTATIONS OF Jak-3 GENE IN PATIENTS WITH AUTOSOMAL SEVERE COMBINED IMMUNE DEFICIENCY (SCID). *Pediatrics*. 1996;98(2):350-351. doi:10.1542/peds.98.2.350b
12. Roifman CM, Zhang J, Chitayat D, Sharfe N. A partial deficiency of interleukin-7R alpha is sufficient to abrogate T-cell development and cause severe combined immunodeficiency. *Blood*. 2000;96(8):2803-2807.
13. Giblett EloiseR, Anderson JeanneE, Cohen F, Pollara B, Meuwissen HilaireJ. ADENOSINE-DEAMINASE DEFICIENCY IN TWO PATIENTS WITH SEVERELY IMPAIRED CELLULAR IMMUNITY. *The Lancet*. 1972;300(7786):1067-1069. doi:10.1016/S0140-6736(72)92345-8
14. Cagdas D, Gur Cetinkaya P, Karaatmaca B, et al. ADA Deficiency: Evaluation of the Clinical and Laboratory Features and the Outcome. *J Clin Immunol*. 2018;38(4):484-493. doi:10.1007/s10875-018-0496-9
15. Lagresle-Peyrou C, Six EM, Picard C, et al. Human adenylate kinase 2 deficiency causes a profound hematopoietic defect associated with sensorineural deafness. *Nat Genet*. 2009;41(1):106-111. doi:10.1038/ng.278
16. Gennery A. Recent advances in understanding RAG deficiencies. *F1000Res*. 2019;8. doi:10.12688/f1000research.17056.1
17. Moshous D, Callebaut I, de Chasseval R, et al. Artemis, a novel DNA double-strand break repair/V(D)J recombination protein, is mutated in human severe combined immune deficiency. *Cell*. 2001;105(2):177-186. doi:10.1016/s0092-8674(01)00309-9
18. van der Burg M, van Dongen JJ, van Gent DC. DNA-PKcs deficiency in human: long predicted, finally found. *Curr Opin Allergy Clin Immunol*. 2009;9(6):503-509. doi:10.1097/ACI.0b013e3283327e41

19. Jiang J, Tang W, An Y, et al. Molecular and immunological characterization of DNA ligase IV deficiency. *Clinical Immunology*. 2016;163:75-83. doi:10.1016/j.clim.2015.12.016
20. Fischer A, de Saint Basile G, Le Deist F. CD3 deficiencies. *Curr Opin Allergy Clin Immunol*. 2005;5(6):491-495. doi:10.1097/01.all.0000191886.12645.79
21. Tchilian EZ, Wallace DL, Wells RS, Flower DR, Morgan G, Beverley PCL. A Deletion in the Gene Encoding the CD45 Antigen in a Patient with SCID. *The Journal of Immunology*. 2001;166(2):1308-1313. doi:10.4049/jimmunol.166.2.1308
22. Hanna S, Etzioni A. MHC class I and II deficiencies. *Journal of Allergy and Clinical Immunology*. 2014;134(2):269-275. doi:10.1016/j.jaci.2014.06.001
23. Sharifinejad N, Jamee M, Zaki-Dizaji M, et al. Clinical, Immunological, and Genetic Features in 49 Patients With ZAP-70 Deficiency: A Systematic Review. *Front Immunol*. 2020;11:831. doi:10.3389/fimmu.2020.00831
24. Notarangelo LD. Primary immunodeficiencies. *Journal of Allergy and Clinical Immunology*. 2010;125(2 SUPPL. 2):S182-S194. doi:10.1016/j.jaci.2009.07.053
25. Kreins AY, Davies EG. Replacing defective thymus function. *Curr Opin Allergy Clin Immunol*. 2020;20(6):541-548. doi:10.1097/ACI.0000000000000695
26. Cunningham-Rundles C, Ponda PP. Molecular defects in T- and B-cell primary immunodeficiency diseases. *Nat Rev Immunol*. 2005;5(11):880-892. doi:10.1038/nri1713
27. James KD, Jenkinson WE, Anderson G. T-cell egress from the thymus: Should I stay or should I go? *J Leukoc Biol*. 2018;104(2):275-284. doi:10.1002/JLB.1MR1217-496R
28. Milner JD, Holland SM. The cup runneth over: lessons from the ever-expanding pool of primary immunodeficiency diseases. *Nat Rev Immunol*. 2013;13(9):635-648. doi:10.1038/nri3493
29. Kohler S, Thiel A. Life after the thymus: CD31+ and CD31- human naive CD4+ T-cell subsets. *Blood*. 2009;113(4):769-774. doi:10.1182/blood-2008-02-139154
30. den Braber I, Mugwagwa T, Vriskoop N, et al. Maintenance of Peripheral Naive T Cells Is Sustained by Thymus Output in Mice but Not Humans. *Immunity*. 2012;36(2):288-297. doi:10.1016/j.immuni.2012.02.006
31. Thome JJC, Grinshpun B, Kumar B V., et al. Long-term maintenance of human naive T cells through in situ homeostasis in lymphoid tissue sites. *Sci Immunol*. 2016;1(6). doi:10.1126/sciimmunol.aah6506
32. King C, Ilic A, Koelsch K, Sarvetnick N. Homeostatic expansion of T cells during immune insufficiency generates autoimmunity. *Cell*. 2004;117(2):265-277. doi:10.1016/s0092-8674(04)00335-6
33. Kimmig S, Przybylski GK, Schmidt CA, et al. Two subsets of naive T helper cells with distinct T cell receptor excision circle content in human adult peripheral blood. *J Exp Med*. 2002;195(6):789-794. doi:10.1084/jem.20011756
34. Prager E, Staffler G, Majdic O, et al. Induction of hyporesponsiveness and impaired T lymphocyte activation by the CD31 receptor:ligand pathway in T cells. *J Immunol*. 2001;166(4):2364-2371. doi:10.4049/jimmunol.166.4.2364
35. Hazenberg MD, Borghans JAM, de Boer RJ, Miedema F. Thymic output: A bad TREC record. *Nat Immunol*. 2003;4(2):97-99. doi:10.1038/ni0203-97
36. Cunningham CA, Helm EY, Fink PJ. Reinterpreting recent thymic emigrant function: defective or adaptive? *Curr Opin Immunol*. 2018;51:1-6. doi:10.1016/j.coi.2017.12.006
37. Leite LFB, Máximo TA, Mosca T, Forte WCN. CD40 Ligand Deficiency. *Allergol Immunopathol (Madr)*. 2020;48(4):409-413. doi:10.1016/j.aller.2019.08.005

38. Game DS, Rogers NJ, Lechler RI. Acquisition of HLA-DR and costimulatory molecules by T cells from allogeneic antigen presenting cells. *Am J Transplant*. 2005;5(7):1614-1625. doi:10.1111/j.1600-6143.2005.00916.x
39. Sallusto F, Lenig D, Förster R, Lipp M, Lanzavecchia A. Two subsets of memory T lymphocytes with distinct homing potentials and effector functions. *Nature*. 1999;401(6754):708-712. doi:10.1038/44385
40. Gattinoni L, Lugli E, Ji Y, et al. A human memory T cell subset with stem cell-like properties. *Nat Med*. 2011;17(10):1290-1297. doi:10.1038/nm.2446
41. Larbi A, Fulop T. From “truly naïve” to “exhausted senescent” T cells: When markers predict functionality. *Cytometry Part A*. 2014;85(1):25-35. doi:10.1002/cyto.a.22351
42. Schubert D, Bode C, Kenefeck R, et al. Autosomal dominant immune dysregulation syndrome in humans with CTLA4 mutations. *Nat Med*. 2014;20(12):1410-1416. doi:10.1038/nm.3746
43. Ogishi M, Yang R, Aytekin C, et al. Inherited PD-1 deficiency underlies tuberculosis and autoimmunity in a child. *Nat Med*. 2021;27(9):1646-1654. doi:10.1038/s41591-021-01388-5
44. Bennett CL, Christie J, Ramsdell F, et al. The immune dysregulation, polyendocrinopathy, enteropathy, X-linked syndrome (IPEX) is caused by mutations of FOXP3. *Nat Genet*. 2001;27(1):20-21. doi:10.1038/83713
45. Fisher GH, Rosenberg FJ, Straus SE, et al. Dominant interfering fas gene mutations impair apoptosis in a human autoimmune lymphoproliferative syndrome. *Cell*. 1995;81(6):935-946. doi:10.1016/0092-8674(95)90013-6
46. Nutt SL, Heavey B, Rolink AG, Busslinger M. Commitment to the B-lymphoid lineage depends on the transcription factor Pax5. *Nature*. 1999;401(6753):556-562. doi:10.1038/44076
47. Corcoran AE, Riddell A, Krooshoop D, Venkitaraman AR. Impaired immunoglobulin gene rearrangement in mice lacking the IL-7 receptor. *Nature*. 1998;391(6670):904-907. doi:10.1038/36122
48. Giliani S, Mori L, De Saint Basile G, et al. Interleukin-7 receptor α (IL-7R α) deficiency: cellular and molecular bases. Analysis of clinical, immunological, and molecular features in 16 novel patients. *Immunol Rev*. 2005;203(1):110-126. doi:10.1111/j.0105-2896.2005.00234.x
49. Kaiser FMP, Janowska I, Menafrá R, et al. IL-7 receptor signaling drives human B-cell progenitor differentiation and expansion. *Blood*. 2023;142(13):1113-1130. doi:10.1182/blood.2023019721
50. Qureshi S, Sheikh MDA, Qamar FN. Autosomal Recessive Agammaglobulinemia - first case with a novel TCF3 mutation from Pakistan. *Clin Immunol*. 2019;198:100-101. doi:10.1016/j.clim.2018.07.016
51. LeBien TW, Tedder TF. B lymphocytes: How they develop and function. *Blood*. 2008;112(5):1570-1580. doi:10.1182/blood-2008-02-078071
52. Noordzij JG, De Bruin-Versteeg S, Comans-Bitter WM, et al. Composition of Precursor B-Cell Compartment in Bone Marrow from Patients with X-Linked Agammaglobulinemia Compared with Healthy Children. *Pediatr Res*. 2002;51(2):159-168. doi:10.1203/00006450-200202000-00007
53. Minegishi Y, Rohrer J, Coustan-Smith E, et al. An essential role for BLNK in human B cell development. *Science*. 1999;286(5446):1954-1957. doi:10.1126/science.286.5446.1954
54. Yel L, Minegishi Y, Coustan-Smith E, et al. Mutations in the Mu Heavy-Chain Gene in Patients with Agammaglobulinemia. *New England Journal of Medicine*. 1996;335(20):1486-1493. doi:10.1056/NEJM199611143352003
55. Wang Y, Kanegane H, Sanal O, et al. Novel Igalpha (CD79a) gene mutation in a Turkish patient with B cell-deficient agammaglobulinemia. *Am J Med Genet*. 2002;108(4):333-336. doi:10.1002/ajmg.10296

56. Dobbs AK, Yang T, Farmer D, Kager L, Parolini O, Conley ME. Cutting edge: a hypomorphic mutation in Igbeta (CD79b) in a patient with immunodeficiency and a leaky defect in B cell development. *J Immunol.* 2007;179(4):2055-2059. doi:10.4049/jimmunol.179.4.2055
57. Minegishi Y, Coustan-Smith E, Wang YH, Cooper MD, Campana D, Conley ME. Mutations in the human lambda5/14.1 gene result in B cell deficiency and agammaglobulinemia. *J Exp Med.* 1998;187(1):71-77. doi:10.1084/jem.187.1.71
58. Lucas CL, Chandra A, Nejentsev S, Condliffe AM, Okkenhaug K. PI3K δ and primary immunodeficiencies. *Nat Rev Immunol.* 2016;16(11):702-714. doi:10.1038/nri.2016.93
59. Smith T, Cunningham-Rundles C. Primary B-cell immunodeficiencies. *Hum Immunol.* 2019;80(6):351-362. doi:10.1016/j.humimm.2018.10.015
60. Beck TC, Gomes AC, Cyster JG, Pereira JP. CXCR4 and a cell-extrinsic mechanism control immature B lymphocyte egress from bone marrow. *Journal of Experimental Medicine.* 2014;211(13):2567-2581. doi:10.1084/jem.20140457
61. Balabanian K, Lagane B, Pablos JL, et al. WHIM syndromes with different genetic anomalies are accounted for by impaired CXCR4 desensitization to CXCL12. Published online 2005. doi:10.1182/blood-2004
62. Bemark M. Translating transitions - How to decipher peripheral human B cell development. *J Biomed Res.* 2015;29(4):264-284. doi:10.7555/JBR.29.20150035
63. Cuss AK, Avery DT, Cannons JL, et al. Expansion of Functionally Immature Transitional B Cells Is Associated with Human-Immunodeficient States Characterized by Impaired Humoral Immunity. *The Journal of Immunology.* 2006;176(3):1506-1516. doi:10.4049/jimmunol.176.3.1506
64. Vossenkämper A, Blair PA, Safinia N, et al. A role for gut-associated lymphoid tissue in shaping the human B cell repertoire. *J Exp Med.* 2013;210(9):1665-1674. doi:10.1084/jem.20122465
65. Sims GP, Ettinger R, Shirota Y, Yarboro CH, Illei GG, Lipsky PE. Identification and characterization of circulating human transitional B cells. *Blood.* 2005;105(11):4390-4398. doi:10.1182/blood-2004-11-4284
66. Kurosaki T, Kometani K, Ise W. Memory B cells. *Nat Rev Immunol.* 2015;15(3):149-159. doi:10.1038/nri3802
67. Weill JC, Weller S, Reynaud CA. Human marginal zone B cells. *Annu Rev Immunol.* 2009;27:267-285. doi:10.1146/annurev.immunol.021908.132607
68. Kaji T, Ishige A, Hikida M, et al. Distinct cellular pathways select germline-encoded and somatically mutated antibodies into immunological memory. *J Exp Med.* 2012;209(11):2079-2097. doi:10.1084/jem.20120127
69. Weisel F, Shlomchik M. Memory B Cells of Mice and Humans. *Annu Rev Immunol.* 2017;35(1):255-284. doi:10.1146/annurev-immunol-041015-055531
70. Elsner RA, Shlomchik MJ. Germinal Center and Extrafollicular B Cell Responses in Vaccination, Immunity, and Autoimmunity. *Immunity.* 2020;53(6):1136-1150. doi:10.1016/j.immuni.2020.11.006
71. Cunningham AF, Gaspal F, Serre K, et al. Salmonella induces a switched antibody response without germinal centers that impedes the extracellular spread of infection. *J Immunol.* 2007;178(10):6200-6207. doi:10.4049/jimmunol.178.10.6200
72. Sangster MY, Nguyen PQT, Topham DJ. Role of Memory B Cells in Hemagglutinin-Specific Antibody Production Following Human Influenza A Virus Infection. *Pathogens.* 2019;8(4). doi:10.3390/pathogens8040167
73. Akkaya M, Akkaya B, Kim AS, et al. Toll-like receptor 9 antagonizes antibody affinity maturation. *Nat Immunol.* 2018;19(3):255-266. doi:10.1038/s41590-018-0052-z

74. Soni C, Wong EB, Domeier PP, et al. B Cell–Intrinsic TLR7 Signaling Is Essential for the Development of Spontaneous Germinal Centers. *The Journal of Immunology*. 2014;193(9):4400-4414. doi:10.4049/jimmunol.1401720
75. Elsner RA, Shlomchik MJ. Germinal Center and Extrafollicular B Cell Responses in Vaccination, Immunity, and Autoimmunity. *Immunity*. 2020;53(6):1136-1150. doi:10.1016/j.immuni.2020.11.006
76. Abbott RK, Lee JH, Menis S, et al. Precursor Frequency and Affinity Determine B Cell Competitive Fitness in Germinal Centers, Tested with Germline-Targeting HIV Vaccine Immunogens. *Immunity*. 2018;48(1):133-146.e6. doi:10.1016/j.immuni.2017.11.023
77. Di Niro R, Lee SJ, Vander Heiden JA, et al. Salmonella Infection Drives Promiscuous B Cell Activation Followed by Extrafollicular Affinity Maturation. *Immunity*. 2015;43(1):120-131. doi:10.1016/j.immuni.2015.06.013
78. Weller S, Faili A, Garcia C, et al. CD40-CD40L independent Ig gene hypermutation suggests a second B cell diversification pathway in humans. *Proc Natl Acad Sci U S A*. 2001;98(3):1166-1170. doi:10.1073/pnas.98.3.1166
79. Jenks SA, Cashman KS, Woodruff MC, Lee FEH, Sanz I. Extrafollicular responses in humans and SLE. *Immunol Rev*. 2019;288(1):136-148. doi:10.1111/imr.12741
80. Herlands RA, William J, Hershberg U, Shlomchik MJ. Anti-chromatin antibodies drive in vivo antigen-specific activation and somatic hypermutation of rheumatoid factor B cells at extrafollicular sites. *Eur J Immunol*. 2007;37(12):3339-3351. doi:10.1002/eji.200737752
81. Amirifar P, Yazdani R, Azizi G, et al. Known and potential molecules associated with altered B cell development leading to predominantly antibody deficiencies. *Pediatric Allergy and Immunology*. 2021;32(8):1601-1615. doi:10.1111/pai.13589
82. Kostmann R. Hereditär reticulos: en ny systemsjukdom (Hereditary reticulosis - a new systemic disease). *Lakartidningen*. 1950;47:2861–2868.
83. Notarangelo LD, Bacchetta R, Casanova JL, Su HC. Human inborn errors of immunity: An expanding universe. *Sci Immunol*. 2020;5(49). doi:10.1126/sciimmunol.abb1662
84. Notarangelo LD, Bacchetta R, Casanova JL, Su HC. Human inborn errors of immunity: An expanding universe. *Sci Immunol*. 2020;5(49). doi:10.1126/sciimmunol.abb1662
85. Abolhassani H, Azizi G, Sharifi L, et al. Global systematic review of primary immunodeficiency registries. *Expert Rev Clin Immunol*. 2020;16(7):717-732. doi:10.1080/1744666X.2020.1801422
86. Kwan A, Abraham RS, Currier R, et al. Newborn screening for severe combined immunodeficiency in 11 screening programs in the United States. *JAMA*. 2014;312(7):729-738. doi:10.1001/jama.2014.9132
87. Argudo-Ramírez A, Martín-Nalda A, Marín-Soria JL, et al. First Universal Newborn Screening Program for Severe Combined Immunodeficiency in Europe. Two-Years' Experience in Catalonia (Spain). *Front Immunol*. 2019;10:2406. doi:10.3389/fimmu.2019.02406
88. Pannicke U, Hönig M, Hess I, et al. Reticular dysgenesis (aleukocytosis) is caused by mutations in the gene encoding mitochondrial adenylate kinase 2. *Nat Genet*. 2009;41(1):101-105. doi:10.1038/ng.265
89. Woodbine L, Neal JA, Sasi NK, et al. PRKDC mutations in a SCID patient with profound neurological abnormalities. *Journal of Clinical Investigation*. 2013;123(7):2969-2980. doi:10.1172/JCI67349
90. Dutrannoy V, Demuth I, Baumann U, et al. Clinical variability and novel mutations in the NHEJ1 gene in patients with a Nijmegen breakage syndrome-like phenotype. *Hum Mutat*. 2010;31(9):1059-1068. doi:10.1002/humu.21315

91. Bradford KL, Moretti FA, Carbonaro-Sarracino DA, Gaspar HB, Kohn DB. Adenosine Deaminase (ADA)-Deficient Severe Combined Immune Deficiency (SCID): Molecular Pathogenesis and Clinical Manifestations. *J Clin Immunol.* 2017;37(7):626-637. doi:10.1007/s10875-017-0433-3
92. Markert ML. Purine nucleoside phosphorylase deficiency. *Immunodeficiency Rev.* 1991;3(1):45-81.
93. Noguchi M, Yi H, Rosenblatt HM, et al. Interleukin-2 receptor gamma chain mutation results in X-linked severe combined immunodeficiency in humans. *Cell.* 1993;73(1):147-157. doi:10.1016/0092-8674(93)90167-o
94. Lin JX, Leonard WJ. The Common Cytokine Receptor γ Chain Family of Cytokines. *Cold Spring Harb Perspect Biol.* 2018;10(9). doi:10.1101/cshperspect.a028449
95. Macchi P, Villa A, Giliani S, et al. Mutations of Jak-3 gene in patients with autosomal severe combined immune deficiency (SCID). *Nature.* 1995;377(6544):65-68. doi:10.1038/377065a0
96. Roifman CM, Zhang J, Chitayat D, Sharfe N. A partial deficiency of interleukin-7R alpha is sufficient to abrogate T-cell development and cause severe combined immunodeficiency. *Blood.* 2000;96(8):2803-2807.
97. Schuetz C, Pannicke U, Jacobsen EM, et al. Lesson from hypomorphic recombination-activating gene (RAG) mutations: Why asymptomatic siblings should also be tested. *J Allergy Clin Immunol.* 2014;133(4):1211-1215. doi:10.1016/j.jaci.2013.10.021
98. Cirillo E, Cancrini C, Azzari C, et al. Clinical, Immunological, and Molecular Features of Typical and Atypical Severe Combined Immunodeficiency: Report of the Italian Primary Immunodeficiency Network. *Front Immunol.* 2019;10:1908. doi:10.3389/fimmu.2019.01908
99. Speckmann C, Doerken S, Aiuti A, et al. A prospective study on the natural history of patients with profound combined immunodeficiency: An interim analysis. *Journal of Allergy and Clinical Immunology.* 2017;139(4):1302-1310.e4. doi:10.1016/j.jaci.2016.07.040
100. Stray-Pedersen A, Jouanguy E, Crequer A, et al. Compound heterozygous CORO1A mutations in siblings with a mucocutaneous-immunodeficiency syndrome of epidermodysplasia verruciformis-HPV, molluscum contagiosum and granulomatous tuberculoid leprosy. *J Clin Immunol.* 2014;34(7):871-890. doi:10.1007/s10875-014-0074-8
101. Rowe JH, Delmonte OM, Keles S, et al. Patients with CD3G mutations reveal a role for human CD3g in Treg diversity and suppressive function. *Blood.* 2018;131(21):2335-2344. doi:10.1182/blood-2018-02-835561
102. Ghosh S, Bienemann K, Boztug K, Borkhardt A. Interleukin-2-inducible T-cell kinase (ITK) deficiency - clinical and molecular aspects. *J Clin Immunol.* 2014;34(8):892-899. doi:10.1007/s10875-014-0110-8
103. Dang TS, Willet JDP, Griffin HR, et al. Defective Leukocyte Adhesion and Chemotaxis Contributes to Combined Immunodeficiency in Humans with Autosomal Recessive MST1 Deficiency. *J Clin Immunol.* 2016;36(2):117-122. doi:10.1007/s10875-016-0232-2
104. Hauck F, Randriamampita C, Martin E, et al. Primary T-cell immunodeficiency with immunodysregulation caused by autosomal recessive LCK deficiency. *J Allergy Clin Immunol.* 2012;130(5):1144-1152.e11. doi:10.1016/j.jaci.2012.07.029
105. Biggs CM, Keles S, Chatila TA. DOCK8 deficiency: Insights into pathophysiology, clinical features and management. *Clin Immunol.* 2017;181:75-82. doi:10.1016/j.clim.2017.06.003
106. Moens L, Gouwy M, Bosch B, et al. Human DOCK2 Deficiency: Report of a Novel Mutation and Evidence for Neutrophil Dysfunction. *J Clin Immunol.* 2019;39(3):298-308. doi:10.1007/s10875-019-00603-w

107. Hanna S, Etzioni A. MHC class I and II deficiencies. *J Allergy Clin Immunol.* 2014;134(2):269-275. doi:10.1016/j.jaci.2014.06.001
108. Massaad MJ, Ramesh N, Geha RS. Wiskott-Aldrich syndrome: a comprehensive review. *Ann N Y Acad Sci.* 2013;1285:26-43. doi:10.1111/nyas.12049
109. Rothblum-Oviatt C, Wright J, Lefton-Greif MA, McGrath-Morrow SA, Crawford TO, Lederman HM. Ataxia telangiectasia: a review. *Orphanet J Rare Dis.* 2016;11(1):159. doi:10.1186/s13023-016-0543-7
110. Gámez-Díaz L, Grimbacher B. Immune checkpoint deficiencies and autoimmune lymphoproliferative syndromes. *Biomed J.* 2021;44(4):400-411. doi:10.1016/j.bj.2021.04.005
111. Hafezi N, Zaki-Dizaji M, Nirouei M, et al. Clinical, immunological, and genetic features in 780 patients with autoimmune lymphoproliferative syndrome (ALPS) and ALPS-like diseases: A systematic review. *Pediatr Allergy Immunol.* 2021;32(7):1519-1532. doi:10.1111/pai.13535
112. Park JH, Lee KH, Jeon B, et al. Immune dysregulation, polyendocrinopathy, enteropathy, X-linked (IPEX) syndrome: A systematic review. *Autoimmun Rev.* 2020;19(6):102526. doi:10.1016/j.autrev.2020.102526
113. Durandy A, Kracker S, Fischer A. Primary antibody deficiencies. *Nat Rev Immunol.* 2013;13(7):519-533. doi:10.1038/nri3466
114. Cardenas-Morales M, Hernandez-Trujillo VP. Agammaglobulinemia: from X-linked to Autosomal Forms of Disease. *Clin Rev Allergy Immunol.* 2022;63(1):22-35. doi:10.1007/s12016-021-08870-5
115. Yazdani R, Fekrvand S, Shahkarami S, et al. The hyper IgM syndromes: Epidemiology, pathogenesis, clinical manifestations, diagnosis and management. *Clinical Immunology.* 2019;198:19-30. doi:10.1016/j.clim.2018.11.007
116. Ahn S, Cunningham-Rundles C. Role of B cells in common variable immune deficiency. *Expert Rev Clin Immunol.* 2009;5(5):557-564. doi:10.1586/eci.09.43
117. Castigli E, Wilson SA, Garibyan L, et al. TACI is mutant in common variable immunodeficiency and IgA deficiency. *Nat Genet.* 2005;37(8):829-834. doi:10.1038/ng1601
118. Fathi N, Mojtahedi H, Nasiri M, et al. How do nuclear factor kappa B (NF- κ B)1 and NF- κ B2 defects lead to the incidence of clinical and immunological manifestations of inborn errors of immunity? *Expert Rev Clin Immunol.* 2023;19(3):329-339. doi:10.1080/1744666X.2023.2174105
119. Yel L. Selective IgA Deficiency. *J Clin Immunol.* 2010;30(1):10-16. doi:10.1007/s10875-009-9357-x
120. Sala P, Colatutto A, Fabbro D, et al. Immunoglobulin K light chain deficiency: A rare, but probably underestimated, humoral immune defect. *Eur J Med Genet.* 2016;59(4):219-222. doi:10.1016/j.ejmg.2016.02.003
121. Bucciol G, Moens L, Bosch B, et al. Lessons learned from the study of human inborn errors of innate immunity. *J Allergy Clin Immunol.* 2019;143(2):507-527. doi:10.1016/j.jaci.2018.07.013
122. Yu L, Wang L, Chen S. Endogenous toll-like receptor ligands and their biological significance. *J Cell Mol Med.* 2010;14(11):2592-2603. doi:10.1111/j.1582-4934.2010.01127.x
123. Kawasaki T, Kawai T. Toll-Like Receptor Signaling Pathways. *Front Immunol.* 2014;5. doi:10.3389/fimmu.2014.00461
124. ESID Registry - Working definitions for clinical diagnosis of PID. *ESID Registry - Working definitions for clinical diagnosis of PID.* 2019;(November):1-205.

125. de Vries E, Alvarez Cardona A, Abdul Latiff AH, et al. Patient-centred screening for primary immunodeficiency, a multi-stage diagnostic protocol designed for non-immunologists: 2011 update. *Clin Exp Immunol*. 2012;167(1):108-119. doi:10.1111/j.1365-2249.2011.04461.x
126. Heimall J, Logan BR, Cowan MJ, et al. Immune reconstitution and survival of 100 SCID patients post-hematopoietic cell transplant: a PIDTC natural history study. *Blood*. 2017;130(25):2718-2727. doi:10.1182/blood-2017-05-781849
127. Slade CA, Bosco JJ, Binh Giang T, et al. Delayed Diagnosis and Complications of Predominantly Antibody Deficiencies in a Cohort of Australian Adults. *Front Immunol*. 2018;9. doi:10.3389/fimmu.2018.00694
128. van Zelm MC, van der Burg M, Langerak AW, van Dongen JJM. PID Comes Full Circle: Applications of V(D)J Recombination Excision Circles in Research, Diagnostics and Newborn Screening of Primary Immunodeficiency Disorders. *Front Immunol*. 2011;2. doi:10.3389/fimmu.2011.00012
129. Myers LA, Patel DD, Puck JM, Buckley RH. Hematopoietic stem cell transplantation for severe combined immunodeficiency in the neonatal period leads to superior thymic output and improved survival. *Blood*. 2002;99(3):872-878. doi:10.1182/blood.v99.3.872
130. Baker MW, Grossman WJ, Laessig RH, et al. Development of a routine newborn screening protocol for severe combined immunodeficiency. *J Allergy Clin Immunol*. 2009;124(3):522-527. doi:10.1016/j.jaci.2009.04.007
131. Nový program časného záchytu onemocnění od roku 2022: screening spinální svalové atrofie (SMA) a kombinované těžké imunodeficiencie (SCID). <https://nsc.uzis.cz/res/file/newsletter/nsc-zpravodaj-13.pdf>.
132. Dorsey MJ, Puck JM. Newborn Screening for Severe Combined Immunodeficiency in the United States. *Immunol Allergy Clin North Am*. 2019;39(1):1-11. doi:10.1016/j.iac.2018.08.002
133. Bucciol G, Meyts I. Recent advances in primary immunodeficiency: From molecular diagnosis to treatment. *F1000Res*. 2020;9. doi:10.12688/f1000research.21553.1
134. Bendall SC, Nolan GP, Roederer M, Chattopadhyay PK. A deep profiler's guide to cytometry. *Trends Immunol*. 2012;33(7):323-332. doi:10.1016/j.it.2012.02.010
135. Shearer WT, Ph D, Dunn E, et al. Scid , and Omenn Syndrome : the Primary Immune. 2015;133(4):1092-1098. doi:10.1016/j.jaci.2013.09.044.ESTABLISHING
136. Müller SM, Ege M, Pottharst A, Schulz AS, Schwarz K, Friedrich W. Transplacentally acquired maternal T lymphocytes in severe combined immunodeficiency: a study of 121 patients. *Blood*. 2001;98(6):1847-1851. doi:10.1182/blood.V98.6.1847
137. Van Dongen JJM, Van Der Burg M, Kalina T, et al. EuroFlow-based flowcytometric diagnostic screening and classification of primary immunodeficiencies of the lymphoid system. *Front Immunol*. 2019;10(JUN):1-21. doi:10.3389/fimmu.2019.01271
138. Kanegane H, Hoshino A, Okano T, et al. Flow cytometry-based diagnosis of primary immunodeficiency diseases. *Allergology International*. 2018;67(1):43-54. doi:10.1016/j.alit.2017.06.003
139. Takashima T, Okamura M, Yeh T wen, et al. Multicolor Flow Cytometry for the Diagnosis of Primary Immunodeficiency Diseases. *J Clin Immunol*. 2017;37(5):486-495. doi:10.1007/s10875-017-0405-7
140. Kalina T, Flores-Montero J, van der Velden VHJ, et al. EuroFlow standardization of flow cytometer instrument settings and immunophenotyping protocols. *Leukemia*. 2012;26(9):1986-2010. doi:10.1038/leu.2012.122
141. Van Dongen JJM, Van Der Burg M, Kalina T, et al. EuroFlow-based flowcytometric diagnostic screening and classification of primary immunodeficiencies of the lymphoid system. *Front Immunol*. 2019;10(JUN):1-21. doi:10.3389/fimmu.2019.01271

142. van der Burg M, Kalina T, Perez-Andres M, et al. The EuroFlow PID Orientation Tube for Flow Cytometric Diagnostic Screening of Primary Immunodeficiencies of the Lymphoid System. *Front Immunol.* 2019;10. doi:10.3389/fimmu.2019.00246
143. Kanegane H, Hoshino A, Okano T, et al. Flow cytometry-based diagnosis of primary immunodeficiency diseases. *Allergology International.* 2018;67(1):43-54. doi:10.1016/j.alit.2017.06.003
144. Deyà-Martínez A, Rivière JG, Roxo-Junior P, et al. Impact of JAK Inhibitors in Pediatric Patients with STAT1 Gain of Function (GOF) Mutations-10 Children and Review of the Literature. *J Clin Immunol.* 2022;42(5):1071-1082. doi:10.1007/s10875-022-01257-x
145. Iyer A, Hamers AAJ, Pillai AB. CyTOF® for the Masses. *Front Immunol.* 2022;13. doi:10.3389/fimmu.2022.815828
146. Newell EW, Sigal N, Bendall SC, Nolan GP, Davis MM. Cytometry by Time-of-Flight Shows Combinatorial Cytokine Expression and Virus-Specific Cell Niches within a Continuum of CD8+ T Cell Phenotypes. *Immunity.* 2012;36(1):142-152. doi:10.1016/j.immuni.2012.01.002
147. Amir E ad D, Davis KL, Tadmor MD, et al. viSNE enables visualization of high dimensional single-cell data and reveals phenotypic heterogeneity of leukemia. *Nat Biotechnol.* 2013;31(6):545-552. doi:10.1038/nbt.2594
148. McInnes L, Healy J, Saul N, Großberger L. UMAP: Uniform Manifold Approximation and Projection. *J Open Source Softw.* 2018;3(29):861. doi:10.21105/JOSS.00861
149. Amodio M, van Dijk D, Srinivasan K, et al. Exploring single-cell data with deep multitasking neural networks. *Nat Methods.* 2019;16(11):1139-1145. doi:10.1038/s41592-019-0576-7
150. Koladiya A, Davis KL. Advances in Clinical Mass Cytometry. *Clin Lab Med.* 2023;43(3):507-519. doi:10.1016/j.cll.2023.05.004
151. Castagnoli R, Delmonte OM, Calzoni E, Notarangelo LD. Hematopoietic Stem Cell Transplantation in Primary Immunodeficiency Diseases: Current Status and Future Perspectives. *Front Pediatr.* 2019;7. doi:10.3389/fped.2019.00295
152. Aiuti A, Slavin S, Aker M, et al. Correction of ADA-SCID by stem cell gene therapy combined with nonmyeloablative conditioning. *Science.* 2002;296(5577):2410-2413. doi:10.1126/science.1070104
153. Cavazzana-Calvo M, Hacein-Bey S, de Saint Basile G, et al. Gene therapy of human severe combined immunodeficiency (SCID)-X1 disease. *Science.* 2000;288(5466):669-672. doi:10.1126/science.288.5466.669
154. Braun CJ, Boztug K, Paruzynski A, et al. Gene therapy for Wiskott-Aldrich syndrome--long-term efficacy and genotoxicity. *Sci Transl Med.* 2014;6(227):227ra33. doi:10.1126/scitranslmed.3007280
155. Garcia-Perez L, van Eggermond M, van Roon L, et al. Successful Preclinical Development of Gene Therapy for Recombinase-Activating Gene-1-Deficient SCID. *Mol Ther Methods Clin Dev.* 2020;17:666-682. doi:10.1016/j.omtm.2020.03.016
156. Fischer A, Hacein-Bey-Abina S. Gene therapy for severe combined immunodeficiencies and beyond. *J Exp Med.* 2020;217(2). doi:10.1084/jem.20190607
157. Bauhofer A, Schimo S, Klausmann M. Benefits of immunoglobulin substitution in primary and secondary immunodeficiencies: Interim analysis of a prospective, long-term non-interventional study. *Int J Clin Pharmacol Ther.* 2021;59(6):417-427. doi:10.5414/CP203952
158. Argudo-Ramírez A, Martín-Nalda A, González de Aledo-Castillo JM, et al. Newborn screening for scid. Experience in Spain (Catalonia). *Int J Neonatal Screen.* 2021;7(3). doi:10.3390/ijns7030046

159. Argudo-Ramírez A, Martín-Nalda A, Marín-Soria JL, et al. First universal newborn screening program for severe combined immunodeficiency in europe. Two-years' experience in catalonia (spain). *Front Immunol.* 2019;10(OCT):1-10. doi:10.3389/fimmu.2019.02406
160. ESID Registry – Working Definitions for Clinical Diagnosis of PID. https://esid.org/content/download/17141/463543/file/ESID_Clin_Crit_omim_orpha_hpo_11_2019fin.pdf
161. Janda A, Schwarz K, van der Burg M, et al. Disturbed B-lymphocyte selection in autoimmune lymphoproliferative syndrome. *Blood.* 2016;127(18):2193-2202. doi:10.1182/blood-2015-04-642488
162. Hao Z, Duncan GS, Seagal J, et al. Fas Receptor Expression in Germinal-Center B Cells Is Essential for T and B Lymphocyte Homeostasis. *Immunity.* 2008;29(4):615-627. doi:10.1016/j.immuni.2008.07.016
163. Rensing-Ehl A, Warnatz K, Fuchs S, et al. Clinical and immunological overlap between autoimmune lymphoproliferative syndrome and common variable immunodeficiency. *Clinical Immunology.* 2010;137(3):357-365. doi:10.1016/j.clim.2010.08.008
164. Bucciol G, Moens L, Bosch B, et al. Lessons learned from the study of human inborn errors of innate immunity. *J Allergy Clin Immunol.* 2019;143(2):507-527. doi:10.1016/j.jaci.2018.07.013
165. Lo YM, Lo ES, Watson N, et al. Two-way cell traffic between mother and fetus: biologic and clinical implications. *Blood.* 1996;88(11):4390-4395.
166. Zhang J, Quintal L, Atkinson A, Williams B, Grunebaum E, Roifman CM. Novel RAG1 Mutation in a Case of Severe Combined Immunodeficiency. *Pediatrics.* 2005;116(3):e445-e449. doi:10.1542/peds.2005-0369
167. Hazenberg MD, Borghans JAM, de Boer RJ, Miedema F. Thymic output: A bad TREC record. *Nat Immunol.* 2003;4(2):97-99. doi:10.1038/ni0203-97
168. Adams SP, Kricke S, Ralph E, et al. A comparison of TRECs and flow cytometry for naïve T cell quantification.
169. Kalina T, Flores-Montero J, van der Velden VHJ, et al. EuroFlow standardization of flow cytometer instrument settings and immunophenotyping protocols. *Leukemia.* 2012;26(9):1986-2010. doi:10.1038/leu.2012.122
170. Schlickeiser S, Streitz M, Sawitzki B. Standardized Multi-Color Flow Cytometry and Computational Biomarker Discovery. In: ; 2016:225-238. doi:10.1007/978-1-4939-3139-2_15
171. Maecker HT, McCoy JP, Nussenblatt R. Standardizing immunophenotyping for the Human Immunology Project. *Nat Rev Immunol.* 2012;12(3):191-200. doi:10.1038/nri3158
172. Streitz M, Miloud T, Kapinsky M, et al. Standardization of whole blood immune phenotype monitoring for clinical trials: panels and methods from the ONE study. *Transplant Res.* 2013;2(1):17. doi:10.1186/2047-1440-2-17
173. Durandy A, Kracker S, Fischer A. Primary antibody deficiencies. *Nat Rev Immunol.* 2013;13(7):519-533. doi:10.1038/nri3466
174. ESID Registry – Working Definitions for Clinical Diagnosis of PID. https://esid.org/content/download/17141/463543/file/ESID_Clin_Crit_omim_orpha_hpo_11_2019fin.pdf
175. Al Kindi M, Mundy J, Sullivan T, et al. Utility of peripheral blood B cell subsets analysis in common variable immunodeficiency. *Clin Exp Immunol.* 2012;167(2):275-281. doi:10.1111/j.1365-2249.2011.04507.x
176. Warnatz K, Denz A, Dräger R, et al. Severe deficiency of switched memory B cells (CD27+IgM-IgD-) in subgroups of patients with common variable immunodeficiency: a new approach to classify a heterogeneous disease. *Blood.* 2002;99(5):1544-1551. doi:10.1182/blood.V99.5.1544
177. Wehr C, Kivioja T, Schmitt C, et al. The EUROclass trial: defining subgroups in common variable immunodeficiency. *Blood.* 2008;111(1):77-85. doi:10.1182/blood-2007-06-091744

178. Piqueras B, Lavenu-Bombléd C, Galicier L, et al. Common variable immunodeficiency patient classification based on impaired B cell memory differentiation correlates with clinical aspects. *J Clin Immunol.* 2003;23(5):385-400. doi:10.1023/A:1025373601374
179. Kalina T. Reproducibility of Flow Cytometry Through Standardization: Opportunities and Challenges. *Cytometry Part A.* 2020;97(2):137-147. doi:10.1002/cyto.a.23901
180. Park LM, Lannigan J, Jaimes MC. OMIP-069: Forty-Color Full Spectrum Flow Cytometry Panel for Deep Immunophenotyping of Major Cell Subsets in Human Peripheral Blood. *Cytometry A.* 2020;97(10):1044-1051. doi:10.1002/cyto.a.24213
181. Iyer A, Hamers AAJ, Pillai AB. CyTOF® for the Masses. *Front Immunol.* 2022;13. doi:10.3389/fimmu.2022.815828
182. McInnes L, Healy J, Saul N, Großberger L. UMAP: Uniform Manifold Approximation and Projection. *J Open Source Softw.* 2018;3(29):861. doi:10.21105/JOSS.00861
183. Amir EAD, Davis KL, Tadmor MD, et al. ViSNE enables visualization of high dimensional single-cell data and reveals phenotypic heterogeneity of leukemia. *Nat Biotechnol.* 2013;31(6):545-552. doi:10.1038/nbt.2594
184. Kratochvíl M, Koladiya A, Vondrášek J. Generalized EmbedSOM on quadtree-structured self-organizing maps. *F1000Res.* 2020;8:2120. doi:10.12688/f1000research.21642.2
185. Guldberg SM, Okholm TLH, McCarthy EE, Spitzer MH. Computational Methods for Single-Cell Proteomics. *Annu Rev Biomed Data Sci.* 2023;6:47-71. doi:10.1146/annurev-biodatasci-020422-050255
186. Bendall SC, Davis KL, Amir EAD, et al. Single-cell trajectory detection uncovers progression and regulatory coordination in human B cell development. *Cell.* 2014;157(3):714-725. doi:10.1016/j.cell.2014.04.005
187. Qiu X, Mao Q, Tang Y, et al. Reversed graph embedding resolves complex single-cell trajectories. *Nat Methods.* 2017;14(10):979-982. doi:10.1038/nmeth.4402
188. Powell JD, Pollizzi KN, Heikamp EB, Horton MR. Regulation of immune responses by mTOR. *Annu Rev Immunol.* 2012;30:39-68. doi:10.1146/annurev-immunol-020711-075024
189. Klemann C, Esquivel M, Magerus-Chatinet A, et al. Evolution of disease activity and biomarkers on and off rapamycin in 28 patients with autoimmune lymphoproliferative syndrome. *Haematologica.* 2017;102(2):e52-e56. doi:10.3324/haematol.2016.153411
190. Demaria O, Pagni PP, Traub S, et al. TLR8 deficiency leads to autoimmunity in mice. *J Clin Invest.* 2010;120(10):3651-3662. doi:10.1172/JCI42081
191. Fillatreau S, Manfroi B, Dörner T. Toll-like receptor signalling in B cells during systemic lupus erythematosus. *Nat Rev Rheumatol.* 2021;17(2):98-108. doi:10.1038/s41584-020-00544-4
192. Bousfiha A, Moundir A, Tangye SG, et al. The 2022 Update of IUIS Phenotypical Classification for Human Inborn Errors of Immunity. *J Clin Immunol.* 2022;42(7):1508-1520. doi:10.1007/s10875-022-01352-z
193. Gies V, Bekaddour N, Dieudonné Y, et al. Beyond Anti-viral Effects of Chloroquine/Hydroxychloroquine. *Front Immunol.* 2020;11:1409. doi:10.3389/fimmu.2020.01409

9. Appendix - attached manuscripts

- 9.1. EuroFlow Standardized Approach to Diagnostic Immunophenotyping of Severe PID in Newborns and Young Children
- 9.2. Defects in memory B-cell and plasma cell subsets expressing different immunoglobulin-subclasses in patients with CVID and immunoglobulin subclass deficiencies
- 9.3. Tvislindi algorithm identifies branching developmental trajectories of human B cell development
- 9.4. Non-apoptotic FAS signaling controls mTOR activation and extrafollicular maturation in human B cells
- 9.5. TLR8/TLR7 dysregulation due to a novel TLR8 mutation causes severe autoimmune hemolytic anemia and autoinflammation in identical twins

9.1. EuroFlow Standardized Approach to Diagnostic Immunophenotyping of Severe PID in Newborns and Young Children



EuroFlow Standardized Approach to Diagnostic Immunophenotyping of Severe PID in Newborns and Young Children

Tomas Kalina^{1†}, Marina Bakardjieva^{1†}, Maartje Blom², Martin Perez-Andres³, Barbara Barendregt⁴, Veronika Kanderová¹, Carolien Bonroy^{5,6}, Jan Philippé^{5,6}, Elena Blanco³, Ingrid Pico-Knijnenburg^{2,4}, Jitse H. M. P. Paping², Beata Wolska-Kuśnierz⁷, Malgorzata Pac⁷, Jakub Tkaczyk⁸, Filomeen Haerynck⁹, Himmet Haluk Akar¹⁰, Renata Formánková¹, Tomáš Freiberger^{11,12}, Michael Svatoň¹, Anna Šedivá¹³, Sonia Arriba-Méndez¹⁴, Alberto Orfao³, Jacques J. M. van Dongen¹⁵ and Mirjam van der Burg^{2,4*}

OPEN ACCESS

Edited by:
Antonio Condino-Neto,
University of São Paulo, Brazil

Reviewed by:
Tomohiro Morio,
Tokyo Medical and Dental
University, Japan
Amos J. Simon,
Sheba Medical Center, Israel

*Correspondence:
Mirjam van der Burg
m.van_der_burg@lumc.nl

†These authors have contributed
equally to this work

Specialty section:
This article was submitted to
Primary Immunodeficiencies,
a section of the journal
Frontiers in Immunology

Received: 23 December 2019

Accepted: 17 February 2020

Published: 19 March 2020

Citation:

Kalina T, Bakardjieva M, Blom M, Perez-Andres M, Barendregt B, Kanderová V, Bonroy C, Philippé J, Blanco E, Pico-Knijnenburg I, Paping JHMP, Wolska-Kuśnierz B, Pac M, Tkaczyk J, Haerynck F, Akar HH, Formánková R, Freiberger T, Svatoň M, Šedivá A, Arriba-Méndez S, Orfao A, van Dongen JJM and van der Burg M (2020) EuroFlow Standardized Approach to Diagnostic Immunophenotyping of Severe PID in Newborns and Young Children. *Front. Immunol.* 11:371. doi: 10.3389/fimmu.2020.00371

¹ Department of Paediatric Haematology and Oncology, Second Faculty of Medicine, Charles University and University Hospital Motol, Prague, Czechia, ² Laboratory for Immunology, Department of Pediatrics, Leiden University Medical Center (LUMC), Leiden, Netherlands, ³ Department of Medicine-Serv. Cytometry, Cancer Research Center (IBMCC-CSIC/USAL), University of Salamanca, Salamanca, Spain, ⁴ Department of Immunology, Erasmus MC, University Medical Center Rotterdam, Rotterdam, Netherlands, ⁵ Department of Diagnostic Sciences, Ghent University, Ghent, Belgium, ⁶ Department of Laboratory Medicine, Ghent University Hospital, Ghent, Belgium, ⁷ Department of Immunology, Children's Memorial Health Institute, Warsaw, Poland, ⁸ Department of Pediatrics, Second Faculty of Medicine, Charles University and University Hospital Motol, Prague, Czechia, ⁹ PID Research Lab, Department of Pediatric Pulmonology and Immunology, Ghent University Hospital, Ghent, Belgium, ¹⁰ Department of Pediatric Immunology and Allergy, Kanuni Sultan Süleyman Training and Research Hospital, Istanbul Health Sciences University, Istanbul, Turkey, ¹¹ Centre for Cardiovascular Surgery and Transplantation, Brno, Czechia, ¹² Medical Faculty, Masaryk University, Brno, Czechia, ¹³ Department of Immunology, University Hospital Motol, Prague, Czechia, ¹⁴ Servicio de Pediatría, Hospital Universitario de Salamanca, Salamanca, Spain, ¹⁵ Department of Immunohematology and Blood Transfusion (IHB), Leiden University Medical Center (LUMC), Leiden, Netherlands

The EuroFlow PID consortium developed a set of flow cytometry tests for evaluation of patients with suspicion of primary immunodeficiency (PID). In this technical report we evaluate the performance of the SCID-RTE tube that explores the presence of recent thymic emigrants (RTE) together with T-cell activation status and maturation stages and discuss its applicability in the context of the broader EuroFlow PID flow cytometry testing algorithm for diagnostic orientation of PID of the lymphoid system. We have analyzed peripheral blood cells of 26 patients diagnosed between birth and 2 years of age with a genetically defined primary immunodeficiency disorder: 15 severe combined immunodeficiency (SCID) patients had disease-causing mutations in *RAG1* or *RAG2* ($n = 4$, two of them presented with Omenn syndrome), *IL2RG* ($n = 4$, one of them with confirmed maternal engraftment), *NHEJ1* ($n = 1$), *CD3E* ($n = 1$), *ADA* ($n = 1$), *JAK3* ($n = 3$, two of them with maternal engraftment) and *DCLRE1C* ($n = 1$) and 11 other PID patients had diverse molecular defects [*ZAP70* ($n = 1$), *WAS* ($n = 2$), *PNP* ($n = 1$), *FOXP3* ($n = 1$), *del22q11.2* (DiGeorge) ($n = 4$), *CDC42* ($n = 1$) and *FAS* ($n = 1$)]. In addition, 44 healthy controls in the same age group were analyzed using the SCID-RTE tube in four EuroFlow laboratories using a standardized 8-color approach. RTE were defined as CD62L+CD45RO-HLA-DR-CD31+ and the activation status was assessed by the

expression of HLA-DR⁺. Naïve CD8⁺ T-lymphocytes and naïve CD4⁺ T-lymphocytes were defined as CD62L⁺CD45RO⁻HLA-DR⁻. With the SCID-RTE tube, we identified patients with PID by low levels or absence of RTE in comparison to controls as well as low levels of naïve CD4⁺ and naïve CD8⁺ lymphocytes. These parameters yielded 100% sensitivity for SCID. All SCID patients had absence of RTE, including the patients with confirmed maternal engraftment or oligoclonally expanded T-cells characteristic for Omenn syndrome. Another dominant finding was the increased numbers of activated CD4⁺HLA-DR⁺ and CD8⁺HLA-DR⁺ lymphocytes. Therefore, the EuroFlow SCID-RTE tube together with the previously published PIDOT tube form a sensitive and complete cytometric diagnostic test suitable for patients suspected of severe PID (SCID or CID) as well as for children identified via newborn screening programs for SCID with low or absent T-cell receptor excision circles (TRECs).

Keywords: flow cytometric immunophenotyping, primary immunodeficiencies (PID), EuroFlow, standardization, severe combined immune deficiency (SCID), diagnosis

INTRODUCTION

Severe combined immunodeficiency (SCID) and combined immunodeficiency (CID) are two of the most severe forms of inherited disorders of the immune system (1, 2) with an incidence of 1:35,000–50,000 newborns. Patients are usually born asymptomatic, but they develop severe (opportunistic) infections, failure to thrive within the first months of life and generally die before the age of 1 year, unless they receive adequate and curative treatment. This includes hematopoietic stem cell transplantation (HSCT). For some genetic forms of SCID gene therapy is available (3, 4). HSCT is indicated immediately after birth, since patients transplanted before the age of 3.5 months or patients without infections have a superior prognosis as compared to those transplanted later or when infectious complications have accumulated (5, 6). In contrast, patients with CID usually do not have complete absence of T-lymphocytes as typically seen in SCID, but they frequently show profound impairment of T-cell immunity leading to severe infections, autoimmunity, and malignancies. Thus, the indication of HSCT for CID is less clear as it is less evident whether the T-cell deficiency is sufficiently severe to justify the risks of HSCT (7).

T-cells are generated in the thymus and released to peripheral blood as antigen inexperienced, naïve T-cells. These cells called “recent thymic emigrants” (RTE) are the recently formed naïve T-cells that are produced in the thymus and their numbers correlate with thymic output (8). To date, disease-causing mutations have been reported in 17 genes leading to SCID, and another 43 genes are reported as being mutated in CID (9, 10). The majority of SCID and CID patients presenting in the first 2 years of life have a defect in T-cell development in the thymus. A complete defect (null mutation) results in absence of T-cells, but hypomorphic (“leaky”) mutations can give rise to an incomplete defect leading to presence of variable numbers of T-cells with poor immune function and inadequate control of autoreactivity. This leads to immunodeficiency and dysregulation such as seen in Omenn syndrome (11). Likewise, variable degree of T-cell

immunodeficiency is found in patients diagnosed with 22q11.2 deletion syndrome (DiGeorge syndrome) (12).

An assay for early detection of SCID via newborn screening (NBS) has become available to identify T-cell lymphopenia directly after birth. This assay is based on measurement of T-cell receptor excision circles (TRECs) via quantitative PCR on dried blood spots (13). TRECs are formed as circular excision products during T-cell receptor gene rearrangement in developing T-cells in the thymus and are a molecular marker for recently formed T-lymphocytes. Absence or strongly reduced levels of TRECs are indicative for T-cell lymphopenia and can identify children who may have SCID. TRECs will not be detected in case of the presence of maternally engrafted T-cells. In addition, TRECs will also be low/absent in patients with Omenn Syndrome because of oligoclonal expansion of the autologous T-cells, which makes the TREC assay also useful in these subtypes of SCID. Follow-up diagnostic testing in case of low or absent TREC contents is needed to confirm the diagnosis by flow cytometric immunophenotyping and subsequently by targeted genetic testing for SCID-CID gene aberrations or broader genetic testing (e.g., WES or WGS) in combination with a SCID or PID filter. It should be noted that low or absent TRECs can also be identified in children with T-cell impairment syndromes [such as 22q11.2 deletion syndrome (14), Down’s syndrome or Ataxia Telangiectasia], and children with T-cell impairment secondary to other neonatal conditions or patients with idiopathic lymphocytopenia (15, 16). Furthermore, low/absent TREC levels can also be found in preterm children or in children from mothers on immunosuppressive therapy (17).

Flow cytometric immunophenotyping of lymphocytes proved useful for the early diagnosis of SCID in patients with clinical symptoms or newborns with low/absent TRECs, showing complete lack of one or more lymphocyte lineages (T-cell, B-cell and NK cell) (15, 18). However, interpretation of this basic flow cytometric screening is not sufficient when T-cells are present, either due to a hypomorphic defect or due to the presence of maternal T-cell engraftment. Maternal T-cell engraftment is a relatively frequent finding in SCID (40% in a cohort of 121

patients from Ulm or 47% in the California cohort) (19, 20). In those cases, a flow cytometric test which allows more detailed phenotyping of the T-cells, including analysis of newly generated T-cells, is warranted. At present there is no consensus on the exact composition of a flow cytometric test, although critical parameters (Naïve T-cells, RTE, activated T-cells) are listed by the European Society for Immunodeficiencies (ESID), the American PID treatment consortium (PID-TC) and by other groups (7, 21).

Flow cytometry allows to discriminate naïve T-cell subsets from antigen experienced memory subsets by presence of typical markers (CD45RA isoform, costimulatory molecules CD27, homing receptor CCR7 and CD62L) and absence of memory markers (CD95 and CD45RO isoform) (22, 23). This is useful for diagnostic evaluation of patients with profound T-cell (function) deficiency, where T-cells are detectable (at normal or even increased levels) as a result of peripheral expansion of memory T-cell clones from either autologous or maternal origin. Immunophenotyping could show a skewed redistribution from naïve to memory and activated phenotypes within T-lymphocytes, which alerts for a possible lymphocyte development defect. Furthermore, newly generated T-cells released from the thymus to the periphery (RTE) can also be identified using flow cytometry. RTE are CD4+ T-cells with the highest TREC levels (24) and a phenotype characterized by expression of CD45RA and CD31 (25, 26). Finally, activated T-cells acquire a memory phenotype and temporary signs of activation, which can be detected via analysis of CD69, CD25, and HLA-DR, among other markers (27).

In this study, the EuroFlow PID group consortium has designed, developed and validated a standardized approach for flow cytometric evaluation of naïve, RTE and activated CD4+ and CD8+ T-cells that would offer a high sensitivity test toward disclosing (S)CID in line with the ESID diagnostic criteria in the settings of a multi-center collaboration study. The here developed 8 color “SCID-RTE tube” complements the recently published PIDOT tube (18, 28) for orientation and screening of primary immunodeficiencies (PID) of the lymphoid system. The combination of the two 8-color tubes (or a single 12-color variant of both tubes) could readily be applied in routine diagnostic screening for patients clinically suspected for having (S)CID, as well as in follow-up diagnostics in NBS programs.

MATERIALS AND METHODS

Patient and Control Samples

Our patient cohort consisted of 26 patients with a genetically defined PID diagnosed between birth and the age of 2 years at participating centers (Table 1). Genetic analysis was performed locally according to the routine procedures of the collaborating laboratories using Sanger sequencing or next generation sequencing (NGS). In addition, 44 healthy controls without any known hematological or immunological disorder in the same age range were also enrolled. The samples have been collected from 2013 to 2018. All 26 patient samples were collected according to the local medical ethics regulations of the participating centers, after informed consent was provided by the subjects, their legal representatives, or both, according

to the Declaration of Helsinki. The study was approved by the local ethics committees of the participating centers: University of Salamanca, Salamanca, Spain (USAL-CSIC 20-02-2013); Charles University, Prague, Czech Republic (15-28541A); Erasmus MC, Rotterdam, The Netherlands (MEC-2013-026); University Hospital Ghent, Belgium (B670201629681/B670201214983) and St. Anne’s University, Brno, Czech Republic (METC 1G2015)-.

SCID-RTE Tube Composition and Staining Protocol

The SCID-RTE tube aims to assess relevant lymphoid subpopulations important in PID diagnostics in a single 8 color test. It includes markers for T-cells (CD3, CD4, CD8, TCR $\gamma\delta$), including their naïve (CD62Lpos, CD45ROneg) and RTE (CD31pos) stages, as well as their activated forms (HLA-DR). Detailed composition and volumes of antibodies used are listed in Table 2.

The samples were processed in four EuroFlow laboratories (Charles University, Prague, Czech Republic; Erasmus MC, Rotterdam, The Netherlands; Ghent University, Ghent, Belgium; University of Salamanca, Salamanca, Spain) following standardized EuroFlow approaches (29, 30) (detailed protocols are publicly available at www.EuroFlow.org). In short, peripheral blood ($n = 66$) or cord blood ($n = 4$) (up to 2 ml) was mixed with ammonium chloride lysing solution (48 ml) and incubated for 15 min at room temperature in order to lyse erythrocytes. Obtained WBC were washed twice with phosphate buffered saline (PBS) containing 0.5% bovine serum albumin (BSA) and 0.09% sodium azide (NaN_3) and subsequently stained with the antibodies listed in Table 2 in a final volume of 100 μl for 30 min at room temperature in the dark. Whenever possible, up to one million cells were processed, or all cells available in lymphopenic PID patients. In each case, at least 2×10^5 cells were stained. Next, the cells were incubated with 2 ml BD FACSTM Lysing Solution (BD Biosciences) for 10 min at room temperature in the dark, washed and resuspended in 250 μl washing solution.

Data Acquisition and Analysis

Data acquisition was performed on BD FACSCanto II, BD LSR II or BD FACSLyric instruments (BD Biosciences) equipped with 405, 488, and 633/640 nm lasers and PMT detectors, following the EuroFlow instrument set-up Standard Operating Protocol (29, 31). Data were analyzed using Infinicyt (Cytognos, Salamanca, Spain) and FlowJo (FlowJo LLC, Ashland, Oregon) software. Normal values for all T-cell subsets were determined as numbers above the 5th percentile of the healthy controls. In case of HLA-DR positive activated T-cells, we determined normal values as below the 95th percentile of the healthy controls (see Table 3). Therefore, specificity was by definition 95%. For sensitivity calculations we divided the number of patients with an abnormal value by the total number of patients measured in each parameter/subset separately (see Table 3). For statistical analysis, GraphPad Prism software Mann-Whitney test was used.

TABLE 1 | Characteristics of patients, WBC and lymphocytes subsets (TBNK) reported by the referring clinician (x 10e3/ μ l).

Category	Case no.	Gender	Disease	Mutation	Protein	WBC	T-cells (abs)	B-cells (abs)	NK-cells (abs)	Age
SCID	Case_1	F	SCID, CD3E deficiency	CD3E exon 6 c.173delT	p.Leu58HisfsX9	13.9	0.32	2.6	1.4	0.3
SCID	Case_2	M	SCID, ADA deficiency	ADA exon 4 homozygous c.302G > A	p.Arg101Gln	2.5	0.03	0	0.01	1.3
SCID	Case_3	M	SCID, JAK3 deficiency with mat.enr.	JAK3 heterozygous c.561delT, c.2066C > T	p.Val188SerfsX14, p.Pro689Leu	11.8	6.31	3.02	0.02	1.8
SCID	Case_4	F	SCID, JAK3 deficiency	JAK3 exon 12 homozygote c.1765G > A (NM_000215)	p.Gly589Ser	6.5	0.03	0.8	0.08	0
SCID	Case_5	F	SCID, JAK3 deficiency with mat.enr.	JAK3 exon 5 c.578G > A, exon 19 c.2712C > A	p.Cys193Tyr	15.5	1.68	0.37	0.1	0.2
SCID	Case_6	M	SCID, Cernunnos/XLF deficiency	NHEJ1 exon 5 homozygote c.532C > T	p.Arg178X	3.4	0.22	0.04	0	0.9
SCID	Case_7	F	SCID, Artemis deficiency	DCLRE1C c.1A > C c.401C > G (compound heterozygote)	M1V, T134R (Met1Val, Thr134Arg)	3.6	0.00132	0	0.0018	0.4
SCID	Case_8	M	SCID, RAG2 deficiency	RAG2 homozygous c.1280_1281insTGGATAT	p.Asn428GlyfsX12	33.1	0.04	0.01	1.61	0.2
SCID	Case_9	M	SCID, RAG2 deficiency	RAG2 c.107G > A	p.Trp36*	2.8	0.04236	0.0444	0.0678	0.2
SCID	Case_10	M	Omenn syndrome, RAG1 deficiency	RAG1 c.983G > A/c.1186C > T (compound heterozygote)	p.Cys328Tyr/p.Arg396Cys	27.9	6.767	0.0303	1.818	0
SCID	Case_11	M	Omenn syndrome, RAG1 deficiency	RAG1 exon 2 c.519del	p.Glu174Serfs*27	8.05	2.15	0	0.429	0.3
SCID	Case_12	M	SCID, IL2RG deficiency with mat.enr.	IL2RG c.270-1G > A	n.d.	3.6	0.04	0.57	0	0.7
SCID	Case_13	M	SCID, IL2RG deficiency	IL2RG c.613G > A	p.Trp174*	9.5	0.001045	0.22325	0.022895	0.7
SCID	Case_14	M	SCID, IL2RG deficiency with mat.enr.	IL2RG c.269+3A > T	n.d.	5.4	0.6804	0.783	0.00891	0.5
SCID	Case_15	M	SCID, IL2RG deficiency	IL2RG exon 5 hemizygoote c.595-1G > T	n.d.	8.6	0	0.6	0.02	0.3
other PID	Case_16	M	CID, PNP deficiency	PNP c.700C > T	p.Arg234X	6.1	0.5	0.07	0.01	1.6
other PID	Case_17	M	ZAP70 deficiency	ZAP70 exon 10 homozygoote c.1193C > T	p.Ile398Ser	11.3	2.18	1.03	0.17	0.6
other PID	Case_18	M	Wiskott-Aldrich syndrome	WAS c.1271_1295del	p.Gly424Glyfs*13	8.4	1.47	0.95	0.25	0.3
other PID	Case_19	M	Wiskott-Aldrich syndrome	WAS c.344A > G	p.His115Arg	4	1.271	0.4305	0.3075	1.1
other PID	Case_20	M	Complete DiGeorge syndrome	del22q11.2		6.7	0.48776	0.003819	0.1206	1.6
other PID	Case_21	F	Complete DiGeorge syndrome	del22q11.2		5.1	0.00126684	0.655	0.504	0.2
other PID	Case_22	F	DiGeorge syndrome	del22q11.2		9.9	0.914354	1.342852	1.008826	0.6
other PID	Case_23	M	DiGeorge syndrome	del22q11.2		6.7	0.97	1.29	0.7	0.3
other PID	Case_24	M	Takenouchi-Kosaki syndrome	CDC42 c.191A > G	p.Tyr64Cys	2.4	0.436	0.094	0.094	1.5
other PID	Case_25	M	IPEX syndrome	FOXP3 c.721T > C	S241P (p.Ser241Pro)	15.135	2.42353	1.013115	0.349624	0.2
other PID	Case_26	M	Autoimmune lymphoproliferative sy	FAS exon 7 heterozygous (frameshift)	n.d.	29.8	20.818	2.146	0.226	0.3

TABLE 2 | Composition of the EuroFlow SCID-RTE tube*.

Marker	Fluorochrome	Clone	Source	Catalog number	$\mu\text{l}/\text{test}$
CD3	APC	SK7	BD Biosciences	345767	2.5
CD4	BV510	OKT4	Biolegend	317443	1.5
CD8	APC-Alexa750	B9.11	Beckman Coulter	A94683	1.5
CD31	PE	MEM-05	Exbio	1P-273-T100	5
CD45RO	FITC	UCHL1	Exbio	1F-498-T100	10
CD62L	BV421	DREG-56	Biolegend	304827	2
HLA-DR	PerCP-Cy5.5	L243	Biolegend	307629	1.5
TCR $\gamma\delta$	PE-Cy7	11F2	BD Biosciences	649806	2.5

*Both the SCID-RTE tube and the PIDOT tube have originally be designed for application in 8-color format. However, because of their strong complementarity, it can be efficient and cost-effective to use a 12-color "combined PIDOT & SCID-RTE variant" by supplementing the PIDOT tube with the CD45RO, CD31, HLA-DR, and CD62L markers.

RESULTS

Composition of the SCID-RTE Tube

The SCID-RTE tube was designed with the purpose of identifying the relevant lymphoid subpopulations important in PID diagnostics of severe PID in newborns, using a single 8-color test. It identifies naïve CD4+ T cells and among them, the RTEs. The definition of naïve T-cells includes a selection of non-activated (HLA-DR negative) cells, together with absence of CD45RO (a memory T-cell marker) and the presence of the naïve T-cell marker L-selectin (CD62L). The definition of RTE uses the naïve T-cell gate and is further complemented by CD31, Platelet endothelial cell adhesion molecule (PECAM-1) (Table 2, Figure 1). After gating T-cells as CD3+ and lymphocytes on FSC and SSC, four markers (CD3, TCR $\gamma\delta$, CD4, and CD8) were used to define TCR $\gamma\delta$ + and TCR $\gamma\delta$ - CD4+, CD8+ and double negative (DN) T-cells (Figure 1A, Supplemental Figure 1). The CD4+ T-cells were further subdivided into RTE, naïve, central memory (CM), effector memory CD45RO+ (EMRO+) and CD45RO- (EMRO-) and activated memory T-cells (Figures 1B,D); for CD8+ T-cells the same subsets were defined except for the RTEs (Figures 1C,D). The total set and hierarchy of T-cell subsets that was identified is listed in Figure 1D. To offer intuitive and fast interpretation of the complete lymphoid compartment we developed a new analysis and visualization strategy for the SCID-RTE tube using principle component analysis (PCA)-based multidimensional views (APS graphs). First, reference plots were generated using a set of 10 samples of healthy donors in Infinicyt software. The lymphocyte populations were manually analyzed and subsequently, the most discriminating projection into a single APS graph was determined (Figure 1E). A software tool for automated identification of the cell populations present in the SCID/RTE tube was built, containing normal blood samples stained with the same antibody combination.

Identification of RTEs by the SCID-RTE Tube in PID Patients

The SCID-RTE tube allows analysis of the naïve and memory subsets of T-cells (Figure 2A) that are abnormally distributed in patients with PID (Figure 2B). Typically, their numbers are

different in childhood compared to the adult age (Figure 3), however within 2 years of age a general threshold for CD4+ RTE (<800 cell/ μl), naïve CD4+ (<1,000 cell/ μl) and naïve CD8+ lymphocytes (<290 cell/ μl) is justified. Notably, the number of RTEs are abundant in childhood, whereas the numbers of activated memory CD4+ and CD8+ T-cells are low (Figures 2A, 3).

SCID patients that present without T-cells (Figure 2B, *IL2RG*) are straightforwardly identified by the SCID-RTE tube, but they never pose a diagnostic dilemma even in a simple T-B-NK flow cytometric assay. However, in SCID and Omenn syndrome patients with paradoxically normal or even increased total absolute numbers of T-cells, the SCID-RTE tube allows detection of the activation status of T-cells (HLA-DR positive). These activated T-cells can be of maternal origin in SCID with maternal engraftment (Figure 2B, *JAK3 with maternal engraftment*) or can be oligoclonal, expanded T-cells in Omenn syndrome patients (Figure 2B, *RAG1 Omenn syndrome*). RTE cells are virtually absent in these patients with T-cell production defects (SCID and Omenn patients). Patients with PNP deficiency and complete DiGeorge syndrome also lack RTEs, but patients with *ZAP70* deficiency, Wiskott-Aldrich Syndrome and ALPS have detectable RTEs (Figure 2B, detailed dot plots shown in Supplemental Figures 2, 3).

Absence of RTEs in SCID Patients

In our current study, we analyzed 15 SCID patients and 11 other PID patients diagnosed before 2 years of age. SCID patients had disease-causing mutations in *RAG1* or *RAG2* ($n = 4$, two of them presented with Omenn syndrome), *IL2RG* ($n = 4$, one of them with confirmed maternal engraftment), *NHEJ1* ($n = 1$), *CD3E* ($n = 1$), *ADA* ($n = 1$), *JAK3* ($n = 3$, two of them with maternal engraftment) and *DCLRE1C* ($n = 1$) (see Table 2 and Supplemental Figure 2).

In the SCID patients, the absolute levels of CD3+ T-cells were strongly reduced ($n = 7$) or undetectable ($n = 5$), but for three patients (20% of our cohort) the absolute CD3+ T-cell counts were in the normal range (see Table 3). These patients were proven to have maternal engrafted T-cells ($n = 2$) or oligoclonally expanded cells characteristic for Omenn syndrome ($n = 1$).

TABLE 3 | Lymphocytes subsets evaluated by SCID-RTE tube.

Patient code	Disease	Category	CD3+ of Lym	CD3+ abs	TCRgd+ of T	TCRgd+ abs	CD4+ T of T	CD4+T abs	CD8+ T of T	CD8+T abs	CD4+RTE of CD4	CD4+RTE abs	Naive CD4+ of CD4	Naive CD4+ abs	Naive CD8+ of CD8	Naive CD8+ abs	HLA-DR+ of CD4	HLA-DR+ CD4+ abs	HLA-DR+ of CD8	HLA-DR+ CD8+ abs
Case_1	CD3E	SCID	7	246	0	0	5	13	93	228	0	0	0	0	2	5	93	12	83	188
Case_2	ADA	SCID	55	18	13	2	1	0	83	15	0	0	0	0	0	0	n/a	n/a	93	14
Case_3	JAK3	SCID	69	5,610	1	67	4	210	94	5,256	0	0	0	1	2	117	64	134	95	4,967
Case_4	JAK3	SCID	2	15	3	0	1	0	85	12	0	0	0	0	0	0	n/a	n/a	99	12
Case_5	JAK3	SCID	80	2,247	0	4	98	2,202	1	23	0	0	0	1	0	0	86	1,896	86	19
Case_6	XLF	SCID	38	294	89	263	0	1	2	7	0	0	0	0	0	0	n/a	n/a	64	5
Case_7	Artemis	SCID	18	84	55	46	38	31	1	1	6	2	6	2	31	0	88	28	44	0
Case_8	RAG2	SCID	2	40	1	1	71	29	1	0	0	0	0	0	17	0	91	26	n/a	n/a
Case_9	RAG2	SCID	32	78	5	4	86	67	5	4	0	0	0	0	3	0	66	44	77	3
Case_10	RAG1	SCID	68	4,621	3	158	43	1,964	44	2,024	0	0	0	0	0	1	85	1,661	86	1,739
Case_11	RAG1	SCID	69	1,916	6	109	88	1,690	3	64	0	0	0	2	1	1	68	1,154	83	53
Case_12	IL2RG	SCID	12	92	0	0	71	65	28	25	0	0	0	0	4	1	94	61	81	20
Case_13	IL2RG	SCID	0	1	5	0	31	0	1	0	0	0	0	0	0	0	n/a	n/a	n/a	n/a
Case_14	IL2RG	SCID	45	677	25	171	48	325	23	156	0	0	1	3	7	11	87	282	94	147
Case_15	IL2RG	SCID	0	1	17	0	58	0	0	0	0	0	0	0	0	0	n/a	n/a	n/a	n/a
Case_16	PNP	other PID	63	281	3	7	48	134	37	105	0	0	0	0	0	0	63	84	99	103
Case_17	ZAP70	other PID	51	1,661	3	47	89	1,482	2	29	24	357	34	505	19	5	17	246	30	9
Case_18	WAS	other PID	50	1,092	4	41	82	891	13	138	53	470	82	730	56	78	3	23	3	4
Case_19	WAS	other PID	57	978	28	271	31	303	38	376	18	55	40	122	6	23	39	119	85	319
Case_20	del22q11.2	other PID	50	328	37	122	15	47	3	9	0	0	0	0	1	0	43	21	65	6
Case_21	del22q11.2	other PID	0	1	10	0	0	0	70	1	0	0	0	0	14	0	n/a	n/a	58	1
Case_22	del22q11.2	other PID	27	1,592	9	138	65	1,030	22	344	56	579	71	729	87	300	5	56	4	14
Case_23	del22q11.2	other PID	33	756	8	63	65	493	22	169	50	246	72	356	87	147	4	20	4	7
Case_24	CDC42	other PID	63	465	39	180	34	159	23	107	40	63	66	105	58	63	6	10	21	22
Case_25	FOXP3	other PID	61	1,664	1	22	70	1,157	22	363	40	465	66	765	81	295	4	48	5	19
Case_26	FAS	other PID	86	12,833	3	444	26	3,324	15	1,912	58	1,938	81	2,692	92	1,761	11	356	5	88
Controls																				
5th percentile			52	2,010	0.7	20	54	1,201	13	335	58	840	72	1,030	60	287	0	9	0	2
95th percentile			86	6,626	7	340	82	4,094	35	2,204	86	2,393	96	3,149	96	1,614	3	66	11	80
Sensitivity other PID			55%	91%	55%	20%	55%	82%	27%	64%	91%	91%	73%	91%	64%	73%	90%	40%	55%	27%
Sensitivity SCID			67%	80%	33%	60%	60%	80%	53%	87%	100%	100%	100%	100%	100%	100%	100%	50%	100%	33%

Absolute counts (abs) as $10e3/\mu\text{l}$. Values outside the normal range are in bold. Range obtained in controls (5th and 95th percentile) is given below the table. Sensitivity to disclose abnormal values in other PID and SCID group is given for each measurement in the bottom two rows. Most informative parameters are highlighted in gray.

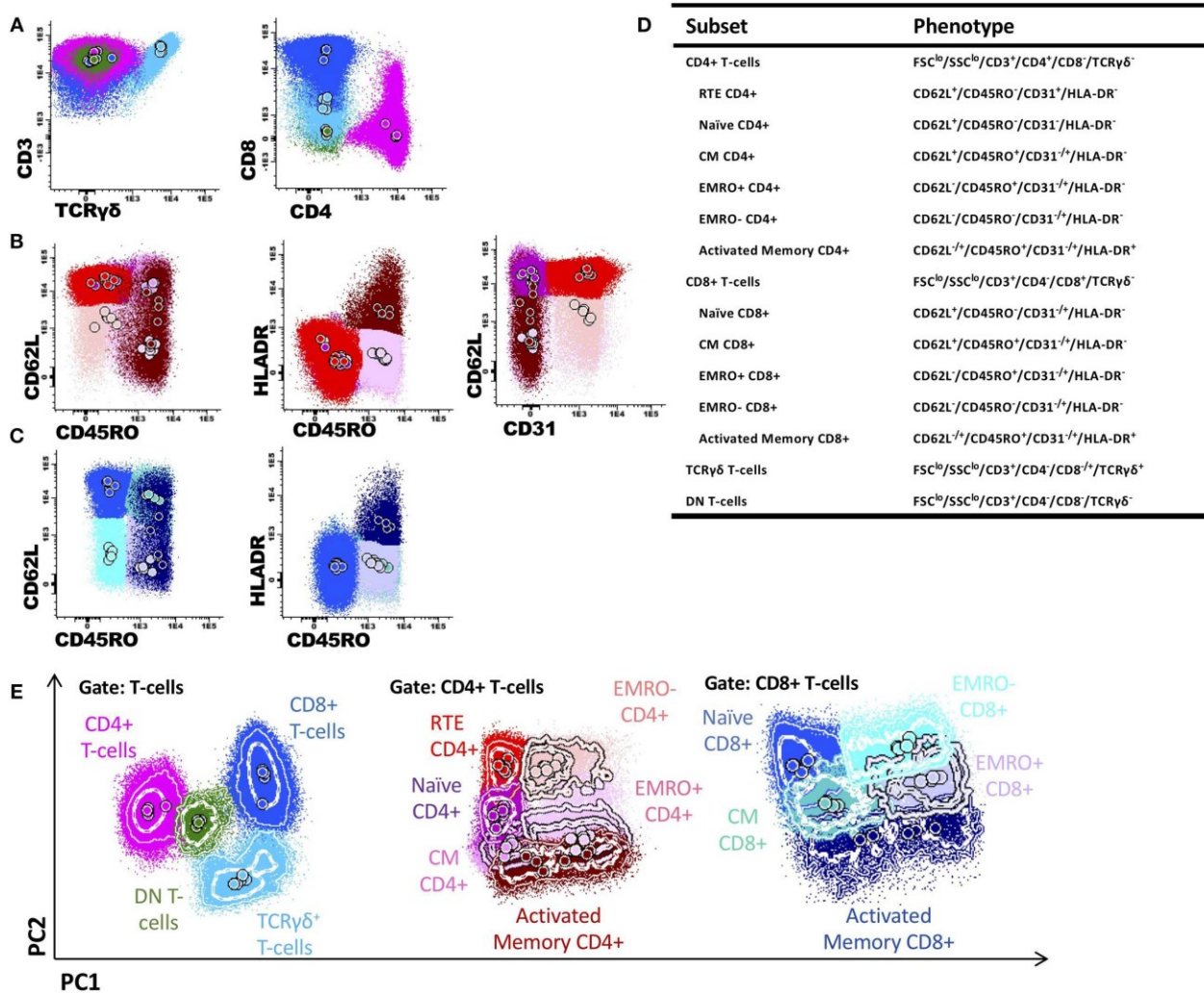


FIGURE 1 | Gating T-cell subsets and generation of a reference principal component analysis representation in an n-dimensional space for SCID-RTE tube. (A) After gating T-cells as CD3⁺ and FSC^{lo} and SSC^{lo}, the markers TCRyδ⁺, in combination with CD4 and CD8 were used to define TCRyδ⁺ T-cells (light blue), CD4⁺CD8⁻TCRyδ⁺ T-cells (pink); CD4⁻CD8⁺ TCRyδ⁺ T-cells (dark blue) and CD4⁻CD8⁻ TCRyδ⁺ double negative T-cells (green). (B) The CD4⁺ T-cell subsets were further subdivided into recent thymic emigrants (RTE; CD62L⁺CD45RO⁻HLDR⁻CD31⁺; red), naïve (CD62L⁺CD45RO⁻HLDR⁻CD31⁻; purple), central memory (CM; CD62L⁺CD45RO⁺HLDR⁻; orchid), effector memory CD45RO⁺ (EMRO⁺; CD62L⁻CD45RO⁺HLDR⁻; mauve), effector memory CD45RO⁻ (EMRO⁻; CD62L⁻CD45RO⁻HLDR⁻; pink) and activated memory (CD45RO⁺HLDR⁺; burgundy) CD4⁺ T cells. (C) The CD8⁺ T-cell maturation subsets were further subdivided into naïve (CD62L⁺CD45RO⁻HLDR⁻; blue), central memory (CM; CD62L⁺CD45RO⁺HLDR⁻; blue-green), effector memory CD45RO⁺ (EMRO⁺; CD62L⁻CD45RO⁺HLDR⁻; cyan) and activated memory (CD45RO⁺HLDR⁺; navy blue) CD8⁺ T cells. (D) Definition and hierarchy of the defined subsets. (E) Principal component analysis representation (APS view) based on the most discriminating parameters for T-cell populations, and CD4⁺ T-cells and CD8⁺ T-cell subsets.

Application of the SCID-RTE tube showed that all SCID patients completely lacked RTE cells and other forms of naïve CD4⁺ and CD8⁺ T cells (Figure 4A), even the patients with normal T-cell counts (due to maternal T-cells or oligoclonal expansion). The T-cells that could be detected had signs of massive activation (64–94% HLA-DR⁺ in CD4⁺ and 44–99% in CD8⁺ T cells) (Figure 4B). Overall, the SCID-RTE tube detected severely decreased or absent numbers of RTE and naïve CD4⁺ and CD8⁺ T-cell subsets in all SCID patients. In the SCID patients with detectable levels of T-cells, the phenotype

was characterized by activation (HLA-DR⁺) and had a memory phenotype (CD45RO⁺).

RTEs in Other Severe PID Diagnosed Before 2 Years of Age

Patients diagnosed with other severe forms of PID (Other PID, n = 11) had diverse molecular defects [ZAP70 (n = 1), WAS (n = 2), PNP (n = 1), FOXP3 (n = 1) del22q11.2 (DiGeorge n = 2; complete DiGeorge n = 2), CDC42 (n = 1) and FAS (n = 1)] (see Table 2 and Supplemental Figure 3). Except for the patient

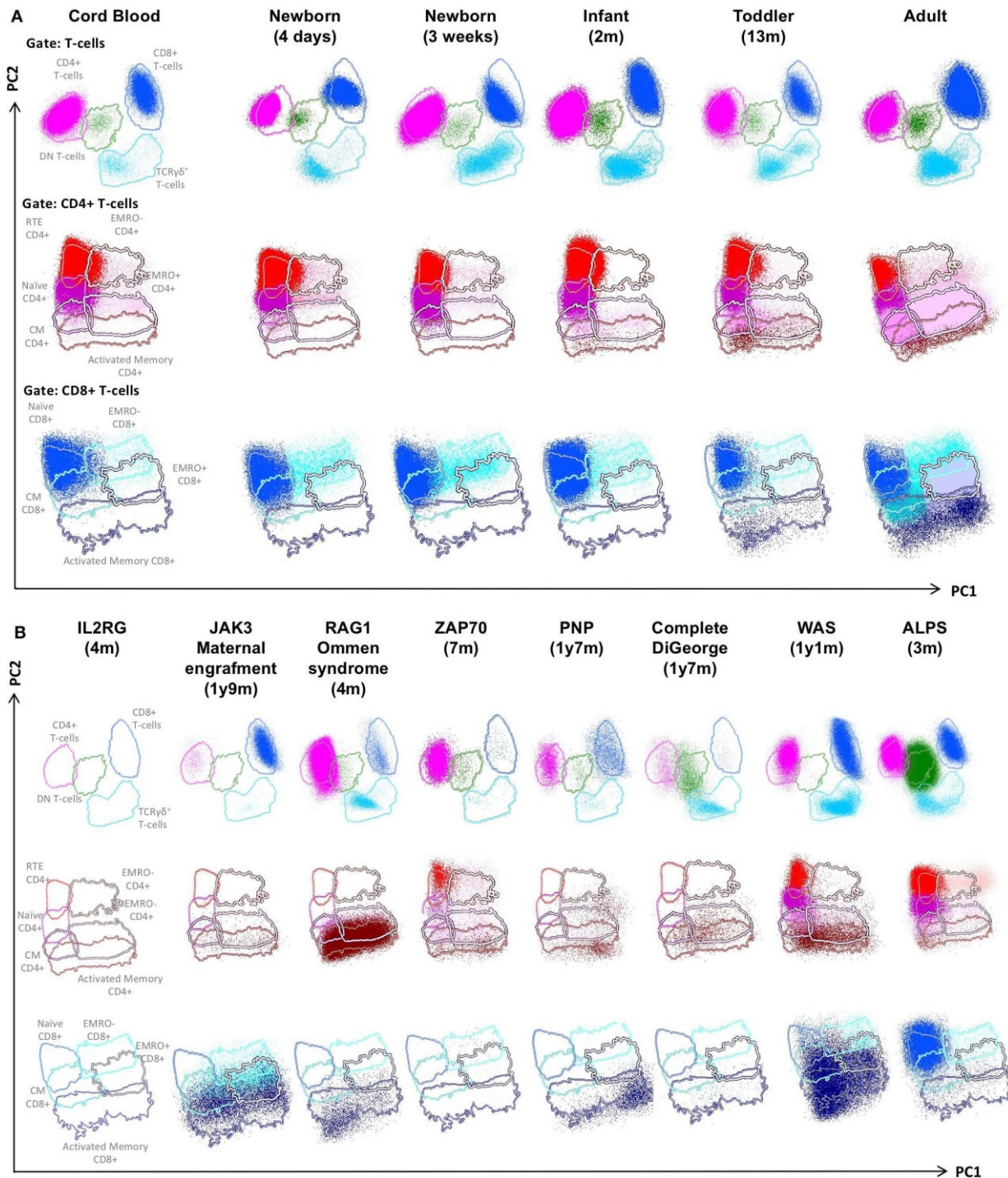
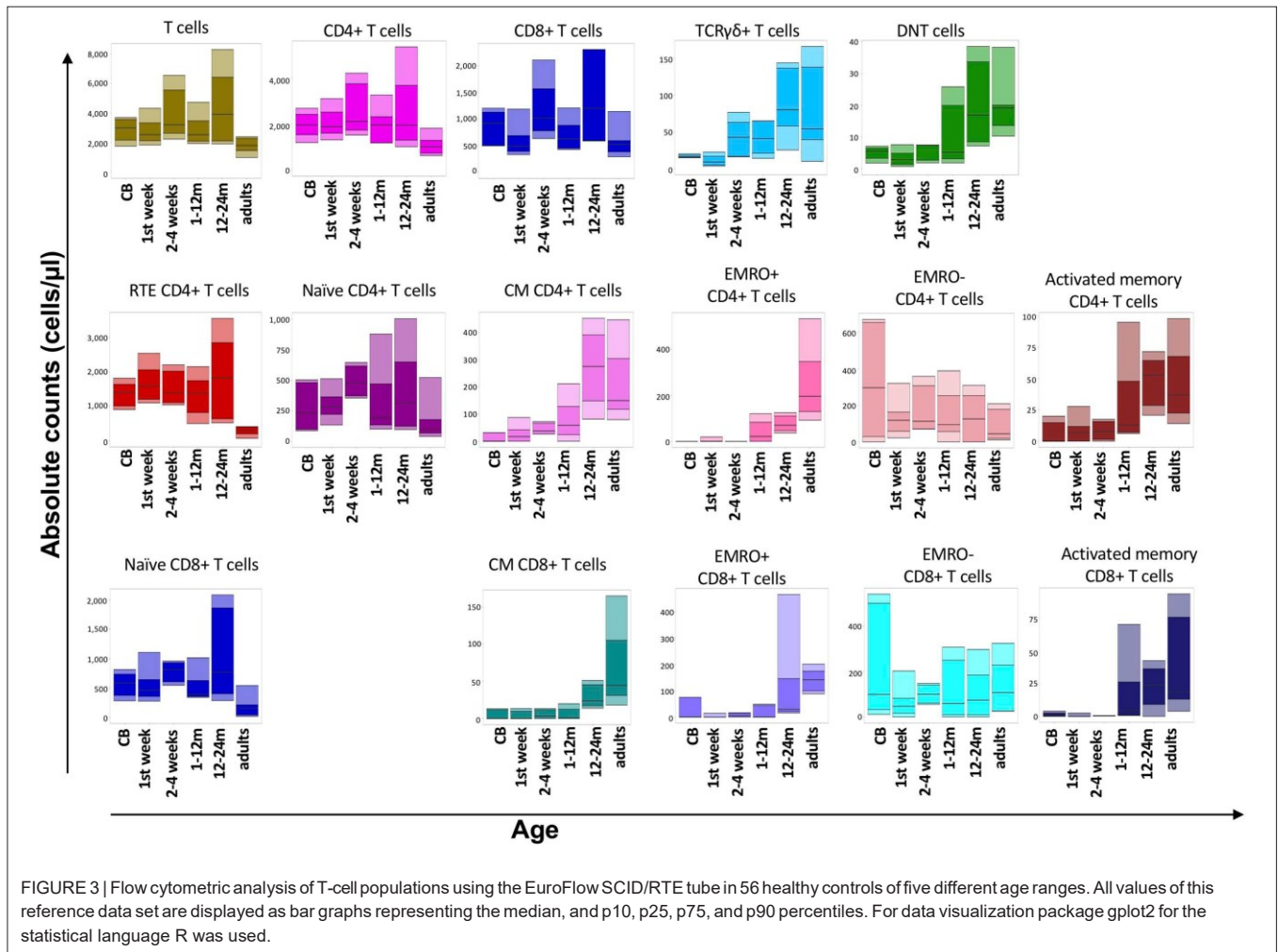


FIGURE 2 | PCA representation of SCID-RTE tube results, showing the distinct blood T-cell subsets in the supervised PCA analysis of blood samples from healthy donors of different age (A) and SCID and CID patients (B). From the top down, APS plots of gated total, CD4+ and CD8+ T-cells are shown. Lines depict a 2 standard deviation boundary of all controls combined. (A) PCA (APS views) of all T-cell subsets of cord blood and peripheral blood from donors of different age. (B) PCA (APS views) of all T-cell subsets of the following patients: a IL2RG-deficient patient, a JAK3-deficient patient with maternal engraftment, a RAG1-deficient Ommen syndrome, a ZAP70-deficient patient, a PNP-deficient patient, a complete DiGeorge syndrome, a Wiskott-Aldrich syndrome (WAS) and an autoimmune lymphoproliferative syndrome (ALPS) patient.



with autoimmune lymphoproliferative syndrome (ALPS) due to FAS mutation, all had decreased absolute counts of CD3+ T-cells compared to controls. However, only one complete DiGeorge patient had <300 T-cells/ μl in the conventional TBNK test, which is considered a diagnostic threshold in SCID patients.

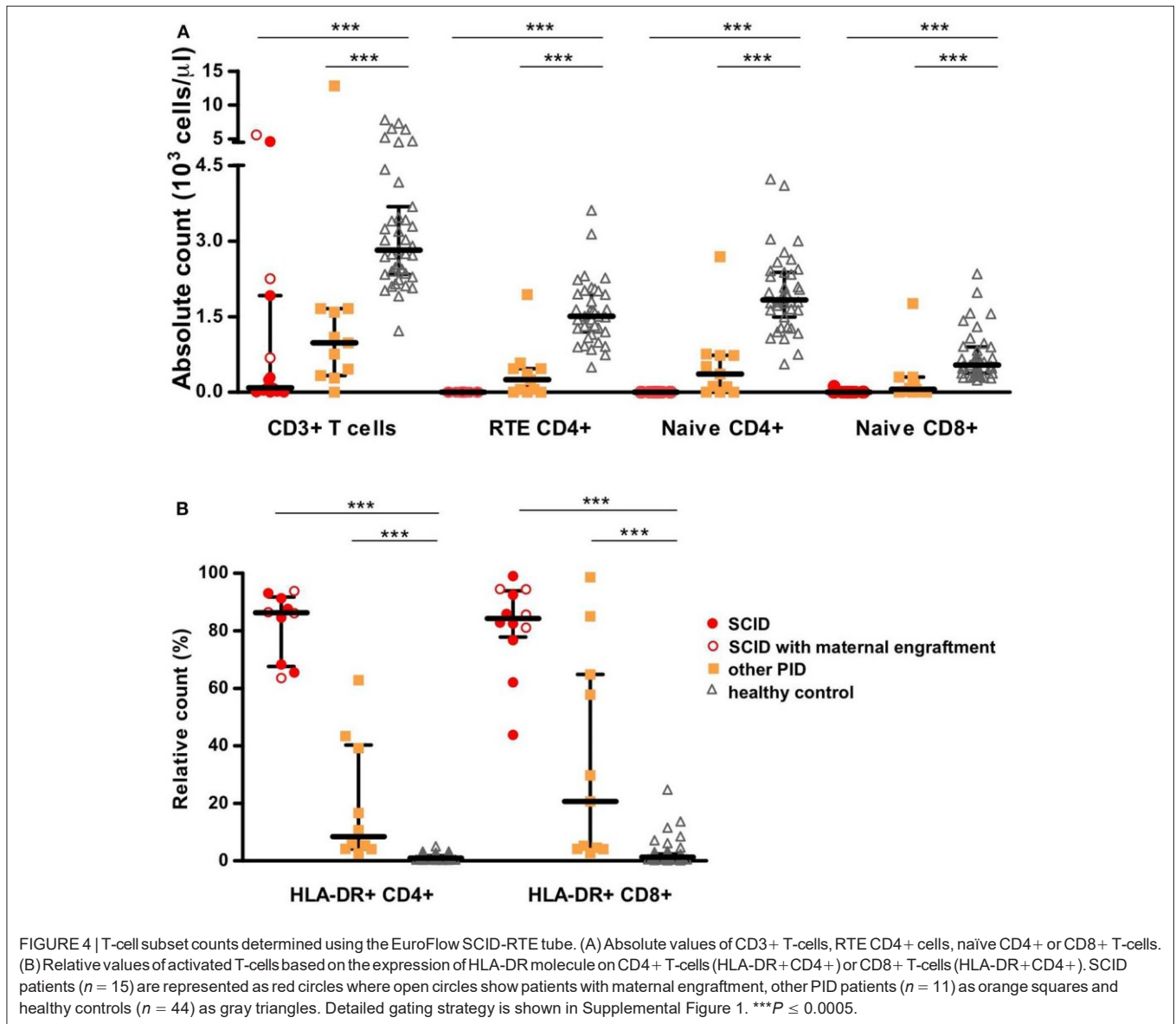
When assessed by the SCID-RTE tube the patients showed a heterogeneous pattern of T-cell subset abnormalities ranging from strongly reduced/absent to normal numbers. However, all of the patients showed at least one abnormality. With the exception of the ALPS patient who presented with normal proportion of naïve CD4+ T-cells (and elevated naïve CD8+ T-cell counts) (32), all had reduced naïve CD4+ T-cells and RTEs below 5th percentile of healthy (Figures 2B, 4A, Table 3). The ALPS patient was characterized by massively increased T-cells especially of double negative T-cells (56% of CD3+TCR $\gamma\delta$ -cells) and activated CD4+ T-cells (11%). As previously described (33), we found a high frequency of TCR $\gamma\delta$ + T cells (9–39% of CD3+ cells), in patients with Wiskott-Aldrich syndrome (WAS) as well as in DiGeorge ($n = 2$) and complete DiGeorge patients. We also identified a high frequency of TCR $\gamma\delta$ + T-cells in CDC42 deficiency. Four had normal total CD8+ T-cell counts, but reduced naïve CD8+ T-cells and showed signs of activation:

WAS, immune dysregulation, polyendocrinopathy, enteropathy, X-linked syndrome (IPEX), DiGeorge (Table 3).

On top of reduction or absence of naïve and RTE subsets of CD4+ T-cells (Table 3), three of the four DiGeorge patients showed decreased CD8+ T cells and their naïve subsets. Activation of T cells (as measured by HLA-DR+) ranged from mild to high. Both patients with WAS had profoundly reduced naïve CD8+ T-cells, reduced naïve CD4+ T-cells and RTE, activation was found in both CD4+ and CD8+ T cells in one of the WAS patients. The complete dataset of findings for all patients is provided in Table 3.

Added Value of SCID-RTE on Top of the PIDOT Tube

The proposed SCID-RTE tube is both a confirmation and extension of the PIDOT tube. As the reduction of naïve T-cells was one of the most important hallmarks of (S)CID and PID in our cohort, as well as in the large group of PID patients published previously (18), we investigated whether the definition of naïve T-cells in the PIDOT tube (CD45RA+CD27+) corresponds to the SCID-RTE tube



definition (CD45RO^{neg}CD62L⁺HLA-DR^{neg}). Indeed, we found that both approaches yield correlating values in the PID patients (Figure 5). Thus, the PIDOT tube is capable of detecting reduction of naïve T-cells and directing the testing toward confirmation with the SCID-RTE tube, which also allows the specific detection of RTEs and activation status, which is particularly important in patients with normal or close to normal T-cell counts.

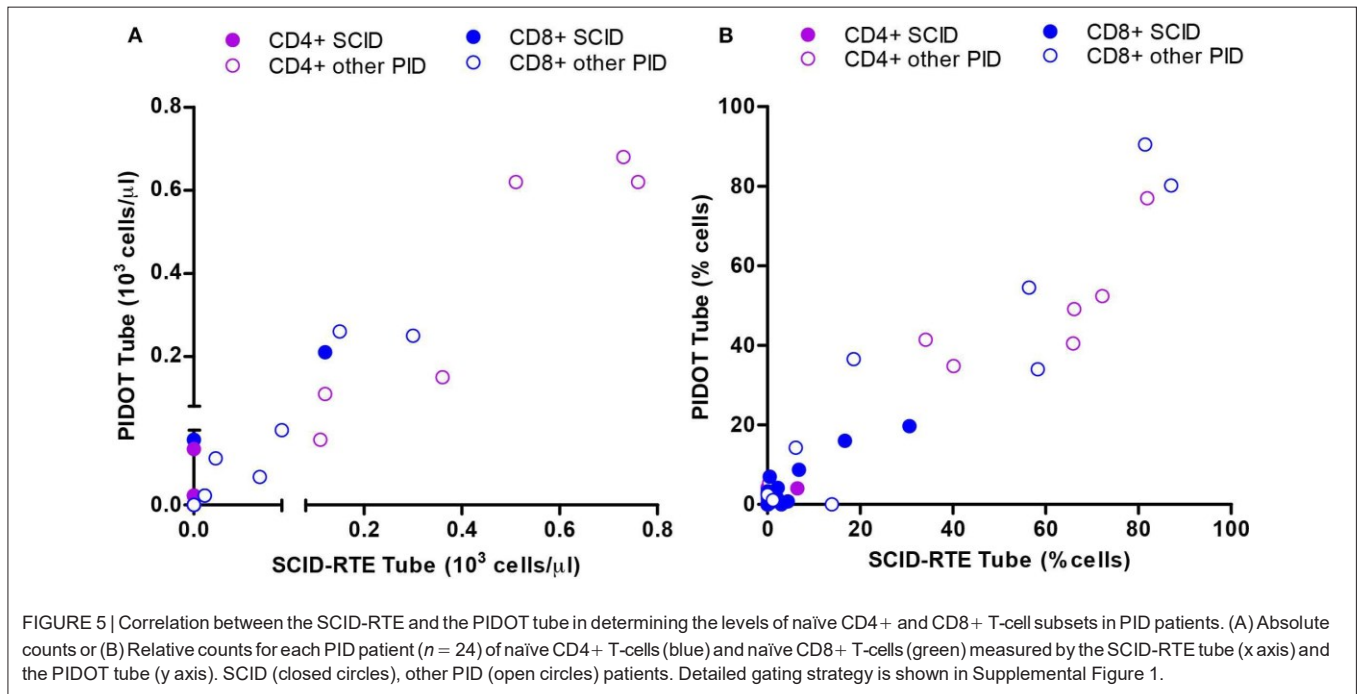
Both the PIDOT tube and the SCID-RTE tube have originally been designed for application in an 8-color format. However, because of their strong complementarity, it can be efficient and cost-effective to use the 12-color combined PIDOT & SCID-RTE variant in cases suspicious of (S)CID, by supplementing the PIDOT tube with the CD45RO, CD31, HLA-DR, and CD62L markers.

Specificity and Sensitivity

Next, we determined the sensitivity of the SCID-RTE tube to find abnormal values (defined as below the 5th percentile, thus allowing for specificity 95%) in our cohort of 15 (S)CID and 11 other PID patients.

The sensitivity of values of naïve CD4+, CD8+, and CD4+ RTE yielded 100% sensitivity to detect (S)CID (see Table 3). This was despite the fact that several (S)CID patients presented with close to normal total T-cells and their basic subsets (CD4+ and CD8+ T-cells). Whenever T-cells were detectable, their activation status (percentage of HLA-DR) was an equally sensitive marker for (S)CID, as the naïve T-cells and RTEs.

However, naïve T-cells and RTEs were also abnormal in the group of other PID, implying that these patients could also be recognized and referred for genetic testing. Thus, it can be



concluded that in case of reduced naïve T-cells and RTEs fast genetic testing is urgently needed.

DISCUSSION

There have been multiple initiatives for establishing comprehensive and detailed reference values of human lymphocyte subsets in children by several groups (34–36). These studies were done by using two to four color flow cytometry. There was no attempt to standardization and no clear indication about the utility of individual subsets' abnormalities for PID diagnostics. Recently, Takashima et al. reported on a detailed set of seven 8–10 color flow cytometry panels used to investigate 75 PID patients, where they also found lack of naïve T-cells in SCID (also with maternal engraftment), Ataxia Telangiectasia and CMCD (37). However, this 7-tube approach would be demanding to use at large scale, and it requires relatively high sample volume for the seven tube-aliquots. With the EuroFlow PID consortium, we developed a standardized approach for flow cytometry testing in PID (38), which includes a tube for screening and orientation (PIDOT) (18), two 8-color tubes for analysis of pre- and post-germinal center B-cells, and an additional isotype tube allowing full characterization of B-cells, including analysis of IgH isotype and subclass distribution within the memory B-cell (MBC) and plasma cell (PCs) compartments (39). The EuroFlow approach offers a systematic approach to diagnostics with a modular design (37).

Here we focused on the feasibility and performance characteristics of the EuroFlow SCID-RTE tube for diagnostic use in (S)CID and severe PID in a cohort of 26 patients, genetically diagnosed before the age of 2 years. The challenge

in revealing SCID patients comes from the fact that a large portion of them presents with detectable T-cells that are either autologous oligoclonal T-cells as seen in Omenn syndrome (40, 41), or arise from maternal engraftment [40% of SCID according to Mueller et al. (19)]. The EuroFlow SCID-RTE tube overcomes the limitations of the basic T, B, NK test that cannot evaluate the nature of the T-cell subsets. In particular, the CD4+ naïve, CD8+ naïve, and CD4+ RTE subsets are shown to be decreased in all SCID and a great majority of other PID in our cohort. The RTE subset was reported as a useful proxy for thymic output measurements (25, 42–45), correlating to TREC levels (43, 45–47), that are used in newborn screening programs for SCID.

Since (S)CID patients harbor deleterious mutations that prevent normal T-cell development, any T-cells in their bloodstream must be expanded T-cells of either autologous oligoclonal origin or maternal origin. In order to improve the RTE definition for patients with putative peripheral expansion of T-cells, we gated not only on CD31+CD45RO-CD4+ T-cells, but we additionally excluded TCR $\gamma\delta$ + and HLA-DR positive cells and restricted the gate to include CD62L positive cells only. Thus, only naïve, non-activated CD4+ T-cells (non-TCR $\gamma\delta$ +) are counted as RTE. This improved the accuracy of the RTE measurements, particularly in other PID patients with massive presence of HLA-DR, where some activated (HLA-DR+) cells would be otherwise considered RTE. HLA-DR was reported as a marker of residual T-cells in Omenn syndrome patients by Saint Basil et al. (27) already in 1991. The biological significance and mode of HLA-DR acquisition by T-cells is thought to be explained by acquisition of the molecule from antigen presenting cell (APC) after T-cell-APC contact (48).

A difficult PID category to be diagnosed with the SCID-RTE tube would be DiGeorge syndrome patients who present with near-normal counts of T-lymphocytes and their subsets. DiGeorge patients have variable clinical presentations, TREC levels and T-cell counts that are generally lower than normal, but vary considerably from patient to patient (14). However, their clinical course rarely requires HSCT. Rare cases of complete DiGeorge patients resembled SCID patients in their immunophenotype and thus pose no diagnostic challenge. While in other PID patients in our cohort, T-cell production (thymopoiesis) is not the mechanism responsible for the immunodeficiency, but their mutation leads to more complex changes broadly termed as dysregulation (WAS, ALPS, IPEX, ZAP70, CID), the SCID-RTE tube was also able to find abnormalities, mainly in the naïve/RTE compartments and in the T cell subset activation status. A CDC42 mutation in a Takenouchi-Kosaki syndrome (49, 50) patient was accidentally found in an infant with failure to thrive, lymphopenia and lymphedema by whole exome sequencing for PID suspicion. Abnormalities in lymphoid cells were clearly revealed by the PIDOT and SCID-RTE tube.

The SCID-RTE tube can also be used in patients with Combined Immunodeficiency (CID), where severe clinical presentation together with laboratory findings indicative of CID can be used for HSCT indication. ESID criteria for CID diagnosis require that apart from severe infection or immune dysregulation or affected family members, two of the four following T-cell criteria must be met: (a) reduced CD3 or CD4 or CD8 T-cells, (b) reduced naïve CD4 and/or CD8 T-cells, (c) elevated TCR $\gamma\delta$ +T-cells, (d) reduced proliferation to mitogen or TCR stimulation (51). All three immunophenotypic criteria can be readily obtained from the SCID-RTE tube, furthermore the threshold counts of CD4+ RTE (<800 cell/ μ l), naïve CD4+ (<1,000 cell/ μ l) and naïve CD8+ lymphocytes (<290 cell/ μ l) are established in multi-center and standardized diagnostic test. We would propose that the SCID-RTE tube can be used whenever there is a high clinical suspicion for SCID or CID. The SCID-RTE tube should be measured together with the PIDOT tube to obtain insight in the lymphocytes' compartment and to screen and diagnose (S)CID in a fast, standardized and efficient manner. It can also be used in a sibling of a SCID patient, immediately after birth or in children with low or absent TRECs as identified via newborn screening. SCID-RTE and PIDOT can yield the required information confirming severe T-cell abnormality or disproving it in a pre-symptomatic phase, but a separate study is needed to validate this approach in a newborn screening program. SCID-RTE can be used in patient where some abnormalities in the T-cell compartment were found by PIDOT tube. Finally, SCID-RTE and PIDOT can serve as a complementary immunophenotyping test for patients with positive TREC findings, where immunophenotyping information can serve to confirm the diagnosis of PID and direct subsequent genetic testing. Moreover, it can offer hints for the decision making process on appropriate conditioning regimen before HSCT. Importantly, the two 8-color SCID-RTE and PIDOT tubes can also be combined into a single 12-color tube for more efficient testing.

In conclusion, we have shown that the EuroFlow SCID-RTE tube is a well-performing, fast and standardized diagnostic test for (S)CID that can be deployed in any laboratory with 8-color flow cytometer.

DATA AVAILABILITY STATEMENT

The datasets generated for this study are available on request to the corresponding author.

ETHICS STATEMENT

The study was approved by the local ethics committees of the participating centers [University of Salamanca, Salamanca, Spain (USAL-CSIC 20-02-2013); Charles University, Prague, Czech Republic (15-28541A); Erasmus MC, Rotterdam, The Netherlands (MEC-2013-026); University Hospital Ghent, Belgium (B670201523515) and St. Anne's University, Brno, Czech Republic (METC 1G2015)]. The ethics committee waived the requirement of written informed consent for participation.

AUTHOR'S NOTE

All authors wish to stress that they are scientifically independent and have full freedom to act without any obligation to industry other than scientific advice to companies in the context of licensed patents. The selection of antibodies by the EuroFlow consortium is always explicitly based on quality, relevance, and continuous availability. Consequently all proposed antibody panels consist of mixtures of antibodies from many different companies.

AUTHOR CONTRIBUTIONS

MBu, TK, AO, and JD contributed to the conception and design of the study. TK, MBa, MBl, MP-A, BB, VK, CB, JP, EB, IP-K, JHMPP, BW-K, MP, JT, FH, HA, RF, TF, MS, AŠ, and SA-M performed the data acquisition and data analysis. MBa, TK, and MBu wrote the manuscript. All authors contributed to manuscript revision, read and approved the submitted version.

FUNDING

MBa was supported by Grant Agency of the Charles university (GAUK316218); MBl by ZonMW project 543002002 (SONNET study); VK by project NV19-05-00332 from Ministry of Health, and TK by project LO1604 from Ministry of Education, Youth and Sports Czech Republic and cytometer instrument was supported by EU-Prague project CZ.2.16/3.1.00/24505. MP-A was supported by a grant from Fundación Mutua Madrileña (Madrid, Spain). The EuroFlow Consortium received support from the FP6-2004-LIFESCIHEALTH-5 program of the European Commission (grant LSHB-CT-2006-018708) as Specific Targeted Research Project (STREP).

SUPPLEMENTARY MATERIAL

The Supplementary Material for this article can be found online at: <https://www.frontiersin.org/articles/10.3389/fimmu.2020.00371/full#supplementary-material>

Supplemental Figure 1 | Detailed gating strategy.

Supplemental Figure 2 | Detailed flow cytometry dot plots for SCID patients.

Supplemental Figure 3 | Detailed flow cytometry dot plots for other PID patients.

REFERENCES

- Fischer A, Le Deist F, Hacein-Bey-Abina S, André-Schmutz I, Basile G de Saint, de Villartay J-P, et al. Severe combined immunodeficiency. A model disease for molecular immunology and therapy. *Immunol Rev.* (2005) 203:98–109. doi: 10.1111/j.0105-2896.2005.00223.x
- Fischer A, Notarangelo LD, Neven B, Cavazzana M, Puck JM. Severe combined immunodeficiencies and related disorders. *Nat Rev Dis Prim.* (2015) 1:15061. doi: 10.1038/nrdp.2015.61
- Cicalese MP, Aiuti A. Clinical applications of gene therapy for primary immunodeficiencies. *Hum Gene Ther.* (2015) 26:210–9. doi: 10.1089/hum.2015.047
- Mamcarz E, Zhou S, Lockey T, Abdelsamed H, Cross SJ, Kang G, et al. Lentiviral gene therapy combined with low-dose busulfan in infants with SCID-X1. *N Engl J Med.* (2019) 380:1525–34. doi: 10.1056/NEJMoa1815408
- Pai S-Y, Logan BR, Griffith LM, Buckley RH, Parrott RE, Dvorak CC, et al. Transplantation outcomes for severe combined immunodeficiency, 2000–2009. *N Engl J Med.* (2014) 371:434–46. doi: 10.1056/NEJMoa1401177
- Heimall J, Logan BR, Cowan MJ, Notarangelo LD, Griffith LM, Puck JM, et al. Immune reconstitution and survival of 100 SCID patients post-hematopoietic cell transplant: a PIDTC natural history study. *Blood.* (2017) 130:2718–27. doi: 10.1182/blood-2017-05-781849
- Speckmann C, Doerken S, Aiuti A, Albert MH, Al-Herz W, Allende LM, et al. A prospective study on the natural history of patients with profound combined immunodeficiency: an interim analysis. *J Allergy Clin Immunol.* (2017) 139:1302–10.e4. doi: 10.1016/j.jaci.2016.07.040
- Douek DC, Vescio RA, Betts MR, Brechley JM, Hill BJ, Zhang L, et al. Assessment of thymic output in adults after haematopoietic stem-cell transplantation and prediction of T-cell reconstitution. *Lancet.* (2000) 355:1875–81. doi: 10.1016/S0140-6736(00)02293-5
- Picard C, Bobby Gaspar H, Al-Herz W, Bousfiha A, Casanova J-L, Chatila T, et al. International union of immunological societies: 2017 primary immunodeficiency diseases committee report on inborn errors of immunity. *J Clin Immunol.* (2018) 96–128. doi: 10.1007/s10875-017-0464-9
- Bousfiha A, Jeddane L, Picard C, Ailal F, Bobby Gaspar H, Al-Herz W, et al. Phenotypic classification for primary immunodeficiencies. *J Clin Immunol.* (2018) 38:129–143. doi: 10.1007/s10875-017-0465-8
- Yu X, Almeida JR, Darko S, Van Der Burg M, Deravin SS, Malech H, et al. Human syndromes of immunodeficiency and dysregulation are characterized by distinct defects in T-cell receptor repertoire development. *J Allergy Clin Immunol.* (2014) 133:1109–15.e14. doi: 10.1016/j.jaci.2013.11.018
- Gennery A R. Immunological aspects of 22q11.2 deletion syndrome. *Cell Mol Life Sci.* (2012) 69:17–27. doi: 10.1007/s00018-011-0842-z
- van der Spek J, Groenwold RHHH, van der Burg M, van Montfrans JM. TREC based newborn screening for severe combined immunodeficiency disease: a systematic review. *J Clin Immunol.* (2015) 35:416–30. doi: 10.1007/s10875-015-0152-6
- Fronková E, Klocperk A, Svaton M, Nováková M, Kotrová M, Kayserová J, et al. The TREC/KREC assay for the diagnosis and monitoring of patients with DiGeorge syndrome. *PLoS ONE.* (2014) 9:e114514. doi: 10.1371/journal.pone.0114514
- Kwan A, Church JA, Cowan MJ, Agarwal R, Kapoor N, Kohn DB, et al. Newborn screening for severe combined immunodeficiency and T-cell lymphopenia in California: results of the first 2 years. *J Allergy Clin Immunol.* (2013) 132:140–50.e7. doi: 10.1016/j.jaci.2013.04.024
- Amatuni GS, Currier RJ, Church JA, Bishop T, Grimbacher E, Nguyen AA-C, et al. Newborn screening for severe combined immunodeficiency and T-cell lymphopenia in California, 2010–2017. *Pediatrics.* (2019) 143:2010–7. doi: 10.1542/peds.2018-2300
- Barbaro M, Ohlsson A, Borte S, Jonsson S, Zetterström RH, King J, et al. Newborn screening for severe primary immunodeficiency diseases in Sweden—a 2-year pilot TREC and KREC screening study. *J Clin Immunol.* (2017) 37:51–60. doi: 10.1007/s10875-016-0347-5
- Van Der Burg M, Kalina T, Perez-Andres M, Vlkova M, Lopez-Granados E, Blanco E, et al. The EuroFlow PID orientation tube for flow cytometric diagnostic screening of primary immunodeficiencies of the lymphoid system. *Front Immunol.* (2019) 10:246. doi: 10.3389/fimmu.2019.00246
- Müller SM, Ege M, Pottharst A, Schulz AS, Schwarz K, Friedrich W. Transplacentally acquired maternal T lymphocytes in severe combined immunodeficiency: a study of 121 patients. *Blood.* (2001) 98:1847–51. doi: 10.1182/blood.V98.6.1847
- Wahlstrom J, Patel K, Eckhart E, Kong D, Horn B, Cowan MJ, et al. Transplacental maternal engraftment and posttransplantation graft-versus-host disease in children with severe combined immunodeficiency. *J Allergy Clin Immunol.* (2017) 139:628–33.e10. doi: 10.1016/j.jaci.2016.04.049
- Roifman CM, Somech R, Kavadas F, Pires L, Nahum A, Dalal I, et al. Defining combined immunodeficiency. *J Allergy Clin Immunol.* (2012) 130:177–83. doi: 10.1016/j.jaci.2012.04.029
- Appay V, van Lier RAW, Sallusto F, Roederer M. Phenotype and function of human T lymphocyte subsets: consensus and issues. *Cytometry A.* (2008) 73:975–83. doi: 10.1002/cyto.a.20643
- Mahnke YD, Brodie TM, Sallusto F, Roederer M, Lugli E. The who's who of T-cell differentiation: human memory T-cell subsets. *Eur J Immunol.* (2013) 43:2797–809. doi: 10.1002/eji.201343751
- Livak F, Schatz DG. T-cell receptor alpha locus V(D)J recombination by-products are abundant in thymocytes and mature T cells. *Mol Cell Biol.* (1996) 16:609–18. Available at: <http://www.ncbi.nlm.nih.gov/pubmed/8552089> doi: 10.1128/MCB.16.2.609
- Kimmig S, Przybylski GK, Schmidt CA, Laurisch K, Möwes B, Radbruch A, et al. Two subsets of naive T helper cells with distinct T cell receptor excision circle content in human adult peripheral blood. *J Exp Med.* (2002) 195:789–94. doi: 10.1084/jem.20011756
- Kohler S, Thiel A. Life after the thymus: CD31+ and CD31-human naive CD4+ T-cell subsets. *Blood.* (2009) 113:769–74. doi: 10.1182/blood-2008-02-139154
- de Saint-Basile G, Le Deist F, de Villartay JP, Cerf-Bensussan N, Journet O, Brousse N, et al. Restricted heterogeneity of T lymphocytes in combined immunodeficiency with hypereosinophilia. (Omenn's syndrome). *J Clin Invest.* (1991) 87:1352–9. doi: 10.1172/JCI115139
- van der Velden VHJ, Flores-Montero J, Perez-Andres M, Martin-Ayuso M, Crespo O, Blanco E, et al. Optimization and testing of dried antibody tube: the EuroFlow LST and PIDOT tubes as examples. *J Immunol Methods.* (2019) 475:112287. doi: 10.1016/j.jim.2017.03.011
- Kalina T, Flores-Montero J, van der Velden VHJ, Martin-Ayuso M, Böttcher S, Ritgen M, et al. EuroFlow standardization of flow cytometer instrument settings and immunophenotyping protocols. *Leukemia.* (2012) 26:1986–2010. doi: 10.1038/leu.2012.122
- Flores-Montero J, Sanoja-Flores L, Paiva B, Puig N, Garcia-Sánchez O, Böttcher S, et al. Next Generation Flow for highly sensitive and standardized detection of minimal residual disease in multiple myeloma. *Leukemia.* (2017) 31:2094–103. doi: 10.1038/leu.2017.29
- Glier H, Novakova M, te Marvelde J, Bijkerk A, Morf D, Thurner D, et al. Comments on EuroFlow standard operating procedures for instrument setup and compensation for BD FACS Canto II, Navios and BD FACS lyric instruments. *J Immunol Methods.* (2019) 475:112680. doi: 10.1016/j.jim.2019.112680

32. Magerus-Chatinet A, Stolzenberg M-C, Loffredo MS, Neven B, Schaffner C, Ducrot N, et al. FAS-L, IL-10, and double-negative CD4-CD8- TCR α/β + T cells are reliable markers of autoimmune lymphoproliferative syndrome. (ALPS) associated with FAS loss of function. *Blood*. (2009) 113:3027-30. doi: 10.1182/blood-2008-09-179630
33. Morio T, Takase K, Okawa H, Oguchi M, Kanbara M, Hiruma F, et al. The increase of non-MHC-restricted cytotoxic cells. (gamma/delta-TCR-bearing T cells or NK cells) and the abnormal differentiation of B cells in Wiskott-Aldrich syndrome. *Clin Immunol Immunopathol*. (1989) 52:279-90. doi: 10.1016/0090-1229(89)90179-7
34. van Gent R, van Tilburg CM, Nibbelke EE, Otto SA, Gaiser JF, Janssens-Korpela PL, et al. Refined characterization and reference values of the pediatric T- and B-cell compartments. *Clin Immunol*. (2009) 133:95-107. doi: 10.1016/j.clim.2009.05.020
35. Schatorjé EJH, Gemen EFA, Driessen GJA, Leuvenink J, van Hout RWNM, de Vries E. Paediatric reference values for the peripheral T cell compartment. *Scand J Immunol*. (2012) 75:436-44. doi: 10.1111/j.1365-3083.2012.02671.x
36. Comans-Bitter WM, De Groot R, Van den Beemd R, Neijens HJ, Hop WCJ, Groeneveld K, et al. Immunophenotyping of blood lymphocytes in childhood: reference values for lymphocyte subpopulations. *J Pediatr*. (1997) 130:388-93. doi: 10.1016/S0022-3476(97)70200-2
37. Takashima T, Okamura M, Yeh T-W, Okano T, Yamashita M, Tanaka K, et al. Multicolor flow cytometry for the diagnosis of primary immunodeficiency diseases. *J Clin Immunol*. (2017) 37:486-95. doi: 10.1007/s10875-017-0405-7
38. Van Dongen JJMM, Van Der Burg M, Kalina T, Perez-Andres M, Mejstrikova E, Vlkova M, et al. EuroFlow-based flowcytometric diagnostic screening and classification of primary immunodeficiencies of the lymphoid system. *Front Immunol*. (2019) 10:1271. doi: 10.3389/fimmu.2019.01271
39. Blanco E, Pérez-Andrés M, Arriba-Méndez S, Contreras-Sanfeliciano T, Criado I, Pelak O, et al. Age-associated distribution of normal B-cell and plasma cell subsets in peripheral blood. *J Allergy Clin Immunol*. (2018) 141:2208-19.e16. doi: 10.1016/j.jaci.2018.02.017
40. Villa A, Notarangelo LD, Roifman CM. Omenn syndrome: inflammation in leaky severe combined immunodeficiency. *J Allergy Clin Immunol*. (2008) 122:1082-6. doi: 10.1016/j.jaci.2008.09.037
41. IJspeert H, Driessen GJ, Moorhouse MJ, Hartwig NG, Wolska-Kusnierz B, Kalwak K, et al. Similar recombination-activating gene. (RAG) mutations result in similar immunobiological effects but in different clinical phenotypes. *J Allergy Clin Immunol*. (2014) 133:1124-33. doi: 10.1016/j.jaci.2013.11.028
42. Hazenberg MD, Borghans J a M, de Boer RJ, Miedema F. Thymic output: a bad TREC record. *Nat Immunol*. (2003) 4:97-9. doi: 10.1038/ni0203-97
43. Tanaskovic S, Fernandez S, Price P, Lee S, French MA. CD31. (PECAM-1) is a marker of recent thymic emigrants among CD4+ T-cells, but not CD8+ T-cells or gammadelta T-cells. *Immunol Cell Biol*. (2010) 88:321-7. doi: 10.1038/icb.2009.108
44. Hazenberg MD, Verschuren MC, Hamann D, Miedema F, van Dongen JJ. T cell receptor excision circles as markers for recent thymic emigrants: basic aspects, technical approach, and guidelines for interpretation. *J Mol Med*. (2001) 79:631-40. doi: 10.1007/s001090100271
45. Hazenberg MD, Otto S a, de Pauw ES, Roelofs H, Fibbe WE, Hamann D, et al. T-cell receptor excision circle and T-cell dynamics after allogeneic stem cell transplantation are related to clinical events. *Blood*. (2002) 99:3449-53. doi: 10.1182/blood.V99.9.3449
46. Hazenberg MD, Otto SA, Cohen Stuart JW, Verschuren MC, Borleffs JC, Boucher Ca, et al. Increased cell division but not thymic dysfunction rapidly affects the T-cell receptor excision circle content of the naive T cell population in HIV-1 infection. *Nat Med*. (2000) 6:1036-42. doi: 10.1038/79549
47. Junge S, Kloeckener-Gruissem B, Zufferey R, Keisker A, Salgo B, Fauchere J-C, et al. Correlation between recent thymic emigrants and CD31+ (PECAM-1) CD4+ T cells in normal individuals during aging and in lymphopenic children. *Eur J Immunol*. (2007) 37:3270-80. doi: 10.1002/eji.200636976
48. Game DS, Rogers NJ, Lechler RI. Acquisition of HLA-DR and costimulatory molecules by T cells from allogeneic antigen presenting cells. *Am J Transplant*. (2005) 5:1614-25. doi: 10.1111/j.1600-6143.2005.00916.x
49. Martinelli S, Krumbach OHF, Pantaleoni F, Coppola S, Amin E, Pannone L, et al. Functional dysregulation of CDC42 causes diverse developmental phenotypes. *Am J Hum Genet*. (2018) 102:309-20. doi: 10.1016/j.ajhg.2017.12.015
50. Takenouchi T, Kosaki R, Niizuma T, Hata K, Kosaki K. Macrothrombocytopenia and developmental delay with a *de novo* CDC42 mutation: yet another locus for thrombocytopenia and developmental delay. *Am J Med Genet A*. (2015) 167A:2822-5. doi: 10.1002/ajmg.a.37275
51. Seidel MG, Kindle G, Gathmann B, Quinti I, Buckland M, van Montfrans J, et al. The European Society for Immunodeficiencies. (ESID) registry working definitions for the clinical diagnosis of inborn errors of immunity. *J Allergy Clin Immunol Pract*. (2019) 7:1763-70. doi: 10.1016/j.jaip.2019.02.004

Conflict of Interest: JD, AO, MBu, MP-A, TK, and EB each report being one of the inventors on the EuroFlow-owned patent PCT/NL 2015/ 050762 (Diagnosis of primary immunodeficiencies). The Infinicyt software is based on intellectual property (IP) of some EuroFlow laboratories (University of Salamanca in Spain and Federal University of Rio de Janeiro in Brazil) and the scientific input of other EuroFlow members. All above mentioned intellectual property and related patents are licensed to Cytognos (Salamanca, ES), which pays royalties to the EuroFlow Consortium. These royalties are exclusively used for continuation of the EuroFlow collaboration and sustainability of the EuroFlow consortium. JD and AO report an Educational Services Agreement from BD Biosciences (San José, CA) and a Scientific Advisor Agreement with Cytognos; all related fees and honoraria are for the involved university departments at Leiden University Medical Center and University of Salamanca, respectively.

The remaining authors declare that the research was conducted in the absence of any commercial or financial relationships that could be construed as a potential conflict of interest.

Copyright © 2020 Kalina, Bakardjieva, Blom, Perez-Andres, Barendregt, Kanderová, Bonroy, Philippé, Blanco, Pico-Knijnenburg, Paping, Wolska-Kusnierz, Pac, Tkaczyk, Haerynck, Akar, Formánková, Freiburger, Svatoň, Šedivá, Arriba-Méndez, Orfao, van Dongen and van der Burg. This is an open-access article distributed under the terms of the Creative Commons Attribution License (CC BY). The use, distribution or reproduction in other forums is permitted, provided the original author(s) and the copyright owner(s) are credited and that the original publication in this journal is cited, in accordance with accepted academic practice. No use, distribution or reproduction is permitted which does not comply with these terms.

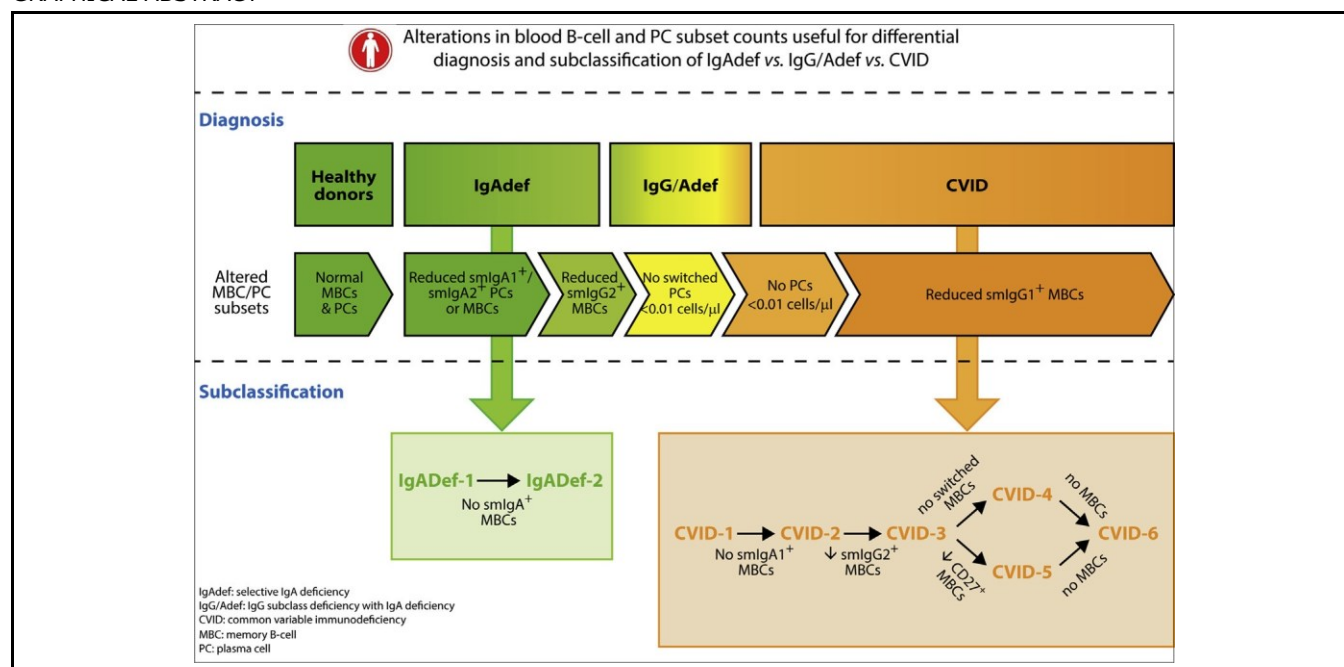
9.2. Defects in memory B-cell and plasma cell subsets expressing different immunoglobulin-subclasses in patients with CVID and immunoglobulin subclass deficiencies

Defects in memory B-cell and plasma cell subsets expressing different immunoglobulin-subclasses in patients with CVID and immunoglobulin subclass deficiencies



Elena Blanco, PhD,^{a,b*} Martín Perez-Andres, PhD,^{a,b*} Sonia Arriba-Mendez, MD, PhD,^c Cristina Serrano, MD,^d Ignacio Criado, PhD,^{a,b} Lucía Del Pino-Molina, PhD,^e Susana Silva, MD, PhD,^f Ignacio Madruga, MD,^g Marina Bakardjieva, MSc,^h Catarina Martins, PhD,ⁱ Ana Serra-Caetano, MSc,^f Alfonso Romero, MD,^j Teresa Contreras-Sanfeliciano, MD,^k Carolien Bonroy, PhD,^l Francisco Sala, MD,^m Alejandro Martín, MD, PhD,^{n,o} Jose María Bastida, MD, PhD,^{n,o} Félix Lorente, MD, PhD,^c Carlos Prieto, PhD,^p Ignacio Davila, MD, PhD,^q Miguel Marcos, MD, PhD,^g Tomas Kalina, MD, PhD,^h Marcela Vlckova, PhD,^r Zita Chovancova, MD, PhD,^r Ana Isabel Cordeiro, MD,^s Jan Philippe, MD, PhD,^l Filomeen Haerynck, MD, PhD,^t Eduardo Lopez-Granados, MD, PhD,^e Ana E. Sousa, PhD,^f Mirjam van der Burg, PhD,^{u,v} Jacques J. M. van Dongen, MD, PhD,^{w,t} and Alberto Orfao, MD, PhD,^{a,b,t} on behalf of the EuroFlow PID group
 Salamanca, Madrid, and Pamplona, Spain; Lisbon, Portugal; Prague and Brno, Czech Republic; Ghent, Belgium; and Rotterdam and Leiden, The Netherlands

GRAPHICAL ABSTRACT



From ^athe Department of Medicine, Cancer Research Centre (IBMCC, USAL-CSIC), Cytometry Service (NUCLEUS), University of Salamanca (USAL), Institute of Biomedical Research of Salamanca (IBSAL), Salamanca, and ^bthe Biomedical Research Networking Centre Consortium of Oncology (CIBERONC), number CB16/12/00400, Instituto de Salud Carlos III, Madrid; ^cServicio de Pediatría and ^dServicio de Bioquímica Clínica, Hospital Universitario de Salamanca; ^eServicio de Inmunología, Fundación Jiménez Díaz, Madrid; the Clinical Immunology Department, University Hospital La Paz and Physiopathology of Lymphocytes in Immunodeficiencies Group, IdiPAZ Institute for Health Research, Madrid; ^fInstituto de Medicina Molecular, Faculdade de Medicina, Universidade de Lisboa, Lisbon; ^gServicio de Medicina Interna, Hospital Universitario de Salamanca, Institute for Biomedical Research of Salamanca, Department of Medicine, University of Salamanca, Salamanca; ^hCLIP, Department of Haematology/Oncology, 2nd Faculty of Medicine, Charles University, Prague; ⁱNOVA Medical School/Faculdade de Ciências Médicas Universidade Nova de Lisboa, Lisbon; ^jCentro de Salud Miguel Armijo, Salamanca;

^kthe Department of Laboratory Medicine and ^lthe Department of Respiratory Diseases and Department of Pediatrics and Genetics, University Hospital Ghent; ^mServicio de Hematología, Hospital de Navarra, Pamplona; ⁿServicio de Hematología, Hospital Universitario de Salamanca, Institute for Biomedical Research of Salamanca, Salamanca; ^othe Biomedical Research Networking Centre Consortium of Oncology (CIBERONC) number CB16/12/00233, Instituto de Salud Carlos III, Madrid; ^pBioinformatics service (NUCLEUS), University of Salamanca, Salamanca; ^qServicio de Alergia, Hospital Universitario de Salamanca, Institute for Biomedical Research of Salamanca, Biomedical and Diagnosis Science Department, University of Salamanca (USAL), Salamanca; ^rthe Department of Clinical Immunology and Allergology, St Anne's University Hospital, and Faculty of Medicine, Masaryk University, Brno; ^sHospital D. Estefânia, CHLC, Lisbon; ^tthe Department of Immunology, Erasmus MC, Rotterdam; ^uDepartment of Pediatrics, Laboratory for Immunology, Leiden University Medical Center, Leiden; and ^vthe Department of Immunohematology and Blood Transfusion, Leiden University Medical Center, Leiden.

Background: Predominantly antibody deficiencies (PADs) are the most prevalent primary immunodeficiencies, but their B-cell defects and underlying genetic alterations remain largely unknown.

Objective: We investigated patients with PADs for the distribution of 41 blood B-cell and plasma cell (PC) subsets, including subsets defined by expression of distinct immunoglobulin heavy chain subclasses.

Methods: Blood samples from 139 patients with PADs, 61 patients with common variable immunodeficiency (CVID), 68 patients with selective IgA deficiency (IgAdef), 10 patients with IgG subclass deficiency with IgA deficiency, and 223 age-matched control subjects were studied by using flow cytometry with EuroFlow immunoglobulin isotype staining. Patients were classified according to their B-cell and PC immune profile, and the obtained patient clusters were correlated with clinical manifestations of PADs.

Results: Decreased counts of blood PCs, memory B cells (MBCs), or both expressing distinct IgA and IgG subclasses were identified in all patients with PADs. In patients with IgAdef, B-cell defects were mainly restricted to surface membrane (sm)IgA¹ PCs and MBCs, with 2 clear subgroups showing strongly decreased numbers of smIgA¹ PCs with mild versus severe smIgA¹ MBC defects and higher frequencies of nonrespiratory tract infections, autoimmunity, and affected family members. Patients with IgG subclass deficiency with IgA deficiency and those with CVID showed defects in both smIgA¹ and smIgG¹ MBCs and PCs.

Reduced numbers of switched PCs were systematically found in patients with CVID (absent in 98%), with 6 different defective MBC (and clinical) profiles: (1) profound decrease in MBC numbers; (2) defective CD27¹ MBCs with almost normal IgG₃¹ MBCs; (3) absence of switched MBCs; and (4) presence of both unswitched and switched MBCs without and; (5) with IgG₂¹ MBCs; and (6) with IgA₁¹ MBCs.

Conclusion: Distinct PAD defective B-cell patterns were identified that are associated with unique clinical profiles. (J Allergy Clin Immunol 2019;144:809-24.)

Key words: Immunodeficiency, primary antibody deficiency, selective IgA deficiency, common variable immunodeficiency, immunophenotyping, immunoglobulins, immunoglobulin subclasses, memory B cells, plasma cells, flow cytometry, diagnosis, classification

Abbreviations used

CVID:	Common variable immunodeficiency
ESID:	European Society for Immunodeficiencies
GC:	Germinal center
HD:	Healthy donor
IgAdef:	Selective IgA deficiency
IgG/Adef:	IgG subclass deficiency with IgA deficiency
IgH:	Immunoglobulin heavy chain
IUIS:	International Union of Immunological Societies
LLN:	Lower limit of normal
MBC:	Memory B cell
NPV:	Negative predictive value
PAD:	Predominantly antibody deficiency
PC:	Plasma cell
PPV:	Positive predictive value
sm:	Surface membrane

Predominantly antibody deficiencies (PADs) are the most prevalent primary immunodeficiencies (50% to 70% of all primary immunodeficiencies)^{1,2} and comprise a heterogeneous spectrum of disorders with defective production of 1 or more immunoglobulin isotypes and/or immunoglobulin subclasses; the underlying pathogenic mechanisms remain largely unknown.^{1,2} Current classification of PADs strongly relies on the affected serum immunoglobulin heavy chain (IgH) isotype and subclass levels and includes (1) selective IgA deficiency (IgAdef) characterized by an isolated defect of serum IgA (prevalence, approximately 1:100-1,000 subjects)³⁻⁵; (2) IgG subclass deficiency with IgA deficiency (IgG/Adef) with reduced IgA and 1 or more IgG subclass serum levels (approximately 15% to 20% of IgA deficiencies)⁶; and (3) common variable immunodeficiency (CVID), which is characterized by low (total) IgG serum levels, decreased IgA and/or IgM levels, and a more severe clinical presentation but a lower prevalence (approximately 1:25,000-50,000 subjects).^{4,5} Although recurrent bacterial infections of the respiratory tract are the clinical hallmark of PADs, clinical manifestations vary substantially among patients, from (almost) asymptomatic cases to patients presenting with recurrent severe infections associated with other noninfectious disorders, such as autoimmunity, allergy, lymphoproliferation and organomegalies, enteropathy, and granulomatous disease.^{1,3,7-10}

*These authors contributed equally to this work as first authors.

†These authors contributed equally to this work as last authors.

E.B. was supported by a grant from the Junta de Castilla y Leon (Fondo Social Europeo, ORDEN EDU/346/2013, Valladolid, Spain). This work was supported by the CB16/12/00400 and CB/16/12/00233 grants (CIBERONC, Instituto de Salud Carlos III, Ministerio de Economía y Competitividad, Madrid, Spain, and FONDOS FEDER), the FIS PI12/00905-FEDER grant (Fondo de Investigación Sanitaria of Instituto de Salud Carlos III, Madrid, Spain) and a grant from Fundación Mutua Madrileña (Madrid, Spain). The coordination and innovation processes of this study were supported by the EuroFlow Consortium.


Disclosure of potential conflict of interest: E. Blanco, M. Perez-Andrés, T. Kalina, M. Vlkova, E. Lopez-Granados, M. van der Burg, J. J. M. van Dongen, and A. Orfao each report being one of the inventors on the EuroFlow-owned patent PCT/NL 2015/050762 (Diagnosis of primary immunodeficiencies), which is licensed to Cytognos, a company that pays royalties to the EuroFlow Consortium. J. J. M. van Dongen and A. Orfao

report an Educational Services Agreement from BD Biosciences. The rest of the authors declare that they have no relevant conflicts of interest.

Received for publication April 17, 2018; Revised January 29, 2019; Accepted for publication February 1, 2019.

Available online February 28, 2019.

Corresponding author: Alberto Orfao, MD, PhD, Department of Medicine, Cancer Research Center, University of Salamanca, Paseo de la Universidad de Coimbra s/n, 37007 Salamanca, Spain. E-mail: orfao@usal.es.

 The CrossMark symbol notifies online readers when updates have been made to the article such as errata or minor corrections

0091-6749
© 2019 The Authors. Published by Elsevier Inc. on behalf of the American Academy of Allergy, Asthma & Immunology. This is an open access article under the CC BY-NC-ND license (<http://creativecommons.org/licenses/by-nc-nd/4.0/>).
<https://doi.org/10.1016/j.jaci.2019.02.017>

Despite extensive efforts, genetic (ie, monogenic) alterations responsible for PADs are detected in less than 10% of cases.^{1,2,11} In such settings altered distributions of distinct blood B- and T-cell subpopulations determined by using flow cytometry might provide key (complementary) diagnostic information, particularly for patients with low serum antibody isotype levels and nonspecific clinical features.^{5,12,13} Thus controversial results have been reported in patients with CVID concerning the potential association between specific B-cell alterations, such as decreased (relative) numbers of CD27⁺ (antigen-experienced) switched B cells in blood and relevant clinical manifestations (eg, splenomegaly, granulomatous disease, and autoimmunity),¹⁴⁻¹⁸ whereas preservation of CD27⁺ class-switched memory B cells (MBCs) has been considered a surrogate marker for the ability to respond to vaccination.⁵ Similarly, decreased CD27⁺ (antigen-experienced) switched B-cell counts in blood have been associated with a worse clinical outcomes in patients with IgAdef,¹⁹ whereas decreased percentages of CD21⁺ B cells and increased proportions of immature/transitional B-cells have both been correlated to distinct CVID clinical profiles.^{15,18,20}

Despite all the above associations, the actual clinical relevance of these B-cell defects in patients with PADs still remains elusive. In addition, a significant clinical and functional B-cell heterogeneity is still observed among patients who present with similar patterns of alteration of B cells by using flow cytometry (eg, reduced numbers of switched MBCs).^{18,21} This is probably due to the limited number of B-cell populations investigated, the lack of appropriate age-matched reference ranges, or both in most studies. For example, in many studies focused on antigen-experienced B cells, no distinction is made between (relative long-living) MBCs and (newly generated) circulating plasma cells (PCs),^{14,15,19} and very few reports have investigated the precise relationship between defects in specific immunoglobulin isotypes and the number of blood B cells and PCs that express them.^{22,23} Moreover, thus far, no study has investigated the IgG₁ to IgG₄, and IgA₁ and IgA₂ subclass distribution within the PC and MBC compartments of patients with PADs. Finally, despite the fact that PADs can present at any age^{1,7,9,13} and major age-related differences exist in the distribution of blood B-cell subsets throughout life,²⁴ most reports on B-cell compartments in patients with PADs do not consider (normal) age-associated variations, and only a few studies subdivided healthy donors (HDs) and patients with PADs into a few (n = 5-3-4) age groups.^{17,20,23} Altogether, this reflects the potential relevance of a more in-depth evaluation of the B-cell compartment and its alterations in patients with PADs versus age-matched control subjects for improved diagnosis and classification of PADs.

Here, for the first time, we investigated the distribution of 41 distinct blood B-cell and PC subsets in 139 patients with PADs versus 223 age-matched control subjects. Based on the B-cell and PC defects encountered, distinct defective immune profiles were identified that are associated with both the diagnostic subtype and clinical manifestations of PADs.

METHODS

Patients and control subjects

Overall, 139 patients with PADs¹ (mean age, 32.6 ± 19 years; range, 4-87 years) and 223 HDs (mean age, 39.6 ± 28 years; range, 4-99 years) were studied. Patients with PADs were subclassified by the International Union of Immunological Societies (IUIS)⁴ and European Society for

Immunodeficiencies (ESID)⁵ criteria into 68 and 42 patients with IgAdef (mean age, 24.6 ± 17 years), respectively; 10 patients with IgG/Adef (mean age, 24.6 ± 14 years); and 61 patients with CVID (mean age, 41.6 ± 17 years). Twenty-six asymptomatic patients with IgAdef (mean age, 24.6 ± 15 years) with serum IgA levels of less than 7 mg/dL did not fulfill the ESID criteria⁵ for IgAdef and are referred to hereafter as ESID² versus ESID¹ IgAdef cases. EDTA-anticoagulated blood samples were collected at 8 different sites and centrally processed in 2 of them after informed consent was provided by each subject, their legal representatives, or both. The study was approved by local ethics committees.

Flow cytometric identification of blood B cells and their subsets

Total B-cell counts and distribution of 41 distinct B-cell subsets were analyzed by using flow cytometry after staining 10⁷ nucleated cells with the EuroFlow 12-color immunoglobulin isotype B-cell tube (see Table E1 in this article's Online Repository at www.jacionline.org) and bulk-lyse standard operating procedure (www.EuroFlow.org), as described elsewhere.^{25,26} Per sample, 5 × 10⁶ or more leukocytes were measured in LSRFortessa X-20 flow cytometers (Becton Dickinson Biosciences, San Jose, Calif). Instrument set-up and calibration were performed according to EuroFlow standard operating procedures (www.EuroFlow.org).²⁷ For data analysis, Infinicyt software (Cytogenes S.L., Salamanca, Spain) was used.

CD19⁺ B-cells and PCs were both identified by using low-to-intermediate forward light scatter and sideward light scatter and subsequently subclassified into 41 different subpopulations based on their maturation stage and expression of distinct immunoglobulin isotypes and immunoglobulin subclasses, as previously described,²⁴ by using the gating strategy detailed in the Methods section and Fig E1 in this article's Online Repository at www.jacionline.org. Briefly, the following B-cell subpopulations were defined based on their staining profile for CD19, CD38, CD24, CD21, CD27, CD5, surface membrane (sm)IgM, and smIgD: (1) CD27⁺CD38^{hi}CD24^{hi}CD5⁺smIgM⁺IgD⁺ immature/transitional B-cells; (2) CD27⁺CD38^{lo}CD24^{hi}CD5^{hi}smIgM⁺IgD⁺ naive B lymphocytes; (3) CD27⁺CD38^{lo}CD5⁺CD24^{hi}smIgM⁺IgD⁺ unswitched MBCs; (4) CD27⁺CD38^{lo}CD5⁺CD24^{hi}smIgM⁺IgD⁺ switched MBCs; and (5) CD27⁺CD38^{hi}CD5⁺CD21⁺CD24⁺ PCs. MBCs and PCs were further subclassified according to their immunoglobulin isotypes and immunoglobulin subclasses into (1) smIgM⁺IgD⁺, smIgD⁺-only, smIgA₁⁺, smIgA₂⁺, smIgG₁⁺, smIgG₂⁺, smIgG₃⁺, and smIgG₄⁺ MBCs and (2) smIgM⁻-only, smIgD⁺-only, smIgA₁⁺, smIgA₂⁺, smIgG₁⁺, smIgG₂⁺, smIgG₃⁺, and smIgG₄⁺ PCs, respectively. Finally, the above subpopulations of naive B lymphocytes and MBCs were placed in further subsets based on CD21 (CD21⁺ vs CD21⁻ naive and MBC subsets) and CD27 expression (CD27⁺ and CD27⁻ MBCs, see Fig E1). Absolute counts were calculated by using total B-cell counts based in a double-platform assay²⁸ and used throughout the study. Intra-laboratory and interlaboratory variability was assessed at the participating centers based on replicate measurements of the same samples to ensure comparable results at distinct sites (see Fig E2 in this article's Online Repository at www.jacionline.org).

Statistical analyses

Statistical analyses were performed with either the R (version 3.2.3; <https://www.r-project.org/>)²⁹ or SPSS (version 23.0; IBM, Armonk, NY) software packages. Kruskal-Wallis and Mann-Whitney *U* tests (for continuous variables) and χ^2 and Fisher exact tests (for categorical variable) were used, respectively, to investigate the statistical significance (set at $P \leq .05$) of differences observed between groups in B-cell subset counts and clinical features. Unsupervised clustering analysis of patient data based on the K-means learning algorithm³⁰ and Euclidean distances was performed by using blood B-cell subset absolute counts normalized by age group (see Table E2 in this article's Online Repository at www.jacionline.org) based on (previously reported) reference values of 140 age-matched subjects²⁴ and extended here to 223 individual Zlog₁₀ values (patient value/minimum normal value)². Age-normalized B-cell/PC subset values per patient were represented in heat maps by using gplots (R package),³¹

and 5th to 95th percentile values were used to define normal ranges per age group defined by a minimum of 20 subjects (see [Table E3](#) in this article's Online Repository at www.jacionline.org). Those B-cell and PC subsets with absolute counts that were less than the method's limit of detection (undetectable; <0.01 cells/mL) in at least 1 subject for more than 1 reference (HD) age group were excluded from the analysis (ie, IgD-only and IgG¹ PCs and MBCs and IgG₁¹, IgG₂¹, and IgG₃¹ PCs).

RESULTS

Blood B-cell and PC subset defects in patients with IgAdef

Once compared with age-matched HDs, most patients with IgAdef displayed normal total B-cell counts (93%), including normal immature/transitional (90%), naive (94%), and MBC (87%) counts (see [Table E4](#) in this article's Online Repository at www.jacionline.org). In contrast, numbers of (total) PCs, although being detected in every case (≥ 0.07 PCs/mL), were decreased in 49% of patients ([Fig 1](#) and see [Table E4](#)). When MBCs and PCs were dissected according to their pattern of expression of immunoglobulin subclasses, a greater frequency of altered cases was observed. Thus smIgA₁¹ and/or smIgA₂¹ PC counts were found to be reduced in blood in 97% of cases, with still detectable residual smIgA¹ PCs in 38% of the patients (PCs expressing both IgA subclasses were found in 26%, smIgA₁¹-only subclasses were found in 9%, and smIgA₂¹-only subclasses were found in 3% of all patients with IgAdef).

In line with these findings, reduced smIgA₁¹ and/or smIgA₂¹ MBC counts were also observed in virtually all patients with IgAdef (99%), although still present in half (50%) of them (both smIgA₁¹ and smIgA₂¹ MBCs were detected in 40% and smIgA₁¹-only MBCs were detected in 10% of all patients with IgAdef; [Fig 2](#) and see [Table E4](#)). Thus decreased smIgA₁¹ or smIgA₂¹ MBC counts showed a sensitivity of 99% with a negative predictive value (NPV) of 100% (see [Table E5](#) in this article's Online Repository at www.jacionline.org), although when combined with decreased smIgA₁¹ or smIgA₂¹ PC counts, reached a 100% sensitivity and NPV (see [Table E6](#) in this article's Online Repository at www.jacionline.org). In turn, absence of the above MBC or PC subpopulations showed a specificity of 100% and positive predictive value (PPV) of 98% for identification of patients with IgAdef (see [Table E6](#)). In contrast, smIgG¹ PCs were present in virtually every patient with IgAdef (91%), with normal smIgG¹ PC counts in 71% of them. Similarly, smIgG₁¹ to smIgG₃¹ MBC counts were only decreased in 13% or fewer patients ([Fig 1](#) and see [Fig E3](#) and [Table E4](#)).

Blood B-cell and PC subset defects in patients with IgG/Adef

Similarly to patients with IgAdef, total peripheral blood B-cell counts, including immature/transitional, naive and MBC counts, were within the normal range in most patients with IgG/Adef (90%, [Fig 2](#) and see [Table E4](#)); in contrast, decreased PC counts were observed in 90% of patients with IgG/Adef, mostly because of a significant decrease in both smIgA¹ and smIgG¹ PC counts (100% and 90%, respectively), which were undetectable in 90% and 50% of cases, respectively. Although total blood MBC counts were within the normal range in 70% of patients with IgG/Adef showed decreased smIgA₁¹ MBC and/or smIgA₂¹ MBC counts in association with decreased smIgG₂¹ MBC counts; meanwhile,

smIgG₁¹ and smIgG₃¹ MBC counts were normal in 80% and 90% of patients with IgG/Adef, respectively ([Fig 1](#) and see [Fig E3](#) and [Table E4](#)).

Based on these results, the observation of undetectable PCs combined with decreased smIgG₂¹ MBC counts also showed a high sensitivity (90%), specificity (96%), and NPV (100%) for IgG/Adef in addition to those MBC and PC populations that identified IgAdef. In contrast, the PPV was only 50% because of the low number of patients with IgG/Adef analyzed ([Fig 1](#) and see [Tables E6](#) and [E7](#) in this article's Online Repository at www.jacionline.org).

Blood B-cell and PC subset defects in patients with CVID

In contrast to patients with IgAdef, total B-cell and PC counts were decreased in around half (51%) and the majority (98%) of patients with CVID, respectively ($P < .001$ vs patients with IgAdef). In addition, immature/transitional and naive B lymphocytes were decreased in 42% and 43% of patients with CVID, mostly at the expense of CD21⁺ B cells ([Fig 2](#) and see the [Results](#) section, [Fig E4](#), and [Table E4](#) in this article's Online Repository at www.jacionline.org), with only 10% and 3% of patients with CVID showing undetectable immature/transitional and naive B cells, respectively ([Fig 2](#) and see [Table E4](#)). Reduced smIgA₁¹ and/or smIgA₂¹ PC counts were found in all patients with CVID, being undetectable in virtually every (98%) case. In line with these findings, only 2% of patients with CVID showed circulating smIgG¹ PCs ([Fig 1](#) and see [Fig E3](#) and [Table E4](#)). Thus the absence of switched PCs was highly accurate (100% specificity, 100% PPV, and 100% NPV, with a sensitivity of 98%) for identification of CVID (see [Table E8](#) in this article's Online Repository at www.jacionline.org). Of note, no other parameter or combination of parameters showed an improved sensitivity, specificity, PPV, and NPV for identification of CVID than the absence of switched PCs or the lack of smIgA₂¹ PCs (see [Table E6](#)). However, the lack of switched PCs was not specific enough for an accurate differential diagnosis among distinct PAD subgroups because 9% of patients with IgAdef and 50% of patients with IgG/Adef also had undetectable switched PCs. Because of this, for a clear-cut discrimination among distinct PAD diagnostic categories, the lack of switched PCs needs to be combined with the absence or decrease in other B-cell subsets in patients with CVID that are typically normal among patients with IgAdef and those with IgG/Adef (eg, smIgG₁¹ or smIgG₂¹ MBCs, or total PCs; [Fig 1](#) and see [Table E4](#)). Interestingly, the (small) subgroup of patients with IgAdef who had undetectable switched PCs also had lower serum IgG levels at diagnosis (data not shown).

Finally, despite abnormally low total MBC counts being observed in most patients with CVID (70%) and being undetectable (<0.01 MBCs/mL) in only 13% of cases, the degree of involvement of MBCs expressing different immunoglobulin isotypes and immunoglobulin subclasses varied significantly. Thus reduced smIgA₁¹ and/or smIgA₂¹ MBC counts were observed in virtually all patients with CVID (98%), being absent in most of them (80%). Regarding MBC subsets expressing distinct IgG subclasses, patients with CVID more frequently showed decreased or absent smIgG₂¹ (95% and 67% of patients, respectively) than smIgG₁¹ MBC counts (90% and 33% [$P > .05$]).

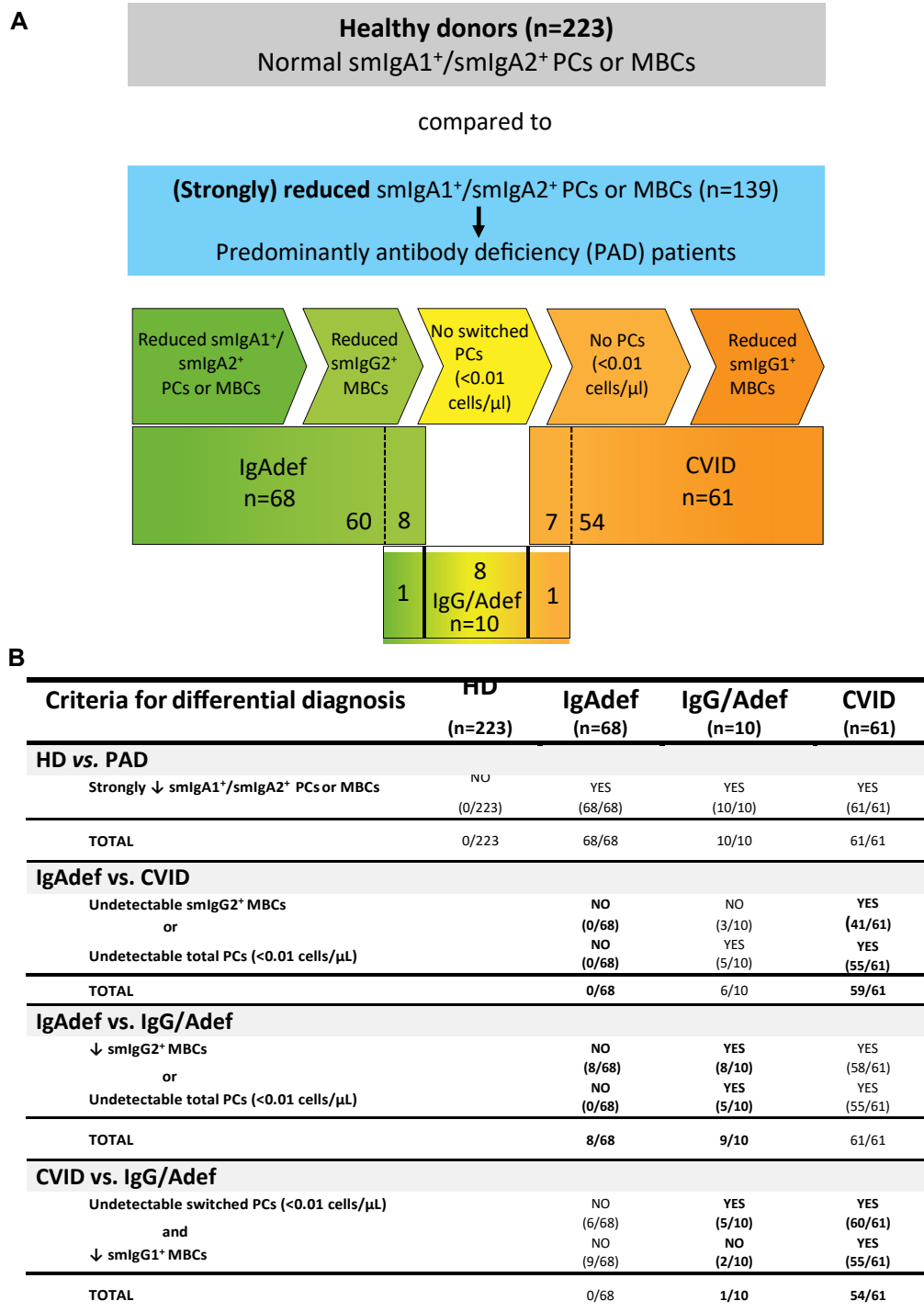


FIG 1. Alterations in blood B-cell and PC subset counts useful for the diagnosis of PADs and for the differential diagnosis of IgAdef versus IgG/Adef versus CVID. A, Scheme illustrating the most useful peripheral blood B-cell subset alterations for the diagnosis of PADs (vs HDs; strongly reduced: absolute numbers lower than the minimum value in HDs) and the differential diagnosis of patients with IgAdef versus patients with IgG/Adef versus patients with CVID are shown. As displayed, these criteria showed a 100% and approximately 98% accuracy in the diagnosis of PADs and the discrimination between IgAdef and CVID, respectively, whereas approximately 10% of cases within both diagnostic subgroups overlapped with 10% and 10% of patients with IgG/Adef, respectively. B, Most useful peripheral blood B-cell subset criteria for the diagnosis of PAD versus HDs and the distinction between patients with IgAdef versus patients with CVID, patients with IgAdef versus patients with IgG/Adef, and patients with CVID versus patients with IgG/Adef are shown, together with the number of cases within the different diagnostic categories that fulfilled these criteria.

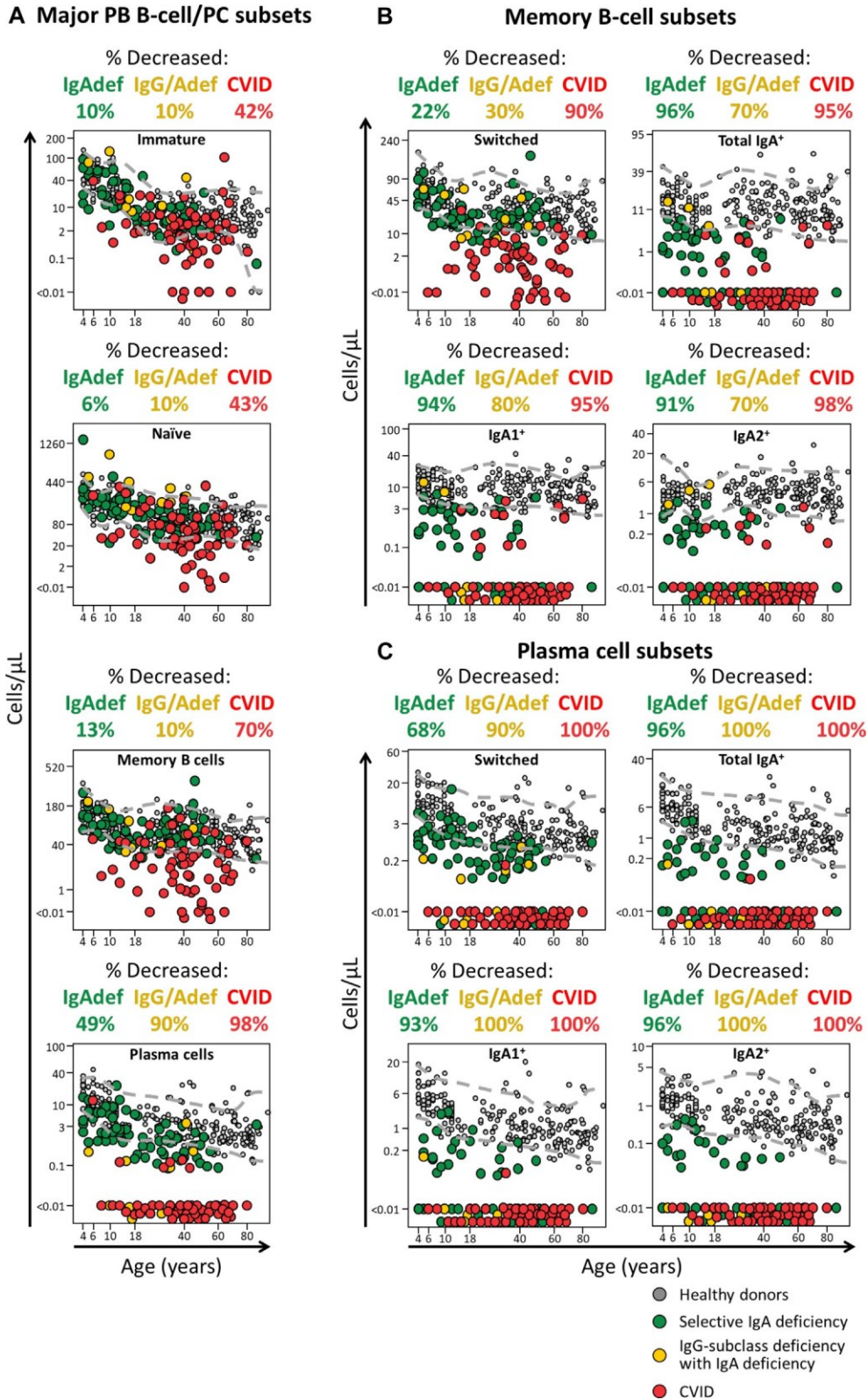


FIG 2. Absolute counts of distinct maturation-associated subpopulations of blood B cells and PCs (A) and total switched, total IgA, and IgA subclass subsets of MBCs (B) and PCs (C) in patients with IgAdef (n 5 68), patients with IgG/Adef (n 5 10), and patients with CVID (n 5 61) versus HDs (n 5 223) grouped by age. Individual cases are represented as green dots (IgAdef), yellow dots (IgG/IgAdef), red dots (CVID), and gray dots (HDs). Dotted gray lines represent age-associated reference 5th and 95th values. Percentages of patients with reduced numbers compared with reference values per age group are depicted above each plot by using the same color code.

and $P < .001$], respectively) and smIgG_3^1 MBC counts (61% and 23%, respectively; $P < .001$; Fig 1 and see Fig E3 and Table E4).

Classification of patients with PADs based on blood B-cell and PC subset immune profiles

Unsupervised clustering analysis identified 5 major immune profiles of altered blood B-cell and PC subset counts in patients with PADs (classification criteria are provided in Table I), which were closely related to the IUIS diagnostic categories of PADs and are termed hereafter PAD-1 to PAD-5 (Fig 3, A).⁴ Thus patients with IgAdef were split between the PAD-1 and PAD-2 clusters (with 1 outlier in PAD-3), and patients with IgG/Adef were split between the PAD-1, PAD-2, and PAD-3 groups, whereas most (54/61) patients with CVID fell into the PAD-3, PAD-4, and PAD-5 clusters, with 7 of 61 outliers falling into the PAD-1 and PAD-2 groups (Fig 3, A).

In detail, PAD-1 included 40 patients with reduced but detectable numbers of smIgA^1 PCs and/or smIgA^1 MBCs (smIgA^1 MBCs and smIgA^1 PCs ranging from <12-fold below the lower limit of normal [LLN] and undetectable to virtually normal counts, respectively). Thirty-two (80%) of 40 PAD-1 cases had been given a previous diagnosis of IgAdef and 2 (5%) of IgG/Adef, and 6 (15%) were patients with CVID with decreased but detectable numbers of IgA_1^1 or IgA_2^1 MBCs with limited effect on the overall number of smIgA^1 MBCs (never decreased >12 times the LLN) and virtually normal IgG_1^1 to IgG_3^1 MBC counts.

PAD-2 was characterized by severely decreased numbers of smIgA^1 MBCs (>40 times below the LLN; absent in 37 of 39 patients) and absence of smIgA^1 PCs but (similarly to PAD-1) virtually normal smIgG_1^1 to smIgG_3^1 MBC counts. This PAD-2 cluster included 35 (90%) patients with IgAdef, 3 (7.5%) patients with IgG/Adef, and 1 (2.5%) patient with CVID who lacked PCs and smIgA^1 MBCs but had normal smIgG^1 MBC numbers.

PAD-3 cases consisted of patients with severely decreased switched smIgG^1 and smIgA^1 PC counts (absent in 34/35 cases) and $\text{smIgA}_1^1/\text{smIgA}_2^1$ MBC counts (absent in 30/36 cases) but presenting with a heterogeneous defect on IgG^1 MBCs, consisting of severely reduced smIgG_2^1 MBC counts (absent in 19/36), with a milder decrease in smIgG_1^1 (86% of cases) and particularly smIgG_3^1 (39% of cases) MBC counts. This subgroup included 30 patients with CVID (83%), 5 patients with IgG/Adef (14%), and 1 patient with IgAdef (3%).

Finally, all PAD-4 and PAD-5 cases had undetectable smIgG_2^1 MBCs (14/14 cases) with severely reduced smIgG_1^1 MBC counts (14/14; absent in 9/14 cases; PAD-4) or no MBCs at all (PAD-5), except for 2 PAD-5 cases who showed detectable IgG_3^1 MBCs at levels of greater than 15-fold below the LLN; all PAD-4 and PAD-5 cases corresponded to CVID.

Blood B-cell and PC immune profiles in patients with IgAdef

Patients with IgAdef were split into 2 subgroups termed hereafter IgAdef-1 and IgAdef-2 (classification criteria are provided in Table I) with different patterns of alteration of smIgA^1 MBCs (Fig 3, B): smIgA_1^1 and/or smIgA_2^1 MBCs were present in the IgAdef-1 group, whereas they were virtually absent in IgAdef-2 cases (Fig 4, B, and Figs E5, A, and E6 in this article's Online Repository at www.jacionline.org). Interestingly, these 2

subgroups did not show a strong association with the ESID diagnostic criteria⁵ for clinical IgAdef, which were met in 53% of IgAdef-1 cases versus 69% of IgAdef-2 cases ($P > .05$; see Table E9, A, in this article's Online Repository at www.jacionline.org). Of note, IgAdef-1 cases were older than IgAdef-2 cases both at the time of analysis (31.6 ± 19 years vs 17.6 ± 13 years, respectively; $P = .001$) and at diagnosis (28.6 ± 19 years vs 14.6 ± 13 years, respectively; $P = .006$), with a similar male/female distribution. Despite no differences being observed in IgM serum levels at diagnosis, serum IgG levels were slightly lower in IgAdef-1 versus IgAdef-2 cases (1305.6 ± 290 vs 1467.6 ± 232 mg/dL, $P = .03$). In turn, although around one third of both IgAdef-1 and IgAdef-2 cases had a past history of recurrent respiratory tract infections at presentation, IgAdef-2 cases showed a greater frequency of other (recurrent) infections (17% vs 0%, respectively; $P = .02$), tissue-specific autoimmunity (31% vs 6%, respectively; $P = .01$), and other family members affected (22% vs 3%, respectively; $P = .03$; Fig 5, A, and see Table E10 in this article's Online Repository at www.jacionline.org).

Blood B-cell and PC immune profiles in patients with CVID

Overall, 6 subgroups of CVID (designated hereafter as CVID-1 to CVID-6) with different patterns of altered B-cell subsets and complete absence of switched PCs in 98% of cases (classification criteria are provided in Table I) were identified (Figs 3, C, and 4, C, and see Figs E5, B, and E6).

The CVID-1 and CVID-2 groups included patients with both detectable smIgMD^1 MBCs and switched MBCs of all smIgG_1 to smIgG_3 subclasses, with CVID-1 (but not CVID-2) cases also presenting normal or slightly reduced IgA_1^1 MBC counts. In contrast, CVID-3 cases showed a more severe smIgG_2^1 MBC defect (>4-fold below the LLN), frequently with undetectable (<0.01 cells/mL) smIgG_3^1 MBCs (17/22 cases). CVID-4 cases had no switched MBCs, whereas CVID-5 cases showed more severe defects involving all CD27⁺ MBC subsets (≥6-fold below the LLN) but almost normal CD27⁺ smIgG_3^1 MBC counts. Finally, CVID-6 cases had severely decreased switched and unswitched MBC counts, including 0.06 or fewer IgG_3^1 MBCs/mL (>15-fold below the LLN; Figs 3, C, and 4, C).

Overall, a close association between the CVID-1 and CVID-6 clusters and the EUROclass classification (see Table E11 in this article's Online Repository at www.jacionline.org)¹⁸ of CVID was observed. Thus EUROclass smB^1 patients were subclassified here into the CVID-1 (58%), CVID-2 (17%), and CVID-3 (25%) clusters, depending on their normal versus low smIgA^1 and smIgG_2^1 MBC counts. EUROclass B^2 patients were included in our CVID-6 cluster, except for 2 cases with less than 1% peripheral blood B cells but preserved MBC counts, who were thereby classified as CVID-4 and CVID-5, respectively. In fact, in 8 of 9 patients classified as B^2 , we could identify naive B cells, and in 4 of 9 cases we could also identify MBCs, despite these cells being severely decreased in 2 of them. In contrast, EUROclass smB^2 patients split across the different CVID-1 to CVID-6 clusters: CVID-1, 2.5%; CVID-2, 10%; CVID-3, 47.5%; CVID-4, 12.5%; CVID-5, 20%; and CVID-6, 7.5% of smB^2 cases (Fig 3, C, and see Table E9, B). Inclusion of other EUROclass parameters, such as CD21 expression (see Table E9, B) or immature/transitional B-cell counts did not result in significantly

TABLE I. Criteria used for subclassification of patients with PAD, patients with IgAdef, and patients with CVID into the PAD-1 to PAD-5, IgAdef-1 to IgAdef-2, and CVID-1 to CVID-6 clusters, respectively

Clusters	MBCs					
	Total MBCs	CD27 ⁺ MBCs	CD21 ⁺ MBCs	smIgM ⁺ IgD ⁺ MBCs	Switched MBCs	smIgA ⁺ MBCs
PAD-1	Normal or Y<2-fold			Normal or Y<1.4-fold	Normal or Y<3-fold	Normal or Y<12-fold
PAD-2	Normal or Y<1.4-fold			Normal or Y<1.1-fold	Normal or Y<2-fold	Y>40-fold or undetectable
PAD-3	Normal or Y<10-fold			Normal or Y<2-fold ^t	Normal or Y<100-fold	Y>2-fold or undetectable
PAD-4	Y1.4-46 fold			Y>2-fold or undetectable [§]	Y>12-fold or undetectable	Undetectable
PAD-5	Y>500-fold or undetectable			Undetectable	Y>190-fold or undetectable	Undetectable
IgAdef-1						Normal or Y<12-fold
IgAdef-2						Y>40-fold or undetectable
CVID-1	Normal	Normal or Y<1.4-fold	Normal or Y<1.8-fold	Normal or Y<1.4-fold	Normal or Y<3-fold	
CVID-2	Normal	Normal	Normal	Normal	Normal or Y<5-fold	
CVID-3	Normal or Y<5-fold [#]	Normal or Y<6-fold [#]	Normal or Y<8-fold [#]	Normal or Y<3-fold	Y>3-100 fold	
CVID-4	Y1.4-30 fold	Y1.3-30 fold	Y1.5-35 fold	Normal or Y<14-fold	Undetectable	
CVID-5	Y5-45 fold	Y>6-fold or undetectable	Y8-1000-fold	Y>3-fold or undetectable	Y>2-80 fold	
CVID-6	Y>500-fold or undetectable	Undetectable	Y>780-fold to undetectable	Undetectable	Y>185-fold or undetectable	

B-cell subpopulations that were not required for patient subclassification are plotted as empty cells. *Undetectable* is defined as less than 0.01 cells/mL. The most relevant subsets for discrimination between 2 or more subgroups are highlighted in boldface.

*Less than 15% of cases showed reduced smIgG₂⁺ MBC counts systematically associated with the presence of switched PCs or normal to less than 2-fold reduced smIgA⁺ MBC counts.

^tThose cases with smIgMD⁺ MBC counts reduced more than 2-fold systematically had normal smIgG⁺ MBC or detectable smIgG⁺ MBC counts.

^tOne case had detectable switched PCs (55-fold below the LLN) associated with decreased smIgG⁺ (>1.5-fold) and smIgG⁺ MBC counts and undetectable smIgA⁺ MBCs.

[§]One case had normal values associated with undetectable switched MBCs.

^kReduced smIgA₁ or smIgA PC counts were observed in all patients with IgAdef except 2 patients who had decreased smIgA⁺ MBC counts.

^zOne CVID case showed detectable but reduced switched PC counts.

[#]When smIgG₂⁺ MBCs were present, these subsets were systematically decreased.

different distributions of smB² patients across our CVID-1 to CVID-6 clusters (data not shown).

When considering the 6 CVID clusters, no overall differences were observed among them regarding age (at time of study and at diagnosis) and immunoglobulin serum levels, whereas significant differences were found in the frequency of autoimmunity ($P = .02$), autoimmune cytopenias ($P = .02$), and (a statistical trend) hepatomegaly ($P = 0.06$). Subsequent pairwise comparisons confirmed a similar age and sex distribution and frequency of recurrent infections (range, 83% to 100%) was observed among the 6 CVID clusters, except for CVID-6 cases, who were significantly older than CVID-2 cases ($P = .04$). In addition, no differences were observed regarding serum immunoglobulin levels at diagnosis and the clinical manifestations of the disease among patients with preserved smIgG₁⁺ MBCs (CVID-1, CVID-2, and CVID-3 cases). Conversely, all CVID-4 cases presented with autoimmunity versus 25% in CVID-1 ($P = .009$), 33% in CVID-2 ($P = 0.03$), and 50% in CVID-3 ($P = 0.04$) cases, including a greater frequency of autoimmune cytopenias (67% vs 0% in CVID-1 and CVID-2 cases and 20% in CVID-3 cases, $P < .05$) and a tendency ($P > .05$) toward a greater frequency of systemic

autoimmunity (50% vs 25% in CVID-1, 0% in CVID-2, and 10% in CVID-3 cases). Although systemic autoimmunity was not detected among CVID-5 cases ($P = .04$ vs CVID-4 cases), these cases more frequently had other adverse clinical features, such as hepatomegaly (44% vs 5% in CVID-3 cases, $P = .02$), autoimmunity (89% vs 25% in CVID-1 cases [$P = .01$], 33% in CVID-2 cases [$P < .05$], and 50% in CVID-3 cases [$P = .05$]), and cytopenias (44% vs 0% in CVID-1 cases, $P = .05$).

Finally, CVID-6 cases displayed a mixed clinical profile between CVID-4 and CVID-5 cases, with a high frequency of autoimmune cytopenias (50%), as well as hepatomegaly (56%), bronchiectasis (80%), and enteropathy (78%; Fig 5, B). Additionally, CVID-6 cases presented with granulomatous disease more frequently than all other CVID patient groups (30% vs 0% to 15%, $P = .06$; Fig 5, B, and see Table E12 in this article's Online Repository at www.jacionline.org).

DISCUSSION

Current IUIS and ESID guidelines for diagnosis and classification of PADs rely on antibody serum levels, response to

MBCs				PCs	
smIgA ₁ ⁺ MBCs	smIgG ₃ ⁺ MBCs	smIgG ₁ ⁺ MBCs	smIgG ₂ ⁺ MBCs	Switched PCs	smIgA ⁺ PCs
	Normal or Y<2-fold	Normal or Y<3-fold	Normal*	Detectable in >80% of cases	Y or undetectable in >90% of cases
	Normal or Y<2-fold	Normal or Y<1.3-fold	Normal*	Detectable in >80% of cases	Undetectable
	Normal or Y<12-fold	Normal or Y<65-fold	Y>1.4-fold or undetectable	Undetectable	Undetectable
	Y>1.2-fold or undetectable	Y>13-fold or undetectable	Undetectable	Undetectable	Undetectable
	Y>15-fold or undetectable	Undetectable	Undetectable	Undetectable	Undetectable
					Y or undetectable ^k
					Undetectable
Normal or Y<2-fold		Normal or Y<3-fold	Normal or Y<11-fold	Undetectable ^f	
Y>34-fold or undetectable		Normal or Y<4-fold	Normal or Y<12-fold	Undetectable	
Y>9-fold or undetectable		Y2-65-fold	Y>4-fold or undetectable	Undetectable	
Undetectable		Undetectable	Undetectable	Undetectable	
Y>20-fold or undetectable		Y>9-fold or undetectable	Y>80-fold or undetectable	Undetectable	
Undetectable		Undetectable	Undetectable	Undetectable	

vaccination, and clinical manifestations of PADs^{4,5,7} in the absence of well-defined genetic markers^{32,33}; in addition, an increased susceptibility to infections and autoimmunity or the existence of affected family members is required for the diagnosis of IgAdef per the ESID⁵ (but not IUIS) criteria. Although the number of affected serum antibody isotypes provides a rough estimation of susceptibility to less (eg, IgAdef) versus more severe (CVID) disease complications in the short term in patients with PADs,^{4,5} it cannot accurately predict the longer-term outcome of individual patients within each PAD subgroup, particularly after immunoglobulin replacement therapy. In these settings B-cell maturation-associated defects identified by using flow cytometry have proved useful for the diagnosis and classification of patients with CVID^{5,18,20} because they more precisely reflect the medium-term B cell-associated protective potential than their corresponding serum antibody isotype levels. However, some of the relationships observed in these studies between B-cell subset defects in blood and clinical manifestations of the disease^{14,15,18} have not been confirmed in other studies.¹⁶ Moreover, patients are usually classified based on relative B-cell subset numbers,^{14,15,18} which might be modified by changes in the other subsets,²⁰ and no

reference values per age group are used,^{14,15,18} which might limit the applicability of these classifications in, for example, children.³⁴ In addition, such B-cell defects have been poorly explored in patients with IgG/Adef and those with IgAdef,^{19,35} whereas the blood distribution of B cells and PCs expressing distinct immunoglobulin subclasses has not been investigated thus far in either patients with CVID or those with IgAdef.

Here, for the first time, we investigated the distribution of MBC and PC subsets that express distinct immunoglobulin isotypes and IgH subclasses in the blood of patients with PADs and correlated the altered immune profiles identified with the diagnostic subgroups and clinical manifestations of the disease. Because the blood B-cell compartment is highly dynamic across a patient's lifetime,^{24,36-39} B-cell defects were defined per age group.

Overall, every patient with CVID, IgG/Adef, or IgAdef studied here showed decreased counts for 1 or more B-cell subsets. This contrasts with previous flow cytometric studies that detected B-cell defects in only 6% to 86% of patients with PADs, namely 77% to 86% in patients with CVID,^{14,15,18,20,23,40,41} 6% to 25% in patients with IgAdef,^{19,35} and 30% in patients with selective IgG subclass deficiency (with or without IgAdef).⁴¹ This high

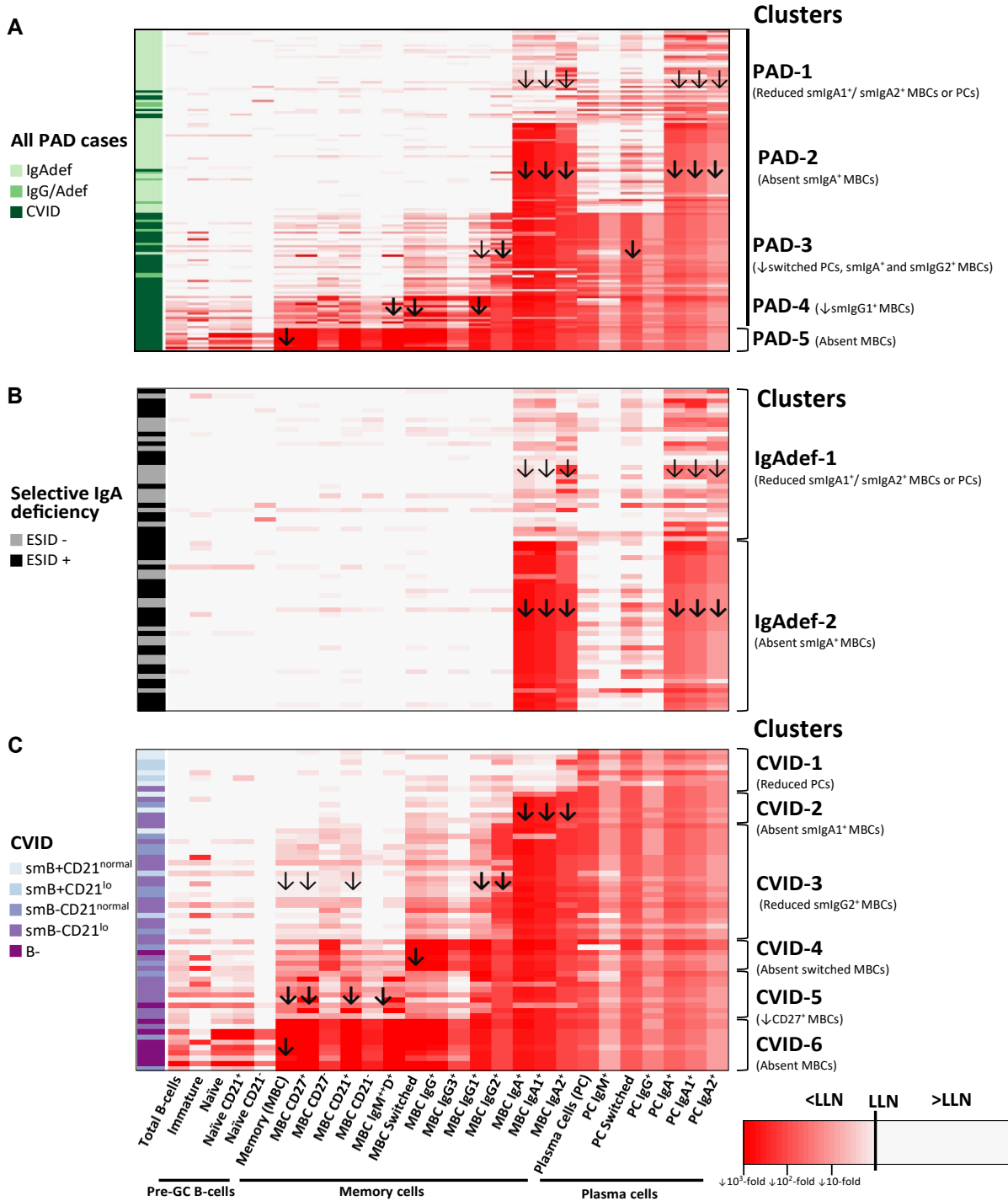
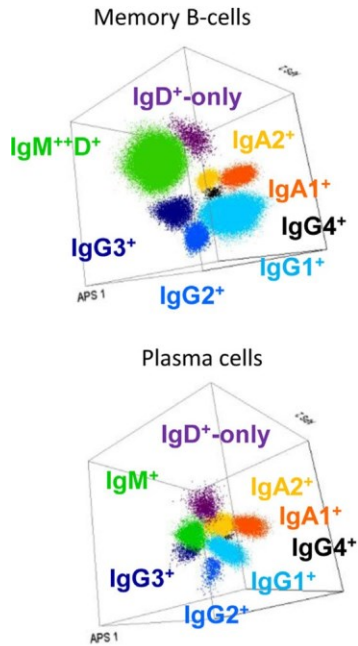
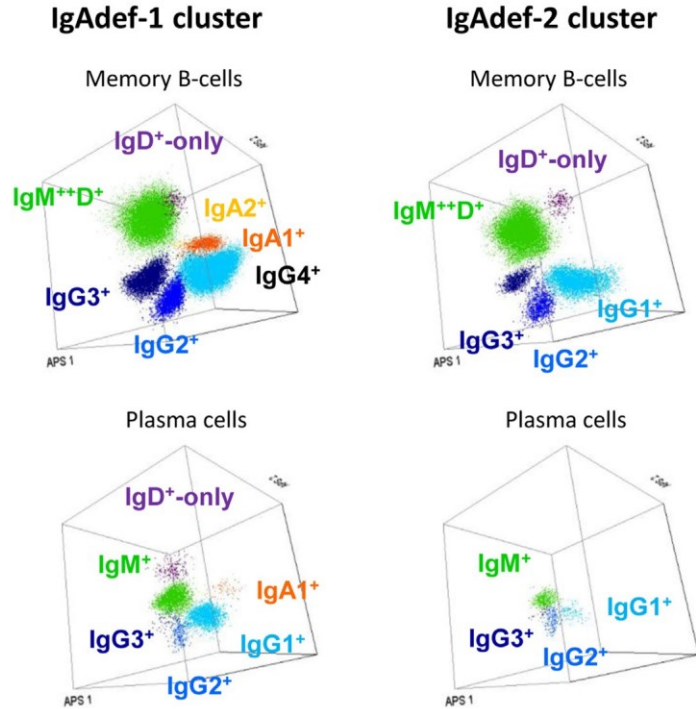


FIG 3. Clustering analysis–based heat map representing all patients with PADs (A) and those with IgAdef (B) and CVID (C) grouped according to their (altered) blood MBC and PC subset immune profiles. Each heat map represents absolute counts of the different B-cell subsets normalized by the LLN in HDs for the corresponding age group (columns) versus individual cases (rows). Higher red color intensities represent a deeper degree of deficiency in a log₁₀ scale compared with the corresponding age-matched LLN. Individual patients (rows) are identified by (1) their IUIS (clinical) diagnosis (Fig 3, A; light green for patients with IgAdef, intermediate green for patients with IgG/Adef, and dark green for patients with CVID); (2) their corresponding ESID IgAdef diagnosis (Fig 3, B), including IgAdef cases that fulfilled (black) or not (gray) the ESID criteria for IgAdef; and (3) CVID EUROclass classification subgroup (Fig 3, C), smB⁺CD21^{normal}, smB⁺CD21^{lo}, smB⁻CD21^{normal}, smB⁻CD21^{lo}, and B2 cells from lighter to darker violet. The here-defined PAD-1 to PAD-5 (Fig 3, A), IgAdef-1 and IgAdef-2 (Fig 3, B), and CVID-1 to CVID-6 (Fig 3, C) clusters identified by using the K-means algorithm, as well as the main characteristics of these groups, are depicted at the right side of each heat map. Black arrows indicate those MBC and PC subsets that contributed most to the specific identification of each patient cluster.

A Healthy donor



B Selective IgA deficiency



c CVID

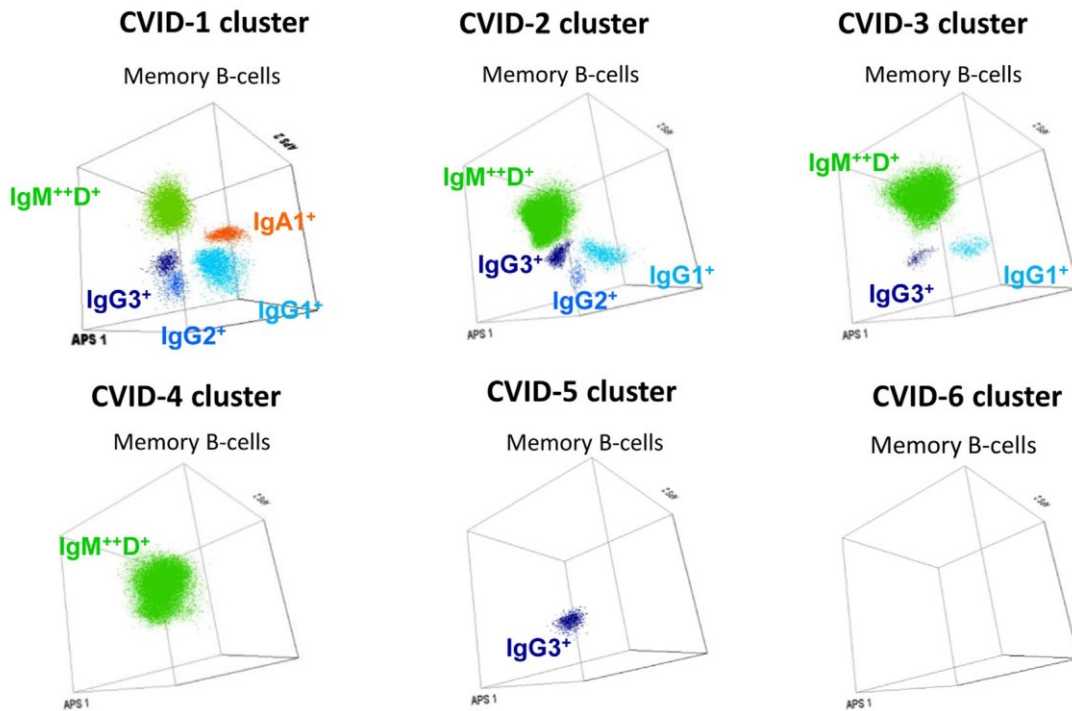


FIG 4. Illustrating dot plot examples of the numeric distribution of blood unswitched and switched MBC and PC subsets expressing different immunoglobulin isotypes and subclasses in a representative HD (A) and in representative patients with IgAdef (B) and CVID (C). Each plot corresponds to 3-dimensional Automated Population Separator (APS) views of principal component 1 (PC1) versus PC2 versus PC3 of the distinct subsets of MBCs and PCs defined by the immunoglobulin isotype and subclass expressed: IgM(D⁺) in green, IgG₁ in light blue, IgG₂ in intermediate blue, IgG₃ in dark blue, IgG₄ in black, IgA₁ in orange, IgA₂ in yellow, and IgD in violet. Additional cases from each group of patients with PADs are displayed in Figs E5 and E6.

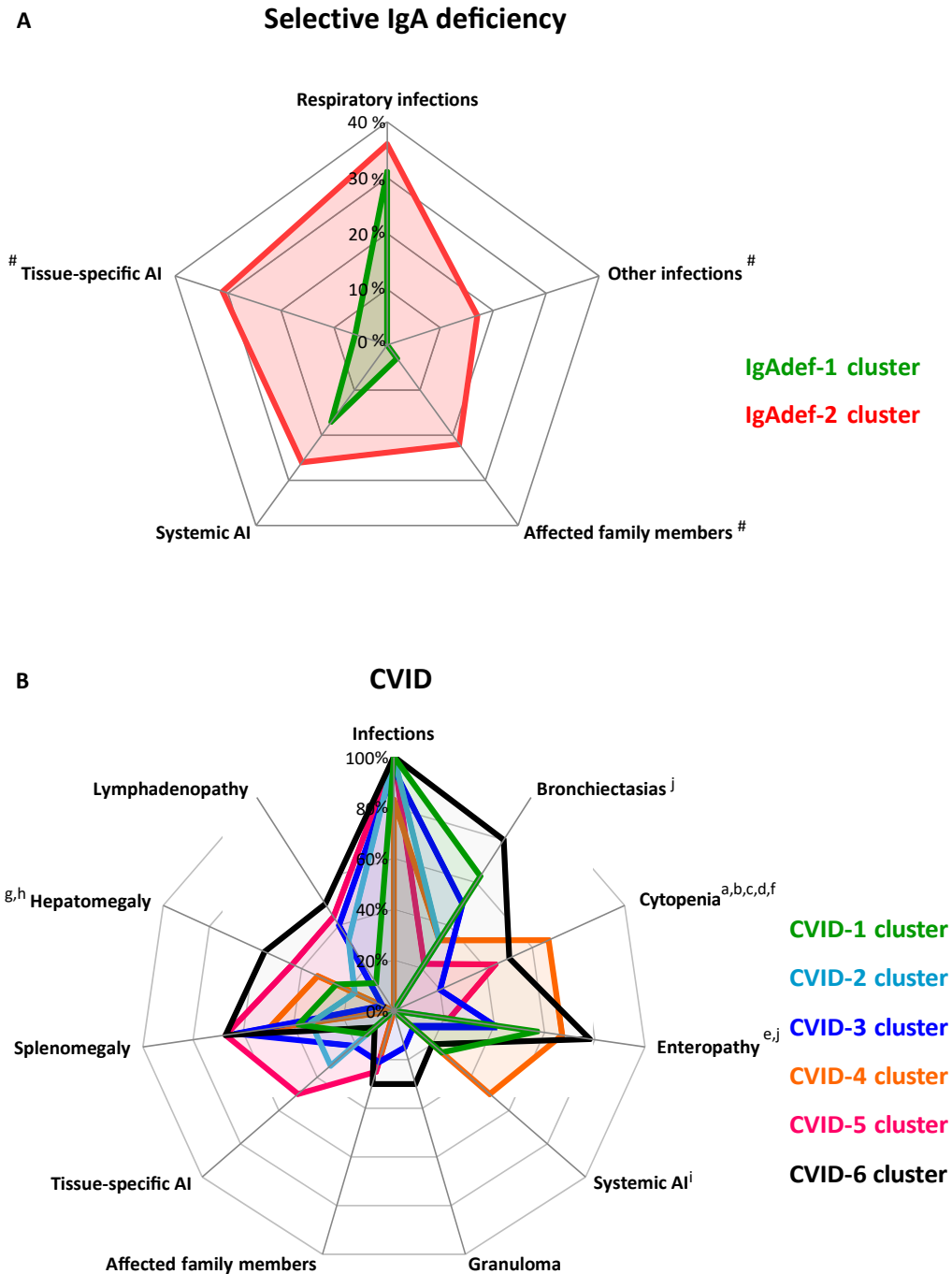


FIG 5. Frequency of distinct clinical manifestations of PADs and the existence (vs absence) of affected family members among the distinct clusters (ie, groups) of patients with IgAdef and those with CVID defined by their distinct patterns of altered blood B-cell and PC subset counts. Radar charts represent the percentage of patients with IgAdef (A) and patients with CVID (B) presenting with each type of clinical manifestation of the disease and the presence of family members affected by PADs. *Colored lines* indicate the distinct patient groups as defined by clustering analysis based on the B-cell and PC subset defects identified (see also Fig 3). # $P \leq .05$ for patients with IgAdef-1 versus IgAdef-2. ^a $P \leq .05$ for CVID-1 versus CVID-4. ^b $P \leq .05$ for CVID-1 versus CVID-5. ^c $P \leq .05$ for CVID-1 versus CVID-6. ^d $P \leq .05$ for CVID-2 versus CVID-4. ^e $P \leq .05$ for CVID-2 versus CVID-6. ^f $P \leq .05$ for CVID-3 versus CVID-4. ^g $P \leq .05$ for CVID-3 versus CVID-5. ^h $P \leq .05$ for CVID-3 versus CVID-6. ⁱ $P \leq .05$ for CVID-4 versus CVID-5. ^j $P \leq .05$ for CVID-5 versus CVID-6. AI, Autoimmunity.

frequency of B-cell defects most likely reflects the more detailed dissection of the blood B-cell and PC compartments together with the greater sensitivity of our method versus previous methods, use of age-matched reference ranges, or both. However, despite the

high sensitivity of the flow cytometric approach used here (similar to that of minimal residual disease detection by using next-generation flow^{25,42}), several minor B-cell subsets, particularly within the smIgG⁺ PC compartment (ie, smIgG⁺ to smIgG⁺

PCs), were undetectable (<0.01 cells/mL) in 1 or more HDs from 2 or more age groups, limiting their potential diagnostic utility. Consequently, these subsets were not considered in the present study. Acquisition of greater numbers of cells with a greater sensitivity will become feasible soon with the new generation of high-speed cytometers and might overcome this limitation.

Recently produced short-lived blood PCs,⁴³ particularly IgA¹ PCs, emerged as the most sensitive population for diagnosis of PADs, followed by switched and nonswitched MBCs, with progressively more severe immunologic defects in the spectrum of IgAdef to IgG/Adef and CVID. Thus decreased smIgA₁¹ and/or smIgA₂¹ PC counts were found in all patients with PADs, except in 2 patients with IgAdef, who showed reduced smIgA₁¹ and smIgA₂¹ MBC counts. In addition, decreased total and/or switched PC counts emerged as a hallmark of CVID, which is in line with previous bone marrow and lymph node findings.^{44,45} Of note, patients with IgAdef showed cellular defects typically restricted to smIgA¹ PCs and MBCs, despite IgG¹ MBC and PC counts also being decreased in 15% and 29% of patients with IgAdef versus 30% and 90% patients with IgG/Adef and 90% and 98% patients with CVID. Nevertheless, compared with a previous study²² in which less than 10% of patients with IgAdef had smIgA¹ MBCs, a greater percentage of our patients with IgAdef showed circulating smIgA¹ MBCs (50%), PCs (approximately 40%), or both. This discrepancy is probably caused by the greater sensitivity of our EuroFlow strategy and method with 5×10^6 or more (vs 5×10^4) cells analyzed.²²

Our findings are in line with those of previous studies demonstrating *S α* -switch recombination in blood B cells from 2 of 4 patients with IgAdef.⁴⁶ Interestingly, patients with IgAdef who showed a preserved IgA-switching capacity (IgAdef-1 cases) displayed a milder clinical phenotype, with less risk factors for CVID progression (eg, autoimmunity)⁴⁷ but a similar prevalence of recurrent respiratory tract infections. In addition, they were younger (both at presentation and at time of analysis) than IgAdef-2 cases, which could potentially reflect progressive accumulation of more severe defects in blood IgA¹ MBCs and PCs in parallel to a greater frequency and severity of clinical manifestations. However, all cases categorized as IgAdef-1 that have been re-evaluated (11/32) after a median follow-up of 25 months (range, 10-52 months) continue to show preserved IgA-switching capacity (data not shown), and none of the 26 IgAdef-2 cases followed since their inclusion in this study have evolved to CVID (median follow-up, 2 years; data not shown). Nonetheless, longer follow-up times are needed to rule out an effect of age at diagnosis on the altered blood B-cell immune profile and clinical manifestations of patients with IgAdef. Altogether, these findings suggest that detailed evaluation of blood B-cell and PC defects might contribute to an improved classification and clinical management of IgAdef patients.

Complete lack of blood switched PCs was the hallmark of CVID. Although reduced switched MBC counts have been extensively reported in patients with CVID,^{14-16,18,20} this is the first time that these cells were dissected at the immunoglobulin subclass level, similar to what is routinely done for serum IgG₁₋₄ levels. Progressive deterioration in IgG-switching capacity was observed in MBCs of patients with CVID, which directly correlated with their consecutive location in the *IGHC* gene locus: IgM $<$ IgG₃ $<$ IgG₁ $<$ IgG₂. In line with these results, Piqueras et al¹⁴ showed a similar pattern of reduced mRNA expression for the different immunoglobulin isotypes/immunoglobulin

subclasses: IgM $>$ IgG₃ \geq IgG₁ $>$ IgG₂ $>$ IgA₁ $>$ IgA₂ $>$ IgG₄. At present, it is well established that downstream IgG subclasses are produced, at least in part, by consecutive switching of B-cells during repeated rounds of MBC response,⁴⁸⁻⁵¹ leading to a greater frequency of somatic hypermutation^{48,50,51} and switch regions bearing remnants of indirect class-switching⁵⁰ in cells expressing downstream immunoglobulin isotypes/immunoglobulin subclasses. Interestingly, we recently identified a similar pattern of sequential production of MBC expressing distinct immunoglobulin subclasses during a lifetime.²⁴

These findings, together with recent observations using genome-wide sequencing approaches, suggest that consecutive switching along the *IGHC* locus might deteriorate in patients with PADs, possibly because of combined hypomorphic/deleterious variants,⁵²⁻⁵⁴ haploinsufficient genes,⁵⁵⁻⁵⁸ and epigenetic modifications⁵⁹ involving B-cell response pathways rather than a single genetic defect. Progressive deterioration of sequential class-switching along the *IGHC* locus, along with reduced MBCs and lack of PCs, leads to a progressively more restricted repertoire and decreased functional capacity of MBCs expressing downstream IgG subclasses. Of note, previous flow cytometric approaches typically excluded patients with CVID with less than 1% B cells from further analyses (and subclassification) caused by insufficient B-cell numbers for robust dissection of its major subsets.^{15,18} However, here we were able to identify B cells also in all patients with CVIDs presenting less than 1% B cells, including circulating blood naive B cells in 8 of 9 cases and MBCs in 4 of 9 cases; this is in contrast to *BTK*-deficient patients evaluated with this same highly sensitive approach, who systematically showed undetectable peripheral blood B cells (data not shown).

Among different approaches used to categorize CVID, the EUROclass classification (see Table E11) is the most widely used because of its clinical utility. This classification allows us to relate alterations in the distribution of peripheral blood B-cell subsets with the presence of clinical manifestations, such as a decrease in MBC counts (smB² group) and the occurrence of splenomegaly, as also confirmed here (see Table E13 in this article's Online Repository at www.jacionline.org). In this regard our proposed stratification criteria for CVID into CVID-1 to CVID-6 clusters based on MBC immunoglobulin isotype and IgH-subclass subset immune profile in blood also showed association with other disease features (eg, autoimmune cytopenias and hepatomegaly) that have been related to a lower survival in patients with CVID¹⁰ but that did not correlate with the EUROclass classification either in the present or other larger previously reported CVID patient series.¹⁸ In addition, the highly sensitive approach used here allowed detection of low blood MBC and PC counts expressing IgG₁ to IgG₄ and IgA₁ to IgA₂ subclasses, demonstrating that most patients with CVID retain the ability for class-switching, including the great majority ($>70\%$) of smB² cases presenting with dramatically reduced numbers of switched MBCs.¹⁸ This is consistent with more laborious functional studies that demonstrated the (residual) capacity of B cells to produce IgG, also among smB² patients.²¹ In fact, our EuroFlow strategy for highly sensitive immunoglobulin subclass analysis of blood B cells and PCs identified 6 CVID subgroups with different IgG-switching patterns and clinical profiles, even within smB² patients with CVIDs. The 3 clinically milder subgroups included patients capable of producing MBCs of the (first 3) IgM/IgD, IgG₃, and IgG₁ immunoglobulin isotypes/subclasses located upstream in

the *IGHC* locus (independently of smIgG₂¹ and IgA¹ MBC counts), who might require less IgG substitution therapy.²¹ In fact, despite patients of all groups having a greater frequency of infection, those within the CVID-1 to CVID-3 groups required less hospital care (data not shown). CVID-4 cases were still capable of CD27¹ unswitched MBC production and typically presented with cytopenias, such as in patients with hyper-IgM syndromes.⁶⁰⁻⁶² However, they had no PCs (including no IgM¹ PCs in all but 1 case), and they showed a typical CVID-related serum antibody profile in the absence of *in vitro* functional defects associated with hyper-IgM syndromes (data not shown).⁶³ Interestingly, 3 of 4 patients with rheumatoid arthritis (an immune complex-mediated autoimmune disease⁶⁴) in our series clustered together in the CVID-4 cluster (data not shown), which only has preserved IgM¹IgD¹ MBCs.

The 2 clinically more severe CVID-5 and (particularly) CVID-6 patient subgroups had dramatically decreased CD27¹ unswitched and switched MBC counts, except for CD27²CD21²IgG₃¹ MBC counts, which were found to be almost normal in CVID-5 (but not CVID-6) cases. From the clinical point of view, CVID-5 and CVID-6 cases specifically showed disease symptoms (eg, organomegalies) reflecting an impaired ability to mount germinal center (GC) responses.^{24,50,65} Altogether, these findings suggest that even if the residual CD27²CD21²smIgG₃¹ MBCs could offer some immune protection in CVID-5 cases, in CVID-5 and CVID-6 cases the underlying immune dysregulation leads to a polyclonal lymphocytic infiltration of secondary lymphoid tissues previously associated with increased risk for lymphoid malignancy in patients with CVID.⁶⁶ In fact, all patients with hematologic tumors were clustered as CVID-5 and CVID-6 cases (see Table E12). Although it is tempting to hypothesize that such stepwise deterioration of IgG-switching capacity might reflect disease progression, no significant differences in age (or time from diagnosis) were observed among the above CVID patient subgroups (except for CVID-6 cases who were older at the time of analysis than CVID-2 cases and the time from diagnosis, which was greater in CVID-6 vs CVID-2 and CVID-3 cases, data not shown).

The most severe CVID immunologic phenotype, CVID-6, also showed significantly reduced pre-GC B-cell counts, reflecting a markedly defective bone marrow B-cell production.^{18,20,45} Most blood B cells in these patients showed an immature/transitional phenotype, reflecting their premature egress from bone marrow,⁴³ whereas residual naive B cells were enriched in the minor CD21^{lo} naive B-cell subset. Reduced pre-GC B-cell counts, together with the low *in vitro* response of both immature and CD21^{lo} naive B cells,^{43,67} might explain the marked antigen-experienced B-cell defect involving all immunoglobulin isotypes found in CVID-6 cases. In line with previous observations,²⁰ these patients also had decreased naive T CD4¹ and T CD8¹ counts versus age-matched HDs and other patients with CVID (data not shown), but they did not fulfill the diagnostic criteria for late-onset combined immunodeficiency.⁵ The potential existence of underlying hypomorphic defects and variants of genes related to the production of lymphocytes (*RAG*, *DCLRE1C*, and *NHEJ1*) previously related to CVID-like clinical phenotypes remains to be more deeply investigated in these CVID-6 cases.⁵²⁻⁵⁴

In summary, detailed dissection of circulating MBCs and PCs in patients with PADs into subsets expressing distinct immunoglobulin subclasses provides complementary information to serum antibody isotype levels and might contribute to a better

understanding of the pathogenesis of PADs and an improved diagnosis, subclassification, and monitoring (particularly in case of immunoglobulin replacement therapy) of the disease. Blood PCs emerged here as the most sensitive diagnostic blood cellular compartment, whereas analysis of blood MBC subsets appeared informative to discriminate patients with different clinical profiles. However, further multicentric studies in large age-matched case-control cohorts are needed to replicate and validate the clinical utility and feasibility of our proposed approach for detailed and sensitive dissection of blood B-cell and PC subsets for the diagnosis and classification of PADs. At the same time, use of EuroFlow databases and tools for automated gating and reporting of flow cytometric data will facilitate its implementation in routine diagnostics.^{68,69}

Key messages

- Evaluation of blood B cells and PCs expressing distinct immunoglobulin subclasses provides a new highly sensitive approach for identification of specific B-cell defects of potential diagnostic relevance in patients with PADs.
- Detailed dissection of blood MBC and PC subsets expressing different immunoglobulin subclasses identifies distinct deficient immune profiles in patients with primary antibody deficiencies, which correlate with both the diagnostic subtype and clinical manifestations of the disease.

REFERENCES

1. Durandy A, Kracker S, Fischer A. Primary antibody deficiencies. *Nat Rev Immunol* 2013;13:519-33.
2. Wood PM. Primary antibody deficiency syndromes. *Curr Opin Hematol* 2010;17:356-61.
3. Wang N, Hammarstrom L. IgA deficiency: what is new? *Curr Opin Allergy Clin Immunol* 2012;12:602-8.
4. Picard C, Bobby Gaspar H, Al-Herz W, Bousfiha A, Casanova J-L, Chatila T, et al. International Union of Immunological Societies: 2017 Primary Immunodeficiency Diseases Committee Report on Inborn Errors of Immunity. *J Clin Immunol* 2018;38:96-128.
5. Abinun M, Albert M, Buckland S.B.C.M, Bustamante J, Cant A, Casanova J-L, et al. ESID registry—working definitions for clinical diagnosis of PID; European Society for Immunodeficiencies. Available at: <https://esid.org/Working-Parties/Registry-Working-Party/Diagnosis-criteria>. Accessed January 10, 2019.
6. Ballou M. Primary immunodeficiency disorders: antibody deficiency. *J Allergy Clin Immunol* 2002;109:581-91.
7. Jolles S. The variable in common variable immunodeficiency: a disease of complex phenotypes. *J Allergy Clin Immunol Pract* 2013;1:545-56.
8. Yazdani R, Azizi G, Abolhassani H, Aghamohammadi A. Selective IgA deficiency: epidemiology, pathogenesis, clinical phenotype, diagnosis, prognosis and management. *Scand J Immunol* 2017;85:3-12.
9. Cunningham-Rundles C. The many faces of common variable immunodeficiency. *Hematology Am Soc Hematol Educ Progr* 2012;2012:301-5.
10. Chapel H, Lucas M, Patel S, Lee M, Cunningham-Rundles C, Resnick E, et al. Confirmation and improvement of criteria for clinical phenotyping in common variable immunodeficiency disorders in replicate cohorts. *J Allergy Clin Immunol* 2012;130:1197-8.
11. Chapel H. Common variable immunodeficiency disorders (CVID)—diagnoses of exclusion, especially combined immune defects. *J Allergy Clin Immunol Pract* 2016;4:1158-9.
12. Bertinchamp R, Gerard L, Boutboul D, Malphettes M, Fieschi C, Oksenhendler E, et al. Exclusion of patients with a severe T-cell defect improves the definition of common variable immunodeficiency. *J Allergy Clin Immunol Pract* 2016;4:1147-57.
13. Bonilla FA, Barlan I, Chapel H, Costa-Carvalho BT, Cunningham-Rundles C, de la Morena MT, et al. International consensus document (ICON): common variable immunodeficiency disorders. *J Allergy Clin Immunol Pract* 2016;4:38-59.

14. Piqueras B, Lavenu-Bombléd C, Galicier L, Bergeron-van der Cruyssen F, Mouthon L, Chevret S, et al. Common variable immunodeficiency patient classification based on impaired B cell memory differentiation correlates with clinical aspects. *J Clin Immunol* 2003;23:385-400.
15. Warnatz K, Denz A, Dräger R, Braun M, Groth C, Wolff-Vorbeck G, et al. Severe deficiency of switched memory B cells (CD27(1)IgM(-)IgD(-)) in subgroups of patients with common variable immunodeficiency: a new approach to classify a heterogeneous disease. *Blood* 2002;99:1544-51.
16. Al Kindi M, Mundy J, Sullivan T, Smith W, Kette F, Smith A, et al. Utility of peripheral blood B cell subsets analysis in common variable immunodeficiency. *Clin Exp Immunol* 2012;167:275-81.
17. Piątosza B, Pac M, Siewiera K, Pietrucha B, Klaudel-Dreszler M, Heropolitańska-Pliszka E, et al. Common variable immune deficiency in children—clinical characteristics varies depending on defect in peripheral B cell maturation. *J Clin Immunol* 2013;33:731-41.
18. Wehr C, Kivioja T, Schmitt C, Ferry B, Witte T, Eren E, et al. The EUROclass trial: defining subgroups in common variable immunodeficiency. *Blood* 2008;111:77-85.
19. Aghamohammadi A, Abolhassani H, Biglari M, Abolmaali S, Moazzami K, Tabatabaeiyan M, et al. Analysis of switched memory B cells in patients with IgA deficiency. *Int Arch Allergy Immunol* 2011;156:462-8.
20. Driessen GJ, van Zelm MC, van Hagen PM, Hartwig NG, Trip M, Warris A, et al. B-cell replication history and somatic hypermutation status identify distinct pathophysiologic backgrounds in common variable immunodeficiency. *Blood* 2011;118:6814-23.
21. Rösel AL, Scheibenbogen C, Schliesser U, Sollwedel A, Hoffmeister B, Hanitsch L, et al. Classification of common variable immunodeficiencies using flow cytometry and a memory B-cell functionality assay. *J Allergy Clin Immunol* 2015;135:198-208.
22. Marasco E, Farroni C, Cascioli S, Marcellini V, Scarsella M, Giorda E, et al. B-cell activation with CD40L or CpG measures the function of B-cell subsets and identifies specific defects in immunodeficient patients. *Eur J Immunol* 2017;47:131-43.
23. Driessen GJ, Dalm VASH, van Hagen PM, Grashoff HA, Hartwig NG, van Rossum AMC, et al. Common variable immunodeficiency and idiopathic primary hypogammaglobulinemia: two different conditions within the same disease spectrum. *Haematologica* 2013;98:1617-23.
24. Blanco E, Perez-Andres M, Arriba-Mendez S, Contreras-Sanfeliciano T, Criado I, Pelak O, et al. Age-associated distribution of normal B-cell and plasma cell subsets in peripheral blood. *J Allergy Clin Immunol* 2018;141:2208-19.
25. Flores-Montero J, Sanoja-Flores L, Paiva B, Puig N, Garcia-Sanchez O, Böttcher S, et al. Next Generation Flow for highly sensitive and standardized detection of minimal residual disease in multiple myeloma. *Leukemia* 2017;31:2094-103.
26. Blanco E, Perez-Andres M, Sanoja-Flores L, Wentink M, Pelak O, Martín-Ayuso M, et al. Selection and validation of antibody clones against IgG and IgA subclasses in switched memory B-cells and plasma cells. *J Immunol Methods* 2017 [Epub ahead of print].
27. Kalina T, Flores-Montero J, van der Velden VHJ, Martín-Ayuso M, Böttcher S, Ritgen M, et al. EuroFlow standardization of flow cytometer instrument settings and immunophenotyping protocols. *Leukemia* 2012;26:1986-2010.
28. Rudolf-Oliveira RCM, Goncalves KT, Martignago ML, Mengatto V, Gaspar PC, de Moraes ACR, et al. Determination of lymphocyte subset reference ranges in peripheral blood of healthy adults by a dual-platform flow cytometry method. *Immunol Lett* 2015;163:96-101.
29. R Core Team. R: a language and environment for statistical computing. Vienna (Austria): R Foundation; 2015.
30. MacQueen J. Some methods for classification and analysis of multivariate observations. In: *Proceedings of the Fifth Berkeley Symposium on Mathematical Statistics and Probability, Volume 1: Statistics*. Berkeley (CA): University of California Press; 1967. pp. 281-97.
31. Warnes GR, Bolker B, Bonebakker L, Gentleman R, Liaw WHA, Lumley T, et al. gplots: various R programming tools for plotting Data. R Packag. version 2.17.0.2015.
32. Bogaert DJA, Dullaers M, Lambrecht BN, Vermaelen KY, De Baere E, Haerynck F. Genes associated with common variable immunodeficiency: one diagnosis to rule them all? *J Med Genet* 2016;53:575-90.
33. Kienzler A-K, Hargreaves CE, Patel SY. The role of genomics in common variable immunodeficiency disorders. *Clin Exp Immunol* 2017;188:326-32.
34. Schatorj e EJH, Gemen EFA, Driessen GJA, Leuvenink J, van Hout RWNM, van der Burg M, et al. Age-matched reference values for B-lymphocyte subpopulations and CVID classifications in children. *Scand J Immunol* 2011;74:502-10.
35. Nechvatalova J, Pikulova Z, Stikarovska D, Pesak S, Vlkova M, Litzman J. B-lymphocyte subpopulations in patients with selective IgA deficiency. *J Clin Immunol* 2012;32:441-8.
36. Piątosza B, Wolska-Kusnierz B, Pac M, Siewiera K, Galkowska E, Bernatowska E. B cell subsets in healthy children: reference values for evaluation of B cell maturation process in peripheral blood. *Cytometry B Clin Cytom* 2010;78:372-81.
37. van Gent R, van Tilburg CM, Nibbelke EE, Otto SA, Gaiser JF, Janssens-Korpela PL, et al. Refined characterization and reference values of the pediatric T- and B-cell compartments. *Clin Immunol* 2009;133:95-107.
38. Morbach H, Eichhorn EM, Liese JG, Girschick HJ. Reference values for B cell subpopulations from infancy to adulthood. *Clin Exp Immunol* 2010;162:271-9.
39. van den Heuvel D, Jansen MAE, Nasserinejad K, Dik WA, van Lochem EG, Bakker-Jonges LE, et al. Effects of nongenetic factors on immune cell dynamics in early childhood: the Generation R Study. *J Allergy Clin Immunol* 2017;139:1923-34.e17.
40. Huck K, Feyen O, Ghosh S, Beltz K, Bellert S, Niehues T. Memory B-cells in healthy and antibody-deficient children. *Clin Immunol* 2009;131:50-9.
41. Bogaert DJA, De Bruyne M, Debacker V, Depuydt P, De Preter K, Bonroy C, et al. The immunophenotypic fingerprint of patients with primary antibody deficiencies is partially present in their asymptomatic first-degree relatives. *Haematologica* 2017;102:192-202.
42. Theunissen P, Mejstrikova E, Sedek L, van der Sluijs-Gelling AJ, Gaipa G, Bartels M, et al. Standardized flow cytometry for highly sensitive MRD measurements in B-cell acute lymphoblastic leukemia. *Blood* 2017;129:347-57.
43. Perez-Andres M, Paiva B, Nieto WG, Caraux A, Schmitz A, Almeida J, et al. Human peripheral blood B-cell compartments: a crossroad in B-cell traffic. *Cytometry B Clin Cytom* 2010;78(suppl 1):S47-60.
44. Unger S, Seidl M, Schmitt-Graeff A, Bohm J, Schrenk K, Wehr C, et al. Ill-defined germinal centers and severely reduced plasma cells are histological hallmarks of lymphadenopathy in patients with common variable immunodeficiency. *J Clin Immunol* 2014;34:615-26.
45. Ochtrop MLG, Goldacker S, May AM, Rizzi M, Draeger R, Hauschke D, et al. T and B lymphocyte abnormalities in bone marrow biopsies of common variable immunodeficiency. *Blood* 2011;118:309-18.
46. Wang Z, Yunis D, Irigoyen M, Kitchens B, Bottaro A, Alt F. Discordance between IgA switching at the DNA level and IgA expression at the mRNA level in IgA-deficient patients. *Clin Immunol* 1999;91:263-70.
47. Aghamohammadi A, Mohammadi J, Parvaneh N, Rezaei N, Moin M, Espanol T, et al. Progression of selective IgA deficiency to common variable immunodeficiency. *Int Arch Allergy Immunol* 2008;147:87-92.
48. Jackson KJL, Wang Y, Collins AM. Human immunoglobulin classes and subclasses show variability in VDJ gene mutation levels. *Immunol Cell Biol* 2014;92:729-33.
49. Collins AM, Jackson KJL. A temporal model of human IgE and IgG antibody function. *Front Immunol* 2013;4:235.
50. Berkowska MA, Driessen GJA, Bikos V, Grosserichter-Wagener C, Stamatopoulos K, Cerutti A, et al. Human memory B cells originate from three distinct germinal center-dependent and -independent maturation pathways. *Blood* 2011;118:2150-8.
51. de Jong BG, IJspeert H, Marques L, van der Burg M, van Dongen JJ, Loos BG, et al. Human IgG2- and IgG4-expressing memory B cells display enhanced molecular and phenotypic signs of maturity and accumulate with age. *Immunol Cell Biol* 2017;95:744-52.
52. Volk T, Pannicke U, Reisli I, Bulashevskaya A, Ritter J, Bjorkman A, et al. DCLRE1C (ARTEMIS) mutations causing phenotypes ranging from atypical severe combined immunodeficiency to mere antibody deficiency. *Hum Mol Genet* 2015;24:7361-72.
53. Abolhassani H, Cheraghi T, Rezaei N, Aghamohammadi A, Hammarstrom L. Common variable immunodeficiency or late-onset combined immunodeficiency: a new hypomorphic JAK3 patient and review of the literature. *J Investig Allergol Clin Immunol* 2015;25:218-20.
54. Abolhassani H, Wang N, Aghamohammadi A, Rezaei N, Lee YN, Frugoni F, et al. A hypomorphic recombination-activating gene 1 (RAG1) mutation resulting in a phenotype resembling common variable immunodeficiency. *J Allergy Clin Immunol* 2014;134:1375-80.
55. Kuehn HS, Boisson B, Cunningham-Rundles C, Reichenbach J, Stray-Pedersen A, Gelfand EW, et al. Loss of B cells in patients with heterozygous mutations in IKAROS. *N Engl J Med* 2016;374:1032-43.
56. Schubert D, Bode C, Kenefek R, Hou TZ, Wing JB, Kennedy A, et al. Autosomal dominant immune dysregulation syndrome in humans with CTLA4 mutations. *Nat Med* 2014;20:1410-6.
57. Fliegau M, Bryant VL, Frede N, Slade C, Woon S-T, Lehnert K, et al. Haploinsufficiency of the NF-kappaB1 subunit p50 in common variable immunodeficiency. *Am J Hum Genet* 2015;97:389-403.
58. Tuijnburg P, Lango Allen H, Burns SO, Greene D, Jansen MH, Staples E, et al. Loss-of-function nuclear factor kappaB subunit 1 (NFKB1) variants are the most common monogenic cause of common variable immunodeficiency in Europeans. *J Allergy Clin Immunol* 2018;142:1285-96.

59. Rodriguez-Cortez VC, del Pino-Molina L, Rodriguez-Ubreva J, Ciudad L, Gomez-Cabrero D, Company C, et al. Monozygotic twins discordant for common variable immunodeficiency reveal impaired DNA demethylation during naïve-to-memory B-cell transition. *Nat Commun* 2015;6:7335.
60. Leven EA, Maffucci P, Ochs HD, Scholl PR, Buckley RH, Fuleihan RL, et al. Hyper IgM Syndrome: a Report from the USIDNET Registry. *J Clin Immunol* 2016;36:490-501.
61. Qamar N, Fuleihan RL. The hyper IgM syndromes. *Clin Rev Allergy Immunol* 2014;46:120-30.
62. de la Morena MT. Clinical phenotypes of hyper-IgM syndromes. *J Allergy Clin Immunol Pract* 2016;4:1023-36.
63. O’Gorman MR, Zaas D, Paniagua M, Corrochano V, Scholl PR, Pachman LM. Development of a rapid whole blood flow cytometry procedure for the diagnosis of X-linked hyper-IgM syndrome patients and carriers. *Clin Immunol Immunopathol* 1997;85:172-81.
64. Derksen VFAM, Huizinga TWJ, van der Woude D. The role of autoantibodies in the pathophysiology of rheumatoid arthritis. *Semin Immunopathol* 2017;39:437-46.
65. Fecteau JF, Côté G, Neron S. A new memory CD27-IgG1 B cell population in peripheral blood expressing VH genes with low frequency of somatic mutation. *J Immunol* 2006;177:3728-36.
66. Chapel H, Lucas M, Lee M, Bjorkander J, Webster D, Grimbacher B, et al. Common variable immunodeficiency disorders: division into distinct clinical phenotypes. *Blood* 2008;112:277-86.
67. Isnardi I, Ng Y, Menard L, Meyers G, Saadoun D, Srdanovic I, et al. Complement receptor 2/CD21- human naïve B cells contain mostly autoreactive unresponsive clones. *Blood* 2010;115:5026-36.
68. Lhermitte L, Mejstrikova E, van der Sluijs-Gelling AJ, Grigore GE, Sedek L, Bras AE, et al. Automated database-guided expert-supervised orientation for immunophenotypic diagnosis and classification of acute leukemia. *Leukemia* 2018;32:874-81.
69. van der Burg M, Kalina T, Perez-Andres M, Vlokova M, Lopez-Granados E, Blanco E, et al. The EuroFlow PID orientation tube for flow cytometric diagnostic screening of primary immunodeficiencies of the lymphoid system. *Front Immunol* 2019, eCollection.

9.3. Tviolindi algorithm identifies branching developmental trajectories of human B cell development

Tviblindi algorithm identifies branching developmental trajectories of human B cell development

Authors:

Marina Bakardjieva¹, Jan Stuchlý^{1,2}, Ondřej Pelák¹, Marjolein Wentink³, Hana Glier¹, David Novák^{1,4,5}, Jitka Stančíková¹, Daniela Kužilková^{1,2}, Iga Janowska^{6,7}, Marta Rizzi^{6,7}, Mirjam van der Burg⁸, Tomáš Kalina^{1,2} *

1 CLIP, Department of Paediatric Haematology and Oncology, Second Faculty of Medicine, Charles University, Prague, Czech Republic.

2 Department of Paediatric Haematology and Oncology, University Hospital Motol, Prague, Czech Republic.

3 Department of Internal Medicine, Erasmus MC, University Medical Center Rotterdam, Rotterdam, Netherlands.

4 Department of Applied Mathematics, Computer Science and Statistics, Ghent University, Krijgslaan 281-S9, Ghent, Belgium

5 Data Mining and Modeling for Biomedicine, Center for Inflammation Research, VIB-UGent, Technologiepark-Zwijnaarde 71, Ghent, Belgium

6 Department of Rheumatology and Clinical Immunology, Freiburg University Medical Center, University of Freiburg, Freiburg, Germany.

7 Center for Chronic Immunodeficiency, University Medical Center Freiburg, Faculty of Medicine, University of Freiburg, Freiburg, Germany.

8 Department of Pediatrics, Laboratory for Pediatric Immunology, Leiden University Medical Center, Leiden, Netherlands.

* Correspondence: _

tomas.kalina@lfmotol.cuni.cz

V Uvalu 84

Prague 150 06

Czech Republic

Abstract

Detailed knowledge of the human B-cell development is crucial for proper interpretation of inborn errors of immunity and for malignant diseases. It is of interest to understand the kinetics of protein expression changes during the B cell development, but also to properly interpret the major and possibly alternative developmental trajectories. We have investigated human bone marrow and peripheral blood samples from healthy individuals with the aim to describe all B-cell developmental trajectories across the two tissues. We validated a 30-parameter mass cytometry panel and demonstrated the utility of “*vaevictis*” visualization of B-cell developmental stages. We used our recently developed trajectory inference tool “*tviblin*” to exhaustively describe all trajectories leading to all developmental ends discovered in the data. Focusing on Natural Effector B cells, we demonstrated the dynamics of expression of nuclear factors (PAX-5, TdT, Ki-67, Bcl-2), cytokine and chemokine receptors (CD127, CXCR4, CXCR5) in relation to the canonical B-cell developmental stage markers (CD34, CD10, sIgM, IgD, CD20, CD27). Lastly, we performed analysis of the expression changes related to developmental branching points (Natural Effector versus Switched Memory B cells, marked by up-regulation of CD73).

In conclusion, we developed, validated and presented a comprehensive set of tools for investigation of B-cell development.

Keywords

B cell development, mass cytometry, trajectory inference, CD73

Introduction

B-cells, together with T-cells, are adaptive immunity constituents responsible for antigen-specific responses and immune system memory. Mature and terminally differentiated B-cells produce high affinity antibodies. B-cells develop from hematopoietic stem cells in the bone marrow, exit to peripheral blood, enter the secondary lymphoid organs upon antigen encounter to mature in the germinal center and recirculate to peripheral blood and eventually home back to the bone marrow as antibody secreting cells. These principles, key developmental stages and molecular mechanisms are largely known and surface molecule expression defining the immunophenotype of each stage are published extensively ¹.

B-cell development abnormalities or complete blocks are found as a result of monogenic lesions in primary immunodeficiency disorders (PIDD) ². Leukemia and lymphoma of B-cell origin is the most common neoplasia in children, defects in B-cell development and regulation are frequent causes of immune dysregulation diseases in both children and adults, making the B-cell development and function an attractive therapeutic target. As B-cell targeted therapies (e.g. anti-CD20 monoclonal antibodies, anti-CD19 CAR-T) become available and their usage is increasing, iatrogenic B-cell developmental failures are becoming common conditions ³.

However, our understanding of the particularities of B-cell developmental abnormalities in those conditions is still incomplete. We currently lack detailed knowledge of the dynamics of additional, non-canonical molecules (new phenotype markers, signaling molecules, therapeutic targets, *in vivo* response to therapy markers). Second, we lack detailed insight into within-a-stage changes, details of transitions or intermediate stages. Third, we lack tools to disclose additional, alternative or non-dominant trajectories potentially present in human patients.

Recent advances in single cell analysis extended the capabilities of clinical flow cytometry beyond 10 parameters, and in another quantum leap forward, spectral ⁴ or mass cytometry ⁵ enabled us to investigate 40 parameters on each cell ⁶. In a proof of principle work of Bendall et al. 2014 ⁷, Wanderlust algorithm was applied to B-cell developmental mass cytometry data, showing assembled progression of markers in a single pathway. We have previously proven that a single 10-color flow cytometry tube is capable of describing the crucial stages of B-cell development and its abnormalities found in PIDD with monogenic lesions in the scope of EuroFlow consortium standardized protocol ⁸. This knowledge is essential, since the inherent assumption of a single-cell trajectory inference is that data contain all markers needed to distinguish all stages and their transition points. Recently, Saelens et al. 2019 ⁹, benchmarked 45 trajectory inference algorithms out of 70 available, concluding that only several would allow for multiple endpoints discovery. Most are built for single-cell RNA data, where the number of cells analyzed is low (10 000) but the number of parameters is high, which contrasts with the mass cytometry dataset, where tens of millions of cells are analyzed with several dozens of parameters. Our objective was to limit the amount of prior information to the starting cell subset, generate all putative random walks and allow for their graphical and user-friendly interrogation and in depth analysis of the selected trajectories.

In the current study, we set out to develop mass cytometry protocol and analytical tools that would allow us to interrogate the B-cell developmental pathways in more detail. We use the 10-color EuroFlow tube as a benchmark. We interrogate the pathways of development leading to terminal cell types expressing either κ light chain or λ light chain across two tissue types.

Methods

Sample cohort composition and preparation

Fresh human bone marrow samples (n=3) were obtained from pediatric patients with excluded hematological disease or immunological disorder or (n=1) from fully recovered patient 1 year after successful B-cell precursor leukemia therapy. Only leftover part of the clinical material was used where Informed consent was given. Study was conducted within a project approved by University hospital Motol ethical board. B cells were isolated from the samples using RosetteSep Human B cell Enrichment Cocktail (Stemcell Technologies, Vancouver, BC, Canada) following manufacturer's instructions. Isolated bone marrow B cells and precursors were cryopreserved in fetal bovine serum containing 10% DMSO in liquid nitrogen. Peripheral B cells were isolated using the same method either from fresh human peripheral blood (n=1) or from buffy coats (n=3), washed with MaxPar Cell Staining Buffer (Standard BioTools, South San Francisco, CA, USA) and used immediately for staining. Bone marrow B cells were thawed for 1 min in 37°C water bath and rested for 30 min in RPMI medium at 37°C in an incubator and washed. Individual samples were barcoded ¹⁰ with a combination of anti-CD45 and anti-HLA-I metal-tagged antibodies listed in (Supplementary table 1) as described previously ¹¹, pooled and further processed in individual tubes.

Sample staining and acquisition

Metal-tagged antibodies were either purchased (Standard BioTools) or conjugated in-house using Maxpar X8 Antibody Labeling Kit (Standard BioTools) according to manufacturer's instructions. Antibodies were validated and titrated for the appropriate concentrations and are listed in (Supplementary table 1). The samples were stained as described previously ¹² and according to the MaxPar Nuclear Antigen Staining with Fresh Fix (Standard BioTools) protocol as described by the manufacturer. Mass cytometry sample acquisition was performed on Helios instrument (Standard BioTools, CyTOF 6.7.1014 software) after preparation according to the manufacturer's recommendation. Flow cytometry measurement of B-cell precursors was performed exactly as in Wentink et al. 2019 ⁸.

Data analysis

Acquired samples were exported into FCS format and analyzed manually using sequential bivariate gating in FlowJo (v10.5, FlowJo LLC) software. First, we gated nucleated cells positive for DNA intercalator tagged with 191/193I_r and next the cells positive for particular CD45 and MHC-class I antibody reagent combinations were gated to resolve the barcodes of the individual bone marrow or peripheral blood samples. Next, cell populations for both mass and flow cytometry panels were defined as described previously ^{8, 13, 14}, gating strategy shown in Supplementary figure 1 and 2. When markers differently expressed by subsets were sought, we used "population comparison" tool in FlowJo, with probability binning and Cox chi-square statistics.

Projection with *vaevictis*

For visualization of the mass cytometry data, we used the deep learning-based dimensionality reduction technique using the *vaevictis* model ¹⁵, one of the autonomous modules integrated in the *tviblinDi*. For the projection, the healthy bone marrow (n=4) and healthy peripheral blood (n=4) samples were manually debarcoded and exported as individual FCS files. Next, only cells defined as CD34+ or CD19+ were concatenated into one FCS file and subsequently used for training of the *vaevictis* algorithm, where all

panel markers were used for the calculation. Such a trained *vaevictis* model was then applied separately to either the set of bone marrow or the set of peripheral blood cells.

Trajectory inference in *tviblinDi*

For trajectory inference (TI), we used our recent framework called *tviblinDi*¹⁵, an algorithm integrating several autonomous modules - pseudotime inference, random walk simulations, real-time topological classification using persistence homology, and autoencoder-based 2D visualization using the *vaevictis* model. For the TI, the same concatenated FCS file as for the *vaevictis* projection was used. As a point of origin, stem cells (CD19⁻CD79 α ⁺TdT⁻CD34⁺) were used. In total, 5000 random walks were probed across the single cell space. Endpoints for further investigation were selected in *tviblinDi* graphical user interface (GUI). Topological landmarks were selected in the persistence homology graph in the GUI. Next, walks clustering together were selected on the dendrogram of persistence homology and visually inspected on the *vaevictis* plot. The pseudotime vs. marker line plots were created and exported from the *tviblinDi* GUI. For manual analysis of the data in FlowJo, an enhanced FCS file was exported from the *tviblinDi* GUI containing all calculated parameters.

Results

In order to study human B-cell development, we designed a 30-parameter mass cytometry panel allowing for simultaneous measurement of B-cell specific phenotypic surface markers and functional intracellular proteins (Supplementary table 1). We validated the correct assignment of the B-cell precursor subsets by the Euroflow 10-parameter flow cytometry diagnostic panel⁸. We found a similar distribution of B-cell subsets (gated as in Supplementary Figure 1) measured in four bone marrow samples by mass cytometry and Euroflow flow cytometry, confirming that the mass cytometry panel can describe the basic stages of the B cell development in the bone marrow (Supplementary Figure 3).

Next, we visualized the B-cell precursor subsets using *vaevictis*, a representation learning dimensionality reduction tool built for development visualization. We could observe that the expected main features of the B-cell precursor to mature B-cell development were apparent on four bone marrow and four peripheral blood samples (Figure 1). *Vaevictis* plots of all of the samples individually can be found in Supplementary Figure 4. Using information of all 30 markers, *vaevictis* positioned the mature B-cells adjacent to the B-cell precursors (Figure 1A and 1B), where the aforementioned gated subsets were ordered from the progenitors to mature cell types. Also, the light chain expression highlighted the κ and λ branching (Figure 1C). Progression of the canonical markers (CD34, TdT, CD10, surface IgM (sIgM), κ chain, λ chain, IgD and CD27) in the plot corresponds with the expected course of B cell development (Figure 1C). Thus, the B-cells and their precursors measured by mass cytometry panel and visualized using *vaevictis* provided bases for interpretation of the putative trajectories of B-cell development.

On the concatenated dataset we selected the developmental point of origin at CD34⁺ Stem cells. The *tviblinDi* algorithm¹⁵ was tasked to construct 5000 random walks directed away from the origin (CD34⁺ Stem cell) with respect to the calculated pseudotime on the nearest neighbor graph (KNNg) of all single cell events. As the KNNg is directed by the pseudotime, endpoints are automatically detected when a random walk reaches a vertex (single-cell event) with no out-going edges. Sixteen endpoints were located in the 6 B-cell subsets corresponding to mature Naive, Natural Effectors and Switched Memory B-cells expressing either κ or λ light chain (Figure 2A). We have selected all endpoints leading to each subset individually. Next, we assembled random walks into different coherent trajectories leading to Natural Effector κ and λ (Figure 2B and C) and to Switched Memory κ and λ (Figure 2D and E) on dendrograms of groups of walks,

grouped with respect to the persistent homology classes (Supplementary figure 5 and 6). In parallel we visualized them on the *vaevictis* plot. Since *tviblin* algorithm and *vaevictis* visualization operate independently in the dataset, we have prioritized abundant walks with particular topology in all dimensions (selected on persistent homology diagram and dendrogram) and those that were transiting through expected cell subsets in a logical sequence (compare Figure 2B, C, D, E to Figure 1A).

For further analysis, we selected the trajectory leading to Natural Effector κ . We aimed to investigate changes of expression of the markers along the selected developmental trajectory manually. The *tviblin* interface (GUI, Supplementary Figure 7) allowed us to add all calculated parameters (*vaevictis* 1, *vaevictis* 2, pseudotime, cell assignment to trajectory) and manually investigate the enhanced FCS file for the expression of selected markers along the pseudotime of the selected trajectory (κ , λ and TdT markers shown) (Supplementary Figure 8). Next, we aligned the relative expression values of TdT, CD10 and sIgM in manually gated (as in Supplementary Figure 2) populations of B cell development (Figure 3A) to their expression over the course of pseudotime in the trajectory (Figure 3B). In agreement between manual analysis and pseudotime inference, we found the maximum level of nuclear TdT in ProB/PreB-I stage, CD10 in PreB-I stage and sIgM in Transitional B-cells (Figure 3B), however, the pseudotime plots showed single cell data with all gradual transitions. Thereafter we examined the dynamics of expression of other markers in the early (Stem cells to Pre-BII) (Figure 3C), mid (Pre-BII to Transitionals) (Figure 3D), and late (Transitionals to Natural Effectors) (Figure 3E) phases of B-cell development. See Supplementary Figure 9 for a continuation of the expression to the Switched Memory subset.

TdT expression in the Pro-B cells was followed by the CD127 (IL-7R), CXCR4, PAX-5, Ki-67 and CD10 expression at Pro-B to Pre-BI transition. Notably, CD127 raised and declined before Ki-67 peaked in Pre-BI while a second (smaller) CD127 peak followed by Ki-67 was seen in Pre-BII, in line with the reported role of IL-7 signaling inducing proliferation in humans¹⁶. Similarly, PAX-5 peak follows the CD127 peak (Figure 3C). The Bcl-2 and CD44 present bimodal expression, peaking at Pro-B stage first and again in mature stages in the peripheral blood (Figure 3D). CD9 peaks within the Immature stage, followed by sIgM, while CD20 and IgD peak at Transitional B-cell stage (Figure 3D). Finally, the CD22 and CXCR5 increase to their peaks at Naive and Effector stage (Figure 3E), respectively, followed by CD73, which is down modulated in the Natural Effector cells and upregulated again in the Switched memory B cells (Supplementary figure 9C). CD27 is known as a B-cell memory marker, but in fact has also bi-modal expression with a first peak at Pre-BI and Pre-BII stages and second peak at memory stages. The expression of CD24 is first elevated in the Pro-B to the Transitional stage only to reach its highest level in Natural Effectors (Figure 3E).

Analyzing the two compartments separately (Figure 4A, 4B), we could see that Transitional, Naive and Natural Effector cells were present in both the bone marrow and the peripheral blood. Their pseudotime position was slightly different suggesting there is a phenotypic difference. Indeed, we found higher expression of CXCR4 and lower expression of CXCR5 in the subsets in the bone marrow compartment (Figure 4C). The comparison of the Switched Memory subsets is shown in Supplementary Figure 10.

Finally, we set out to find and describe the branching points of discovered trajectories. We easily identified the position of the branching of trajectories to Naive κ and λ endpoints when plotting the κ light chain versus pseudotime (Figure 5A). As expected, the branching point was located at the Pre-BII to Immature transition on a *vaevictis* projection (Figure 5B). Following analogous principle, we investigated the branching point in the development of cells into natural effector and Switched Memory cells (the selection of random walks on dendrograms can be seen in Supplementary figure 11). After selecting the two trajectories based on the respective endpoints, we sought differentially expressed markers by the endpoint subsets. CD73 was the most different of all markers measured. Plotting the two trajectories versus CD73, we found a branching

point at a trajectory segment where CD73 started to increase on the way to the switched memory B-cells (Figure 5C). The branching point was topologically located at the Naïve B-cells (Figure 5D). While examining the trajectory to natural effector B-cell endpoint, we noticed that CD73 was heterogeneous and investigating of the dendrogram of walks we found two similar trajectories, one devoid of CD73 expression and a second with only transient increase of CD73 expression (Supplementary figure 12). The expression of CD73 was preceded by CXCR5, a germinal center homing marker.

Conclusions and discussion

We presented a single cell analysis solution for interrogation of B-cell developmental trajectories on multiple samples of relevant tissues (bone marrow and peripheral blood). We designed and validated a mass cytometry panel capable of evaluating 30-markers plus 5 sample barcodes. We compared its performance to a benchmark of EuroFlow 10-color cytometry assay. We showed a practical, feasible and scalable *vaevictis* projection calculation based on deep learning.

This tool is designed to create a continuous representation of the data rather than isolated clusters allowing a clear interpretation of the dynamics in the data (as compared of other currently used methods t-SNE¹⁷ or UMAP¹⁸). Due to the naïve importance sampling, numerically dominant populations are not overrepresented in the 2D plot and the running time is basically insensitive to the size of the original dataset. The deep learning architecture allows for direct reuses of the trained representation on a newly acquired sample (if performed in a standardized manner).

Thus, uniquely, samples of different donors (affected and unaffected) and of multiple tissues (central and peripheral) can be probed with thousands of putative pathways, that are defined only by a starting point, markers used and the overall definition of cells belonging to the pool of relevant cell type (here stem cells and B-cell lineage).

All trajectories found are visually presented for interrogation, diverse terminal ends can be selected and individual trajectories are assembled into relevant pathways for further exploration. Recent mathematical apparatus based on persistence homology calculations is used to quantitatively describe similarities of trajectories that can be assembled together.

Notably, trajectories found in our dataset correspond to the known theory of B-cell development, they logically transit from the central organ of hematopoiesis (bone marrow) to the periphery (blood). When dissected in detail, they show expected sequences of canonical markers, but add detail to the transition points and provide dynamic information about the expression of markers within known stages. For example, CD127 peaking before PAX-5 is in line with a recent study showing an important role of CD127 (IL-7RA) signaling in promoting PAX-5 expression¹⁶. While CD27 is conventionally used for phenotypic description of memory B cell subsets in the periphery, we show its upregulation also in the Pre-B stages, as shown earlier by Vaskova et al. 2008¹⁹. The transient downregulation of CXCR4 and simultaneous CD9 upregulation which we see within the Pre-BI stage is in line with Leung et al. 2011²⁰, who observed that CD9 levels are enhanced after SDF-1 stimulation suggesting that CD9 plays a role in the SDF-1/CXCR4 axis known to be essential in HSC/progenitor homing. The expression profile of CD24 along the calculated pseudotime follows the experimental findings of studies^{21, 22} showing the highest peak of expression in Transitional B cells (followed by a decrease in Naive cells) and the second in memory B cells. While the mature B-cell stages were immunophenotypically similar in the bone marrow and peripheral blood (found in the same regions on *vaevictis* plot), we could find quantitative difference in the CXCR4 and CXCR5 expression, known homing receptors^{23, 24}. Our approach allowed us to investigate multiple developmental endpoints resulting from trajectories' branching. The CD73, a known marker of switched memory B-cells²⁵ gradually increased until the switched memory B-cell stage, while it remained negative or only transiently increased towards the natural effector B-cell stage. While the branching point was found at naïve B-cell stage, the heterogeneous expression of CD73 together with CXCR5 expression suggested that there are

still alternative trajectories among the natural effector B-cells. One extrafollicular trajectory seems defined by the absence of CXCR5 and CD73 (CXCR5 and CD73 negative), while a second trajectory, defined by a transient expression of CXCR5, may describe cells that passage transiently in the germinal center. Indeed, the distinction between extrafollicular B cells and natural effector-B cells is still unclear ²⁶, and our analysis can provide insights on marker definition to dissect distinct cell fates.

Unlike the so far published algorithms that oversimplify the trajectory inference showing single dominant trajectory or two trajectories with a single branching point (e.g. Wishbone ²⁷), we could analyze multiple branching points and bring quantitative expression information as well as topological information about the branching point. The theoretical limitation is the number of investigated markers and choice of tissues and samples. This can be overcome by using *tviblini* on a single-cell RNASeq or better yet CITE-Seq dataset combining the protein markers with gene expression and enriching the mass cytometry panel in the next iteration. We can generalize, that *tviblini* algorithm can reliably show the sequence of expression of surface markers as well as nuclear transcription factors. We could anticipate that our mass cytometry panel and *tviblini* could be used to compare healthy reference with affected (intrinsic or extrinsic factors) development to discover alternative pathways, new branching points or alternative endpoints. These deviations could potentially disclose targetable processes for therapy of PID and/or B-cell neoplasia.

Acknowledgements

We wish to thank to Daniel Thurner, Pavla Luknarova and Katerina Rejlova for their superb technical assistance. TK and JS were supported by grant 23-05561S from The Czech Science Foundation. TK, DK and JS were funded by the European Union - Next Generation EU (Czech Recovery Plan) - Project National Cancer Research Institute LX22NPO5102. DN was funded by the FWO (Fonds Wetenschappelijk Onderzoek) and conducted as part of the FWO Strategic Basic research project 1S40421N.

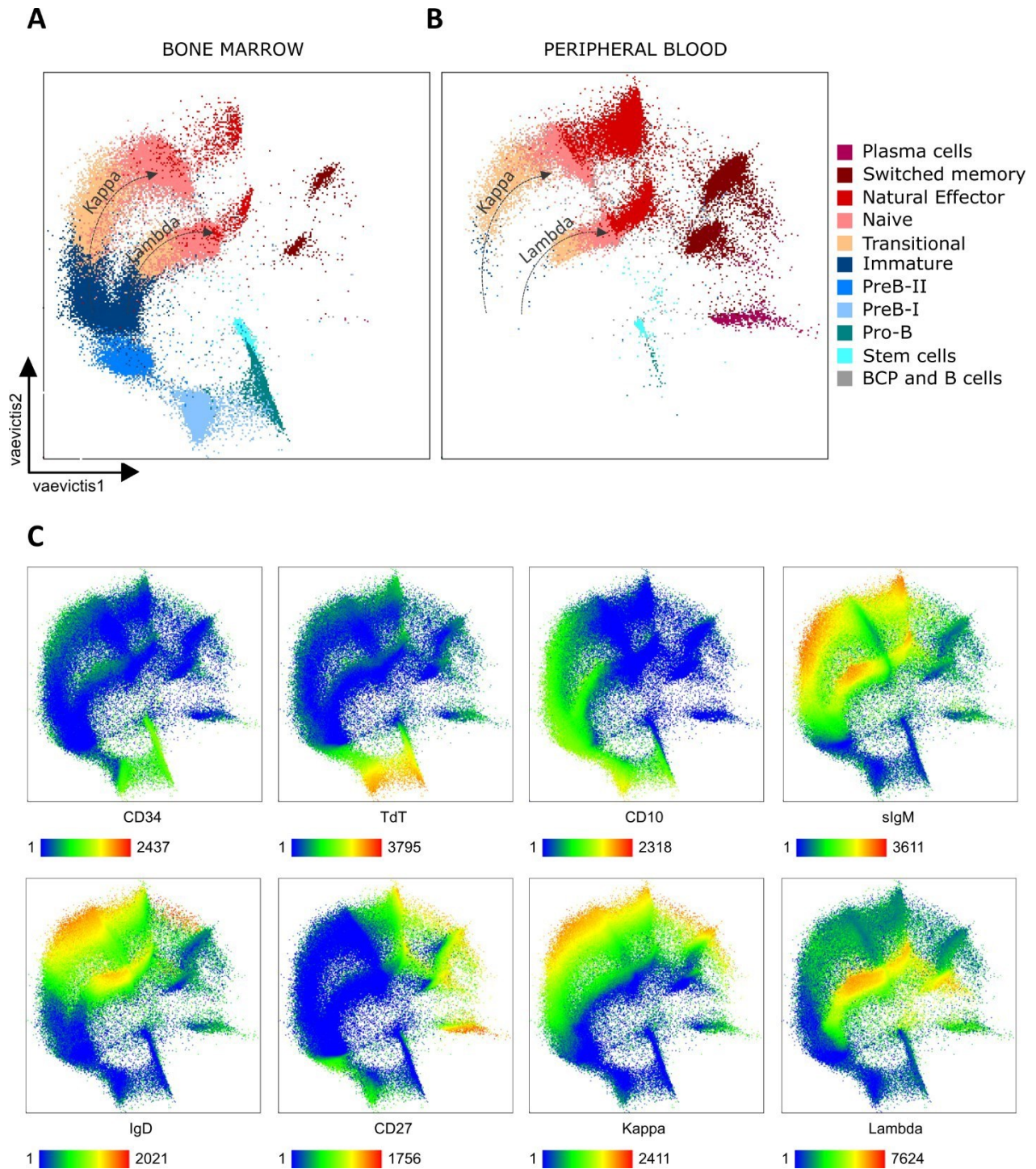


Figure 1. Vaevictis dimensionality reduction of BCPs and B cells in bone marrow and peripheral blood. (A) Healthy bone marrow (n=4, concatenated) and (B) peripheral blood (n=4, concatenated) BCPs and B cells with manually gated populations applied to the visualization in color, with annotation and counts of the individual subsets. Dotted arrows highlight kappa and lambda B cells (compare to panel C) (C) Visualization of the entire merged data with the expression of chosen canonical markers using a heatmap color gradient where green represents the lowest expression and red the highest.

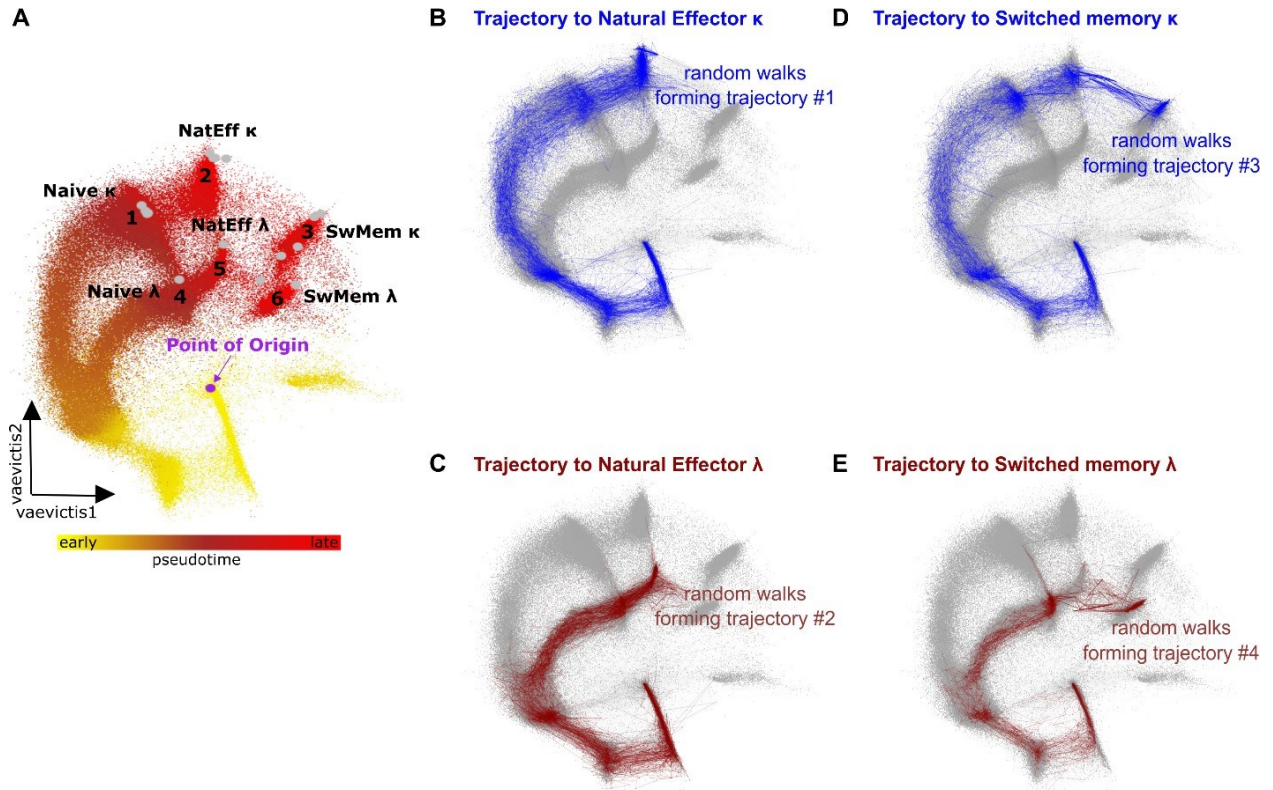


Figure 2. B cell developmental endpoints and trajectories leading to Natural Effector and Switched memory κ and λ B cells constructed by *tviblindi*. (A) Groups of endpoints (1-6) represented as gray dots are located in clusters corresponding to Naïve (1;4), Natural Effector (2;5) and Switched memory (3;6) cells in the vaevictis visualization colored by pseudotime. Yellow color indicates the earliest pseudotime, bright red color indicates the latest pseudotime. The purple dot indicates the Point of origin at gated CD34+ Stem cells. Vaevictis visualization with displayed trajectories to (B) Natural Effector κ and (C) λ B cells and (D) Switched Memory κ and (E) λ B cells constructed by *tviblindi* (for a selection of trajectory group see (Supplementary figure 5 and 6).

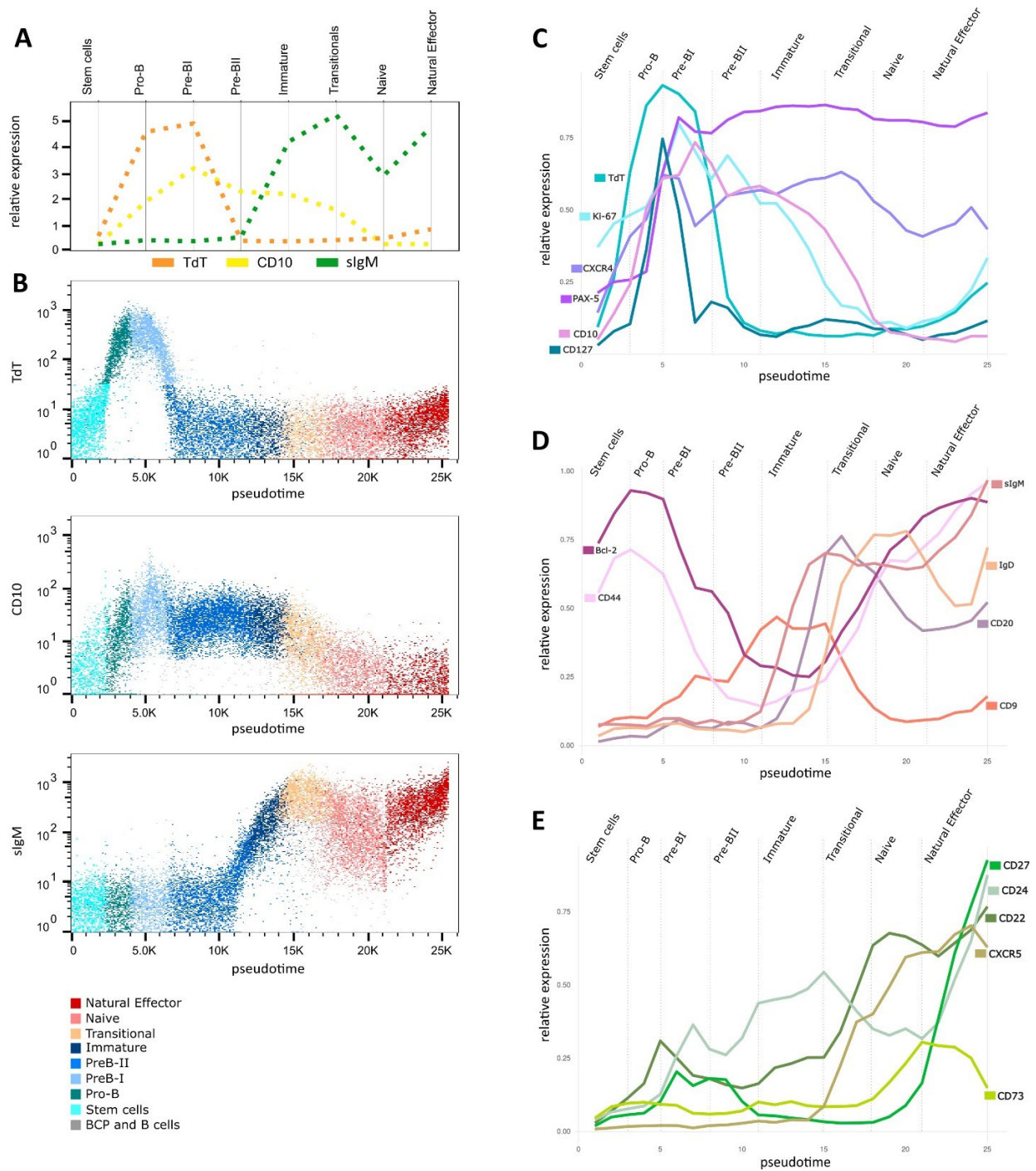


Figure 3. Detailed analysis of the trajectory leading to Natural Effector κ cells. (A) Median expression of TdT (orange), CD10 (yellow) and sIgM (green) from manually gated populations correlate with (B) the expression of TdT, CD10 and sIgM on the pseudotime vs. marker dot plots with manually gated populations overlaid in color. Pseudotime line plots showing the average expression of markers upregulated in the early (C), mid (D) and late (E) phase of the development, manually annotated by the gated stages.

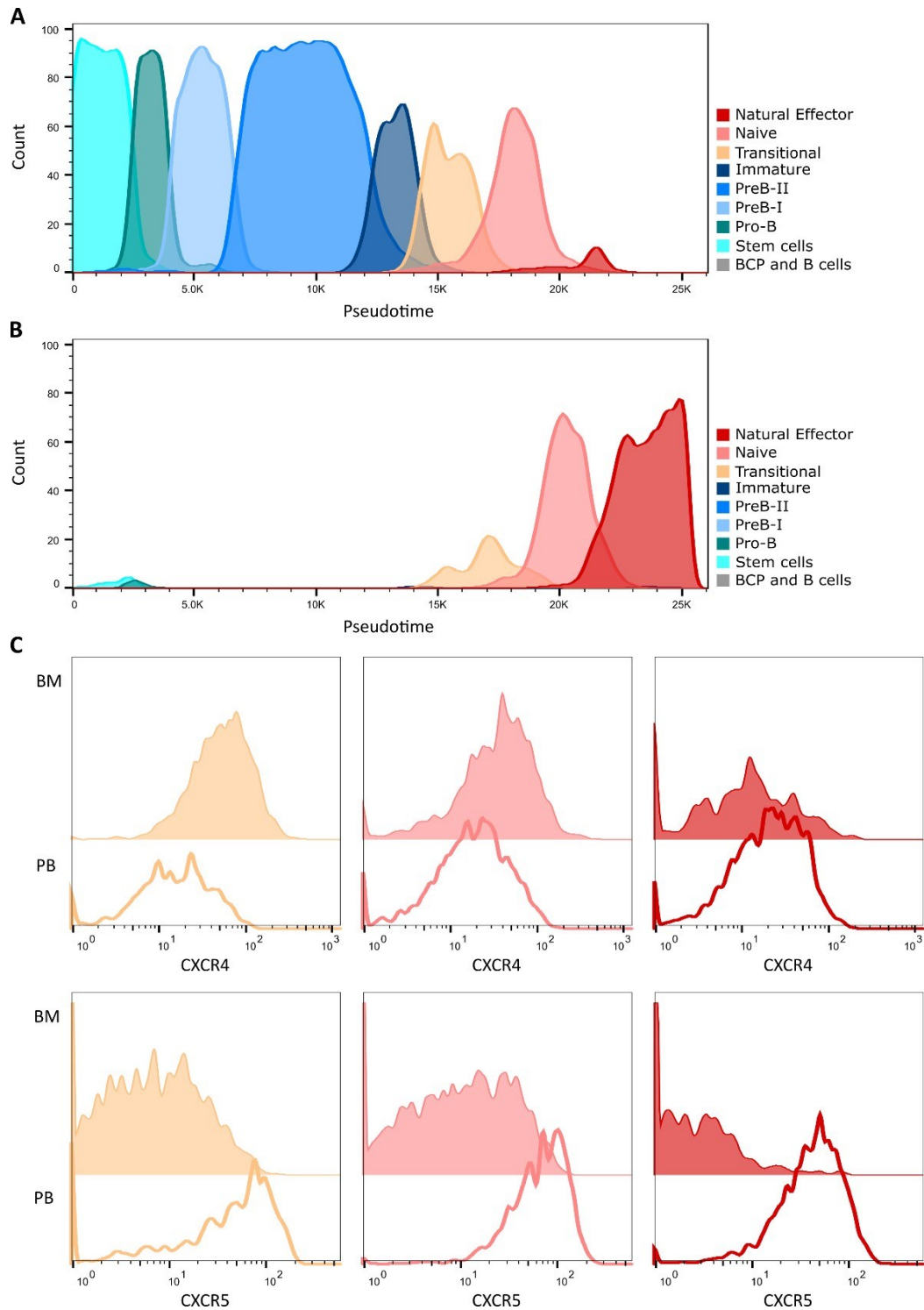


Figure 4. Contribution of the BCP and B-cell stages to the bone marrow and peripheral blood compartments. Individual populations are shown as histograms in the data set divided into (A) bone marrow (n=4, concatenated) and (B) peripheral blood (n=4, concatenated). (C) Differential expression of the markers CXCR4 (top row) and CXCR5 (bottom row) in the populations which are present in both of the compartments. Solid line histograms indicate subsets present in the peripheral blood (PB). Filled histograms indicate subsets present in the bone marrow (BM).

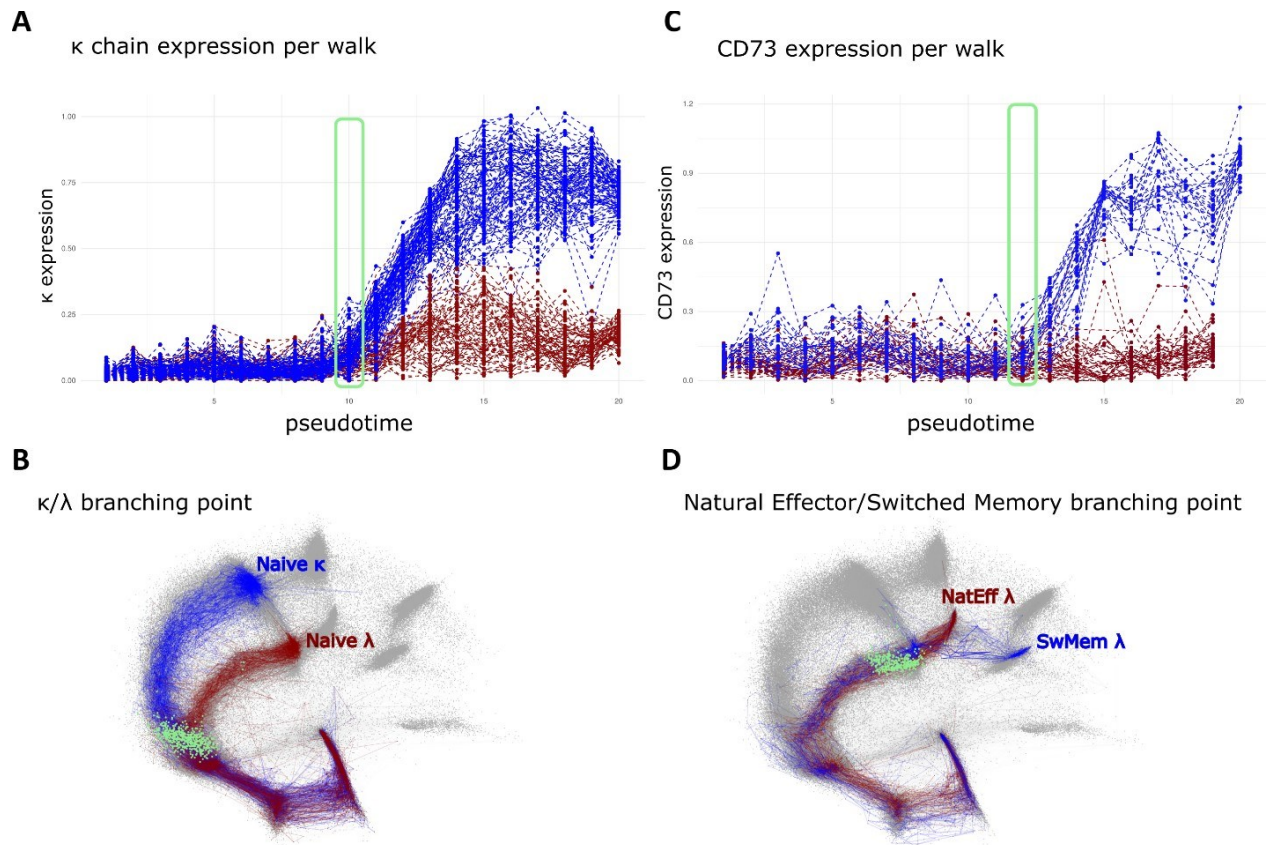


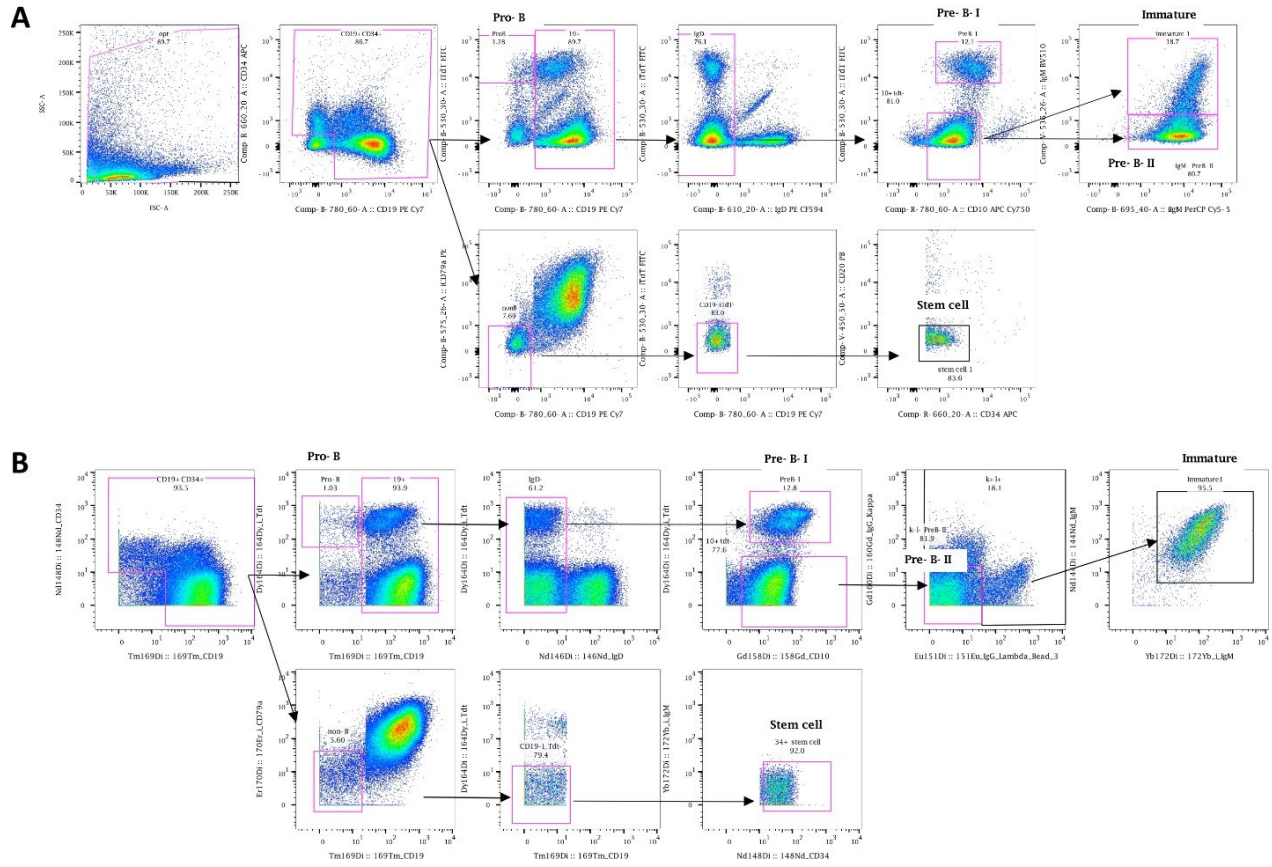
Figure 5. Identification of branching points in trajectories leading to the selected endpoints. (A) Pseudotime line plot showing expression of the κ chain for the selected trajectories leading to Naive κ (blue) and Naive λ (red) ends. The green rectangle indicates the branching point of trajectories and is projected as green dots in the *vaevictis* plot. (B) *Vaevictis* plot showing trajectories to Naive κ (blue) and Naive λ (red) subsets with projection of cells (green) located in the branching point. (C) Pseudotime line plot showing the expression of the CD73 for the selected trajectories leading to Switched memory λ (blue) and Natural Effector λ (red) ends. The green rectangle indicates the branching point of trajectories and is projected as green dots in the *vaevictis* plot. (D) *Vaevictis* plot showing trajectories to Natural Effector λ (red) and Switched memory λ (blue) endpoints with projection of cells (green) located in the branching point.

References

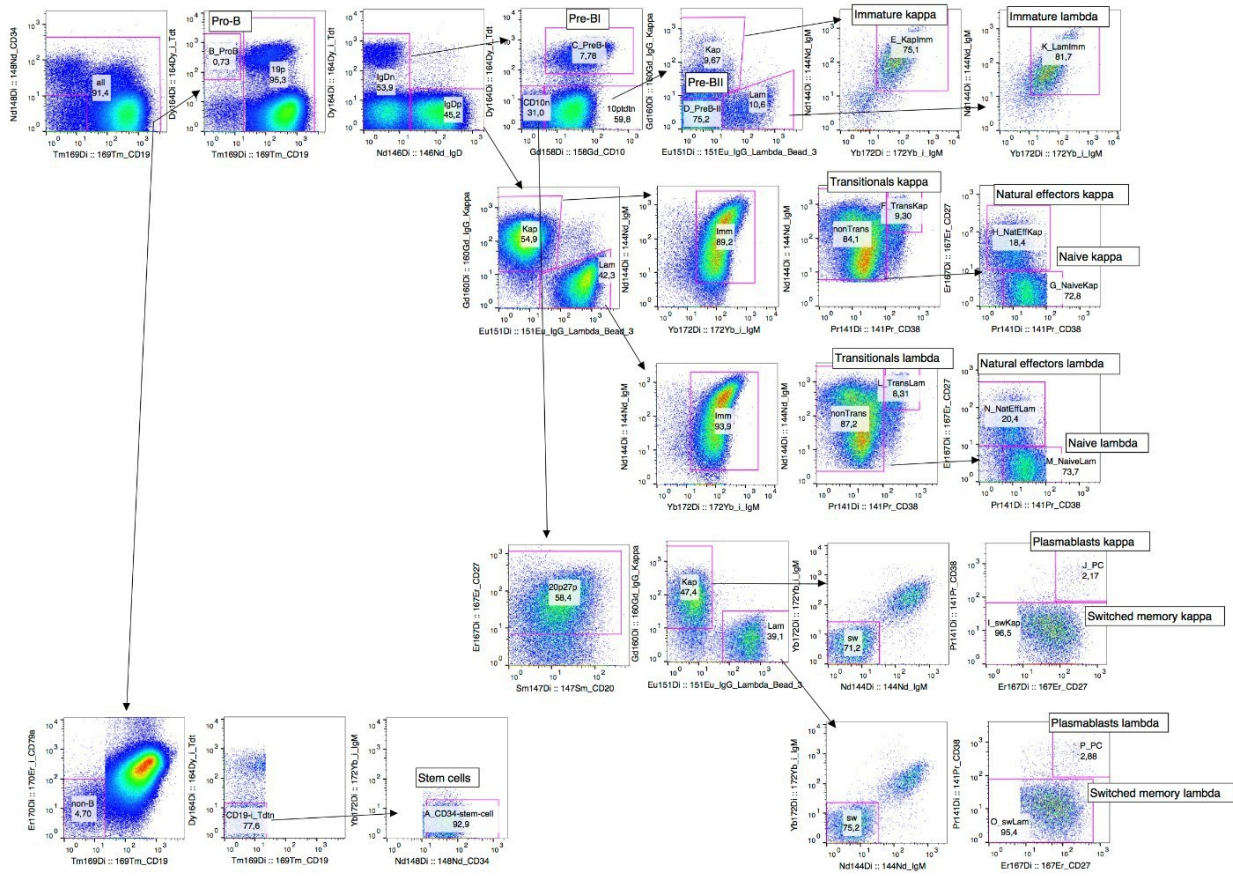
1. Lebien TW, Tedder TF. B lymphocytes: How they develop and function. *Blood*. 2008;112(5):1570-1580. doi:10.1182/blood-2008-02-078071
2. Bousfiha A, Moundir A, Tangye SG, et al. The 2022 Update of IUIS Phenotypical Classification for Human Inborn Errors of Immunity. *J Clin Immunol*. 2022;42(7):1508-1520. doi:10.1007/s10875-022-01352-z
3. Sacks D, Baxter B, Campbell BCV, et al. Multisociety Consensus Quality Improvement Revised Consensus Statement for Endovascular Therapy of Acute Ischemic Stroke. *International Journal of Stroke*. 2018;13(6):612-632. doi:10.1177/1747493018778713
4. Park LM, Lannigan J, Jaimes MC. OMIP-069: Forty-Color Full Spectrum Flow Cytometry Panel for Deep Immunophenotyping of Major Cell Subsets in Human Peripheral Blood. *Cytometry Part A*. 2020;97(10):1044-1051. doi:10.1002/cyto.a.24213
5. Koladiya A, Davis KL. Advances in Clinical Mass Cytometry. *Clin Lab Med*. 2023;43(3):507-519. doi:10.1016/j.cll.2023.05.004
6. Bendall SC, Nolan GP, Roederer M, Chattopadhyay PK. A deep profiler's guide to cytometry. *Trends Immunol*. 2012;33(7):323-332. doi:10.1016/j.it.2012.02.010
7. Bendall SC, Davis KL, Amir EAD, et al. Single-cell trajectory detection uncovers progression and regulatory coordination in human B cell development. *Cell*. 2014;157(3):714-725. doi:10.1016/j.cell.2014.04.005
8. Wentink MWJ, Kalina T, Perez-Andres M, et al. Delineating Human B Cell Precursor Development With Genetically Identified PID Cases as a Model. *Front Immunol*. 2019;10(November):1-12. doi:10.3389/fimmu.2019.02680
9. Saelens W, Cannoodt R, Todorov H, Saeys Y. A comparison of single-cell trajectory inference methods. *Nat Biotechnol*. 2019;37(5):547-554. doi:10.1038/s41587-019-0071-9
10. Kudlacova J, Kuzilkova D, Barta F, et al. Hybrid Macromolecular Constructs as a Platform for Spectral Nanoprobes for Advanced Cellular Barcoding in Flow Cytometry. *Macromol Biosci*. 2023;2300306:1-12. doi:10.1002/mabi.202300306
11. Mei HE, Leipold MD, Schulz AR, Chester C, Maecker HT. Barcoding of Live Human Peripheral Blood Mononuclear Cells for Multiplexed Mass Cytometry. *The Journal of Immunology*. 2015;194(4):2022-2031. doi:10.4049/jimmunol.1402661
12. Kuzilkova D, Bugarin C, Rejlova K, et al. Either IL-7 activation of JAK-STAT or BEZ inhibition of PI3K-AKT-mTOR pathways dominates the single-cell phosphosignature of ex vivo treated pediatric T-cell acute lymphoblastic leukemia cells. *Haematologica*. 2022;107(6):1293-1310. doi:10.3324/haematol.2021.278796
13. Van Dongen JJM, Van Der Burg M, Kalina T, et al. EuroFlow-based flowcytometric diagnostic screening and classification of primary immunodeficiencies of the lymphoid system. *Front Immunol*. 2019;10(JUN):1-21. doi:10.3389/fimmu.2019.01271
14. Van Zelm MC, Szczepański T, Van Der Burg M, Van Dongen JJM. Replication history of B lymphocytes reveals homeostatic proliferation and extensive antigen-induced B cell expansion. *Journal of Experimental Medicine*. 2007;204(3):645-655. doi:10.1084/jem.20060964
15. Stuchly J, Novak D, Brdickova N, et al. Deconstructing Complexity: A Computational Topology Approach to Trajectory Inference in the Human Thymus with tvblindi. doi:10.1101/2023.07.13.547329
16. Kaiser FMP, Janowska I, Menafrá R, et al. IL-7 receptor signaling drives human B-cell progenitor differentiation and expansion. *Blood*. 2023;142(13):1113-1130. doi:10.1182/blood.2023019721

17. Amir EAD, Davis KL, Tadmor MD, et al. ViSNE enables visualization of high dimensional single-cell data and reveals phenotypic heterogeneity of leukemia. *Nat Biotechnol.* 2013;31(6):545-552. doi:10.1038/nbt.2594
18. McInnes L, Healy J, Saul N, Großberger L. UMAP: Uniform Manifold Approximation and Projection. *J Open Source Softw.* 2018;3(29):861. doi:10.21105/JOSS.00861
19. Vaskova M, Fronkova E, Starkova J, Kalina T, Mejstrikova E, Hrusak O. CD44 and CD27 delineate B-precursor stages with different recombination status and with an uneven distribution in nonmalignant and malignant hematopoiesis. *Tissue Antigens.* 2008;71(1):57-66. doi:10.1111/j.1399-0039.2007.00968.x
20. Leung KT, Chan KYY, Ng PC, et al. The tetraspanin CD9 regulates migration, adhesion, and homing of human cord blood CD34+ hematopoietic stem and progenitor cells. *Blood.* 2011;117(6):1840-1850. doi:10.1182/blood-2010-04-281329
21. Carrion C, Guérin E, Gachard N, le Guyader A, Giraut S, Feuillard J. Adult Bone Marrow Three-Dimensional Phenotypic Landscape of B-Cell Differentiation. *Cytometry B Clin Cytom.* 2019;96(1):30-38. doi:10.1002/cyto.b.21747
22. Mensah FFK, Armstrong CW, Reddy V, et al. CD24 expression and B cell maturation shows a novel link with energy metabolism: Potential implications for patients with myalgic encephalomyelitis/chronic fatigue syndrome. *Front Immunol.* 2018;9. doi:10.3389/fimmu.2018.02421
23. Reif K, Ekland EH, Ohl L, et al. Balanced responsiveness to chemoattractants from adjacent zones determines B-cell position. 2002;416. doi: 10.1038/416094a
24. Zehentmeier S, Pereira JP. Cell circuits and niches controlling B cell development. *Immunol Rev.* 2019;289(1):142-157. doi:10.1111/imr.12749
25. Schena F, Volpi S, Faliti CE, et al. Dependence of Immunoglobulin Class Switch Recombination in B Cells on Vesicular Release of ATP and CD73 Ectonucleotidase Activity. *Cell Rep.* 2013;3(6):1824-1831. doi:10.1016/j.celrep.2013.05.022
26. Elsner RA, Shlomchik MJ. Germinal Center and Extrafollicular B Cell Responses in Vaccination, Immunity, and Autoimmunity. *Immunity.* 2020;53(6):1136-1150. doi:10.1016/j.immuni.2020.11.006
27. Setty M, Tadmor MD, Reich-Zeliger S, et al. Wishbone identifies bifurcating developmental trajectories from single-cell data. *Nat Biotechnol.* doi:10.1038/nbt.3569

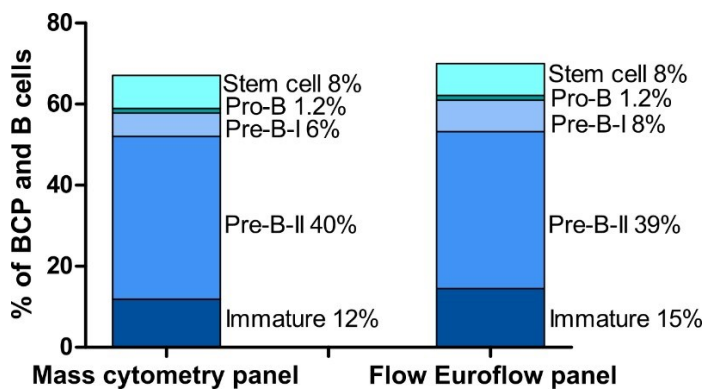
Supplementary data



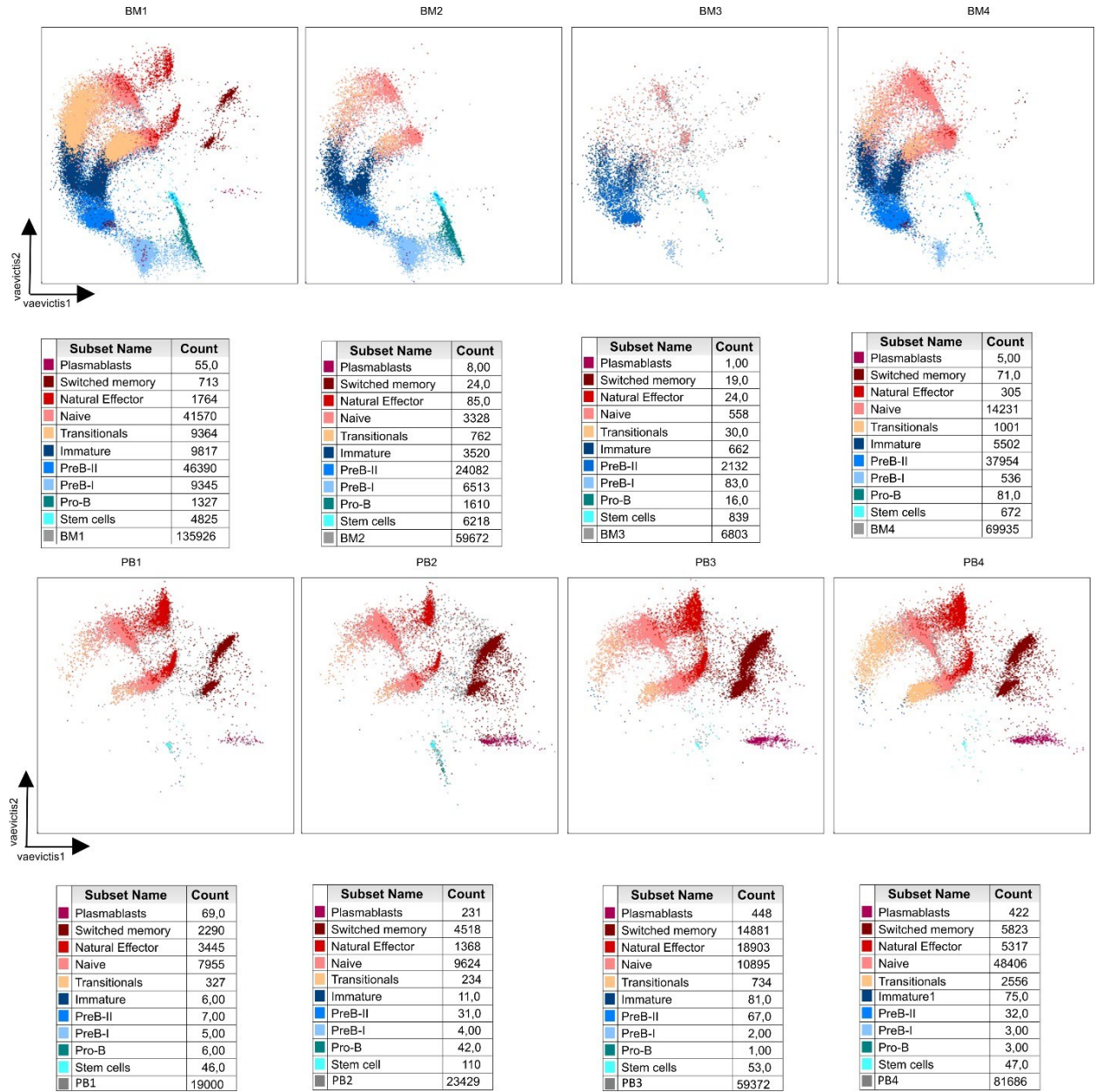
Supplementary Figure 1. Gating strategy for the flow cytometry (A) and CyTOF (B) data. Representative results from the same healthy bone marrow sample measured in parallel.



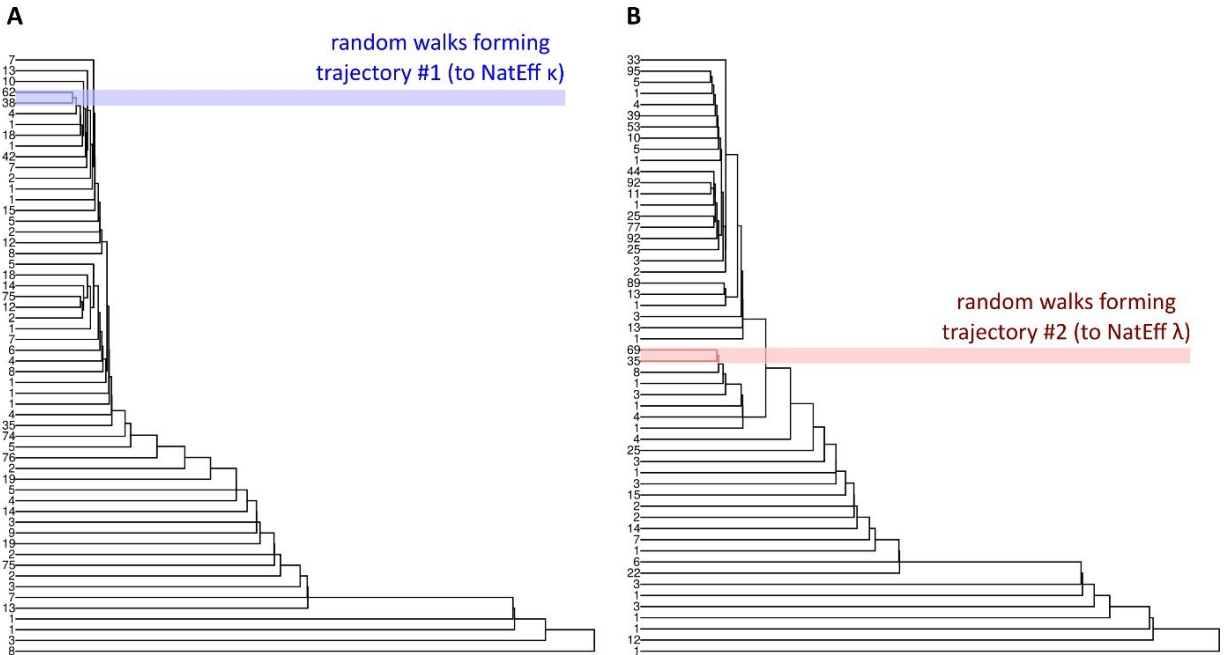
Supplementary figure 2. Gating strategy for the CyTOF data from healthy donor bone marrow and peripheral blood samples.



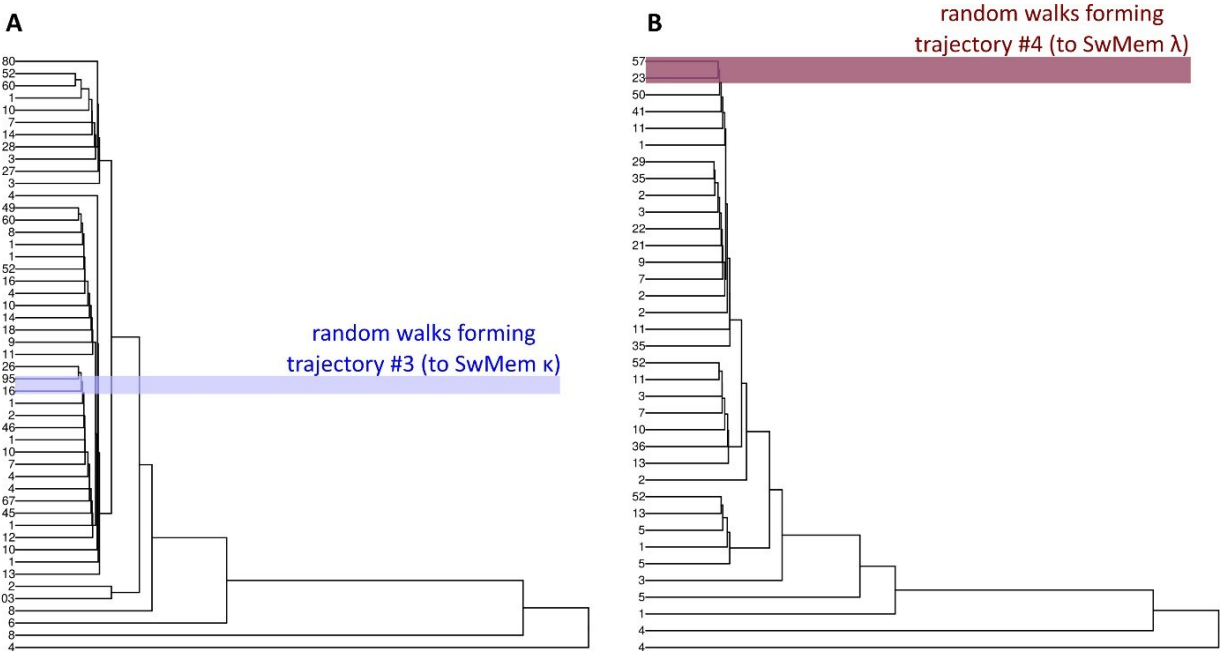
Supplementary Figure 3. Distribution of B-cell precursor populations correlates between the novel mass cytometry panel (left) and previously validated flow Euroflow panel (right). Colors indicate individual populations with percentage representation within both of the panels. Stem cells were defined as CD19-CD79 α -TdT-CD34+, Pro-B cells as CD19-TdT+CD34+, Pre-B-I cells as CD19+TdT+CD34+, Pre-B-II cells as CD19+CD10+IgM+IgM- and Immature cells as CD19+CD10+IgM+IgM+. Results from 4 different healthy bone marrow samples measured in parallel.



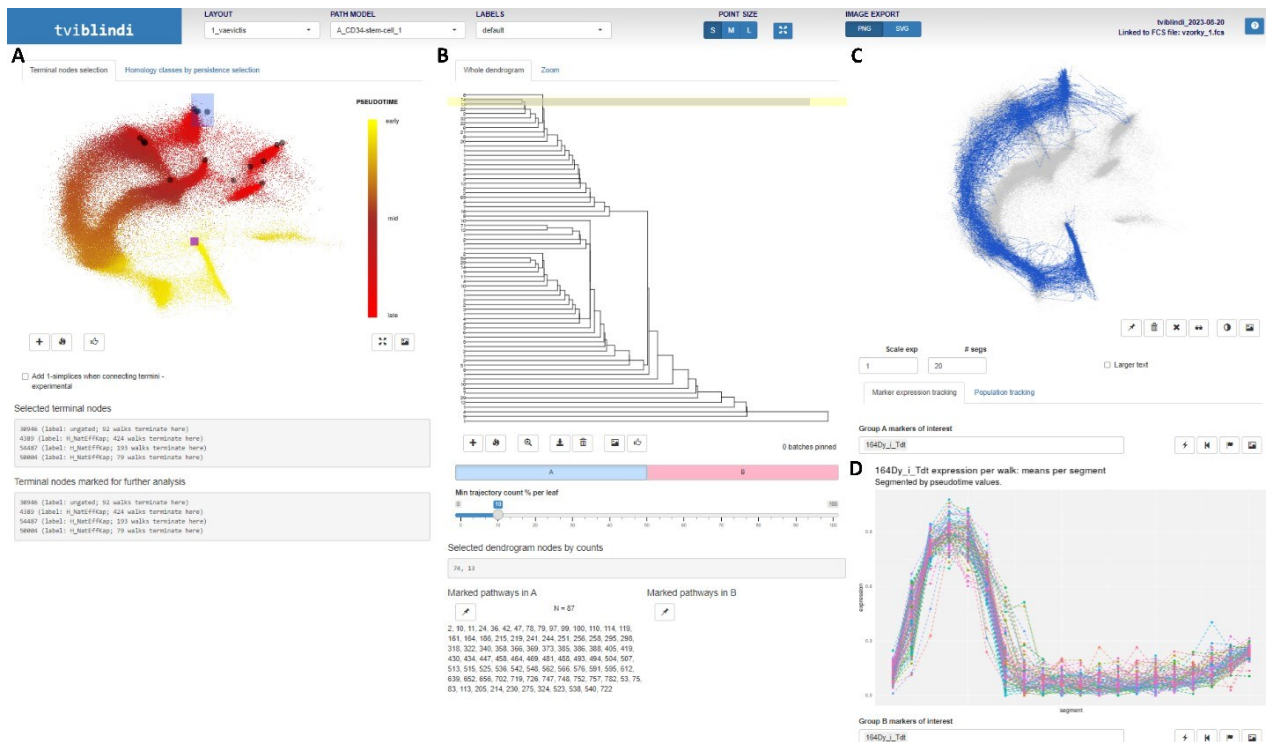
Supplementary Figure 4. Vaevictis dimensionality reduction of BCPs and B cells in bone marrow and peripheral blood for the individual samples. Visualization of the four healthy donor bone marrow samples (top row, BM1-BM4) and the four healthy donor peripheral blood samples (bottom row, PB1-PB4) with manually gated populations applied to the graph in color, with annotation and counts of the individual subsets.



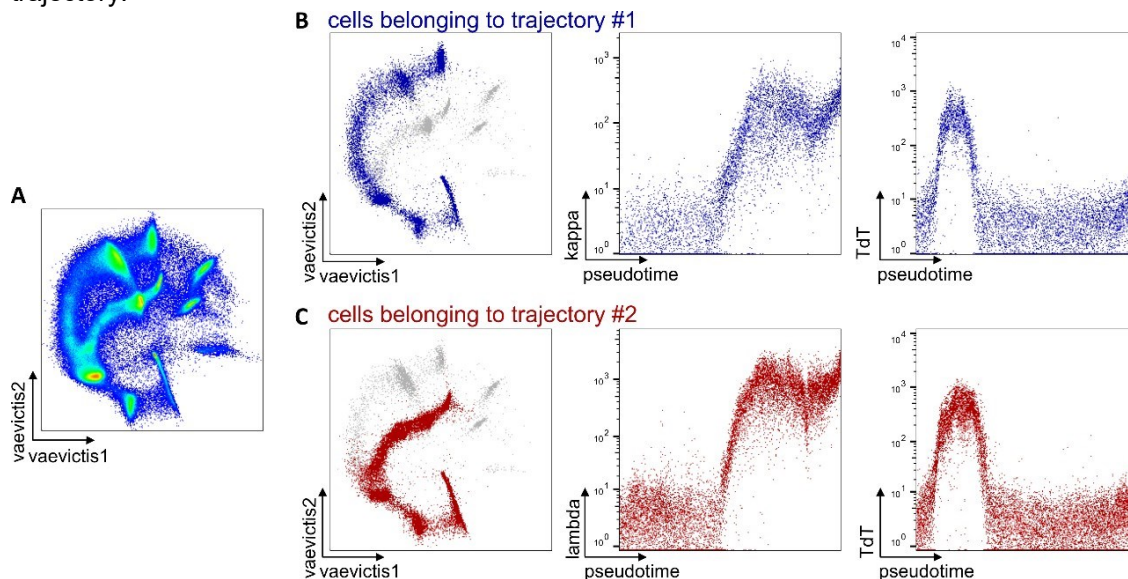
Supplementary Figure 5. Hierarchical clustering dendrogram for Natural Effector κ and λ developmental trajectories. Dendrograms show clustering of all random walks leading to developmental endpoints located in the (A) Natural Effector κ and (B) Natural Effector λ clusters. Leaves represent the groups of random walks with similar topology. In blue is highlighted the selected group of walks representing developmental trajectory to Natural Effector κ cells. In red is highlighted the group of walks representing developmental trajectory to Natural Effector λ cells.



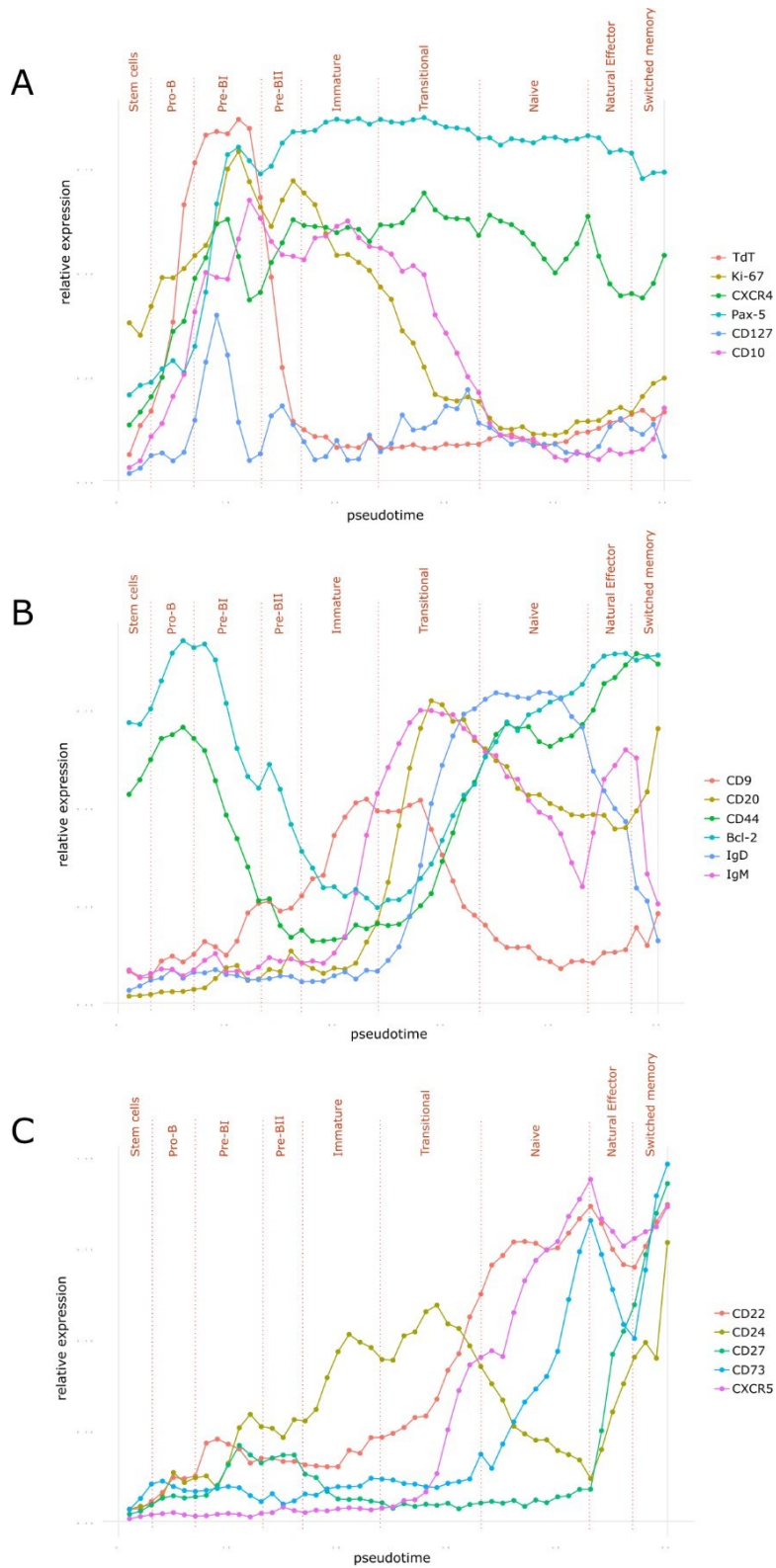
Supplementary Figure 6. Hierarchical clustering dendrogram for Switched Memory κ and λ developmental trajectories. Dendrograms show clustering of all random walks leading to developmental endpoints located in the (A) Switched Memory κ and (B) Switched Memory λ clusters. Leaves represent the random walks and their abundance. In blue is highlighted the selected group of walks representing developmental trajectory to Switched Memory κ cells (A) and Switched Memory λ cells (B).



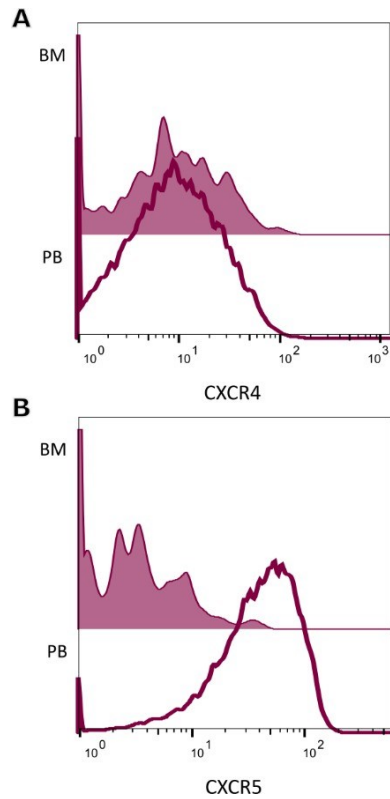
Supplementary Figure 7. tviblindi graphical user interface (GUI). (A) vaevictis plot with selected terminal endpoints located in the Natural Effector kappa cluster, (B) hierarchical clustering dendrogram with selection of random walks forming the trajectory leading to Natural Effector kappa cluster, (C) vaevictis plot with random walks selected in (B), (D) lineplot with the expression of TdT along pseudotime of the selected trajectory.



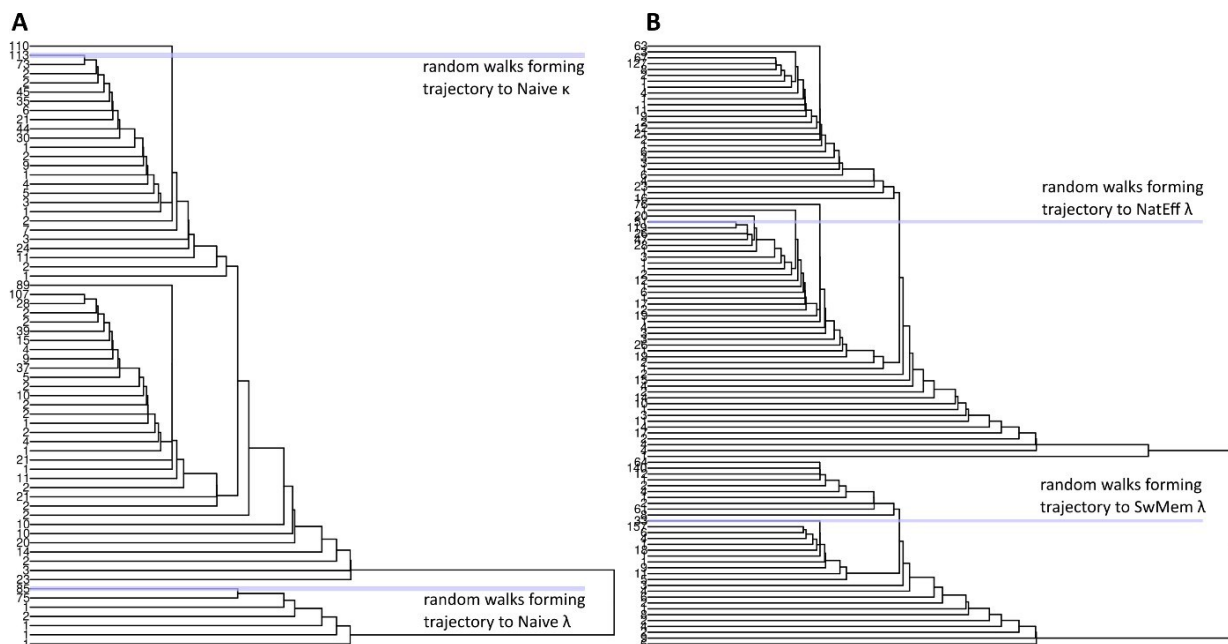
Supplementary Figure 8. Manual analysis of trajectories constructed by tviblindi (at the cellular level) using enhanced FCS file. Vaevictis visualization of (A) the entire data set and (B, C) with colored cells belonging to the selected trajectory ending at the Natural Effector κ (blue) and λ (red) subsets in FlowJo. Expression of κ , λ and TdT markers along pseudotime.



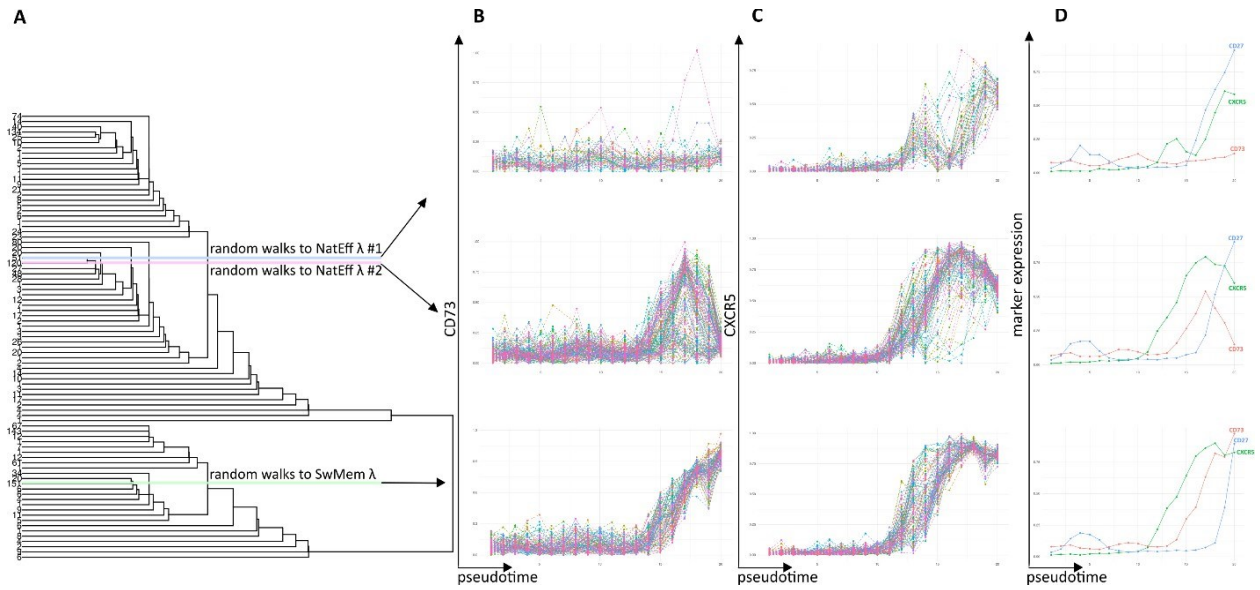
Supplementary Figure 9. Detailed analysis of the trajectory leading to Switched memory κ cells. Pseudotime line plots showing the average expression of markers upregulated in the early (A), mid (B) and late (C) phase of the development.



Supplementary Figure 10. Differential expression of the markers CXCR4 (A) and CXCR5 (B) in Switched memory cells present in both bone marrow (BM) and peripheral blood (PB) compartments. Solid line histograms indicate subsets present in the PB. Filled histograms indicate subsets present in the BM.



Supplementary Figure 11. Hierarchical clustering dendrograms. For the developmental branching of (A) Naive κ and λ cells and (B) Natural Effector λ and Switched memory λ cells. In blue are highlighted the groups of random walks representing the developmental trajectories to (A) Naive κ and λ cells and (B) Natural Effector λ and Switched memory λ cells.

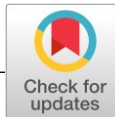


Supplementary Figure 12. Differential expression of the markers CD73 and CXCR5 in trajectories leading to Natural Effector and Switched memory cells. (A) Dendrogram with selection of random walks forming the trajectory to Natural Effector λ #1(blue), #2 (pink) and Switched memory λ (green). The trajectory to Natural Effector λ #1 shows no upregulation of CD73 (B, top) and transient expression of CXCR5 (C, top). The trajectory to Natural Effector λ #2 (B, mid) shows heterogeneous expression of CD73 and upregulation of CXCR5 (C, mid). The trajectory to Switched memory λ shows clear upregulation of both CD73 (B, bottom) and CXCR5 (C, bottom). (D) Lineplots for the different trajectories with dynamics of expression of CD73, CXCR5 and CD27.

marker	clone	tag	µl per 100 µl cell suspension	manufacturer
BARCODES				
CD45	HI30	Y89	1	Fluidigm
CD45	MEM-28	110Cd	2	Exbio
CD45	MEM-28	113In	1	Exbio
HLA-I	W6/32	116Cd	2	Bxcell
HLA-I	W6/32	175Lu	1	Bxcell
SURFACE MARKERS				
CD38	HIT2	141Pr	2	Exbio
IgM	MHM-88	144Nd	1	Biologend
CD24	ML5	145Nd	2	Biologend
IgD	IA6-2	146Nd	1	Fluidigm
CD20	2H7	147Sm	1	Fluidigm
CD34	581	148Nd	2	Fluidigm
CD127	A019D5	149Sm	2	Fluidigm
Ig light chain lambda	MHL-38	151Eu	1	Fluidigm
CD135	BV10A4	156Gd	4	Exbio
CD10	HI10a	158Gd	1	Fluidigm
CD22	HIB22	159Tb	2	Fluidigm
Ig light chain kappa	MHK-49	160Gd	1	Fluidigm
CD9	MEM-61	161Dy	2	Exbio
CD25	MEM-181	162Dy	4	Exbio
CD44	MEM-85	163Dy	2	Exbio
CD27	L128	167Er	1	Fluidigm
CD19	HIB19	169Tm	2	Fluidigm
CXCR5	REA103	171Yb	2	Miltenyi
CXCR4	REA649	173Yb	2	Miltenyi
HLA-DR	L243	174Yb	1	Fluidigm
CD73	AD2	176Yb	2	Exbio
INTRACELLULAR MARKERS				
Caspase 3 (Cleaved)	D3E9	142Nd	2	Fluidigm
cPARP	F21-852	143Nd	1	Fluidigm
PAX-5	1H9	150Nd	2	Biologend
Caspase 7 (Cleaved)	D6H1	152Sm	1	Fluidigm
BCL-2	Bcl-2/100	153Eu	2	Exbio
Tdt	E17-1519	164Dy	1	Fluidigm
Biotin	1D4-C5	165Ho	1	Fluidigm
Ki-67	B56	168Er	1	Fluidigm
CD79a	HM57	170Er	2	Exbio
IgM	MHM-88	172Yb	1	Fluidigm
LINEAGE NEGATIVE MARKERS				
CD3	UCHT1	biotin	2	Exbio
CD16	3G8	biotin	2	Biologend
CD33	HIM3-4	biotin	2	Exbio
CD66b	G10F5	biotin	2	Biologend
DNA INTERCALATOR				
		191Ir/193Ir	1	Fluidigm

Supplementary table 1. Mass cytometry panel of markers used for staining of the samples. The marker in brackets (ilgM) was excluded from the manual analysis due to poor performance.

9.4. Non-apoptotic FAS signaling controls mTOR activation and extrafollicular maturation in human B cells



IMMUNODEFICIENCY

Non-apoptotic FAS signaling controls mTOR activation and extrafollicular maturation in human B cells

Julian Staniek^{1,2}, Tomas Kalina³, Geoffroy Andrieux^{4,5}, Melanie Boerries^{4,5}, Iga Janowska¹, Manuel Fuentes⁶, Paula Díez^{6,7}, Marina Bakardjieva³, Jitka Stancikova³, Jan Raabe¹, Julika Neumann¹, Sabine Schwenk¹, Leonardo Arpesella¹, Jan Stuchly³, Vladimír Benes⁸, Rodrigo García Valiente⁶, Jonatan Fernández García⁶, Rita Carsetti⁹, Eva Piano Mortari⁹, Albert Catala¹⁰, Oscar de la Calle¹¹, Georgios Sogkas¹², Bénédicte Neven¹³, Frédéric Rieux-Laucat¹⁴, Aude Magerus¹⁴, Olaf Neth¹⁵, Peter Olbrich¹⁵, Reinhard E. Voll^{1,16}, Laia Alsina^{10,17}, Luis M. Allende¹⁸, Luis I. Gonzalez-Granado^{19,20}, Chiara Böhler¹, Jens Thiel^{1,21}, Nils Venhoff¹, Raquel Lorenzetti^{1,21}, Klaus Warnatz^{1,16,22}, Susanne Unger^{1,16}, Maximilian Seidl^{23,24}, Dirk Mielenz²⁵, Pascal Schneider²⁶, Stephan Ehl^{16,27,28}, Anne Rensing-Ehl¹⁶, Cristian Roberto Smulski^{16,29}, Marta Rizzi^{1,16,28,30*}

copyright © 2024 authors, some rights reserved; exclusive licensee American Association for the Advancement of Science. No claim to original U.S. Government Works

Defective FAS (CD95/Apo-1/TNFRSF6) signaling causes autoimmune lymphoproliferative syndrome (ALPS). Hypergammaglobulinemia is a common feature in ALPS with FAS mutations (ALPS-FAS), but paradoxically, fewer conventional memory cells differentiate from FAS-expressing germinal center (GC) B cells. Resistance to FAS-induced apoptosis does not explain this phenotype. We tested the hypothesis that defective non-apoptotic FAS signaling may contribute to impaired B cell differentiation in ALPS. We analyzed secondary lymphoid organs of patients with ALPS-FAS and found low numbers of memory B cells, fewer GC B cells, and an expanded extrafollicular (EF) B cell response. Enhanced mTOR activity has been shown to favor EF versus GC fate decision, and we found enhanced PI3K/mTOR and BCR signaling in ALPS-FAS splenic B cells. Modeling initial T-dependent B cell activation with CD40L in vitro, we showed that FAS competent cells with transient FAS ligation showed specifically decreased mTOR axis activation without apoptosis. Mechanistically, transient FAS engagement with involvement of caspase-8 induced nuclear exclusion of PTEN, leading to mTOR inhibition. In addition, FASL-dependent PTEN nuclear exclusion and mTOR modulation were defective in patients with ALPS-FAS. In the early phase of activation, FAS stimulation promoted expression of genes related to GC initiation at the expense of processes related to the EF response. Hence, our data suggest that non-apoptotic FAS signaling acts as molecular switch between EF versus GC fate decisions via regulation of the mTOR axis and transcription. The defect of this modulatory circuit may explain the observed hypergammaglobulinemia and low memory B cell numbers in ALPS.

INTRODUCTION

Disrupted FAS (also known as CD95, TNFRSF6, or APO-1) signaling due to dominant-negative mutations in FAS or loss of FAS expression is linked to autoimmune lymphoproliferative syndrome (ALPS-FAS) in humans (1) and to an ALPS/systemic lupus erythematosus (SLE) phenotype in MRL/lpr mice (2). Beyond the development of autoimmunity with autoantibodies and lymphoproliferation, most patients with ALPS show hypergammaglobulinemia, fewer circulating class-switched memory cells, and marginal zone (MZ)-like B cells but normal numbers of transitional and naïve B cells as well as plasmablasts (3, 4). Histological analysis revealed defective MZ areas and rare, small germinal centers (GCs) (3). Conditional *Fas* deletion in B cells in mice is sufficient to induce B and T cell lymphoproliferation, defects in B cell memory repertoire, disruption of secondary lymphoid organ (SLO) structure, and autoimmunity (5, 6). *Fas*-deficient MRL/lpr mice show an enhanced extrafollicular (EF) response with proliferative plasmablast production and somatic hypermutation outside of GCs (7–9). In addition, akin to the polyreactive nature of the memory compartment in ALPS (10), immunoglobulin G (IgG) autoantibodies in MRL/lpr mice have characteristics of an EF response, with lower affinity, dominant IgG3 isotype, and a broader antigen recognition profile (11). The enhanced EF response in MRL/lpr mice and reduced memory cells in ALPS suggest an involvement of FAS in the regulation of

cell fate decisions that cannot be fully explained by its apoptosis-inducing function.

After initial activation at the T-B border, naïve B cells will either rapidly differentiate into antibody-secreting cells (ASCs) or EF memory cells in the EF space (12, 13) or move into the GC and give rise to conventional memory cells (14) and long-lived plasma cells (15). The human EF response comprises CD11c⁺ activated naïve B cells (aN) and their double negative 2 (DN2) descendants, which express the transcription factor T-bet and lack CD21, CD27, IgD, and CXCR5 (16). EF B cells are comprised in the CD21^{low}/age-associated B cell population, reported in other conditions (16–19). aN and DN2 are precursors of bona fide short-lived ASCs and enriched in self-reactive specificities (20, 21). Whereas both T-dependent and T-independent signals can drive EF B cell activation and maturation, it is unclear which receptors contribute to B cell rewiring to GC maturation in humans. The GC fate is regulated by the differential expression of transcription factors IRF4 (22) and IRF8 (23) and requires MYC (24), which is indispensable in early GC B cells before the expression of GC master regulator BCL6 (24). The phosphoinositide 3-kinase (PI3K)/mammalian target of rapamycin (mTOR) pathway (25, 26) guides B cell fate decisions. Upon PI3K activation, 3-phosphoinositide-dependent kinase 1 (PDK1) and the mTOR complex 2 (mTORC2) mediate site-specific Akt phosphorylation, which

results in mTORC1 activation (27) and phosphorylation of ribosomal protein S6. PTEN is an inositol phosphatase that directly counteracts PI3K activity by dephosphorylating phosphatidylinositol 3,4,5-trisphosphate (PIP₃). PTEN expression and function is regulated by subcellular localization (28). Hyperactivation of mTOR promotes rapid plasma cell differentiation (29), and mTORC1 inactivation in B cells abrogates the generation of ASCs in mice (30). Available data suggest that high PI3K/Akt/mTOR signaling favors EF B cell differentiation. In SLE, reduced PTEN expression correlates with disease activity (31), and EF atypical memory cells show hyperactive mTOR signaling pathway (32). Increased proportions of EF B cells in blood have been described in active SLE and in severe coronavirus disease 2019 (COVID-19) (21, 33, 34). Expansion of EF B cells in patients with gain-of-function mutations in the PI3K signaling pathway (17) suggests a role for the mTOR pathway in directing fate decisions during initial B cell activation. On the basis of the enhanced EF response in MRL/lpr mice and reduced GC-derived memory cells in patients with ALPS-FAS, we hypothesize that FAS may play a role in EF versus GC fate decisions.

¹Department of Rheumatology and clinical immunology, university medical center Freiburg, Faculty of medicine, university of Freiburg, Freiburg, germany. ²Faculty of Biology, university of Freiburg, Freiburg, germany. ³Department of Paediatric haematology and oncology, Second Faculty of medicine, Charles University, Prague, Czech Republic. ⁴Institute of medical Bioinformatics and Systems medicine, university medical center Freiburg, Faculty of medicine, university of Freiburg, Freiburg, germany. ⁵German cancer consortium (DKTK), partner site Freiburg, and German cancer Research center (DKFZ), Heidelberg, germany. ⁶Department of medicine and general cytometry Service-nucleus, Proteomics unit, ciBeRonc cB16/12/00400, cancer Research center (iBmcc/cSic/uSal/iBSal), universidad de Salamanca, Salamanca, Spain. ⁷Department of immunology, Leiden University Medical Center, Leiden, Netherlands. ⁸Genomics core Facility, European Molecular Biology Laboratory, Heidelberg, Germany. ⁹B cell unit, immunology Research area, Bambino Gesù children's hospital, IRCCS, Rome, Italy. ¹⁰Department of hematology, Institut de Recerca Hospital Sant Joan de Déu Barcelona, Barcelona, Spain. ¹¹Immunology Department, Hospital de la Santa Creu i Sant Pau, Barcelona, Spain. ¹²Department of Rheumatology and immunology, Hannover Medical School, Hannover, Germany. ¹³Pediatric hematology-immunology and Rheumatology Department, University Hospital Necker-Enfants Malades, Paris, France. ¹⁴Université de Paris, Laboratory of Immunogenetics of Pediatric Autoimmune Diseases, Imagine Institute, INSERM UMR 1163, Paris, France. ¹⁵Department of Paediatric Infectious Diseases, Rheumatology and immunology, Hospital Universitario Virgen del Rocío (HuVR), Instituto de Biomedicina de Sevilla (iBiS), Universidad de Sevilla/cSic, Red de Investigación Traslacional en Infectología Pediátrica RiTiP, Sevilla, Spain. ¹⁶Center for chronic immunodeficiency, University Medical Center Freiburg, Faculty of medicine, University of Freiburg, Freiburg, Germany. ¹⁷Clinical immunology and Primary Immunodeficiencies unit, Department of Pediatric Allergy and Clinical Immunology, Hospital Sant Joan de Déu Barcelona, Barcelona, Spain. ¹⁸Department of immunology, Hospital Universitario 12 de Octubre, Madrid, Spain. ¹⁹Primary Immunodeficiencies unit, Department of Pediatrics, Research Institute Hospital 12 Octubre (i+12), Madrid, Spain. ²⁰School of medicine, Complutense University, Madrid, Spain. ²¹Division of Rheumatology and clinical immunology, Medical University Graz, Graz, Austria. ²²Department of immunology, University Hospital Zurich, Zurich, Switzerland. ²³Department of Pathology, University Medical Center Freiburg, Freiburg, Germany. ²⁴Institute of Pathology, Heinrich-Heine University and University Hospital of Düsseldorf, Düsseldorf, Germany. ²⁵Division of molecular immunology, Department of Internal Medicine III, Nikolaus Fiebiger Zentrum, Friedrich-Alexander-University Erlangen-Nürnberg, Erlangen, Germany. ²⁶Department of Immunobiology, Faculty of Biology and Medicine, University of Lausanne, Lausanne, Switzerland. ²⁷Center for Pediatrics and Adolescent Medicine, University Medical Center Freiburg, Faculty of medicine, University of Freiburg, Freiburg, Germany. ²⁸ciBSS—centre for integrative Biological Signalling Studies, University of Freiburg, Freiburg, Germany. ²⁹Medical Physics Department, Centro Atómico Bariloche, Comisión Nacional de Energía Atómica (CNEA), Consejo Nacional de Investigaciones Científicas y Técnicas (CONICET), San Carlos de Bariloche, Argentina. ³⁰Division of clinical and experimental immunology, Institute of Immunology, Center for Pathophysiology, Infectiology and Immunology, Medical University of Vienna, Vienna, Austria.

*corresponding author. email: marta.rizzi@uniklinik-freiburg.de, marta.rizzi@meduniwien.ac.at

FAS can mediate apoptotic and non-apoptotic signaling (35, 36). Membrane-bound multimeric FAS ligand (FASL; also known as TNFSF6, CD95L, or CD178) binding to FAS recruits FAS-associated protein with death domain (FADD), pro-caspase-8, and c-FLIP to form the death-inducing signaling complex (DISC). This induces auto-proteolytic activation of caspase-8 and the activation of downstream executioner caspases (e.g., caspase-3) that promote apoptosis. In activated B cells, FAS-mediated apoptosis is counterbalanced by CD40-induced signals that require nuclear factor κ B (NF- κ B) or PI3K activation (37, 38). However, the components of the DISC can induce activation of the NF- κ B, mitogen-activated protein kinase (MAPK), and PI3K pathways (39). The soluble form of FASL can induce cell migration via PI3K signaling (40) in activated T cells and promotes memory B cell development into plasmablasts without affecting naïve B cells (41). In the context of T-B interactions, membrane-bound FASL expressed by T cells (42) seems to be more relevant. In mice carrying the palmitoylation-defective *Fas C194V* mutation, cells are unable to undergo apoptosis but can mediate non-apoptotic signaling. When the MRL/lpr mouse is reconstituted with *C194V Fas*, the auto-immune phenotype is reverted (43). Hence, non-apoptotic signaling through FAS may be involved in regulation of self-reactive B cells.

Here, we analyzed spleens and lymph nodes (LNs) of patients with ALPS-FAS and found an expansion of the EF B cell compartment associated with a reduced frequency of GC and conventional class-switched memory B cells. In-depth signaling studies showed increased B cell receptor (BCR) and mTOR signaling especially in EF B cells. We demonstrated that FAS signaling can modulate CD40-induced mTOR activation in healthy naïve B cells by regulating PTEN nuclear exclusion and that activation of caspase-8 contributes to this process. In ALPS-FAS B cells, FASL-dependent PTEN nuclear exclusion and mTOR modulation were defective. Last, in healthy CD40L-activated naïve B cells, transient stimulation of FAS changes expression of genes favoring the GC fate over the EF response. Together, our findings describe a physiological role of non-apoptotic FAS signaling in modulating the EF versus GC commitment upon early activation in human B cells.

RESULTS

Human spleens and tonsils show distinct compositions of EF and GC B cell populations

To allow a meaningful comparison of the B cell compartment in ALPS-FAS SLOs, we first profiled SLOs from healthy donors (HDs) ($n = 14$) and included markers for isotype specificity, homing and complement receptors, memory and plasma cells, and differentiation and activation status (fig. S1A and table S1). We compared B cell composition within tonsils ($n = 7$) and spleens ($n = 7$) (Fig. 1A). Uniform Manifold Approximation and Projection (UMAP) algorithm (44) for dimensionality reduction showed a phenotypic separation between tonsil and spleen (Fig. 1B). Primary populations such as naïve, pre-GC, GC, memory-like B cells (containing conventional CD27⁺ memory cells), and ASCs (Fig. 1, C and D, and fig. S1, B to D) were projected onto the composite UMAP and found to be only partially overlapping in location and size between tonsil and spleen (Fig. 1C). In particular, low memory-like but high GC B cell frequency was found in tonsils compared with spleen (Fig. 1E), in line with published data (45, 46). Primary populations were further delineated in nonredundant secondary populations. Describing the EF B cell populations (21), in the naïve compartment, we identified

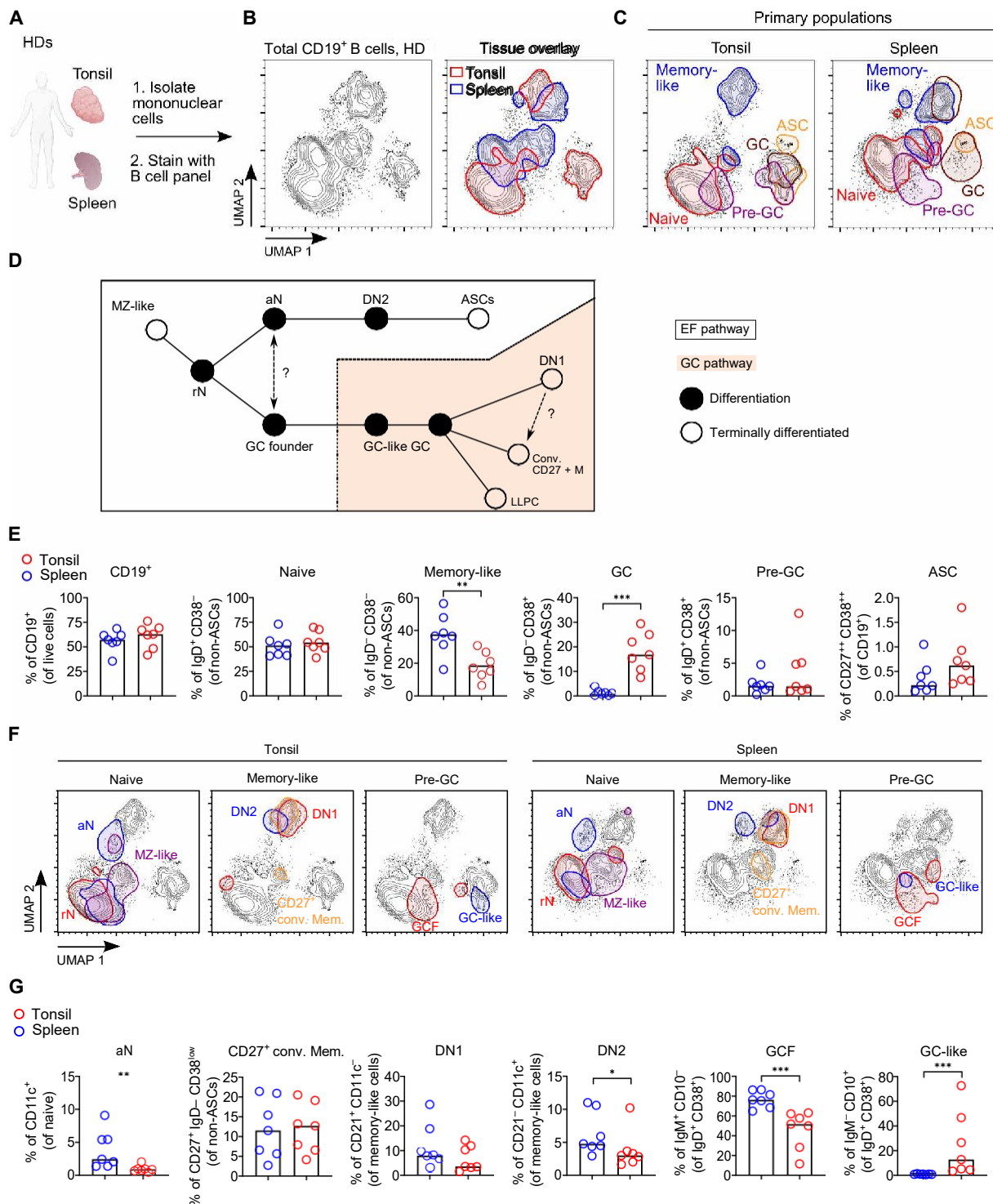


Fig. 1. Predominance of EF response in spleen and of GC response in tonsils in HDs. (A) experimental overview. generated with BioRender.com. (B) umaP projection of composite hD samples from CD19⁺ cells of tonsils (n = 7) and spleens (n = 7) analyzed by spectral flow cytometry (table S1). composite sample was derived from 10,000 representative cells from each sample. overlaid regions indicate the outermost boundaries of 90% equal probability contouring. (C) overlay of indicated primary B cell populations (gated as in fig. S1B) on composite umaP projection. (D) illustration of analyzed populations of the eF and gc pathways in human S10s. (E) Frequencies of CD19⁺ cells and primary B cell populations within indicated parent gates in hD tonsils and spleens. (F) Secondary B cell populations (gated as in fig. S1, B to D) overlaid on the composite umaP projection of respective tissues. (G) Frequencies of secondary B cell populations within indicated parent gates in hD tonsils and spleens. (e and g) median. Statistical significance was calculated using unpaired mann-Whitney test, and only significant results are indicated: *P < 0.05; **P < 0.01; ***P < 0.001. gcF, gc founder; cD27⁺ conv. mem., conventional cD27⁺ memory.

resting (CD11c⁻, rN) and activated (CD11c⁺, aN) naïve cells (Fig. 1, D and F, and fig. S1C). aN cells were more frequent in spleen samples (Fig. 1G) and expressed FAS (fig. S1E). aN cells differentiate into DN2 cells (CD27⁻IgD⁻CXCR5⁻CD21⁺) that express CD11c and FAS (fig. S1, D and E). DN1 cells (CD27⁻IgD⁻CXCR5⁺CD21⁺FAS^{low}) are transcriptionally and phenotypically very similar to their putative descendant CD27⁺ conventional memory cells (Fig. 1F and fig. S1E) (21). DN1 and DN2 tended to show a higher frequency in spleen compared with tonsils (Fig. 1G and fig. S1D). The frequency of MZ-like B cells was similar between both compartments (fig. S1F). The pre-GC B cell population (IgD⁺CD38⁺) can be divided into GC founders (CD10⁻) that are more frequent in the spleen (Fig. 1, D, F, and G, and fig. S1D) versus more committed GC-like cells (CD10⁺) (47) present at a higher frequency in the tonsil (Fig. 1, D, F, and G, and fig. S1D). Therefore, we proceeded to study the EF pathway in the spleen and GCs in tonsil samples.

The EF response is enhanced and class-switched memory B cell formation is reduced in patients with ALPS-FAS

To investigate whether FAS mutation affects the composition of the B cell compartment and thus B cell differentiation in SLOs, we compared four ALPS-FAS spleens (table S2) with seven HD spleens using the above-described flow cytometric approach. We observed a lower B cell frequency in ALPS-FAS spleens compared with HDs. Patients with ALPS-FAS do not have B lymphopenia, and this is likely because of the relative expansion of the T cell compartment (fig. S2A). The composite UMAP projecting total CD19⁺ cells revealed a phenotypic separation between the two groups, and three regions of interest (ROIs) were identified (Fig. 2, A and B, and fig. S2B). In ROI 1, aN B cells and DN2 cells are mapped (Fig. 2B), and these subsets were more frequent in patients with ALPS, with an increased DN2/DN1 ratio in patients (Fig. 2C). The identity of aN and DN2 B cells was confirmed by reduced levels of follicular homing receptor CXCR5 and increased expression of the tissue homing mediator CXCR3 (fig. S2C) (21). Memory and naïve B cells mapped in ROIs 2 and 3, respectively (Fig. 2A and fig. S2B). ALPS-FAS spleens showed decreased frequency of CD27⁺ conventional memory cells (Fig. 2C) and an enrichment of naïve follicular B cells (Fig. 2C) compared with controls. Hence, the EF B cell maturation pathway is enhanced in spleens of patients with ALPS-FAS.

Upon T-B cell interaction, a fraction of rN B cells develop into GC founder and GC-like cells that move into the GC and can be distinguished by the expression of CD10, IgD, and IgM (Fig. 1D and fig. S1D). We studied the early phase of GC maturation in LNs of two patients with ALPS-FAS. We compared healthy tonsils with ALPS-FAS LNs, as done in other studies (48, 49), because of the absence of active GCs in healthy LNs (fig. S2D). The tissue UMAP overlay showed a large overlap between HD tonsils and ALPS-FAS LNs (fig. S2E) but identified two ROIs that showed considerable separation between the two groups (Fig. 2, D and E). ROI A comprised GC B cells that were reduced in frequency in ALPS-FAS LNs (Fig. 2, E and F). In addition, within the pre-GC cells, ALPS-FAS LNs showed an accumulation of GC founder cells (CD10⁻IgM⁺) and a reduction of more committed CD10⁺IgM⁻ GC-like cells (Fig. 2, E and F). The reduced ratio between GC-like and GC founder cells indicated a defective maturation of GC founder into GC B cells in ALPS-FAS, which is in line with the previously reported small size of GCs in patients with ALPS-FAS (3). In spleens, ALPS-FAS and control samples showed similar but very low frequencies of GC

B cells (fig. S2F). We observed a positive correlation between aN and DN2 cells in both patients and controls. We also observed a negative correlation between aN and GC B cells in both groups (fig. S2G). These data support the concept that EF and GC responses represent alternative fates for activated naïve B cells, and in patients with ALPS, expansion of EF B cells occurs at the expense of the GC maturation pathway. In LNs and tonsils, ROI B mapped to CD27⁺ conventional memory B cells that were reduced in ALPS-FAS (Fig. 2, D and F). In ALPS-FAS spleens and LNs, we observed reduced frequencies of IgG1-2⁻ and IgA1-2⁻ expressing B cells and similar frequencies of IgG3⁺ and IgG4⁺ cells compared with controls (Fig. 2, G and H, and fig. S2H). By contrast, ASCs had a similar frequency between patients and controls both in spleen and in LN and tonsils (fig. S2I). Hence, conventional memory B cells are reduced in SLOs of patients with ALPS-FAS, indicating that their differentiation is defective in ALPS.

To extend the observations from the SLOs, we studied peripheral blood of untreated patients with ALPS-FAS. We confirmed a normal frequency of B cells, and in line with previous reports (4), we found reduced class-switched memory and MZ-like B cells and normal frequencies of ASCs (fig. S3, A and B). We found significantly increased aN B cells and reduced DN1 cells (fig. S3, A and B). Although the increase in frequency of DN2 cells was not found in all patients, the increased ratio between DN2 and DN1 cells was pointing to an EF expansion in patients with ALPS-FAS compared with controls (fig. S3B). As for isotype and subclass distribution within the B cells, we found a significant reduction of IgG1 and a lower, albeit not significant, IgG2-switched isotype frequency. No significant differences were found within the other isotypes, including IgG3 (fig. S3C), which is associated with EF origin (11, 21). Hence, deep phenotyping in peripheral blood of patients with ALPS-FAS confirmed the skewed maturation of B cells with a deficient development of conventional memory B cells and enhanced proportion of EF response. As for the T cell compartment, higher frequency of T cells was found in ALPS-FAS spleens, but the CD4 and CD8 frequency was similar in patients and controls (fig. S3, D and E). Proliferative FAS-controlled CD45RA⁺CD38⁺ double-negative T (DNT) cells (50) were expanded (fig. S3, D and E). We observed similar frequencies of both mature EF-resident CXCR5^{low}PD-1^{low} T helper cells (42) and CXCR5⁺PD-1⁺ mature T follicular helper (T_{FH}) cells in both groups (fig. S3, D and F). As expected, the two populations showed differential expression of interleukin-7R (IL-7R) and CCR7 (fig. S3G) and expressed FASL (fig. S3G), suggesting that FAS can be engaged by FASL-expressing T cells in situ in both the EF space and the GC.

B cells from ALPS-FAS SLOs show enhanced BCR and mTOR signaling

To identify signaling pathways involved in defective B cell maturation, we studied ALPS-FAS spleens ex vivo by mass cytometry [cytometry by time of flight (CyTOF)] with a panel including 11 phosphoproteins downstream of major signaling pathways (fig. S4A and tables S3 to S5). The UMAP projection calculated including all phosphoproteins and the multivariate chi-square analysis (51) showed a substantial segregation between ALPS and HD splenic CD19⁺ cells (Fig. 3A). Increased mTOR signaling as identified by pS6 and pAkt (T308) and increased BCR signaling as identified by pBTK, pLyn, and pPLCγ2 (Fig. 3B and fig. S4B) mostly contributed to the difference between ALPS and controls. We focused our analysis on the EF response that was expanded in ALPS-FAS spleens. We found consistently enhanced mTOR and BCR signaling in rN, aN, DN1,

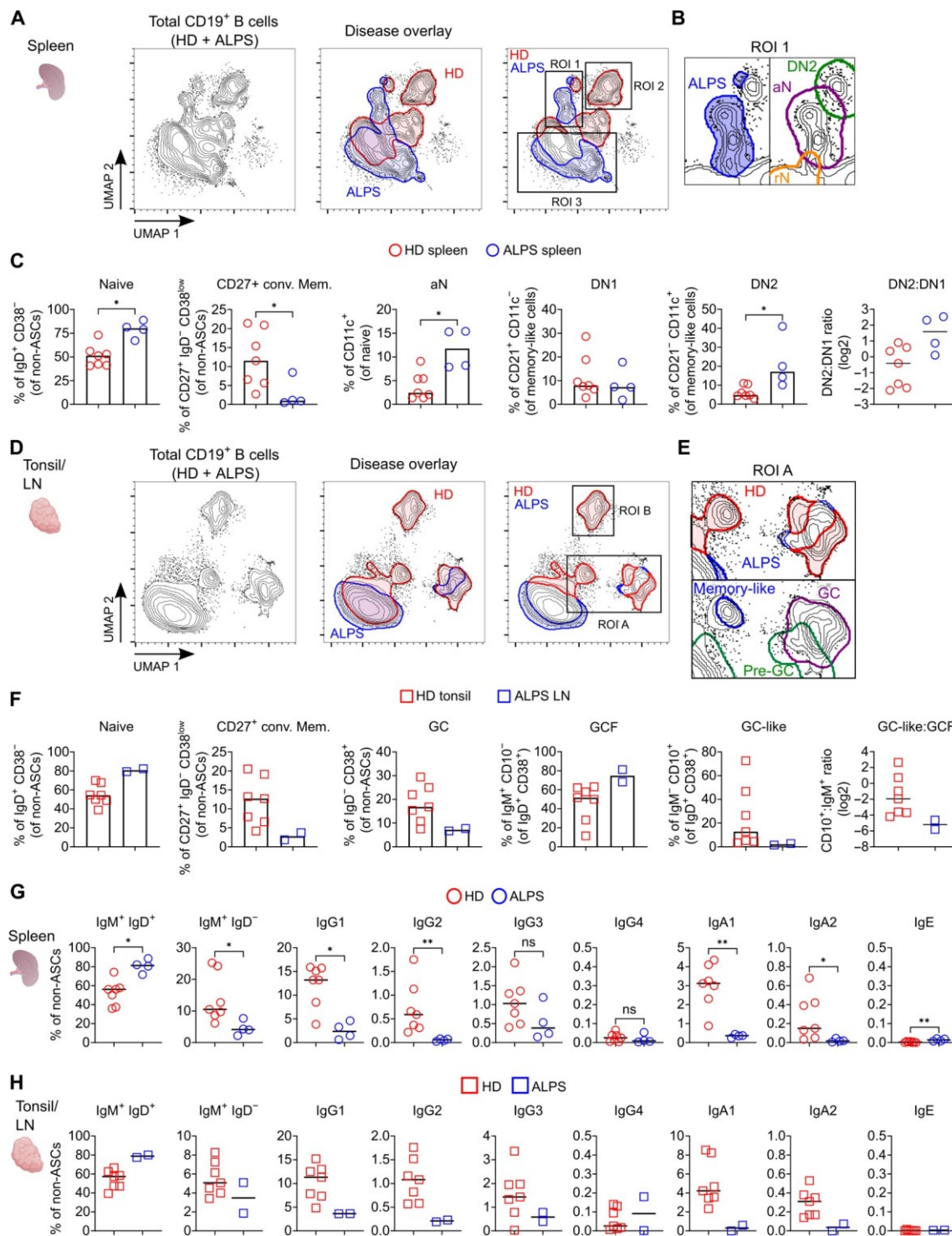


Fig. 2. Enhanced EF response, reduced conventional memory, and GC B cells in ALPS SLOs. (A) umaP projection of composite hD ($n = 7$) and aLPS-FaS ($n = 4$; see table S2 for clinical information) samples from splenic $CD19^+$ cells analyzed by spectral flow cytometry as in Fig. 1. overlaid regions denote the outermost boundaries of 90% equal probability contouring from aLPS and hD. Regions of interest: Roi 1, Roi 2, and Roi 3. (B) Zoom in on Roi 1. Disease state and B cell populations highlighted. overlay of indicated populations (gated as in fig. S1, B to e) on composite umaP projection. (C) Frequencies of B cell subpopulations in aLPS and hD spleens. Ratio of the Dn2:Dn1 frequency in both groups. (D) umaP projection of composite tonsillar hD ($n = 7$) and lns aLPS-FaS ($n = 2$) samples from $CD19^+$ cells. Regions of interest: Roi a and Roi B. (E) Zoom in on Roi a. Disease state and B cell populations highlighted. (F) Frequencies of B cell subpopulations within indicated parent gates in hD tonsils and aLPS lns. Ratio of the gc-like:gCF frequency in both groups. (G and H) Surface ig subclass distribution in spleen (g) and tonsils and lns (h) (gated as in fig. S2h) in hDs and aLPS. (c and f to h) median. Statistical significance was calculated using unpaired mann-Whitney test when $n \geq 3$, and significant results are indicated: * $P < 0.05$; ** $P < 0.01$. ns, not significant.

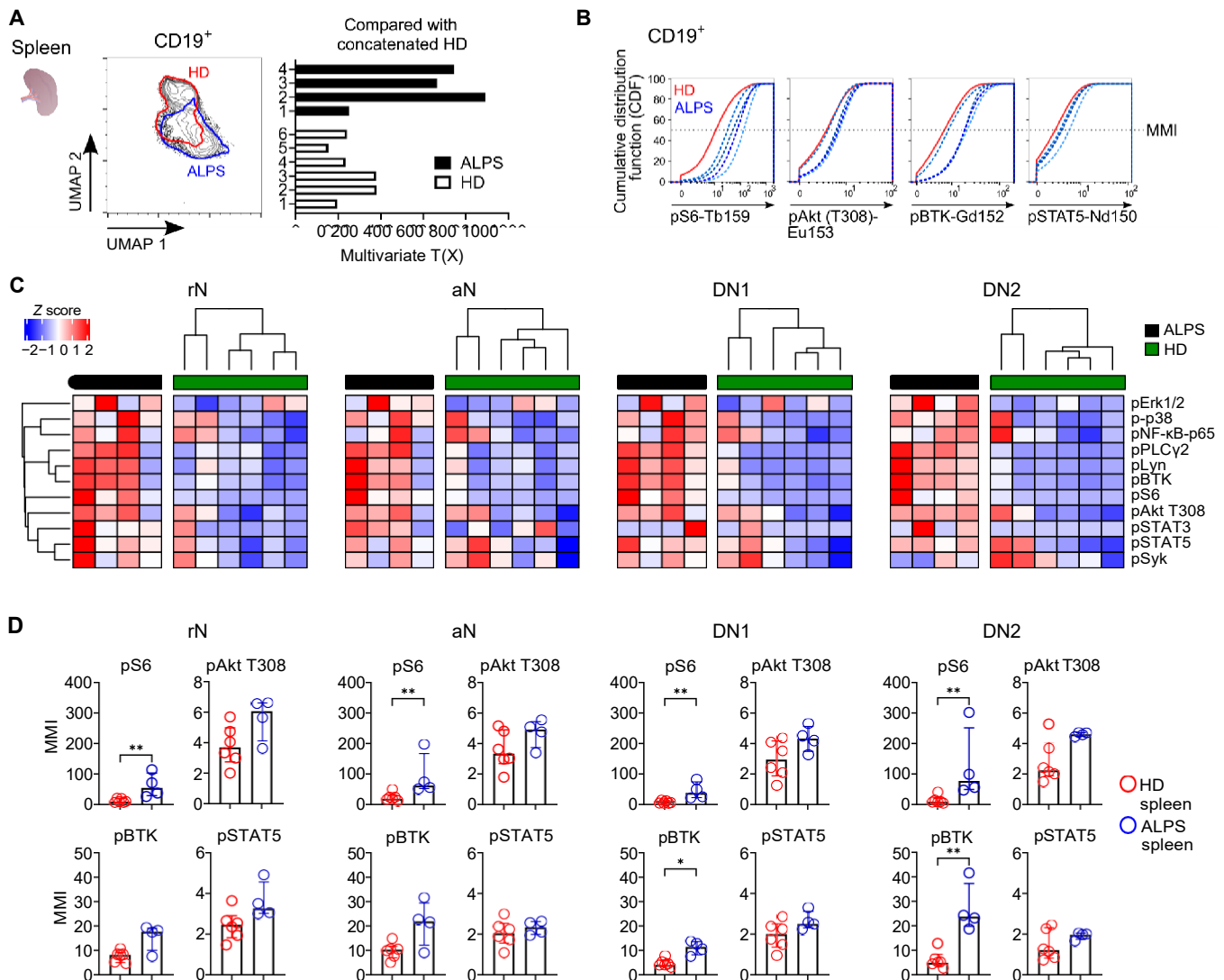


Fig. 3. Dysregulated activation in B cells from ALPS SLOs. (A) umaP projection of composite hD ($n = 6$) and aLPS-FaS ($n = 4$) samples from splenic $CD19^+$ cells analyzed by cytoF. composite sample was derived from all cells analyzed with the panel outlined in tables S3 to S5. overlaid regions denote the outermost boundaries of 90% equal probability contouring from the indicated disease state. multivariate $t(X)$ plot shows results from a chi-square test with modified binning of each individual sample against a concatenated hD sample. (B) cumulative distribution function (CDF) plots of indicated phosphoproteins from $CD19^+$ cells of the concatenated hD sample (red line) and four samples from patients with aLPS-FaS (blue shaded dotted lines). intersection of a given distribution, with the dashed line identifying its median metal intensity (mmi). (C) heatmaps of z scores of listed phosphoproteins in splenic B cell populations. Rows and columns were clustered using single agglomeration method on euclidean distance. (D) mmi of indicated phosphoproteins in indicated splenic B cell populations. median \pm iQR. Statistical significance was calculated using unpaired mann-Whitney test, and significant results are indicated: * $P < 0.05$; ** $P < 0.01$.

and DN2 cells of patients with ALPS-FAS (Fig. 3C and fig. S4C). In particular, we observed a significant increase of pS6 in all ALPS-FAS B cell subpopulations (Fig. 3, C and D), whereas significantly increased pBTK levels were restricted to DN1 and DN2 cells. In contrast, signal transducer and activator of transcription 5 (STAT5) and STAT3 phosphorylation was not globally dysregulated in ALPS-FAS splenic B cells, suggesting only a minor contribution of the cytokine microenvironment to the enhanced signaling in ALPS-FAS B cells. These data supported previous observations that the EF response is associated with increased mTOR and BCR signaling (52, 53), thus suggesting that non-apoptotic FAS signaling may contribute to the control of B cell activation.

CD40L-activated human B cells are partially resistant to FAS-induced apoptosis

Upon initial activation at the T-B border, B cells remain in the EF space for 2 to 3 days before moving into the GC (12). During this time, B cells get in contact with multiple T cells for a time span that can vary from 15 min to few hours (54), and FASL expressed by EF-resident T helper cells (42) can transiently engage FAS. Following the hypothesis that non-apoptotic FAS signaling contributes to the control of mTOR activity, we established an in vitro model of early B cell activation. Here, HD B cells were stimulated with CD40L overnight, resulting in FAS expression in naïve ($CD27^-$) and memory ($CD27^+$) cells (Fig. 4A and fig. S5, A and B) so that every B cell

bound the multimeric form of FASL (Fig. 4B) (55). FASL stimulation induced activation of caspase-3 that corresponded with lower expression of CD19 (Fig. 4C) and was time and dose dependent (Fig. 4, D to F). Caspase-3 activation was initially detected after 2 hours of incubation with FASL (Fig. 4D), and after 4 hours, only 30% of activated naïve and memory B cells displayed early and/or late apoptotic features (Fig. 4, D and E, and fig. S5C). In a dose response to FASL incubation for 4 hours, active caspase-3 was detected at minimal intensity at 12.5 ng/ml of FASL concentration and progressively increased, reaching a plateau between 100 and 200 ng/ml [Fig. 4F, median effective concentration (EC_{50}) = 46.9 ng/ml]. All successive studies were then conducted with a FASL concentration of 100 ng/ml, by which the maximal activation of caspase-3 at 4 hours was observed. To study whether FASL stimulation resulted in delayed apoptotic events, we loaded CD40L-stimulated B cells treated with FASL for 4 hours with PhiPhiLux G1D2, a fluorogenic quenched molecule linked to the caspase-3 substrate sequence DEVDGI (Fig. 4G). Survival of sorted active caspase-3-negative cells was comparable between FASL-treated and untreated cells after 1 and 2 days of culture (Fig. 4, H and I), indicating that B cells that do not activate caspase-3 after 4 hours of FAS engagement are not prompted to undergo apoptosis at later times. CD40L stimulation induces expression of anti-apoptotic molecules (37, 56). Accordingly, comparison of the transcriptome between CD40L-activated and resting naïve B cells displayed enrichment in gene sets related to metabolism, biosynthesis, and apoptosis (table S6 and fig. S5D). Among the latter, we found increased expression of c-FLIP, an apoptosis inhibitor that binds to FADD and caspase-8 (57), and of the BCL-2 family members BCL-2 and BCL-xL. Furthermore, we observed reduced levels of caspase-8 and caspase-10 compared with unstimulated cells (fig. S5D and table S6). We also found increased c-FLIP and stable caspase-8 and caspase-10 protein expression in CD40L-activated B cells (fig. S5E). Thus, in line with previous reports showing that B cells become sensitive to FASL-induced apoptosis after 2 days of activation (58), most recent CD40L-activated naïve B cells with short-term FAS engagement did not result in apoptosis.

FAS engagement modulates mTOR signaling in non-apoptotic B cells

On the basis of the above-described *in vitro* model, we studied signaling pathways triggered by FASL in apoptosis-protected B cells by CyTOF (tables S3 to S5). We compared overnight CD40L-activated primary HD B cells (CD40L) incubated for 4 hours with FASL (CD40L + FASL) or FASL in the presence of poly-caspase inhibitor Q-VD (CD40L + FASL + Q-VD). At 4 hours of FASL stimulation, we can readily distinguish apoptotic events on the basis of activation of caspase-3. Poly-caspase inhibitor Q-VD was used to assess the impact of caspase activity (fig. S6A). UMAP analysis comprising all markers included in the panel identified two clusters A and B (Fig. 5A, top). The size of cluster B was increased in unstimulated and FASL-treated cells and was associated with apoptosis markers (cPARP⁺, aCasp-3⁺, Bcl-2⁻, Bax⁺, CD20⁺), and cluster A represented non-apoptotic cells (cPARP⁻, aCasp-3⁻, Bcl-2⁺, Bax⁻, CD20⁺) (fig. S6, B and C). Hence, we analyzed signaling in non-apoptotic cPARP⁻ naïve (CD27⁻) and memory (CD27⁺) B cells (fig. S6D). Induction of phosphorylation of S6, Akt (S473), NF- κ B p65, and p38 MAPK was observed in CD40L-stimulated cells (Fig. 5B and fig. S6, E and F). Additional stimulation with FASL specifically reduced pS6 and pAkt (S473) levels, in particular in naïve B cells (Fig. 5B). To identify

FASL-induced changes in HD B cells, we compared the median intensities of surface markers and phosphoproteins analyzed by CyTOF in CD40L + FASL- or CD40L + FASL + Q-VD-treated naïve (CD27⁻) or memory (CD27⁺) cells versus CD40L control cells (Fig. 5C). Heatmap analysis showed that most surface and intracellular markers were stable upon 4 hours of FASL stimulation, including pNF- κ B p65 and p-p38 MAPK in both populations. Expression of total Akt and S6 proteins was constant by both CyTOF and conventional flow cytometry, whereas pS6 and pAkt (S473) were consistently reduced (Fig. 5C and fig. S6, G to I). 4E-BP1 phosphorylation at residue T37/46 is mTORC1 dependent, but nonsensitive to the mTOR inhibitor rapamycin (59), and was not modulated by FASL in our culture (Fig. 5C). Hence, FAS engagement resulted in a specific modulation of the CD40L-induced phosphorylation of Akt and S6, especially in naïve B cells, and less prominently in memory B cells, suggesting control of PI3K/Akt/mTOR pathway in B cells. We confirmed these data using conventional flow cytometry (Fig. 5E). Here, apoptotic cells were excluded combining CD19 expression, a fixable live/dead staining, cell size, and caspase-3 activation (fig. S6G; see Material and Methods for details). FASL-induced signaling modulation of pS6 and pAkt (S473) was reversed by the poly-caspase inhibitor Q-VD (Fig. 5E). Naïve B cells from patients with ALPS-FAS were unable to modulate CD40-induced mTOR activation in response to FASL (Fig. 5, F and G).

Looking at the dynamics of signaling modulation in HD CD40L-activated naïve B cells, reduction of S6 phosphorylation was observed already at very low concentrations of FASL [1.5 ng/ml, Fig. 5H, median inhibitory concentration (IC_{50}) = 2.43 ng/ml], lower than what was required to induce caspase-3 activation (IC_{50} = 46.9 ng/ml, see Fig. 4F). Down-modulation of pS6 reached a plateau with FASL (25 ng/ml). These data suggest that mTOR modulation is independent of caspase-3 induction in naïve B cells. Activation of B cells via CD40 may result in bimodal distribution of pS6 (Fig. 5D). To study whether high pS6 activation corresponded to high FAS expression and enhanced susceptibility to apoptosis, we studied FAS expression and S6 phosphorylation in CD40L-activated B cells. In CD40L dose-response studies, low doses of CD40L readily induced FAS expression, whereas higher concentrations of CD40L were required to induce S6 phosphorylation (Fig. 5I). Hence, expression of FAS and pS6 is independent in response to CD40L. Together, these data suggest that FAS-dependent reduction of pS6 is not due to early apoptosis of pS6^{high} cells. Functionally, mTOR signaling is often linked to cell proliferation (27, 60). To assess proliferation, naïve B cells were activated with CD40L overnight followed by stimulation with FASL for 4 hours, and subsequently, magnetically sorted non-apoptotic cells were cultivated with CD40L and IL-21. FASL stimulation for 4 hours did not change the proliferation pattern of apoptosis-protected cells at day 3 or 6 of culture (Fig. 5J).

FASL regulates both mTORC1 and mTORC2 signaling in CD40L-activated naïve B cells via active caspase-8

We next analyzed the kinetic of FASL-mediated changes of CD40L-induced signaling pathways in non-apoptotic cells by phosphoflow and Western blot. The phosphorylation of Akt and the regulation of its activity are complex, and Akt is thought to be downstream and upstream of mTORC1 and mTORC2, respectively (27). The mechanisms of mTORC2 activation are not fully understood but likely involve PI3K-produced PIP₃ (fig. S7A). As shown in Figs. 5 and 6, CD40L can induce Akt phosphorylation at S473 via mTORC2 and

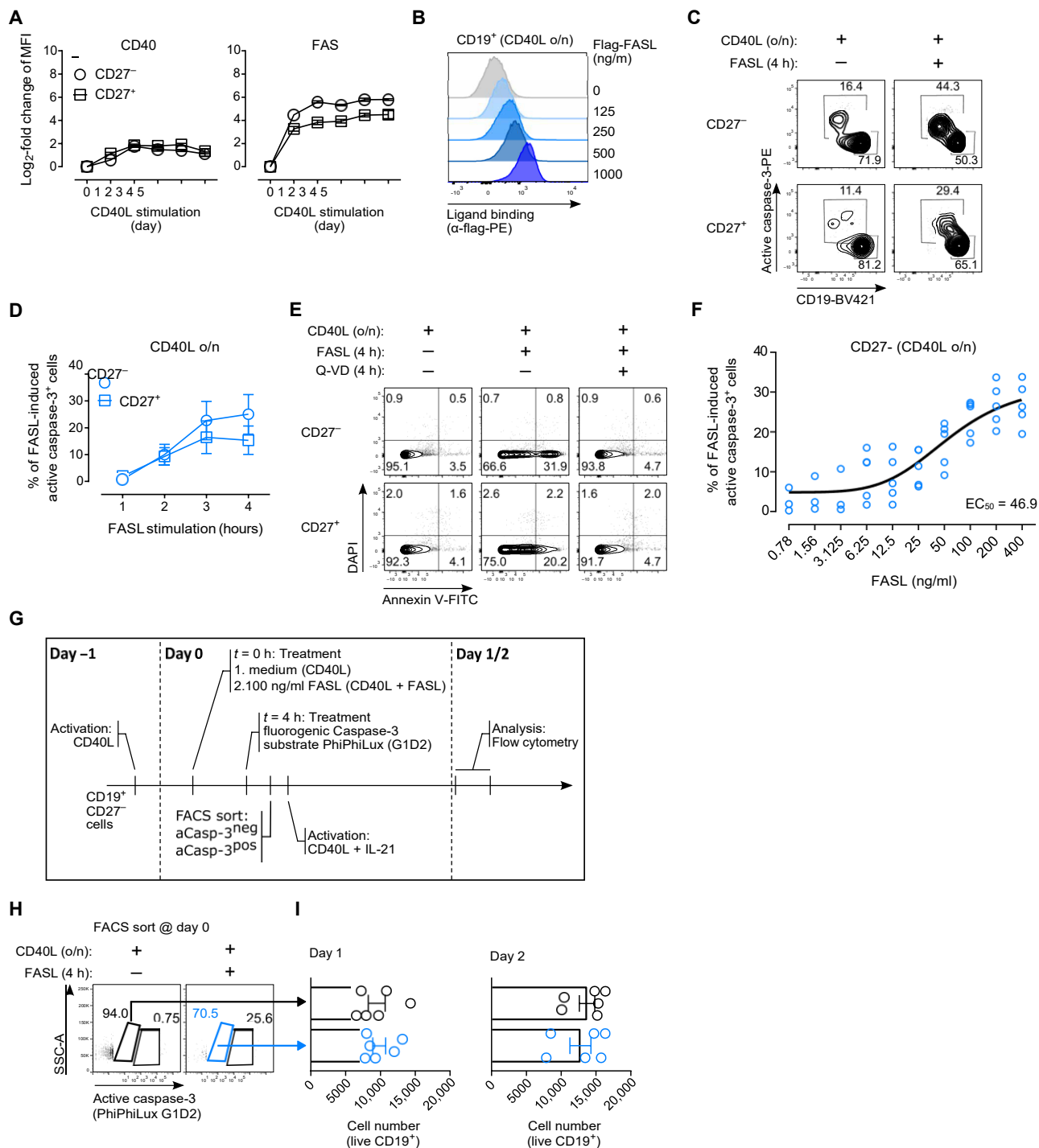


Fig. 4. CD40L-activated human B cells are partially resistant to FAS-induced apoptosis. (A) CD40 and FaS expression in CD40L-activated CD27⁻ and CD27⁺ hD B cells, depicted as log₂-fold change of median fluorescence intensity (mFI) compared with expression at day 0. (B) Representative flag-tagged flag-FaSI binding at indicated concentrations in overnight (o/n) CD40L-activated B cells. (C) overnight CD40L-activated CD27⁻ and CD27⁺ B cells were stimulated or not with FaSI for 4 hours. active caspase-3 and CD19 expression was analyzed by flow cytometry. (D) time course of FaSI-induced caspase-3 activation in overnight CD40L-stimulated CD27⁻ and CD27⁺ B cells. Frequencies of active caspase-3⁺ cells in CD40L-stimulated controls were subtracted. (E) annexin V and DaPI staining in overnight CD40L-activated CD27⁻ and CD27⁺ B cells in response to 4 hours of FaSI ± Q-VD. (F) Dose response of 4-hour FaSI-induced caspase-3 activation in overnight CD40L-activated CD27⁻ B cells. Frequencies of active caspase-3⁺ cells in CD40L-stimulated controls were subtracted. nonlinear fit in black. (G) experimental setup. B cells were stimulated as indicated and loaded with fluorogenic caspase-3 substrate PhiPhiLuxG1D2. (H) B cells were sorted on the basis of PhiPhiLuxG1D2 signal (i.e., active caspase-3) and (I) cultured with CD40L + il-21, and live cells were analyzed 1 and 2 days later by flow cytometry. (a) n = 4 in triplicates; (B) representative of n = 5; (c and D) n = 3; (e) representative of n ≥ 3; (F) n ≥ 3; (h and i) n = 3 in duplicates. (i) two-tailed paired Student's t test. (c to e and h) FaSI used at 100 ng/ml and Q-VD at 20 μM.

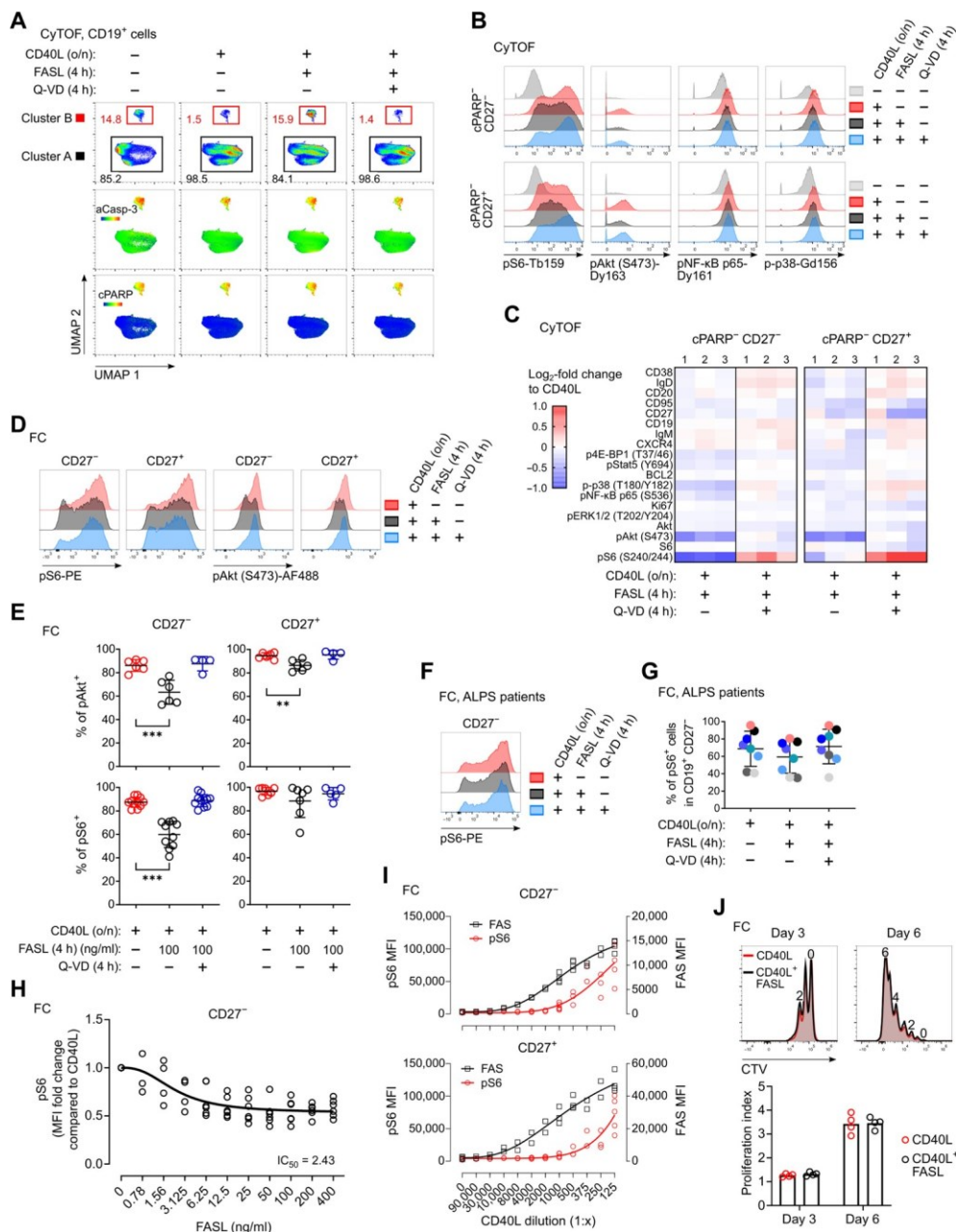


Fig. 5. FAS engagement modulates mTOR signaling in apoptosis-protected B cells. human B cells were activated with CD40I overnight or left untreated. cD40I-stimulated cells were cultured for 4 hours with FaSI ± Q-VD (see fig. S6a) and analyzed by cytoF or flow cytometry (Fc). (A) umaP projection of nucleated CD19⁺ cells; percentage of cells in clusters a and B is indicated. expression of active caspase-3 (casp-3) and cleaved PaRP (cPaRP). colors express median intensity scaled to the maximal expression. (B) Representative histograms of indicated markers. (C) heatmap summarizes log₂-fold change in the mmi of indicated markers in response to 4-hour FaSI ± Q-VD normalized to CD40I-stimulated cells in indicated cells. each column represents a biological replicate. (D) Representative expression of indicated markers in overnight CD40I-activated B cells after 4-hour FaSI ± Q-VD (see fig. S6g for gating). (E) Percentages of pakt- and pS6-positive overnight CD40I-activated CD27⁻ and CD27⁺ B cells in response to 4-hour FaSI ± Q-VD. (F) Representative expression of pS6 in CD27⁻ overnight CD40I-activated aIPS-FaS B cells after 4-hour FaSI ± Q-VD. (G) Fc. Percentages of pS6-positive overnight CD40I-activated CD27⁻ B cells derived from patients with aIPS-FaS carrying distinct FAS mutations in response to 4-hour FaSI ± Q-VD. each color identifies an individual patient. (H) Fc. Dose response of FaSI-induced changes of pS6 expression in overnight CD40I-activated CD27⁻ B cells. Fold change of pS6 mFi to CD40I-treated control cells is depicted. nonlinear fit in black. (I) Fc. Dose response to overnight CD40I stimulation (dilution factor in the x axis) in CD27⁻ and CD27⁺ B cells. expression of pS6 (red) and FaS (black) depicted as mFi. nonlinear fit in red (pS6) and black (FaS). (J) CD27⁻ B cells were loaded with celltrace Violet (ctV) and then activated overnight with CD40I (cd40I) followed by 4 hours of stimulation with FaSI (cd40I + FaSI). annexin V⁺ apoptotic cells were magnetically depleted, and non-apoptotic cells were further cultivated in the presence of CD40I and il-21. top, representative histogram. Bottom, proliferation index reflects the number of divisions of cells that underwent at least one division. (a to c) concatenated data from n=3; (D and e) n≥3; (g) n=8; (h) n≥3; (i) n≥2; (J) n=4. (e and g) mean ± Sem. one-way anova, followed by Dunnett's multiple comparison test; significant results are indicated. **P_{adj} < 0.01; ***P_{adj} < 0.001. (J) mean. FaSI used at 100 ng/ml and Q-VD at 20 μm, unless otherwise indicated.

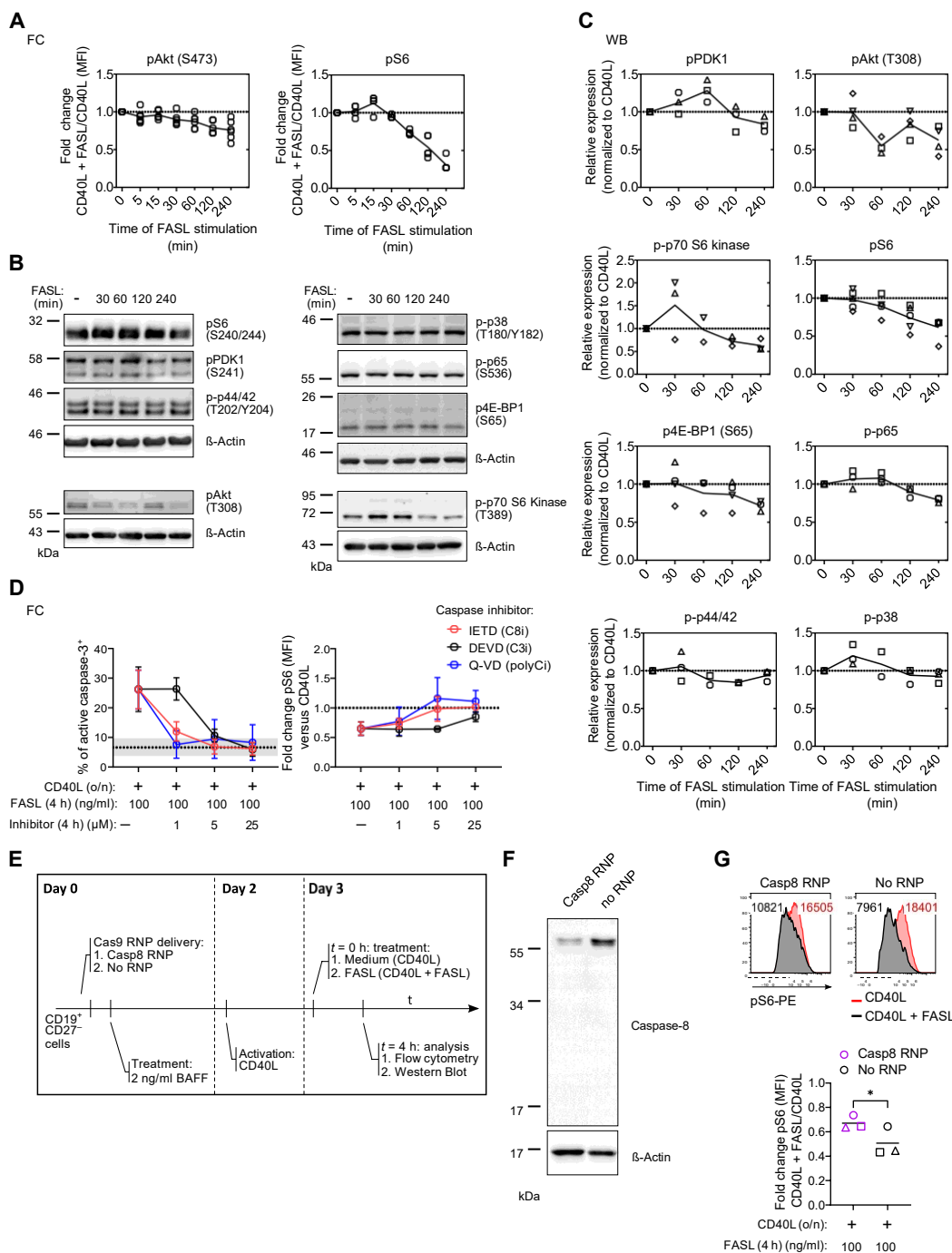


Fig. 6. Non-apoptotic FAS signaling regulates mTORC1 and mTORC2 dependent on caspase-8 activity. (A) Fc. time course of overnight cD401-activated cD27⁺ B cells in response to FaSI. Data are depicted as fold change of mFi to cD401-treated control cells. (B) overnight cD401-activated cD27⁺ B cells were stimulated with FaSI for indicated periods of time. early apoptotic cells were magnetically depleted, and live cells were analyzed by Western blot (WB). Representative WB analysis of indicated phosphoproteins. Lanes 2 to 5 of the original immunoblot were mirrored horizontally to match the order of time points. (C) Densitometric quantification of WB experiments. Intensities of phosphoproteins were normalized to the corresponding β-actin or Ponceau S signals. Relative expression was calculated compared with the cD401-activated control cells (dashed line). (D) overnight cD401-activated cells were stimulated with FaSI for 4 hours in the presence of scalar doses of caspase-8 (ietd) inhibitor, caspase-3 (DeVD) inhibitor, or poly-caspase inhibitor (Q-VD). activation of caspase-3, depicted as % of active caspase-3⁺ cells (left) and pS6 expression, depicted as fold change of pS6 mFi versus cD401-activated control cells (right). (E) experimental setup for cRiSPR-cas9-mediated deletion of caspase-8 in hD cD27⁺ B cells. electroporation with cas9 RnPs targeting caspase-8 (casp8 RNP) or without RnPs (no RNP). (F) Representative WB shows expression of caspase-8 and β-actin in cRiSPR-cas9-edited cells. (G) pS6 expression was analyzed in cRiSPR-cas9-edited cells after overnight cD401 activation ± 4-hour FaSI. Representative histograms show pS6 expression in cells electroporated with casp8 RnPs or no RnPs. mFi values are depicted. Bottom, fold change of pS6 mFi in FaSI-stimulated versus cD401-treated control cells. (a) n ≥ 5; (b) representative of n=3; (c) n=3; (D) n ≥ 3; (F and G) n=3. (a and c) mean. (D) mean ± SD. Dashed line indicates cD401 control level; gray area mean ± SD of cD401 control. (g) mean. two-tailed paired Student's t test. *P < 0.05. FaSI used at 100 ng/ml.

phosphorylation of PDK1 at S241, which in turn promotes Akt phosphorylation at T308. Akt T308 phosphorylation is required for mTORC1 activation and S6 phosphorylation. Thus, Akt T308 phosphorylation can be used as a proxy for mTORC1 activity and Akt S473 phosphorylation for mTORC2. To test whether non-apoptotic FAS signaling would modulate both mTORC1 and mTORC2, we assessed phospho-PDK1 S241, phospho-Akt T308, phospho-p70 S6K, phospho-S6 S240/244, phospho-4E-BP1 (S65) (reflecting mTORC1 activity), and phospho-Akt S473 (reflecting mTORC2). As determined by phosphoflow, phosphorylation of S6 and Akt S473 was reduced progressively upon FAS stimulation in CD40L-stimulated naïve B cells (Fig. 6A). Modulation of Akt S473 phosphorylation suggested an involvement of mTORC2 upon FAS engagement. Time course experiments showed that mTORC1 signaling was modulated at 3 to 4 hours (Fig. 6, B and C). PDK1 phosphorylation was also modulated, implying a role for PIP₃ and PTEN upstream of Akt. In contrast, p38 MAPK and NF- κ B signaling were induced by FASL stimulation within 30 min of incubation but were not followed by a signal down-modulation, and p42/p44 [extracellular signal-regulated kinase 1/2 (Erk1/2)] phosphorylation was unchanged by FAS engagement (Fig. 6, B and C, and fig. S7B). Hence, FASL modulates both mTORC1 and mTORC2 signaling, with a slight predominance for mTORC1.

Poly-caspase inhibitor Q-VD protected from FAS-induced down-modulation of pAkt (S473) and pS6 (Fig. 5D), implicating proximal caspases in this non-apoptotic function of FAS. To understand which caspase mediated this effect, we used specific caspase inhibitors. Caspase-8 inhibitor IETD restored S6 phosphorylation and apoptosis induction already at low concentrations, similarly to Q-VD control. In contrast, 5 μ M of executioner caspase-3 inhibitor DEVD inhibited apoptosis but was unable to restore S6 phosphorylation (Fig. 6D). At high DEVD concentration of 25 μ M, pS6 levels were similar to the CD40L control. However, at this concentration, DEVD also inhibited caspase-8 activity (fig. S7, C and D), further evidence of the role of caspase-8 in this process. To corroborate the contribution of caspase-8, we genetically deleted caspase-8 by CRISPR-Cas9 in primary naïve B cells with a ribonucleoprotein (RNP)-based approach (Fig. 6E). Caspase-8 expression was significantly reduced in CD40L-activated naïve B cells targeted with caspase-8 (Casp8) RNPs (Fig. 6F), resulting in increased resistance to FASL-induced apoptosis (fig. S7E). Intriguingly, reduced caspase-8 expression was associated with reduced down-modulation of pS6 in response to FASL (Fig. 6G and fig. S7F). Thus, FAS triggering in CD40L-activated naïve B cells results in modulation of mTORC1 and mTORC2 signaling and involves caspase-8.

Changes in protein expression in response to FASL identify a cross-talk between FAS and CD40 signaling

To understand the cross-talk between CD40L activation, FAS non-apoptotic signaling, and mTOR modulation, we studied changes in the proteome of activated primary HD B cells using a high-throughput tandem mass spectrometry (MS/MS) approach (61). We compared overnight CD40L-activated naïve B cells incubated for 4 hours with FASL (CD40L + FASL) or FASL in the presence of poly-caspase inhibitor Q-VD (CD40L + FASL + Q-VD) (fig. S8A). Subcellular fractions were isolated and clustered closely together, respectively, acknowledging MS/MS dataset robustness (fig. S8B). Because the DISC is assembled in the cytoplasmic tail of FAS, we compared the cytoplasmic fractions of FASL- with CD40L-treated control cells and

identified 278 differentially regulated proteins (absolute log₂-fold change >5), of which 125 were down- and 153 up-regulated in FASL-treated cells (Fig. 7, A and B, and table S7).

We found several proteins involved in the regulation of B cell signaling and function (Fig. 7C), and we focused on ubiquitin-specific processing protease 7 (USP7 or HAUSP) (Fig. 7C), which contains tumor necrosis factor (TNF) receptor-associated factor (TRAF) domains and binds TRAF family proteins (62). USP7 has been implicated in the ubiquitination and thereby subcellular localization of PTEN via a PML-DAXX molecular network (63, 64). Interaction between PML and DAXX has been shown in mouse B lymphocytes (65). In human myeloid leukemia, USP7-induced deubiquitination results in PTEN nuclear exclusion (66). Cytoplasmic USP7 abundance was significantly increased in FASL-treated compared with FASL-untreated cells (Fig. 7, C and D). In addition, the interactome of the main independent components identified by MS was obtained from the BioGRID database (67) and suggested a network linking CD40 and FAS signaling via members of the TRAF family, USP7, PTEN, and DAXX (Fig. 7E). We confirmed expression of USP7, DAXX, and PTEN in CD40L-activated naïve B cells (fig. S8C), indicating that all elements of this potential regulatory circuit are present in human B cells. DAXX has previously been reported to bind to the death domain of FAS (68, 69). In HD-derived lymphoblastoid cell lines (LCLs), FASL binding induced DAXX recruitment to FAS receptor complexes (fig. S8D), whereas this process was less evident in three of the four analyzed LCLs derived from patients with ALPS-FAS (fig. S8E). Following the hypothesis that active USP7 can deubiquitinate PTEN favoring its translocation from the nucleus to the cytoplasm, we tracked PTEN localization in primary naïve B cells by confocal microscopy. We observed that 4 hours of FASL stimulation in overnight CD40L-activated naïve B cells induced nuclear exclusion of PTEN and, consequently, a significant reduction in the ratio of nuclear PTEN versus cytoplasmic PTEN (Fig. 7, F and G, and fig. S8F). Nuclear exclusion of PTEN in response to FASL stimulation was not observed in ALPS-FAS patients' naïve B cells (Fig. 7G), and PTEN expression *ex vivo* was similar between patients with ALPS-FAS and controls in naïve B cells (Fig. 7H). These data are in line with the failure of ALPS-FAS B cells to modulate S6 phosphorylation in response to FASL (Fig. 5, F and G). In HD CD40L-activated naïve B cells, FASL stimulation slightly but significantly reduced expression of PTEN (Fig. 7I). In addition, phospho-PTEN was reduced in a subfraction of naïve B cells (Fig. 7J). Phosphorylation of PTEN reduces PTEN activity and increases stability (70, 71). Hence, together with PTEN nuclear exclusion, reduction of PTEN phosphorylation may contribute to FAS-induced modulation of PI3K signaling.

On the basis of literature data, the presence of the signaling components in human naïve B cells, the recruitment of DAXX to FAS, and immunofluorescence detection of PTEN, we hypothesize that FAS engagement induces the recruitment of DAXX to FAS, which may release the PML-DAXX inhibition of USP7. USP7 could in turn deubiquitinate PTEN, resulting in its nuclear exclusion, licensing PTEN to counteract cytoplasmic activity of CD40-induced PI3K/Akt/mTOR pathway (fig. S8G).

FASL regulates transcription in recently activated naïve B cells

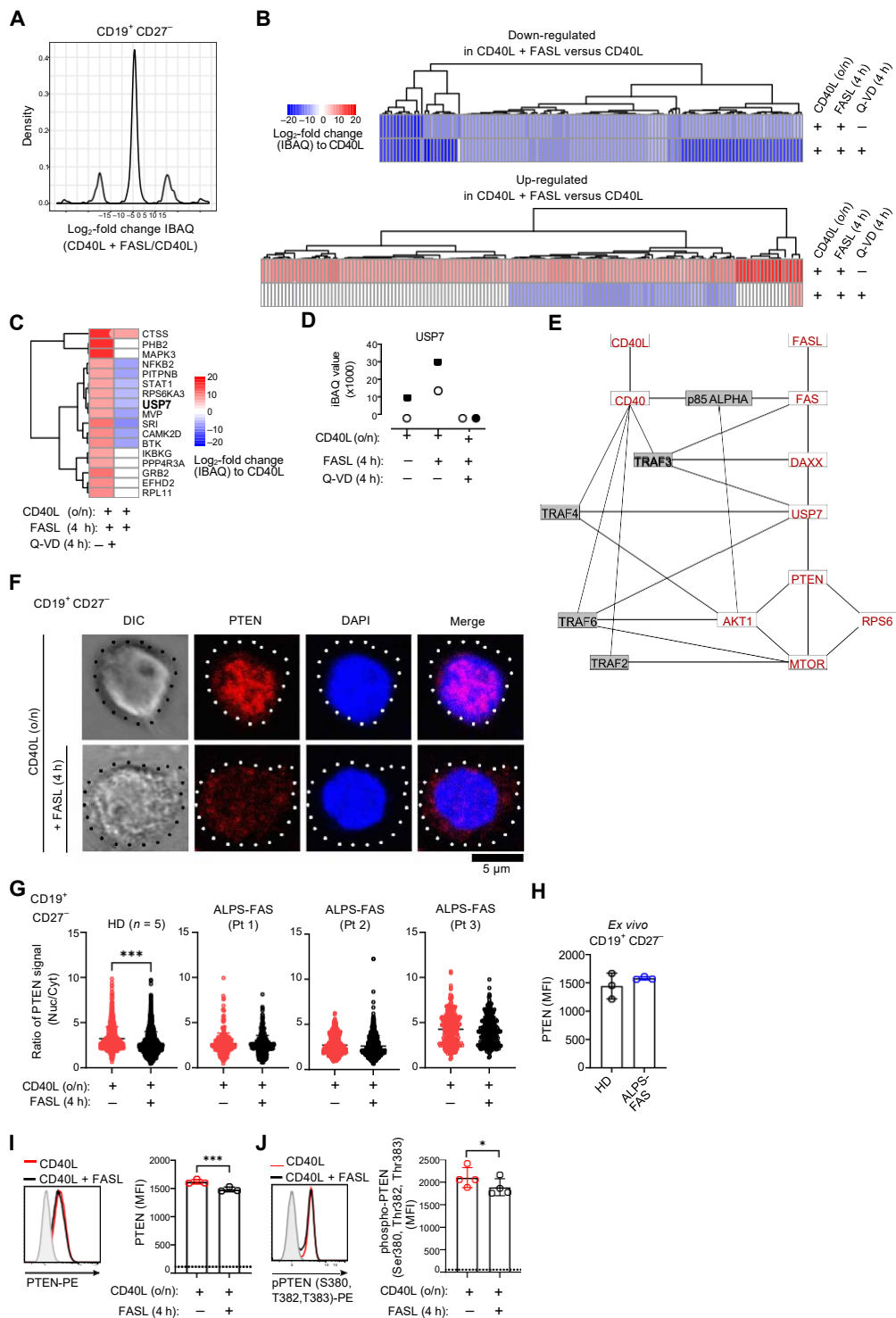
Modulation of signaling can result in cell fate decisions that are driven by transcriptional changes. FAS signaling has been previously associated with induction of gene expression (72, 73). We performed

Fig. 7. FAS-induced changes in protein expression result in PTEN nuclear exclusion in CD40L-activated naïve B cells.

overnight cD40L-stimulated CD27⁺ B cells were cultured for 4 hours with FaSI ± Q-VD, followed by Ic-mS/mS analysis. (A) Distribution of log₂-fold change of iBaQ values between CD40L + FaSI-treated and CD40L-treated control cells in the cytoplasmic fraction. (B) heatmaps display log₂-fold change of iBaQ values of down-regulated and up-regulated proteins in cD40L + FaSI/cD40L. (C) heatmap shows log₂-fold change of iBaQ values of selected candidate proteins. (D) iBaQ values of uSP7 in all in vitro conditions. each symbol represents a biological replicate. (E) Protein-protein interactions from the Biogrid interactome database based on experimental data and curated databases.

Proteins in red are investigated in this study. (F) Representative confocal image of overnight cD40L-activated CD27⁺ B cells ± 4-hour FaSI. Staining of Pten and DaPi. Dotted line indicates cytoplasmic membrane region. (G) Quantification of the ratio of Pten signal nucleus/cytoplasm.

each dot corresponds to a single cell, hDs (n = 5), and patients with aLPS-FaS (n = 3). (H) Pten mFi in ex vivo CD27⁺ B cells of hDs (n = 3) and patients with aLPS-FaS (n = 3). (I) Representative histograms of Pten expression in CD27⁺ B cells activated overnight with cD40L ± 4-hour FaSI and statistical analysis of Pten mFi. gray histogram shows fluorescence minus one (Fmo). (J) Representative histograms of phospho-Pten (S380, T382, and T383) expression in CD27⁺ B cells activated overnight with cD40L ± 4-hour FaSI and statistical analysis of phospho-Pten mFi. gray histogram shows Fmo. (a to d) mean ± SD. (g to h) two-tailed unpaired Student's *t* test; (i and j) two-tailed paired Student's *t* test; significant results are indicated: **P* < 0.05; ****P* < 0.001. FaSI used at 100 ng/ml and Q-VD at 20 μm.



RNA sequencing (RNA-seq) of overnight CD40L-activated primary human naïve B cells followed by FASL stimulation or by FASL and the caspase inhibitor Q-VD for 4 hours. Using VennUpset diagrams, we explored differentially expressed genes (DEGs) in CD40L + FASL-stimulated versus CD40L control cells to the transcriptional changes dependent on FASL, in CD40L + FASL- versus CD40L +

FASL + Q-VD-treated cells to find changes dependent on caspase activity, and in CD40L + FASL + Q-VD versus CD40L to dissect caspase activity-independent gene expression changes (fig. S9A). The scatterplots showed that genes that were up-regulated upon FASL stimulation were also positively regulated when comparing CD40L + FASL + Q-VD versus CD40L (*R* = 0.48, *P* < 0.001) and

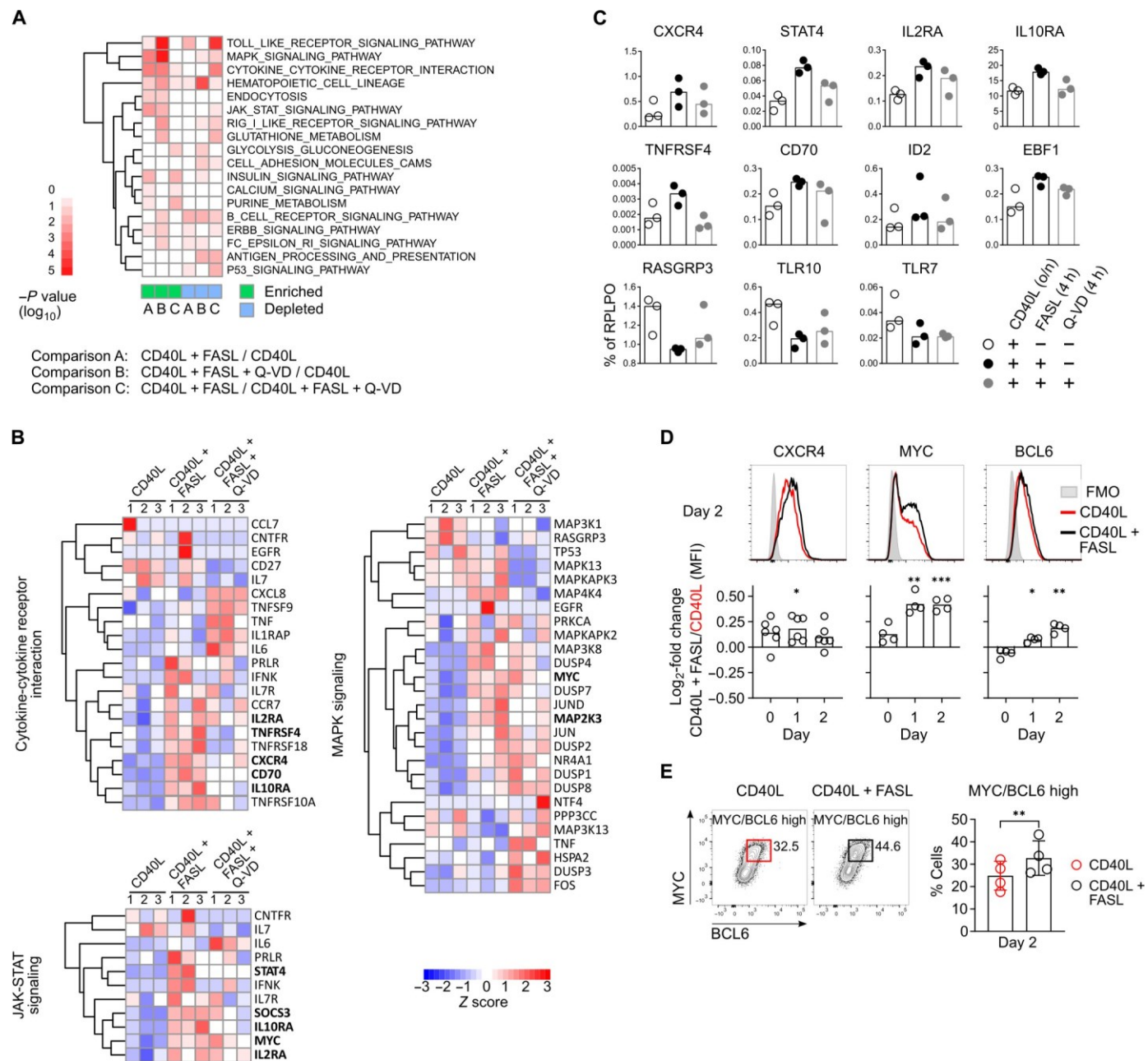


Fig. 8. FAS transcriptionally regulates B cell signaling and cell-cell interaction-related genes and induces MYC and CXCR4 expression. (A) Rna-seq of overnight cD40L-stimulated cD27⁺ B cells cultured for 4 hours with FaSl ± Q-VD. Kyoto encyclopedia of genes and genomes (Kegg) pathway analysis of Degr in indicated comparisons. Gene sets were clustered using complete agglomeration method on euclidean distance. (B) Heatmap shows Degr annotated to pathways included in the Kegg pathway analysis. Row-wise z score values are represented. Genes were clustered using complete agglomeration method on euclidean distance. Each column represents a biological replicate. (C) qPCR analysis of genes selected from (B). (D) overnight cD40L-activated cD27⁺ B cells were stimulated with FaSl for 4 hours. early apoptotic cells were magnetically depleted, and enriched non-apoptotic cells were further cultivated in the presence of cD40L and il-21 (see fig. S9D). expression of cXcR4, myc, and Bcl6 was assessed by Fc from days 0 to 2 of culture. Representative histograms show expression at day 2. Data are expressed as log₂-fold change of cD40L control cells. (E) coexpression of myc and Bcl6 at day 2 of culture and statistical analysis of myc/Bcl6^{high}-expressing cells. (a to c) n = 3; (D) n ≥ 4; (e) n = 4. (c) Bars indicate median. (D) Bars indicate mean. one-sample t test with Bonferroni's post hoc correction; significant results are indicated: *P_{adj} < 0.0167; **P_{adj} < 0.01; ***P_{adj} < 0.001. (e) Bars indicate mean ± SD. two-tailed paired Student's t test. **P < 0.01. FaSl used at 100 ng/ml and Q-VD at 20 μm.

CD40L + FASL versus CD40L + FASL + Q-VD (R = 0.68, P < 0.001) and vice versa (fig. S9B). These results suggested that most genes specifically regulated by FASL were caspase activity dependent. Gene Set Enrichment Analysis (74–76) revealed signatures that

included Toll-like receptor (TLR) signaling, cytokine-cytokine receptor interaction, MAPK signaling, and Janus kinase-STAT signaling pathways (Fig. 8A and table S8). FASL induced increased expression of cytokine and chemokine interactors (CXCR4, IL2RA,

IL10RA, and *CD70*), regulators of cytokine signaling (*STAT4* and *SOCS3*), and key players of MAPK signaling (*MAP2K3* and *MYC*) (Fig. 8B). We validated the expression of selected transcripts by quantitative polymerase chain reaction (qPCR) (Fig. 8C). FASL stimulation in CD40L-activated naïve B cells down-modulated genes related to the interferon (IFN) response (fig. S9F) and to TLR signaling (*TLR7* and *TLR10*) (Fig. 8, A and C), which are key features of the EF B cell differentiation (77). At the same time, CD40L + FASL-treated cells showed enhanced *IL-10RA* expression (Fig. 8, B and C), which was reported to suppress T-bet expression (78). Gene Set Enrichment Analysis also showed strong up-regulation in CD40L + FASL-stimulated B cells of gene signatures associated with responses to MYC and TNF (fig. S9C and table S9). Up-regulation of MYC and *BCL6* induction is linked to GC formation (24) and *CXCR4* to GC polarization (79). We analyzed whether FASL-induced transcriptional changes would also translate to the protein level. To this end, overnight CD40L-activated naïve B cells were stimulated with FASL for 4 hours, and non-apoptotic cells were then magnetically sorted and cultivated in vitro with CD40L and IL-21 (fig. S9D). In CD40L + FASL-treated cells, FAS expression decreased over 2 days (fig. S9E), acknowledging the initial 4 hours of FAS engagement and signaling in all cells. Transient FASL incubation induced rapid protein expression of *CXCR4* that persisted over 2 days and a progressive expression of MYC (Fig. 8D). CD40L + FASL-treated cells acquired the phenotype of GC-like cells coexpressing MYC and *BCL6* at a greater frequency (Fig. 8E), suggesting that non-apoptotic FAS signaling facilitates GC commitment. EF responses result in rapid plasmablast production (20, 77, 80). To substantiate the role of FAS signaling in regulating GC versus EF commitment, we monitored ASC differentiation in an identical setting as described above (fig. S9D). After 3 and 6 days of activation, differentiation to plasmablasts occurred less frequently in FASL-treated naïve B cells compared with CD40L only-treated controls (fig. S9, F and G). In the absence of FASL signaling, rapid plasmablast differentiation occurs. Together, our results suggest that FAS-induced non-apoptotic signaling contributes to the regulation of genes governing developmental decisions in activated B cells.

DISCUSSION

We found an expansion of the EF B cell response and a reduction of the GC pathway in SLOs of patients with FAS deficiency. The bias in development toward the EF pathway was associated with enhanced activation of the BCR, PI3K, and mTOR signaling pathway in ALPS-FAS B cells. In vitro modeling of initial T-dependent B cell activation with CD40L in HDs showed that transient FAS signaling can modulate the mTOR pathway by mediating PTEN nuclear exclusion with an involvement of caspase-8. FAS-dependent regulation of the mTOR pathway and PTEN nuclear exclusion were defective in patients with ALPS-FAS. Transient FAS signaling in CD40L-activated B cells resulted in transcriptional changes and affected plasmablast development. Hence, our data imply non-apoptotic FAS signaling as a molecular switch between EF and GC fates in activated naïve B cells.

Early activated B cells spend 2 to 3 days in the EF space before moving into the GC (12), integrating signals derived from BCR, T cells, and cytokines. In this phase, the quantity of signal seems to be more important than the quality. In mice, mTORC1 signaling is required in the early phase of EF plasmablast differentiation because

it induces unfolded protein response-related genes (81), and RAPTOR mutation results in both disturbed mTORC1 activation and defective EF responses (30). In human activated PI3K- δ syndrome (APDS), caused by mutations in *PIK3CD* and *PIK3R1*, hyperactive mTOR is linked to defective class-switch recombination (CSR) and conventional memory formation and enhanced formation of EF ($CD21^{\text{low}}$ T-bet⁺) B cells and ASCs (17, 82, 83). Defective CSR was also observed in mouse models with conditional deletion of the PI3K inhibitor *PIK3IP1* (84). We showed that in FAS-competent B cells, FAS engagement can modulate mTOR activation in vitro, and this modulation was abrogated in ALPS-FAS patients' B cells. In-depth ex vivo analysis of SLOs, the site where B cells are naturally activated, revealed hyperactive mTOR signaling in splenic EF B cells (aN and DN2). This increase in PI3K/Akt signaling has been indirectly confirmed in peripheral naïve B cells of patients with ALPS-FAS by increased expression of the phosphatase CD148 that can be used as proxy for previous PI3K/Akt activation (85). Therefore, high mTOR activity in ALPS may drive EF and ASC development at the expense of GC and memory formation, explaining hypergammaglobulinemia, enhanced EF B cell compartment, and low memory B cells (4, 10). Mechanistically, in CD40L-activated HD B cells, we showed that FAS engagement results in PTEN nuclear exclusion, a process that was defective in ALPS-FAS B cells. Dysregulation of PTEN activity and enhanced PI3K signaling has been linked in humans to autoimmunity (17, 31) and defects in memory formation (86). Furthermore, CD40-FAS interaction could potentially contribute to the modulation of the mTOR axis as receptor heteromerization of CD40 and FAS was shown to regulate CD40-induced NF- κ B responses in human B cells (87).

EF B cell differentiation is controlled by several signals. First, it is favored by intrinsic BCR affinity for the antigen (53, 80). Therefore, the enhanced BCR signaling, observed in EF B cells in ALPS-FAS spleens, may contribute to the expansion of the EF response in ALPS. Whether FAS contributes to the regulation of BCR signaling directly has not been addressed in this study. Second, T cell help plays a role, as shown by low frequencies of EF ($CD21^{\text{low}}$ T-bet⁺) B cells in patients with disruptive mutations in *CD40*, *IL-21 receptor*, *IFN- γ receptor*, and *STAT1* (loss of function) (17). In addition, TLR signaling favors EF development (33), and whereas IFN signaling promotes the expression of T-bet (88, 89), IL-10 signaling inhibits it (78). On the other side, expression of MYC marks GC initiation before the induction of the GC master regulator *BCL6* (24, 90). MYC is down-regulated in EF ($CD21^{\text{low}}$ T-bet⁺) B cells (91). Our transcriptome analysis shows that FAS signaling down-regulated transcription of genes related to the EF response (IFN and TLR), and enhanced expression related to the GC fate, such as *MYC*, *IL10RA*, and *CXCR4* in human CD40L-activated naïve B cells. These data, together with the changes in MYC and *BCL6* protein expression in CD40L + FASL-stimulated B cells and the delayed in vitro plasmablast development, substantiate the role of FAS in guiding GC versus EF differentiation.

FAS expression is rapidly induced in all naïve B cells upon CD40L activation, and FASL-induced apoptotic and non-apoptotic signals have a different dynamic. Modulation of PI3K signaling occurs rapidly at low concentration of FASL, whereas caspase-3 activation requires higher concentration of FASL and longer incubation. These data imply that modulation of signaling and apoptosis are two independent events and that the former does not require activation of caspase-3. Different factors guide apoptotic versus non-apoptotic

outcome of FAS signaling, for example, FAS expression and post-translational modifications (43), localization within the membrane [e.g., recruitment to lipid rafts (92)], concomitant signaling [e.g., BCR signaling (93)], and composition of the DISC (94). As for the latter, we analyzed the role of caspase-8 in the control of FAS-dependent mTOR modulation. Caspase-8 mediates non-apoptotic functions in a different cellular system, from activation of NF- κ B to MAPKs (95). Patients deficient in caspase-8 show a main defect in T cell activation and immunodeficiency—not always associated with the classical ALPS phenotype (96, 97). We show that pharmacological inhibition of caspase-8 or (partial) genetic knockout of caspase-8 restored S6 phosphorylation in CD40L-activated naïve B cells, implying a role for caspase-8 in this FAS function.

The present study was limited by the rarity of patients with ALPS-FAS and the availability of patient material, in particular, of tissue specimens of LN and spleen. To overcome this limitation, we analyzed peripheral blood mononuclear cells (PBMCs) of a larger ALPS-FAS cohort. To corroborate our *ex vivo* studies, we established *in vitro* models of early B cell activation that can only partially reproduce *in vivo* processes. The mechanistic studies (e.g., proteomics, transcriptome, extensive phosphoflow, and Western blot signaling analysis) to study the role of FAS in modulating CD40 activation in B cells were performed in healthy primary B cells. Because of the paucity of samples from patients with ALPS-FAS, only selected features (e.g., pS6 phosphorylation, PTEN translocation, and DAXX recruitment) were confirmed in patient-derived samples. We showed that caspase-8 is involved in non-apoptotic FAS signaling in this context using specific inhibitors and CRISPR-Cas9-mediated deletion of caspase-8 in primary B cells. The cytoplasmic localization of caspase-8 did not allow the sorting of knockout cells for the experiments. Thus, a mixture of knockout and wild-type cells was used, limiting a definitive interpretation of the data and requiring further studies to dissect the molecular cues linking caspase-8 activation and the mTOR signaling pathway. In summary, we showed that FAS specifically regulates human B cell activation, by modulating CD40-induced mTOR signaling, and promotes the transcription of genes important for B cell fate decisions. These data suggest that non-apoptotic FAS signaling contributes to developmental decisions of activated B cells. In ALPS, the mTOR inhibitor rapamycin efficiently reduces both lymphoproliferation and autoimmunity (98, 99). Whereas the reduction of DNTs can be explained by their dependence on mTOR signaling (50), the effect on autoimmunity and B cells is not yet understood. The few memory B cells formed in ALPS show high frequency of polyreactive specificities and high somatic hypermutation (10). Hence, autoimmunity in ALPS may be a result of both, a bias toward the EF response and an impaired deletion of polyreactive GC-derived memory B cells. The dysregulation of non-apoptotic FAS signaling may explain the low frequency of memory cells, the enhanced EF response associated with hypergammaglobulinemia, and the efficacy of rapamycin on autoimmunity in ALPS. In addition, it may pave the way for the development of new treatment strategies for autoimmune diseases specifically targeting the FAS/mTOR signaling pathway.

MATERIALS AND METHODS

Study design

This study aimed to investigate FAS signaling in human B cell activation and differentiation. We performed *ex vivo* and

in vitro experiments analyzing B cells from blood and SLOs of HDs and patients with ALPS-FAS. We studied the phenotype and signaling pathway activation in B cells derived from HDs and patients with ALPS-FAS *ex vivo*. Using *in vitro* modeling of human B cell activation, we corroborated these findings analyzing signaling pathways, apoptosis, the proteome, and the transcriptome in response to FASL stimulation. Biological and technical replicates were used to validate the findings, and experiments were performed at least twice.

Human material

Buffy coats and leukocyte reduction system chambers were purchased from the blood bank of the University Medical Center Freiburg (University Freiburg Ethics Approval: 147/15). Healthy control PBMCs were provided from the IR and Freeze Biobank, University Medical Center Freiburg. Tonsillar cells and LN cells of healthy controls sourced from tonsillectomy or excisional biopsies (University Freiburg Ethics Approval: 121/11). Control spleens derived from patients who underwent splenectomy because of blood vessel malformations were used in the study. None of the patients had known immunodeficiency, autoimmune disease, tumors, and recent or acute infections. LNs, splenic samples, and blood were obtained under local ethics-approved protocols (University Freiburg Ethics Approval: 47/19; ethic committee of CPP Ile-de-France: CPP IDF2 DC-2014-22722015-03-03 AF). In accordance with the Declaration of Helsinki, informed consent was obtained from all patients or parents, as well as healthy controls.

Patients' description

PBMCs, LNs, and splenic cells were collected from patients with ALPS-FAS. Clinical characteristics are listed in table S2 (100). Epstein-Barr virus-immortalized LCLs from four patients with ALPS-FAS were used.

PBMC and SLO cell isolation

PBMCs were purified from blood by density gradient centrifugation. Total (EasySep Human B Cell Isolation Kit), CD27⁻ naïve B cells (EasySep Human Naive B cell Isolation Kit), or CD27⁺ memory B cells (EasySep Human Memory B Cell Isolation Kit) (all STEMCELL Technologies) were isolated following the manufacturer's instructions. Mononuclear cells were isolated from tonsillar, LN, and splenic specimens by mechanical disruption. Minced tissue was pressed through a 380- μ m meshed sieve followed by filtration.

Cell culture

Magnetically isolated B cells were plated at the concentration of 0.75×10^6 to 1.5×10^6 cells/ml in enriched Iscove's modified Dulbecco's medium (IMDM; Thermo Fisher Scientific) supplemented with 10% heat-inactivated fetal calf serum (FCS), penicillin, streptomycin, insulin, apo-transferrin, nonessential amino acids, glutamine, and reduced glutathione as described earlier (101). Cells were activated with CD40L and IL-21 as described (101) and Fc-hFASL (P.S.'s laboratory) or flag-tagged FASL (soluble) (Enzo). Working concentrations of poly-caspase inhibitor Q-VD, caspase-3 inhibitor Z-DEVD-FMK, and caspase-8 inhibitor Z-IETD-FMK (all R&D Systems) were determined by analyzing FASL-induced apoptosis in overnight CD40L-activated B cells in the presence of serial dilutions of caspase inhibitors. Inhibitors were added at concentrations (1 to 25 μ M) indicated in figure legends. Apoptotic cells were magnetically depleted using the EasySep Dead Cell Removal (Annexin V)

Kit (STEMCELL Technologies) according to the manufacturer's instructions, or apoptotic active caspase-3⁺ cells were excluded by fluorescence-activated cell sorting (see the "Apoptotic cell exclusion and sorting of live cells" section). LCLs were maintained in IMDM supplemented with 10% FCS, penicillin, and streptomycin.

Cell proliferation assay

The cell proliferation assay was performed using the CellTrace Violet Cell Proliferation Kit (Thermo Fisher Scientific) according to the manufacturers' instructions. Proliferation was monitored by flow cytometry, and the proliferation index (102) was calculated.

CRISPR-Cas9 in primary human B cells

CRISPR-Cas9 deletion was carried out using the Neon Transfection System (Invitrogen) to deliver Cas9 RNPs into freshly isolated human naïve B cells according to the genome editing method by Integrated DNA Technologies (IDT). CRISPR RNAs (crRNAs) targeting exon 1 of human caspase-8 (*CASP8*) were designed using the CRISPOR (<http://crispor.tefor.net/>) (103) and the IDT crRNA design tools (<https://eu.idtdna.com/>) and purchased at IDT. The sequences of the used *CASP8* crRNAs with AGG protospacer adjacent motifs are as follows: GCCTGGACTACATTCCGCAA and GATGTTATTCCAGAGACTCC. crRNA and tracer RNAs (tracrRNA) at 200 μ M were mixed at equimolar concentrations with IDTE buffer (10 mM tris, 0.1 mM EDTA) to a concentration of 44 μ M and hybridized at 95°C for 5 min. Next, the crRNA:tracrRNA duplex was cooled slowly to room temperature (RT), mixed with Cas9 enzyme (36 μ M), and incubated for 20 min at RT to form the RNP complex. Naïve B cells were washed with phosphate-buffered saline (PBS), resuspended in electroporation buffer T (Thermo Fisher Scientific), and added to the RNP complex. Electroporation enhancer (10.8 μ M; all IDT) was added, and cells were electroporated with the Neon Transfection System 10 μ L Kit (Thermo Fisher Scientific) at 2350 V, 20-ms width, and 1 pulse. Cells were then rested in IMDM without antibiotics and rested for 15 min. Thereafter, cells were cultivated in enriched IMDM without antibiotics with B cell activating factor (BAFF) (2 ng/ml, Adipogen Life Sciences) for 2 days.

Flow cytometry

Single-cell suspensions were stained for 20 min at RT (CXCR3, CXCR4, CXCR5, CCR7, CD127, TCR $\gamma\delta$) or for 15 min at 4°C with corresponding antibodies. In SLOs, B cell subsets were characterized as follows (fig. S1B): CD27⁺⁺ CD38⁺⁺ ASCs. Among non-ASCs, IgD⁺ CD38^{low} naïve B cells, IgD⁻ CD38^{low} (memory-like) cells, CD38⁺ IgD⁺ pre-GC, and CD38⁺ IgD⁻ GC B cells (16, 104). Then, nonredundant secondary B cell subsets were identified as gated in figs. S1 (B to D) and S3A (16, 33, 47, 104). Identity of primary and secondary populations was reviewed by backgating using CD19, CD20, CD38, IgD, IgM, CD10, CD24, CD27, CD95, CXCR3, and CXCR5. In in vitro experiments with peripheral B cells, naïve cells were defined as CD27⁻ and antigen-experienced B cells as CD27⁺ (fig. S5A). Intracellular staining was performed using the IntraPrep Kit (Beckman Coulter) according to the manufacturer's instructions. To study phospho-proteins, samples were fixed with Cytotfix Fixation Buffer (BD Biosciences) or FoxP3 Transcription Factor Staining Buffer Set (Thermo Fisher Scientific). After surface staining, cells were either permeabilized with Phosflow Perm Buffer III (BD Biosciences) or washed in FoxP3 Permeabilization Buffer (Thermo Fisher Scientific), and phospho-proteins were stained for

30 min at RT. When using unconjugated or biotinylated primary antibodies, cells were stained with donkey anti-rabbit IgG-phycoerythrin (PE) antibody (Jackson ImmunoResearch) or streptavidin-BV421 or streptavidin-allophycocyanin (APC) in a subsequent staining step for 15 min at RT. Acquisition was performed on BD FACSCanto II (BD Biosciences) or Cytex Aurora (Cytex Biosciences) and analyzed with FlowJo software (FlowJo, BD Biosciences). For a complete list of antibodies, refer to table S10.

Mass cytometry

Isotope-tagged mass cytometry antibodies were purchased as conjugates (Fluidigm) or conjugated in-house using the Maxpar Antibody Labeling Kit (Fluidigm) according to the manufacturer's instructions. After conjugation, Antibody Stabilizer PBS (Candor Bioscience GmbH) was added in a 1:2 ratio. Optimal concentration for each antibody was determined by antibody titration. All purified antibodies used are listed in tables S3 to S5. For in vitro experiments, cells were fixed with Maxpar Fix I Buffer (Fluidigm), washed, and barcoded (0.5×10^6 cells) with barcoding antibodies (table S3) for 30 min at RT. For analyses of ex vivo specimens, sample sets (four to six samples per experiment) were assembled with the same ratio of patients versus controls in each barcoded set. Twenty percent of samples were measured twice to ensure consistency. Barcoded cells were washed in Maxpar Cell Staining Buffer (Fluidigm) and pooled. Surface antibody mixture (table S4) was added and incubated for 30 min at RT. Cells were washed and permeabilized in 80% ice-cold methanol for 30 min on ice, then stained with intracellular antibody mixtures (table S5) for 30 min at RT, resuspended in Maxpar Fix and Perm Buffer (Fluidigm) with iridium (Ir) intercalator (Fluidigm), and stained overnight at 4°C. For SLOs, specimens were fixed and permeabilized for 30 min at RT using the FoxP3 Transcription Factor Staining Buffer Set (Thermo Fisher Scientific). For acquisition, cells were washed twice in Maxpar Cell Staining Buffer and once in Maxpar deionized water (Fluidigm) before dilution in 20% EQ Four Element Calibration Beads (Fluidigm). The sample was then filtered through a 35- μ m mesh (BD Biosciences) and acquired with a CyTOF2 instrument (Fluidigm). Data were gated on Ir-positive nucleated cells, debarcoded, and exported as FCS files.

Apoptotic cell exclusion and sorting of live cells

Dead cell exclusion was performed by 4',6-diamidino-2-phenylindole (DAPI; Thermo Fisher Scientific) or by Zombie NIR/Aqua Fixable Viability Kit (both BioLegend) staining. Cells with features of early apoptosis were identified by flow cytometry using forward scatter (FSC) and side scatter (SSC) and a combination of CD19 expression and cell size or CD19 expression and activation of caspase-3 or annexin V surface expression (Fig. 4, C and E, and fig. S6G). Early apoptotic cells were excluded by CyTOF as shown in fig. S6 (B to D). For cell sorting, cells were incubated with 10 μ M of the fluorogenic caspase-3 substrate PhiPhiLux G1D2 (OncoImmunit Inc.) supplemented with 10% FCS for 30 min at 37°C. Cells were washed, and PhiPhiLux G1D2-negative (i.e., negative for active caspase-3) cells were sorted using a FACSMelody cell sorter (BD Biosciences).

Proteomic analysis

Naïve B cells (1.0×10^7 per condition) were washed with PBS, and subcellular fractions were extracted as described earlier (61). For liquid chromatography (LC)-MS/MS analysis, samples were processed as previously described (70). Details are provided in

Supplementary Methods. Data were analyzed using the MaxQuant and Perseus suite (v.1.6.0.1) packages versus the *Homo sapiens* Next-Prot proteome database. Averaged intensity-based absolute quantification (iBAQ) intensities were calculated per condition for all detected proteins. Principal components analysis was performed on the log₂ iBAQ intensities. Log₂-fold change between the iBAQ values in CD40L + FASL- versus CD40L-treated cells in the cytoplasmic fraction was calculated, and thresholds of -5 and +5 were determined empirically on the basis of the log₂-fold distribution (Fig. 7A). Protein-protein interactions of the main independent components identified by MS were obtained using the BioGRID interactome database (67) and merged in Cytoscape.

Immunoblotting and immunoprecipitation

Human naïve B cells were lysed for 10 min on ice in lysis buffer (50 mM Tris-HCl, 137.5 mM NaCl, 0.5 mM EDTA, 10% glycerol, 1% IGEPAL, 1 mM Na₃VO₄) containing phosphatase and protease inhibitors (Sigma-Aldrich). For immunoprecipitations, 2.0 × 10⁷ LCLs were incubated with Fc-hFASL (200 ng/ml) and solubilized in lysis buffer. Protein lysates were incubated with protein G Sepharose beads (GE Healthcare) and processed as described earlier (105). Immunoprecipitates and whole protein lysates were separated by 12 or 14% SDS-polyacrylamide gel electrophoresis before electrophoretic transfer onto nitrocellulose membranes (GE Healthcare). After Ponceau S staining, membranes were probed with antibodies listed in the “Reagents, software, and algorithms” section and then incubated with horseradish peroxidase-conjugated anti-rabbit (Jackson ImmunoResearch) and anti-mouse (Sigma-Aldrich) antibodies, respectively, and developed using SuperSignal West Pico PLUS Chemiluminescent or Pierce ECL Western Blotting Substrate (both Thermo Fisher Scientific). Densitometric analysis was performed using the Fusion-Capt software (Vilber Lourmat). After rolling ball subtraction, intensities were normalized to the β-actin or Ponceau S signal of corresponding samples. Relative expression was calculated compared with CD40L-activated control cells.

Immunofluorescence

Naïve B cells were stimulated in Lab-Tek II Chamber Slides (Thermo Fisher Scientific) coated with poly-d-lysine (Sigma-Aldrich) or U96 well plates. Cells were fixed with 4% paraformaldehyde for 10 min at RT and permeabilized with 0.5% Triton X-100 for 10 min at RT. Cells were then incubated with Image-iT Fx Signal Enhancer (Thermo Fisher Scientific) for 30 min at RT, followed by a blocking step with 4% donkey serum (Abcam) for 1 hour at RT. Next, cells were incubated with rabbit anti-PTEN overnight at 4°C in 1% donkey serum. Then, cells were incubated with donkey anti-rabbit A647 for 45 min or 2 hours at RT, and nuclei were counterstained with DAPI for 10 min at RT. Lab-Tek II chamber slides were mounted with ProLong Diamond Antifade Mountant (Thermo Fisher Scientific). Cells from U96 well plates were transferred in PBS to Cellvis 96-well glass-bottom plates (Cellvis, P96-1.5H-N). Images were acquired by confocal laser scanning microscopy using a 63× objective (Leica TCS SP2 AOBs) or 40× objective (Zeiss LSM710). Fluorescence intensity was determined from at least five images per donor, using the ImageJ software package Fiji.

RNA sequencing

RNA was extracted from naïve B cells using the RNeasy Mini Kit (Qiagen) according to the manufacturer’s instructions. On-column

deoxyribonuclease I treatment (Qiagen) was performed during RNA extraction according to the manufacturer’s instructions. Quality of RNA specimens was checked using the Fragment Analyzer (Advanced Analytical Technologies) applying Standard or High Sensitivity RNA Analysis Kits according to the manufacturer’s instructions. Barcoded stranded mRNA-seq libraries were prepared from high-quality total RNA samples (~100 ng per sample) using the Illumina TruSeq RNA Sample Preparation v2 Kit (Illumina) implemented on the liquid handling robot Beckman FXP2. Obtained libraries that passed the QC step were subjected to NextSeq 500 (Illumina) unidirectional sequencing.

Quantification and statistical analysis

To determine PTEN localization using the ImageJ software package Fiji, nuclear and cytoplasmic regions were detected in the focal plane. After PTEN signal intensity was calculated in both regions, PTEN localization was reported as a ratio of PTEN signal nucleus versus cytoplasm. Cytoscape equipped with the Biogrid plugin was used to predict protein-protein interactions. Statistical analysis was performed with GraphPad Prism (GraphPad Software) and R. Statistical details are listed in figure legends and supplementary figure legends. Data are represented as mean ± SEM or ± SD or median ± interquartile range (IQR) as indicated. Unpaired or paired two-tailed Student’s *t* test and unpaired Mann-Whitney test were used for differences between two groups. A one-sample *t* test (versus a value of 0) with Bonferroni’s post hoc correction was used in Fig. 8D. One-way analysis of variance (ANOVA) followed by Dunnett’s multiple comparison test was used for differences between more than two groups and repeated-measures two-way ANOVA with Šidák’s multiple comparisons test when responses were affected by two factors. Non-linear fitting with least squares regression was calculated when indicated. *n* represents the number of biological replicates. Statistics were calculated when *n* ≥ 3. *P* values of less than 0.05 were considered significant (**P* ≤ 0.05; ***P* ≤ 0.01; ****P* ≤ 0.001) and are reported in figures and supplementary figures.

Reagents, software, and algorithms

Refer to the respective tables for a complete list of antibodies (table S10); chemicals, reagents, and commercial assays (table S11); oligonucleotides (table S12); and software and algorithms (table S13) used in this study.

Supplementary Materials

This PDF file includes:

methods
Figs. S1 to S9
tables S1 to S5
legends for tables S6 to S9
tables S10 to S13

Other Supplementary Material for this manuscript includes the following:

Data file S1
tables S6 to S9
mDaR Reproducibility checklist

REFERENCES AND NOTES

1. F. Rieux-Iaucat, F. Le Deist, C. Hivroz, I. A. Roberts, K. M. Debatin, A. Fischer, J. P. de Villartay, mutations in Fas associated with human lymphoproliferative syndrome and autoimmunity. *Science* **268**, 1347–1349 (1995).
2. R. Watanabe-Fukunaga, C. I. Brannan, N. G. Copeland, N. A. Jenkins, S. Nagata, Lymphoproliferation disorder in mice explained by defects in Fas antigen that mediates apoptosis. *Nature* **356**, 314–317 (1992).

3. B. Neven, J. Bruneau, M. C. Stolzenberg, I. Meyts, A. Magerus-Chatinet, I. Moens, N. Lanzarotti, S. Weller, D. Amiranoff, B. Florin, B. Bader-Meunier, G. Ieверger, A. Ferster, C. Chantrain, S. Blanche, C. Picard, T. J. Molina, N. Brousse, A. Durandy, M. Rizzi, X. Bossuyt, A. Fischer, F. Rieux-Laucat, Defective anti-polysaccharide response and splenic marginal zone disorganization in aLPS patients. *Blood* **124**, 1597–1609 (2014).
4. A. Janda, M. Gomes, M. Abinun, S. Hambleton, A. Cant, F. Shackley, T. Flood, C. Waruuru, K. Beutel, K. Siepermann, G. Dueckers, T. Niehues, T. Wiesel, V. Schuster, M. G. Seidel, M. Minkov, K. Sirkia, M. V. Kopp, M. Korhonen, K. Schwarz, S. Ehl, C. Speckmann, Clinical and immunological overlap between autoimmune lymphoproliferative syndrome and common variable immunodeficiency. *Clin. Immunol.* **137**, 357–365 (2010).
5. Z. Hao, G. S. Duncan, J. Seagal, Y. W. Su, C. Hong, J. Haight, N. J. Chen, A. Elia, A. Wakeham, W. Y. Li, J. Iiepa, G. A. Wood, S. Casola, K. Rajewsky, T. W. Mak, Fas receptor expression in germinal-center B cells is essential for T and B lymphocyte homeostasis. *Immunity* **29**, 615–627 (2008).
6. Y. Takahashi, H. Ohta, T. Takemori, Fas is required for clonal selection in germinal centers and the subsequent establishment of the memory B cell repertoire. *Immunity* **14**, 181–192 (2001).
7. K. M. Nickerson, S. Smita, K. B. Hoehn, A. D. Marinov, K. B. Thomas, J. T. Kos, Y. Yang, S. I. Bastacky, C. T. Watson, S. H. Kleinstein, M. J. Shlomchik, Age-associated B cells are heterogeneous and dynamic drivers of autoimmunity in mice. *J. Exp. Med.* **220**, e20211346 (2023).
8. J. M. Odegard, B. R. Marks, I. D. DiPlacido, A. C. Poholek, D. H. Kono, C. Dong, R. A. Flavell, J. Craft, IcoS-dependent extrafollicular helper T cells elicit IgG production via IL-21 in systemic autoimmunity. *J. Exp. Med.* **205**, 2873–2886 (2008).
9. J. William, C. Euler, S. Christensen, M. J. Shlomchik, Evolution of autoantibody responses via somatic hypermutation outside of germinal centers. *Science* **297**, 2066–2070 (2002).
10. A. Janda, K. Schwarz, M. Van Der Burg, W. Vach, H. Ijspeert, M. R. Iorenz, M. Elgizouli, K. Pieper, P. Fisch, J. Hagel, R. Iorenzetti, M. Seidl, J. Roesler, F. Hauck, E. Traggi, C. Speckmann, A. Rensing-Ehl, S. Ehl, H. Eibel, M. Rizzi, Disturbed B-lymphocyte selection in autoimmune lymphoproliferative syndrome. *Blood* **127**, 2193–2202 (2016).
11. J. Suurmond, Y. Atisha-Fregoso, A. N. Barlev, S. A. Calderon, M. C. Mackay, C. Aranow, B. Diamond, Patterns of ana⁺ B cells for SLE patient stratification. *JCI Insight* **4**, e127885 (2019).
12. J. A. Roco, I. Mesin, S. C. Binder, C. Nefzger, P. Gonzalez-Figueroa, P. F. Canete, J. Ellyard, Q. Shen, P. A. Robert, J. Cappello, H. Vohra, Y. Zhang, C. R. Nowosad, A. Schiepers, I. M. Corcoran, K.-M. Toellner, J. M. Polo, M. Meyer-Hermann, G. D. Victoria, C. G. Vinuesa, Class-switch recombination occurs infrequently in germinal centers. *Immunity* **51**, 337–350.e7 (2019).
13. C. Viant, T. Wirthmiller, M. A. Eltanbouly, S. T. Chen, M. Cipolla, V. Ramos, T. Y. Oliveira, I. Stamatatos, M. C. Nussenzweig, Germinal center-dependent and -independent memory B cells produced throughout the immune response. *J. Exp. Med.* **218**, e20202489 (2021).
14. T. Inoue, R. Shinnakasu, C. Kawai, W. Ise, E. Kawakami, N. Sax, T. Oki, T. Kitamura, K. Yamashita, H. Fukuyama, T. Kurosaki, Exit from germinal center to become quiescent memory B cells depends on metabolic reprogramming and provision of a survival signal. *J. Exp. Med.* **218**, e20200866 (2021).
15. F. J. Weisel, G. V. Zuccarino-Catania, M. Chikina, M. J. Shlomchik, A temporal switch in the germinal center determines differential output of memory B and plasma cells. *Immunity* **44**, 116–130 (2016).
16. I. Sanz, C. Wei, S. A. Jenks, K. S. Cashman, C. Tipton, M. C. Woodruff, J. Hom, F. E. Iee, Challenges and opportunities for consistent classification of human B cell and plasma cell populations. *Front. Immunol.* **10**, 2458 (2019).
17. B. Keller, V. Strohmeier, I. Harder, S. Unger, K. J. Payne, G. Andrieux, M. Boerries, P. T. Felixberger, J. J. M. Landry, A. Nieters, A. Rensing-Ehl, U. Salzer, N. Frede, S. Usadel, R. Elling, C. Speckmann, I. Hainmann, E. Ralph, K. Gilmour, M. W. J. Wentink, M. Van Der Burg, H. S. Kuehn, S. D. Rosenzweig, U. Kolsch, H. Von Bernuth, P. Kaiser-Iabusch, F. Gothe, S. Hambleton, A. D. Vlasea, A. Garcia Garcia, I. Alsina, G. Markelj, T. Avcin, J. Vasconcelos, M. Guedes, J. Y. Ding, C. I. Ku, B. Shadur, D. T. Avery, N. Venhoff, J. Thiel, H. Becker, I. Erazo-Borras, C. M. Trujillo-Vargas, J. I. Franco, C. Fieschi, S. Okada, P. E. Gray, G. Uzel, J. I. Casanova, M. Fliegau, B. Grimbacher, H. Eibel, S. Ehl, R. E. Voll, M. Rizzi, P. Stepensky, V. Benes, C. S. Ma, C. Bossen, S. G. Tangye, K. Warnatz, The expansion of human t-bet^{hi}CD11^{low} B cells is T cell dependent. *Sci. Immunol.* **6**, (2021).
18. I. C. Mouat, E. Goldberg, M. S. Horwitz, Age-associated B cells in autoimmune diseases. *Sci. Adv.* **79**, 402 (2022).
19. I. C. Mouat, M. S. Horwitz, Age-associated B cells in viral infection. *PLOS Pathog.* **18**, e1010297 (2022).
20. M. C. Woodruff, R. P. Ramonell, N. S. Haddad, F. A. Anam, M. E. Rudolph, T. A. Walker, A. D. Truong, A. N. Dixit, J. E. Han, M. Cabrera-Mora, M. C. Runnstrom, R. Bugrovsky, J. Hom, E. C. Connolly, I. Albizua, V. Javia, K. S. Cashman, D. C. Nguyen, S. Kyu, A. Singh Saini, M. Piazza, C. M. Tipton, A. Khosroshahi, G. Gibson, G. S. Martin, C. I. Maier, A. Esper, S. A. Jenks, F. E. Iee, I. Sanz, Dysregulated naive B cells and de novo autoreactivity in severe COVID-19. *Nature* **611**, 139–147 (2022).
21. S. A. Jenks, K. S. Cashman, E. Zumaquero, U. M. Marigorta, A. V. Patel, X. Wang, D. Tomar, M. C. Woodruff, Z. Simon, R. Bugrovsky, E. I. Blalock, C. D. Scharer, C. M. Tipton, C. Wei, S. S. Lim, M. Petri, T. B. Niewold, J. H. Anolik, G. Gibson, F. E. Iee, J. M. Boss, F. E. Iund, I. Sanz, Distinct effector B cells induced by unregulated toll-like receptor 7 contribute to pathogenic responses in systemic lupus erythematosus. *Immunity* **49**, 725–739.e6 (2018).
22. K. Ochial, M. Maischein-Cline, G. Simonetti, J. Chen, R. Rosenthal, R. Brink, A. S. Chong, U. Klein, A. R. Dinner, H. Singh, R. Sciammas, Transcriptional regulation of germinal center B and plasma cell fates by dynamical control of IRF4. *Immunity* **38**, 918–929 (2013).
23. H. Xu, V. K. Chaudhri, Z. Wu, K. Biliouris, K. Dienger-Stambaugh, Y. Rochman, H. Singh, Regulation of bifurcating B cell trajectories by mutual antagonism between transcription factors IRF4 and IRF8. *Nat. Immunol.* **16**, 1274–1281 (2015).
24. D. P. Calado, Y. Sasaki, S. A. Godinho, A. Pellerin, K. Kochert, B. P. Sleckman, I. M. De Alboran, M. Janz, S. Rodig, K. Rajewsky, The cell-cycle regulator c-myc is essential for the formation and maintenance of germinal centers. *Nat. Immunol.* **13**, 1092–1100 (2012).
25. J. G. Cyster, C. D. C. Allen, B cell responses: cell interaction dynamics and decisions. *Cell* **177**, 524–540 (2019).
26. J. J. Iimon, D. A. Fruman, Akt and mTOR in B cell activation and differentiation. *Front. Immunol.* **3**, 228 (2012).
27. J. Jellusova, R. C. Rickert, The PI3K pathway in B cell metabolism. *Crit. Rev. Biochem. Mol. Biol.* **51**, 359–378 (2016).
28. M. S. Song, A. Carracedo, I. Salmena, S. J. Song, A. Egia, M. Malumbres, P. P. Pandolfi, Nuclear Pten regulates the aPc-Cdh1 tumor-suppressive complex in a phosphatase-independent manner. *Cell* **144**, 187–199 (2011).
29. S. Benhamron, S. P. Pattanayak, M. Berger, B. Tirosh, mTOR activation promotes plasma cell differentiation and bypasses XBP-1 for immunoglobulin secretion. *Mol. Cell. Biol.* **35**, 153–166 (2015).
30. D. D. Jones, B. T. Gaudette, J. R. Wilmore, I. Chernova, A. Bortnick, B. M. Weiss, D. Allman, mTOR has distinct functions in generating versus sustaining humoral immunity. *J. Clin. Invest.* **126**, 4250–4261 (2016).
31. X. N. Wu, Y. X. Ye, J. W. Niu, Y. Li, X. Li, X. You, H. Chen, I. D. Zhao, X. F. Zeng, F. C. Zhang, F. I. Tang, W. He, X. T. Cao, X. Zhang, P. E. Iipsky, Defective Pten regulation contributes to B cell hyperresponsiveness in systemic lupus erythematosus. *Sci. Transl. Med.* **6**, 246ra299 (2014).
32. C. Wu, Q. Fu, Q. Guo, S. Chen, S. Goswami, S. Sun, T. Li, X. Cao, F. Chu, Z. Chen, M. Iiu, Y. Iiu, T. Fu, P. Hao, Y. Hao, N. Shen, C. Bao, X. Zhang, I. Lupus-associated atypical memory B cells are mTORC1-hyperactivated and functionally dysregulated. *Ann. Rheum. Dis.* **78**, 1090–1100 (2019).
33. M. C. Woodruff, R. P. Ramonell, D. C. Nguyen, K. S. Cashman, A. S. Saini, N. S. Haddad, A. M. Iey, S. Kyu, J. C. Howell, T. Ozturk, S. Iee, N. Suryadevara, J. B. Case, R. Bugrovsky, W. Chen, J. Estrada, A. Morrison-Porter, A. Derrico, F. A. Anam, M. Sharma, H. M. Wu, S. N. Ie, S. A. Jenks, C. M. Tipton, B. Staiteh, J. I. Daiss, E. Ghosn, M. S. Diamond, R. H. Carnahan, J. E. Crowe Jr, W. T. Hu, F. E. Iee, I. Sanz, Extrafollicular B cell responses correlate with neutralizing antibodies and morbidity in COVID-19. *Nat. Immunol.* **21**, 1506–1516 (2020).
34. C. M. Tipton, C. F. Fucile, J. Darce, A. Chida, T. Ichikawa, I. Gregoret, S. Schieferl, J. Hom, S. Jenks, R. J. Feldman, R. Mehr, C. Wei, F. E. Iee, W. C. Cheung, A. F. Rosenberg, I. Sanz, Diversity, cellular origin and autoreactivity of antibody-secreting cell population expansions in acute systemic lupus erythematosus. *Nat. Immunol.* **16**, 755–765 (2015).
35. M. E. Peter, R. C. Budd, J. Desbarats, S. M. Hedrick, A. O. Hueber, M. K. Newell, I. B. Owen, R. M. Pope, J. Tschopp, H. Wajant, D. Wallach, R. H. Wiltrout, M. Zornig, D. H. Lynch, The cD95 receptor: apoptosis revisited. *Cell* **129**, 447–450 (2007).
36. A. Strasser, P. J. Jost, S. Nagata, The many roles of Fas receptor signaling in the immune system. *Immunity* **30**, 180–192 (2009).
37. R. J. Benson, B. S. Hostager, G. A. Bishop, Rapid cD40-mediated rescue from cD95-induced apoptosis requires TNFR-associated factor-6 and PI3K. *Eur. J. Immunol.* **36**, 2535–2543 (2006).
38. H. H. Iee, H. Dadgostar, Q. Cheng, J. Shu, G. Cheng, nF-kB-mediated up-regulation of Bcl-x and Bfl-1/a1 is required for cD40 survival signaling in B lymphocytes. *Proc. Natl. Acad. Sci. U.S.A.* **96**, 9136–9141 (1999).
39. R. M. Siegel, Caspases at the crossroads of immune-cell life and death. *Nat. Rev. Immunol.* **6**, 308–317 (2006).
40. S. Tazuin, B. Chaigne-Delalande, E. Selva, N. Khadra, S. Daburon, C. Contin-Bordes, P. Blanco, J. Ie Seyec, T. Ducret, I. Counillon, J. F. Moreau, P. Hofman, P. Vacher, P. Iegembre, The naturally processed cD95i elicits a c-yes/calcium/PI3K-driven cell migration pathway. *PLOS Biol.* **9**, e1001090 (2011).
41. S. D. Van Asten, P. P. Unger, C. Marsman, S. Bliss, T. Jorritsma, N. M. Thielens, S. M. Van Ham, R. M. Spaapen, Soluble Fas ligand enhances suboptimal cD401/iL-21-mediated human memory B cell differentiation into antibody-secreting cells. *J. Immunol.* **207**, 449–458 (2021).

42. S. e. Benteibibel, n. Schmitt, J. Bancheureau, h. ueno, human tonsil *B-cell lymphoma 6 (BCL6)*-expressing $CD4^+$ t-cell subset specialized for B-cell help outside germinal centers. *Proc. Natl. Acad. Sci. U.S.A.* **108**, e488–e497 (2011).
43. a. c. cruz, m. Ramaswamy, c. ouyang, c. a. Klebanoff, P. Sengupta, t. n. yamamoto, F. meylan, S. K. thomas, n. Richoz, R. eil, S. Price, R. casellas, V. K. Rao, J. Hippincott-Schwartz, n. P. Restifo, R. m. Siegel, Fas/CD95 prevents autoimmunity independently of lipid raft localization and efficient apoptosis induction. *Nat. Commun.* **7**, 13895 (2016).
44. I. mcinnes, J. healy, umap: uniform manifold approximation and projection for dimension reduction. arXiv:1802.03426 [stat.ml] (2018).
45. a. Kibler, B. Budeus, e. homp, K. Bronischewski, V. Berg, I. Sellmann, F. murke, a. heinold, F. m. heinemann, m. lindemann, i. Bekeredjian-Ding, P. a. horn, c. J. Kirschning, R. Kupperts, m. Seifert, Systematic memory B cell archiving and random display shape the human splenic marginal zone throughout life. *J. Exp. Med.* **218**, e20201952 (2021).
46. J. c. Weill, S. Weller, c. a. Reynaud, human marginal zone B cells. *Annu. Rev. Immunol.* **27**, 267–285 (2009).
47. S. Lebecque, o. de Bouteiller, c. arpin, J. Bancheureau, y. J. Iiu, germinal center founder cells display propensity for apoptosis before onset of somatic mutation. *J. Exp. Med.* **185**, 563–572 (1997).
48. B. Vidal-Rubio, m. Sanchez-carril, J. oliver-morales, a. gonzález-Fernandez, F. gambón-Deza, changes in human lymphocyte subpopulations in tonsils and regional lymph nodes of human head and neck squamous carcinoma compared to control lymph nodes. *BMC Immunol.* **2**, 2 (2001).
49. S. unger, m. Seidl, P. van Schouwenburg, m. Rakhmanov, a. Bulashevskaya, n. Frede, B. grimbacher, J. Pfeiffer, K. Schrenk, I. munoz, I. hanitsch, i. Stumpf, F. Kaiser, o. hausmann, F. Kollert, S. goldacker, m. van der Burg, B. Keller, K. Warnatz, the t(h)1 phenotype of follicular helper t cells indicates an IFN- γ -associated immune dysregulation in patients with $CD21$ low common variable immunodeficiency. *J. Allergy Clin. Immunol.* **141**, 730–740 (2018).
50. m. e. maccari, S. Fuchs, P. Kury, g. andrieux, S. Völkl, B. Bengsch, m. R. Iorenz, m. heeg, J. Rohr, S. Jäggle, c. n. castro, m. groß, u. Warthorst, c. König, i. Fuchs, c. Speckmann, J. thalhammer, F. g. Kapp, m. g. Seidel, g. Dückers, S. Schönberger, c. Schütz, m. Führer, R. Kobbe, D. holzinger, c. Klemann, P. Smisek, S. owens, g. horneff, R. Kolb, n. naumann-Bartsch, m. miano, J. Staniek, m. Rizzi, t. Kalina, P. Schneider, a. erxleben, R. Backofen, a. ekici, c. m. niemeyer, K. Warnatz, B. grimbacher, h. eibel, a. mackensen, a. P. Frei, K. Schwarz, m. Boerries, S. eh, a. Rensing-ehl, a distinct $CD38^+CD45Ra^+$ population of $CD4^+$, $CD8^+$, and double-negative t cells is controlled by Fas. *J. Exp. Med.* **218**, e20192191 (2021).
51. m. Roederer, W. moore, a. treister, R. R. hardy, I. a. herzenberg, Probability binning comparison: a metric for quantitating multivariate distribution differences. *Cytometry* **45**, 47–55 (2001).
52. a. J. Wishnie, t. chwat-edelstein, m. attaway, B. Q. Vuong, Bcr affinity influences t-B interactions and B cell development in secondary lymphoid organs. *Front. Immunol.* **12**, 703918 (2021).
53. D. Paus, t. g. Phan, t. D. chan, S. gardam, a. Basten, R. Brink, antigen recognition strength regulates the choice between extrafollicular plasma cell and germinal center B cell differentiation. *J. Exp. Med.* **203**, 1081–1091 (2006).
54. t. okada, m. J. miller, i. Parker, m. F. Krummel, m. neighbors, S. B. hartley, a. o'garra, m. D. cahan, J. g. cyster, antigen-engaged B cells undergo chemotaxis toward the zone and form motile conjugates with helper t cells. *PLoS Biol.* **3**, e150 (2005).
55. n. holler, a. tardivel, m. Kovacovics-Bankowski, S. hertig, o. gaide, F. martinon, a. tincl, D. Deperthes, S. calderara, t. Schulthess, J. engel, P. Schneider, J. tschopp, two adjacent trimeric Fas ligands are required for Fas signaling and formation of a death-inducing signaling complex. *Mol. Cell. Biol.* **23**, 1428–1440 (2003).
56. a. hennino, m. Berard, P. h. Krammer, t. DeFrance, Flice-inhibitory protein is a key regulator of germinal center B cell apoptosis. *J. Exp. Med.* **193**, 447–458 (2001).
57. m. irmler, m. thome, m. hahne, P. Schneider, K. hofmann, V. Steiner, J.-I. Bodmer, m. Schröter, K. Burns, c. mattmann, D. Rimoldi, I. e. French, J. tschopp, inhibition of death receptor signals by cellular FIP. *Nature* **388**, 190–195 (1997).
58. e. J. Schattner, K. B. elkon, D. h. yoo, J. tumang, P. h. Krammer, m. K. crow, S. m. Friedman, $CD40$ ligation induces apo-1/Fas expression on human B lymphocytes and facilitates apoptosis through the apo-1/Fas pathway. *J. Exp. Med.* **182**, 1557–1565 (1995).
59. a. y. choo, S. o. yoon, S. g. Kim, P. P. Roux, J. B. Blenis, Rapamycin differentially inhibits S6Ks and 4e-BP1 to mediate cell-type-specific repression of mRNA translation. *Proc. Natl. Acad. Sci. U.S.A.* **105**, 17414–17419 (2008).
60. R. a. Saxton, D. m. Sabatini, mTOR signaling in growth, metabolism, and disease. *Cell* **168**, 960–976 (2017).
61. P. Diez, c. Droste, R. m. Degano, m. gonzalez-munoz, n. ibarrola, m. Perez-andres, a. garin-muga, V. Segura, g. marko-Varga, J. IaBaer, a. orfao, F. J. corrales, J. De Ias Rivas, m. Fuentes, integration of proteomics and transcriptomics data sets for the analysis of a lymphoma B-cell line in the context of the chromosome-centric human Proteome Project. *J. Proteome Res.* **14**, 3530–3540 (2015).
62. R. Q. Kim, W. J. van Dijk, t. K. Sixma, Structure of uSP7 catalytic domain and three ubl-domains reveals a connector α -helix with regulatory role. *J. Struct. Biol.* **195**, 11–18 (2016).
63. m. S. Song, I. Salmena, a. carracedo, a. egia, F. Io-coco, J. teruya-Feldstein, P. P. Pandolfi, the deubiquitylation and localization of Pten are regulated by a hausP-Pml network. *Nature* **455**, 813–817 (2008).
64. I. c. trotman, X. Wang, a. alimonti, Z. chen, J. teruya-Feldstein, h. yang, n. P. Pavletich, B. S. carver, c. cordon-cardo, h. erdjument-Bromage, P. tempst, S. g. chi, h. J. Kim, t. misteli, X. Jiang, P. P. Pandolfi, ubiquitination regulates Pten nuclear import and tumor suppression. *Cell* **128**, 141–156 (2007).
65. S. Zhong, P. Salomoni, S. Ronchetti, a. guo, D. Ruggiero, P. P. Pandolfi, Promyelocytic leukemia protein (Pml) and Daxx participate in a novel nuclear pathway for apoptosis. *J. Exp. Med.* **191**, 631–640 (2000).
66. a. morotti, c. Panuzzo, S. crivellaro, B. Pergolizzi, u. Familiari, a. h. Berger, g. Sglio, P. P. Pandolfi, Bcr-Abl disrupts Pten nuclear-cytoplasmic shuttling through phosphorylation-dependent activation of hausP. *Leukemia* **28**, 1326–1333 (2014).
67. R. oughtred, J. Rust, c. chang, B. J. Breitkreutz, c. Stark, a. Willems, I. Boucher, g. Ieung, n. Kolas, F. Zhang, S. Dolma, J. coulombe-huntington, a. chatr-aryamontri, K. Dolinski, m. tyers, the BioGRID database: a comprehensive biomedical resource of curated protein, genetic, and chemical interactions. *Protein Sci.* **30**, 187–200 (2021).
68. X. yang, R. Khosravi-Far, h. y. chang, D. Baltimore, Daxx, a novel Fas-binding protein that activates Jnk and apoptosis. *Cell* **89**, 1067–1076 (1997).
69. a. Villunger, D. c. huang, n. holler, J. tschopp, a. Strasser, Fas ligand-induced c-Jun kinase activation in lymphoid cells requires extensive receptor aggregation but is independent of DaXX, and Fas-mediated cell death does not involve DaXX, RIP, or RaiDD. *J. Immunol.* **165**, 1337–1343 (2000).
70. F. Vazquez, S. Ramaswamy, n. nakamura, W. R. Sellers, Phosphorylation of the Pten tail regulates protein stability and function. *J. Immunol.* **20**, 5010–5018 (2000).
71. J. torres, R. Pulido, the tumor suppressor Pten is phosphorylated by the protein kinase cK2 at its c terminus. implications for Pten stability to proteasome-mediated degradation. *J. Biol. Chem.* **276**, 993–998 (2001).
72. g. m. Z. horste, D. Przybylski, m. a. Schramm, c. Wang, a. Schnell, y. Iee, R. Sobel, a. Regev, V. K. Kuchroo, Fas promotes t helper 17 cell differentiation and inhibits t helper 1 cell development by binding and sequestering transcription factor Stat1. *Immunity* **48**, 556–569.e7 (2018).
73. y. Shen, Z. Song, X. Iu, Z. ma, c. Iu, B. Zhang, y. chen, m. Duan, I. apetoh, X. Ii, J. guo, y. miao, g. Zhang, D. yang, Z. cai, J. Wang, Fas signaling-mediated th9 cell differentiation favors bowel inflammation and antitumor functions. *Nat. Commun.* **10**, 2924 (2019).
74. W. Iuo, m. S. Friedman, K. Shedden, K. D. hankenson, P. J. Woolf, gage: generally applicable gene set enrichment for pathway analysis. *BMC Bioinformatics* **10**, 161 (2009).
75. a. Subramanian, P. tamayo, V. K. mootha, S. mukherjee, B. I. ebert, m. a. gillette, a. Paulovich, S. I. Pomeroy, t. R. golub, e. S. Iander, J. P. mesirov, gene set enrichment analysis: a knowledge-based approach for interpreting genome-wide expression profiles. *Proc. Natl. Acad. Sci. U.S.A.* **102**, 15545–15550 (2005).
76. a. Iiberzon, c. Birger, h. thorvaldsdóttir, m. ghandi, J. P. mesirov, P. tamayo, the molecular Signatures Database (mSigDB) hallmark gene set collection. *Cell Syst.* **1**, 417–425 (2015).
77. R. a. elsner, m. J. Shlomchik, germinal center and extrafollicular B cell responses in vaccination, immunity, and autoimmunity. *Immunity* **53**, 1136–1150 (2020).
78. J. J. guthmiller, a. c. graham, R. a. Zander, R. I. Pope, n. S. Butler, cutting edge: il-10 is essential for the generation of germinal center B cell responses and anti-*Plasmodium* humoral immunity. *J. Immunol.* **198**, 617–622 (2017).
79. g. D. Victoria, D. Dominguez-Sola, a. B. holmes, S. Deroubaix, R. Dalla-Favera, m. c. nussenzweig, identification of human germinal center light and dark zone cells and their relationship to human B-cell lymphomas. *Blood* **120**, 2240–2248 (2012).
80. S. a. Jenks, K. S. cashman, m. c. Woodruff, F. e. Iee, i. Sanz, extrafollicular responses in humans and Sle. *Immunol. Rev.* **288**, 136–148 (2019).
81. B. t. gaudette, D. D. Jones, a. Bortnick, y. argon, D. allman, mtoRc1 coordinates an immediate unfolded protein response-related transcriptome in activated B cells preceding antibody secretion. *Nat. Commun.* **11**, 723 (2020).
82. c. I. Lucas, h. S. Kuehn, F. Zhao, J. e. niemela, e. K. Deenick, u. Palendira, D. t. avery, I. moens, J. I. cannons, m. Biancalana, J. Stoddard, W. ouyang, D. m. Frucht, V. K. Rao, t. P. atkinson, a. agharahami, a. a. hussey, I. R. Folio, K. n. olivier, t. a. Fleisher, S. Pittaluga, S. m. holland, J. i. cohen, J. B. oliveira, S. g. tangye, P. I. Schwartzberg, m. J. Ienardo, g. uzel, Dominant-activating germline mutations in the gene encoding the Pi(3)K catalytic subunit p110 δ result in t cell senescence and human immunodeficiency. *Nat. Immunol.* **15**, 88–97 (2014).
83. m. Wentink, V. Dalm, a. c. Iankester, P. a. van Schouwenburg, I. Scholvinck, t. Kalina, R. Zachova, a. Sediva, a. Iambeck, i. Pico-Knijnenburg, J. J. van Dongen, m. Pac, e. Bernatowska, m. van hagen, g. Driessen, m. van der Burg, genetic defects in Pi3K δ

- effect B-cell differentiation and maturation leading to hypogammaglobulinemia and recurrent infections. *Clin. Immunol.* **176**, 77–86 (2017).
84. K. Ottens, J. Schneider, I. P. Kane, A. B. Satterthwaite, PIK3IP1 promotes extrafollicular class switching in t-dependent immune responses. *J. Immunol.* **205**, 2100–2108 (2020).
85. e. m. cox, m. el-Behi, S. Ries, J. F. Vogt, V. Kohlhaas, t. michna, B. manfroi, m. al-maarri, F. Wanke, B. tirosh, c. Pongdarre, h. Iezeau, n. yogev, R. mittenzwei, m. Descatoire, S. Weller, J. c. Weill, c. a. Reynaud, P. Boudinot, I. Jouneau, S. tenzer, u. Distler, a. Rensing-ehl, c. König, J. Staniek, m. Rizzi, a. magérus, F. Rieux-Iaucat, F. t. Wunderlich, n. hövelmeyer, S. Fillatreau, aKt activity orchestrates marginal zone B cell development in mice and humans. *Cell Rep.* **42**, 112378 (2023).
86. g. J. Driessen, h. ijspeert, m. Wentink, h. g. yntema, P. m. van hagen, a. van Strien, g. Bucciol, o. cogulu, m. trip, W. nillesen, e. a. Peeters, i. Pico-Knijnenburg, B. h. Barendregt, m. Rizzi, J. J. van Dongen, n. Kutukculer, m. van der Burg, increased PI3K/akt activity and deregulated humoral immune response in human Pten deficiency. *J. Allergy Clin. Immunol.* **138**, 1744–1747.e5 (2016).
87. c. R. Smulski, m. Decossas, n. chekka, J. Beyrath, I. Willen, g. guichard, R. Iorenzetti, m. Rizzi, h. eibel, P. Schneider, S. Fournel, hetero-oligomerization between the tNF receptor superfamily members cd40, Fas and tRaiR2 modulate cd40 signalling. *Cell Death Dis.* **8**, e2601 (2017).
88. P. Kochayoo, P. thawornpan, K. Wangriatisak, S. changrob, c. Ieepiyasakulchai, I. Khawawitsut, J. h. adams, P. chootong, interferon- γ signal drives differentiation of t-bet(hi) atypical memory B cells into plasma cells following Plasmodium vivax infection. *Sci. Rep.* **12**, 4842 (2022).
89. R. yang, D. t. avery, human t-bet governs the generation of a distinct subset of cD11c^{hi}cD21^{low} B cells. *Sci. Immunol.* **7**, eabq3277 (2022).
90. D. Dominguez-Sola, g. D. Victoria, c. y. ying, R. t. Phan, m. Saito, m. c. nussenzweig, R. Dalla-Favera, the proto-oncogene myc is required for selection in the germinal center and cyclic reentry. *Nat. Immunol.* **13**, 1083–1091 (2012).
91. i. isnardi, y. S. ng, I. menard, g. meyers, D. Saadoun, i. Srdanovic, J. Samuels, J. Berman, J. h. Buckner, c. cunningham-Rundles, e. meffre, complement receptor 2/cD21- human naive B cells contain mostly autoreactive unresponsive clones. *Blood* **115**, 5026–5036 (2010).
92. J. R. muppidi, R. m. Siegel, ligand-independent redistribution of Fas (cD95) into lipid rafts mediates clonotypic t cell death. *Nat. Immunol.* **5**, 182–189 (2004).
93. J. Wang, a. a. Iobito, F. Shen, F. hornung, a. Winoto, m. J. Ienardo, inhibition of Fas-mediated apoptosis by the B cell antigen receptor through c-Flip. *Eur. J. Immunol.* **30**, 155–163 (2000).
94. i. n. Iavrik, P. h. Krammer, Regulation of cD95/Fas signaling at the DiSc. *Cell Death Differ.* **19**, 36–41 (2012).
95. J. maelfait, R. Beyaert, non-apoptotic functions of caspase-8. *Biochem. Pharmacol.* **76**, 1365–1373 (2008).
96. V. Kanderova, h. grombirikova, i. Zentsova, K. Reblova, a. Klocperk, m. Fejtкова, m. Bloomfield, B. Ravcukova, t. Kalina, t. Freiburger, a. Sediva, lymphoproliferation, immunodeficiency and early-onset inflammatory bowel disease associated with a novel mutation in caspase 8. *Haematologica* **104**, e32–e34 (2019).
97. h. J. chun, I. Zheng, m. ahmad, J. Wang, c. K. Speirs, R. m. Siegel, J. K. Dale, J. Puck, J. Davis, c. g. hall, S. Skoda-Smith, t. P. atkinson, S. e. Straus, m. J. Ienardo, Pleiotropic defects in lymphocyte activation caused by caspase-8 mutations lead to human immunodeficiency. *Nature* **419**, 395–399 (2002).
98. c. Klemann, m. esquivel, a. magerus-chatinet, m. R. Iorenz, i. Fuchs, n. neveux, m. castelle, J. Rohr, c. B. da Cunha, m. ebinger, R. Kobbe, B. Kremens, F. Kollert, e. gambineri, K. Iehberg, m. g. Seidel, K. Siepermann, t. Voelker, V. Schuster, S. goldacker, K. Schwarz, c. Speckmann, c. Picard, a. Fischer, F. Rieux-Iaucat, S. ehl, a. Rensing-ehl, B. neven, evolution of disease activity and biomarkers on and off rapamycin in 28 patients with autoimmune lymphoproliferative syndrome. *Haematologica* **102**, e52–e56 (2017).
99. D. t. teachey, R. greiner, a. Seif, e. attiyeh, J. Bleesing, J. choi, c. manno, e. Rappaport, D. Schwabe, c. Sheen, K. e. Sullivan, h. Zhuang, D. S. Wechsler, S. a. grupp, treatment with sirolimus results in complete responses in patients with autoimmune lymphoproliferative syndrome. *Br. J. Haematol.* **145**, 101–106 (2009).
100. J. B. oliveira, J. J. Bleesing, u. Dianzani, t. a. Fleisher, e. S. Jaffe, m. J. Ienardo, F. Rieux-Iaucat, R. m. Siegel, h. c. Su, D. t. teachey, V. K. Rao, Revised diagnostic criteria and classification for the autoimmune lymphoproliferative syndrome (alPS): Report from the 2009 nih international Workshop. *Blood* **116**, e35–e40 (2010).
101. K. Warnatz, u. Salzer, m. Rizzi, B. Fischer, S. guttenberger, J. Bohm, a. K. Kienzler, Q. Pan-hammarstrom, I. hammarstrom, m. Rakhmanov, m. Schlesier, B. grimbacher, h. h. Peter, h. eibel, B-cell activating factor receptor deficiency is associated with an adult-onset antibody deficiency syndrome in humans. *Proc. Natl. Acad. Sci. U.S.A.* **106**, 13945–13950 (2009).
102. m. Roederer, interpretation of cellular proliferation data: avoid the panglossian. *Cytometry A* **79**, 95–101 (2011).
103. J. P. concordet, m. haeussler, cRiSPoR: intuitive guide selection for cRiSPR/cas9 genome editing experiments and screens. *Nucleic Acids Res.* **46**, W242–W245 (2018).
104. a. cossarizza, h. D. chang, a. Radbruch, S. abrignani, R. addo, m. akdis, i. andr , F. andreatta, F. annunziato, e. arranz, P. Bacher, S. Bari, V. Barnaba, J. Barros-martins, D. Baumjohann, c. g. Beccaria, D. Bernardo, D. a. Boardman, J. Borger, c. Böttcher, I. Borkmann, m. Burns, D. h. Busch, g. cameron, i. cammara, a. cassotta, y. chang, F. g. chirdo, e. christakou, I. Čičin-Šain, I. cook, a. J. corbett, R. cornelis, I. cosmi, m. S. Davey, S. De Biasi, g. De Simone, g. Del Zotto, m. Delacher, F. Di Rosa, J. Di Santo, a. Diefenbach, J. Dong, t. Dörner, R. J. Dress, c. a. Dutertre, S. B. g. eckle, P. eede, m. evrard, c. S. Falk, m. Feuerer, S. Fillatreau, a. Fiz-Iopez, m. Follo, g. a. Foulds, J. Fröbel, n. gagliani, g. galletti, a. gangaev, n. garbi, J. a. garrote, J. geginat, n. a. gherardin, I. gibellini, F. ginhoux, D. i. godfrey, P. gruarin, c. haftmann, I. hansmann, c. m. harpur, a. c. hayday, g. heine, D. c. hernández, m. herrmann, o. hoelsken, Q. huang, S. huber, J. e. huber, J. huehn, m. hundemer, W. y. K. hwang, m. iannacone, S. m. ivison, h. m. Jäck, P. K. Jani, B. Keller, n. Kessler, S. Ketelaars, I. Knop, J. Knopf, h. F. Koay, K. Kobow, K. Kriegsmann, h. Kristyanto, a. Krueger, J. F. Kuehne, h. Kunze-Schumacher, P. Kvistborg, i. Kwok, D. Iatorre, D. Ienz, m. K. Ievings, a. c. Iino, F. Iiotta, h. m. Iong, e. Iugli, K. n. macdonald, I. maggi, m. K. maini, F. maір, c. manta, R. a. manz, m. F. mashreghi, a. mazzoni, J. mccluskey, h. e. mei, F. melchers, S. melzer, D. mielenz, I. monin, I. moretta, g. multhoff, I. e. mu oz, m. mu oz-Ruiz, F. muscate, a. natalini, K. neuemann, I. g. ng, a. niedobitek, J. niemi, I. n. almeida, S. notarbartolo, I. ostendorf, I. J. Pallett, a. a. Patel, g. i. Percin, g. Peruzzi, m. Pinti, a. g. Pockley, K. Pracht, i. Prinz, i. Pujol-autonell, n. Pulvirenti, I. Quatrini, K. m. Quinn, h. Radbruch, h. Rhys, m. B. Rodrigo, c. Romagnani, c. Saggau, S. Sakaguchi, F. Sallusto, I. Sanderink, i. Sandrock, c. Schauer, a. Scheffold, h. u. Scherer, m. Schiemann, F. a. Schildberg, K. Schober, J. Schoen, W. Schuh, t. Sch ler, a. R. Schulz, S. Schulz, J. Schulze, S. Simonetti, J. Singh, K. m. Sitnik, R. Stark, S. Starossom, c. Stehle, F. Szelinski, I. tan, a. tarnok, J. tornack, t. i. m. tree, J. J. P. van Beek, W. van de Veen, K. van gisbergen, c. Vasco, n. a. Verheyden, a. von Borstel, K. a. Ward-hartstonge, K. Warnatz, c. Waskow, a. Wiedemann, a. Wilharm, J. Wing, o. Wirz, J. Wittner, J. h. m. yang, J. yang, guidelines for the use of flow cytometry and cell sorting in immunological studies (third edition). *Eur. J. Immunol.* **51**, 2708–3145 (2021).
105. P. Schneider, I. Willen, c. R. Smulski, tools and techniques to study ligand-receptor interactions and receptor activation by tNF superfamily members. *Methods Enzymol.* **545**, 103–125 (2014).

Acknowledgments: We thank cytoF2 operator D. thurner for his tireless work and m. Follo and J. Bodinek-Wersing from the lighthouse core Facility at the university medical center Freiburg for help with immunofluorescence analysis and cell sorting. We also thank the iR-Biobank and the Freeze Biobank, center for Biobanking at the medical center and Faculty of medicine, university of Freiburg, Freiburg, germany. **Funding:** this work was supported by grants from the Dfg (SFB1160, B02 to m.R.; a04 to K.W.; Z02 to m. Boerries; Z01 to m.S.; a01 to S.e.; SFB850, c9, Z1 to m. Boerries; SFB1479—project id: 441891347-S1 to m. Boerries; SFB1453—project id: 431984000 to m. Boerries; tRR167, Z01 to m. Boerries; tRR130, P12 to R.e.v.; project id: 468499998 to m.R.; tRR353, a01 to m.R.), by the german Federal ministry of education and Research (BmbF) within the framework of the e:med research and funding concept confirm (FKZ O12X1708F to m. Boerries), and by miRacum within the medical informatics Funding Scheme (FKZ O12Z1801B to m. Boerries). J. Staniek was supported by an eFIS-il Short-term Fellowship and the Wissenschaftliche gesellschaft Freiburg. t.K., m. Bakardjieva, and J. Stuchly were funded by nPu Io1604 from ministry of education, youth and Sports, and cytoF2 instrument was financed through operational Program Prague competitiveness (cz.2.16/3.1.00/21540). P.D. was supported by a JcyI-eDu/346/2013 scholarship. P.S. is supported by the Swiss national Science Foundation (grant 310030a_176256). m.F. acknowledges financial support from the Spanish health institute carlos iii (iSciii) for the grants FIS Pi17/01930 and cB16/12/00400. c.R.S. was supported by the national Research council (conicet) and by a grant from Foncyt (Pict-2018-01107). the Proteomics unit belongs to ProteoRed, PRB3-iSciii, supported by grant Pt17/0019/0023, of the Pe i + D + i 2017-2020, funded by iSciii and FeDeR. a.R.-e. is supported by the Wilhelm Sander Stiftung (1 027 087 401). I.i.g.-g. is supported by instituto de Salud carlos iii (iSciii) through the project FIS-Pi21/01642 and cofunded by the european union. o.d.l.c. was supported by the Spanish ministerio de ciencia e innovacion (grant PiD2020-112526RB-I00, funded by mcin/aei/10.13039/501100011033). the study was supported by the institut national de la Sant  et de la Recherche m dicale (inSeRm) and by government grants from the agence nationale de la Recherche as part of the “investment for the Future” program (anR-10-iahu-01 and anR-18-RhuS-0010), the ligue contre le cancer-comit  de Paris, Fondation aRc pour la recherche sur le cancer, the centre de R f rence D ficits immunitaires h r ditaires (ceReDiH), the agence nationale de la Recherche (anR-14-ce14-0026-01 “Iumugene” to F.R.-I.), and the Fondation pour la Recherche m dicale (equipe FRm eQu202103012670). lighthouse core Facility is funded in part by the medical Faculty, university of Freiburg (project numbers 2021/a2-Fol; 2021/B3-Fol) and the Dfg (project number 450392965). **Author contributions:** m.R. and J. Staniek conceptualized and designed the research. J. Staniek, i.J., m. Bakardjieva, J. Stancikova, c.B., J.R., J.n., S.S., I. arpesella, and R.I. performed experiments. a.c., o.d.l.c., B.n.,

F.R.-I., a.m., o.n., P.o., g.S., I. alsina, I.m.a., I.i.g.-g., K.W., and S.e. provided a IPS patient material clinical data. e.P.m., R.c., S.u., K.W., and m.S. provided S10 material from healthy controls. m.F., P.D., J.F.g., and R.g.V. contributed to I c-mS/mS analysis and V.B. to Rna-seq analysis. g.a., J. Stuchly, and m. Boerries performed bioinformatic analysis. P.S. provided key reagents, and P.S., S.e., a.R.-e., R.e.V., and c.R.S. provided specialist advice. J. Staniek, t.K., g.a., J. Stuchly, and m.R. analyzed and interpreted data. J. Staniek, t.K., n.V., J.t., D.m., a.R.-e., c.R.S., and m.R. discussed the data. J. Staniek and g.a. prepared figures, and J. Staniek and m.R. wrote the manuscript with input from all authors. all authors have read the manuscript and approved the submitted version. **Competing interests:** the authors declare that they have no

competing interests. **Data and materials availability:** Rna-seq data are available at ncBi geo under accession gSe145513. I c-mS/mS data are available via ProteomeXchange with identifier PXD017601. Raw data used to generate figures and supplementary figures are included in data file S1.

Submitted 4 august 2023
accepted 8 December 2023
Published 12 January 2024
10.1126/sciimmunol.adj5948

9.5. TLR8/TLR7 dysregulation due to a novel TLR8 mutation causes severe autoimmune hemolytic anemia and autoinflammation in identical twins

RESEARCH ARTICLE

TLR8/TLR7 dysregulation due to a novel *TLR8* mutation causes severe autoimmune hemolytic anemia and autoinflammation in identical twins

Martina Fejtikova¹  | Martina Sukova² | Katerina Hlozkova¹ |
 Karolina Skvarova Kramarova¹  | Marketa Rackova¹  | David Jakubec^{3,4} |
 Marina Bakardjieva¹  | Marketa Bloomfield^{5,6}  | Adam Klocperk⁶  |
 Zuzana Parackova⁶  | Anna Sediva⁶  | Jahnvi Aluri⁷ | Michaela Novakova¹  |
 Tomas Kalina¹  | Eva Fronkova¹ | Ondrej Hrusak¹ | Hana Malcova⁸ |
 Petr Sedlacek² | Zuzana Liba⁹ | Martin Kudr⁹ | Jan Stary² | Megan A. Cooper⁷ |
 Michael Svaton¹  | Veronika Kanderova¹ 

¹CLIP- Childhood Leukaemia Investigation Prague, Department of Paediatric Haematology and Oncology, Second Faculty of Medicine, Charles University and University Hospital Motol, Prague, Czech Republic

²Department of Paediatric Haematology and Oncology, Second Faculty of Medicine, Charles University and University Hospital Motol, Prague, Czech Republic

³Bioinformatics Group, Institute of Organic Chemistry and Biochemistry, Czech Academy of Sciences, Prague, Czech Republic

⁴Department of Software Engineering, Faculty of Mathematics and Physics, Charles University, Prague, Czech Republic

⁵Department of Paediatrics, First Faculty of Medicine, Charles University and Thomayer University Hospital, Prague, Czech Republic

⁶Department of Immunology, Second Faculty of Medicine, Charles University and University Hospital Motol, Prague, Czech Republic

⁷Division of Rheumatology/Immunology, Department of Pediatrics, Washington University School of Medicine, St. Louis, Missouri, USA

⁸Department of Paediatric and Adult Rheumatology, University Hospital Motol, Prague, Czech Republic

⁹Department of Paediatric Neurology, Second Faculty of Medicine, Charles University and University Hospital Motol, Prague, Czech Republic

Correspondence

Veronika Kanderova and Michael Svaton, CLIP - Childhood Leukemia Investigation Prague, Department of Pediatric Hematology and Oncology, Second Faculty of Medicine, Charles University and University Hospital Motol, V Uvalu 84, 15006, Prague 5, Czech Republic.
 Email: veronika.kanderova@lfmotol.cuni.cz (V. K.) and michael.svaton@lfmotol.cuni.cz (M. S.)

Funding information

This work was supported by grants obtained from the Ministry of Health of the Czech Republic no. NV18-05-00162, NV18-07-00430 and NV19-05-00332, Charles University projects PRIMUS/19/MED/04 and GA UK 362119, European Regional Development Fund projects CZ.2.16/3.1.00/

Abstract

Our study presents a novel germline c.1715G>T (p.G572V) mutation in the gene encoding Toll-like receptor 8 (*TLR8*) causing an autoimmune and autoinflammatory disorder in a family with monozygotic male twins, who suffer from severe autoimmune hemolytic anemia worsening with infections, and autoinflammation presenting as fevers, enteritis, arthritis, and CNS vasculitis. The pathogenicity of the mutation was confirmed by in vitro assays on transfected cell lines and primary cells. The p. G572V mutation causes impaired stability of the TLR8 protein, cross-reactivity to TLR7 ligands and reduced ability of TLR8 to attenuate TLR7 signaling. This imbalance toward TLR7-dependent signaling leads to increased pro-inflammatory responses, such as nuclear factor- κ B (NF- κ B) activation and production of pro-inflammatory cytokines IL-1 β , IL-6, and TNF α . This unique *TLR8* mutation with partial TLR8 protein loss and hyperinflammatory phenotype mediated by TLR7 ligands represents a novel

Michael Svaton and Veronika Kanderova contributed equally to this work.

24505 and CZ.02.1.01/0.0/0.0/16_019/0000729, the Jeffrey Modell Foundation and the St. Louis Children's Hospital Foundation. Institutional support was provided from the Ministry of Education, Youth and Sports of the Czech Republic project for the conceptual development of research organization - University Hospital Motol 00064203

inborn error of immunity with childhood-onset and a good response to TLR7 inhibition.

1 | INTRODUCTION

The innate immune system serves as the first line of defense against infection. It employs pattern recognition receptors (PRRs) that recognize evolutionarily conserved molecular structures of microorganisms. Toll-like receptors (TLRs), a family of PRRs, are a group of single-spanning membrane proteins found on the surface or in endosomes of immune cells. Defects in TLR signaling pathways described in IRAK4 or MyD88 deficiencies are associated with bacterial susceptibility and impaired inflammatory responses to infection.¹ Conversely, gain-of-function in TLR8 leads to hyperresponsiveness to TLR8 ligands, hyperproduction of inflammatory cytokines, neutropenia and bone marrow failure.² The phylogenetically related endosomal TLR8 and TLR7 both detect viral and bacterial single-stranded (ss)RNA.^{3,4} TLR8 is predominantly expressed in monocytes/macrophages, myeloid dendritic cells (mDCs), and granulocytes, whereas TLR7 in plasmacytoid dendritic cells (pDCs), B-cells, and monocytes/macrophages.^{5,6} The stimulation of TLRs generally activates NF- κ B, mitogen-activated protein-kinases (MAPK), and interferon (IFN) response factors, which subsequently trigger the transcription of inflammatory cytokines, chemokines and costimulatory molecules.³ The signaling pathways downstream of TLR8 and TLR7 vary in different cell types. In monocytes, TLR8 activation promotes a strong NF- κ B activation, type I IFN response and the production of Th1 polarizing cytokines, whereas TLR7 preferentially activates MAPK signaling and the production of Th17 polarizing cytokines. Interestingly, TLR7 inhibits TLR8-mediated type I IFN response.⁷ Consistently, during the maturation of DCs, TLR8 and TLR7 negatively regulate each other.⁸ A direct or indirect intraendosomal physical interaction of TLR8 and TLR7 is suggested to play a role in balancing these inflammatory outcomes.⁹ Interestingly, because of their high homology, mutations near the ligand-binding site 1 of TLR8 can increase selectivity to TLR7-specific ligands.¹⁰

In addition to external pathogens, TLRs respond to endogenous ligands, such as the self-RNA within anti-ribonucleoprotein autoantibodies that drive systemic lupus erythematosus (SLE)¹¹ or rheumatoid arthritis¹² in mice. Interestingly, overexpression of human TLR8¹³ or murine TLR7^{14,15} is sufficient to drive autoimmune inflammation in mice; and murine TLR8 deficiency also leads to autoimmunity and autoinflammation by increasing TLR7-dependent responses.^{16,17} Here, we present the first report of human partial TLR8 protein deficiency combined with TLR8/TLR7 dysregulation underlying severe autoimmune and inflammatory phenotypes.

2 | METHODS

2.1 | Whole exome sequencing

Sequencing libraries were prepared from DNA isolated from peripheral blood mononuclear cells (PBMCs) of one of the patients using the SureSelect Human All Exon V6+UTRs kit (Agilent Technologies, Santa Clara, CA) and sequenced on the NextSeq 500 Instrument (Illumina, San Diego, CA) according to the manufacturer's instructions. Resulting reads were aligned to the hg19 human reference genome with BWA.¹⁸ Variant calling was performed with VarScan2¹⁹ and samtools,²⁰ and variant annotation and filtering was done in Ingenuity[®] Variant Analysis (QIAGEN, Hilden, Germany) with a custom panel of potential candidate genes. No other potentially pathogenic mutations were identified from the Whole Exome Sequencing data in neither *TLR8*, *TLR7* nor any other known primary immunodeficiency (PID)-related genes.²¹ No pathogenic variants in the *TLR8* gene have been reported in the ClinVar database at the time of this study. Other patients with *TLR8* gene mutations were identified via the GeneMatcher database,²² and a collaboration that led to the publication of the gain-of-function cases by Aluri et al.² was established. The gnomAD database reports eight individuals who are hemizygous for a putative loss-of-function variant without confirmation of these variant calls or information on their phenotypes.

2.2 | Sanger sequencing

DNA was isolated from PBMCs of both siblings and their parents and used for PCR amplification of the p.G572 surrounding area of the *TLR8* gene using the forward 5'-GCAATGCTCAAGTGTAAAGTGGGA and the reverse 5'-TACCAGGGACTTGCTTTCCAG primers. The expression of both alleles in mother's cells was confirmed using the cDNA obtained from sorted monocytes as described below with the forward 5'-GCTCTTACTGAATTGTCGACTTG and the reverse 5'-GCAACTCGAGACGAGGAACT primers. The amplicons were sequenced using BigDye Terminator 3.1 Cycle Sequencing Kit (Thermo Fischer Scientific, Waltham, CA) on 3730 DNA Analyzer (Thermo Fischer Scientific) according to manufacturer's instructions.

2.3 | Cell sorting

Monocytes were isolated on an FACS Aria III sorter (BD Biosciences [BD], San Jose, CA) based on Forward Scatter (FSC), Side Scatter

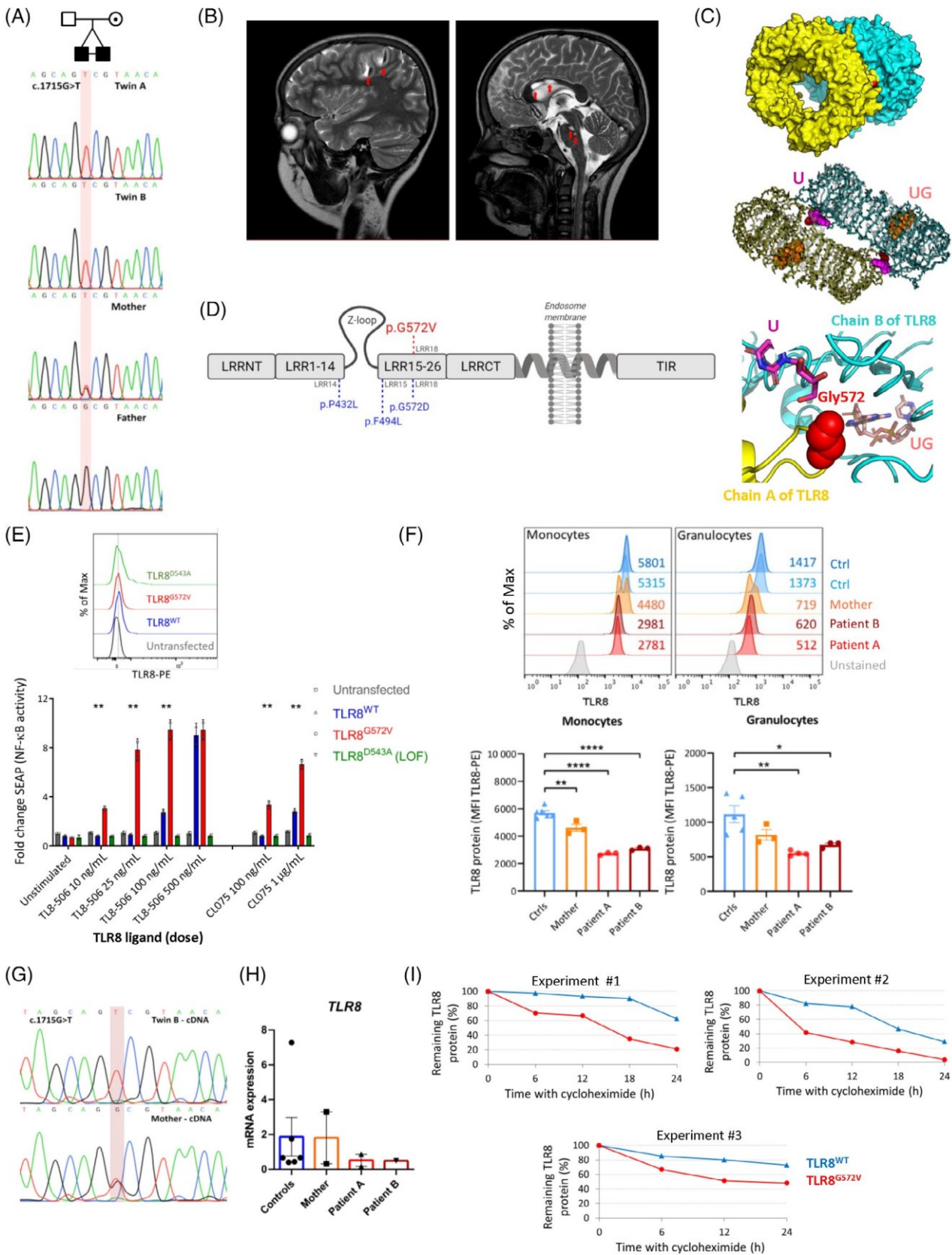


FIGURE 1 Legend on next page.

(SSC), CD45-Pacific Blue, and CD14-APC (Exbio, Vestec, Czech Republic) from the peripheral blood of both patients, their mother and healthy controls. T-cell subpopulations were sorted according to FSC, SSC and TCR $\alpha\beta$ +CD4+CD127+CD25-(non-Treg) (or CD8+) CCR7+CD45RO- (naive T-cells), TCR $\alpha\beta$ +CD4+CD127+CD25-(non-Treg) (or CD8+) CCR7+CD45RO+ (central memory T-cells), TCR $\alpha\beta$ +CD4+CD127+CD25-(non-Treg) (or CD8+) CCR7-CD45RO+ (effector memory T-cells), TCR $\alpha\beta$ +CD4+CD127+CD25-(non-Treg) (or CD8+) CCR7-CD45RO- (terminally differentiated T-cells), TCR $\alpha\beta$ +CD4+CD127dim/-CD25+ (Treg), TCR $\alpha\beta$ +CD8+CD45RO-CCR7+CD127+CD95+ (stem cell memory T-cells), and TCR $\alpha\beta$ +CD4+CD127+CD25-(non-Treg)CD45RO+CXCR5+ (follicular helper T-cells) using TCR $\alpha\beta$ -APC, CCR7-PE-Cy7, and CD8-APC-Alexa Fluor 750 (Beckman Coulter [BC], Miami, FL), CD4-Alexa Fluor 700 and CD45RO-FITC (Exbio), CD127-PE-CF594, CD25-PE, and CXCR5-Brilliant Violet (BV) 421 (BD), and PD-1-BV605, CD95-BV510, and HLA-DR-PerCP-Cy5.5 (Biolegend, San Diego, CA).

2.4 | T-cell receptor β repertoire sequencing

DNA was isolated from the above listed T-cell subpopulations with the QIAamp DNA Micro Kit (Qiagen) and used for the preparation of sequencing libraries according to the EuroClonality-NGS working group protocol for the complete TRB-VJ gene rearrangements.²³ Final libraries were sequenced on the MiSeq instrument (Illumina) according to the manufacturer's instructions, and the data were analyzed using the ARResT/Interrogate application.²⁴ Only clonotypes with productive TRB-VJ rearrangements were selected and filtered based on their frequency in all reads obtained from each sample.

2.5 | *TLR8* and *TLR7* mRNA quantification

Total RNA was isolated from specific cell populations sorted from PBMCs using the FACS Aria III (BD) using the RNeasy Mini Kit (Qiagen) and transcribed to cDNA by an iScript kit (Bio-Rad, Hercules, CA). Gene expression levels of *TLR7* and *TLR8* were determined using TaqMan Gene Expression Assays for *TLR7* (Hs00152971_m1), *TLR8*

(Hs00152972_m1), and the *GAPDH* (Hs99999905_m1) gene that was used for normalization; the qPCR reactions were performed on the Applied Biosystems 7500 Fast Real-Time PCR System (all Thermo Fisher Scientific). The gene expression was normalized to *GAPDH* control gene expression in three healthy donors using the delta-delta Ct method.

2.6 | Cell lines

HEK293 and HEK293T cell lines were purchased from American Type Culture Collection (Manassas, VA) and cultured in Dulbecco's Modified Eagle Medium (DMEM) supplemented with 10% fetal bovine serum (FBS) and antibiotics/antimycotics (all from Thermo Fisher Scientific).

2.7 | Plasmids

Plasmids encoding the mutant TRL8 (TLR8^{G572V} or TLR8^{D543A}) were prepared from the TLR8^{WT} construct (pUNO1-hTLR8b, NM_138636, InvivoGen, San Diego, CA) by site-directed mutagenesis (QuikChange™II XL Site-Directed Mutagenesis kit, Agilent Technologies, Santa Clara, CA) using the primer pairs 5'-TAAATTCTAGATGATGTGTTACGACTGCTATTCTGAAATAGTGTGAA-3' and 5'-TTCACACTATTTTCAAGAATGACGATCGTAACACATCATCTAGAATTTA-3' (for TLR8^{G572V}) or 5'-CAC TAGCATTATCAAAGGCTAGTCTATTGTTTGTCAAATCC-3' and 5'-GG ATTTGACAACAATAGACTAGCCTTTGATAATGCTAGTGCTCTTA-3' (for TLR8^{D543A}). Successful mutagenesis was confirmed by Sanger sequencing. TLR8^{D543A} served as a negative control.²

2.8 | Cycloheximide chase assay

HEK293 and HEK293T cells were seeded in 6-well plates and transfected 24 h later with 4 μ g of TLR8^{WT} or TLR8^{G572V} plasmid using Lipofectamine 3000 (Thermo Fisher Scientific) according to the manufacturer's protocol. After 48 h, proteosynthesis was inhibited using 50 μ g/mL cycloheximide (Sigma Aldrich, Merck). TLR8 protein level

FIGURE 1 *TLR8* c.1715G>T mutation and partial TLR8 protein deficiency. A pedigree of the family and Sanger sequencing of the DNA (A). Large frontoparietal hemorrhagic lesions (red arrows) with smaller postischemic lesions in the brain stem and corpus callosum (smaller arrows) (B). TLR8 dimer from side view (PDB 3W3G16, G572 in red, top), structure of the liganded TLR8 dimer (middle) and detail of the interaction between G572 (in red) and the ssRNA40 degradation products (bottom)—uridine in ligand binding site 1 and UG dinucleotide in ligand binding site 2, PDB 4R08317 (C).²⁶ Linear diagram of TLR8 containing an N-terminal domain (LRRNT), a leucine-rich repeat (LRR) ligand recognition domain connected with the Z-loop between LRR 14 and 15, a C-terminal domain (LRRCT), a transmembrane domain anchoring TLR8 to the endosomal membrane and a Toll/interleukin-1 receptor (TIR) domain for signal transduction. Published mutations in LRR14, LRR15 and LRR18 are depicted in blue,² and the novel G572V mutation in LRR18 is in red (D). NF- κ B transcriptional activity of TLR8^{WT}- and TLR8^{G572V}-containing HEK cells upon TL8-506/CL075 stimulation (E). Basal TLR8 protein levels (F). Sanger sequencing of the monocyte cDNA (G). The relative expression of *TLR8* mRNA (H). Enhanced degradation of mutant TLR8^{G572V} protein compared to TLR8^{WT} (I). Data acquired in two (H) and three (E, F, I) independent experiments, the results are expressed as the mean \pm SEM. Histograms show representative data, MFI in numbers. * $p < .05$, ** $p < .005$, *** $p < .0001$ (unpaired t -test). Protein structures visualized using PyMOL 2.3.0 [Color figure can be viewed at wileyonlinelibrary.com]

TABLE 1 Genetics and clinical characteristics

Patient	Patient A	Patient B
Sex	Male	Male
Current age (years)	11	11
Genetic variant		
Chromosome	X	X
Position (hg19)	12938874	12938874
Gene symbol	<i>TLR8</i>	<i>TLR8</i>
Transcript change	c.1715G>T	c.1715G>T
Transcript	NM_138636	NM_138636
Protein Change	p.G572V	p.G572V
Inheritance	Inherited from mother	Inherited from mother
CADD	25	25
PolyPhen2	0.999	0.999
SIFT	0	0
PhyloP	6.07	6.07
gnomAD AF	Not present	Not present
Clinical manifestation		
Age of onset	1.5 years	7 months
Primary manifestation	Noninfectious cervical lymphadenopathy with xanthogranuloma, acute AIHA (6 years)	Transient red cell aplasia acute AIHA (2.5 years)
Chronic AIHA	Yes (positive for anti-red blood cell antibodies, C3d fragments and cold agglutinins)	Yes (positive for anti-red blood cell antibodies, C3d fragments and cold agglutinins)
Coombs testing	Positive (high)	Positive (high)
Thrombocytopenia	Transient during a flare of AIHA	No
Platelet antibody	No	No
Neutropenia	No	No
Episodes of pancytopenia	No	No
Lymphadenopathy	Yes	Yes
Hepatosplenomegaly	Yes	Yes
GI disease	Recurrent noninfectious enteritis	IBD-like disease, biliary obstruction during hemolysis
Lung disease	No	No
Mouth sores	Mild episodes	Mild episodes
Tracheal/larynx sx	URTIs	URTIs
Hypogammaglobulinemia	Often lower IgG (correlating with CRP—infections)	Often lower IgG (correlating with CRP, SAA—infections)
Infections	<i>HHV6</i> , varicella and recurrent shingles, URTIs, <i>Salmonella enteritis</i> , <i>Clostridium enterocolitis</i>	URTIs, <i>Salmonella enteritis</i> , shingles
Skin and joints	Erythema nodosum	Erythema nodosum, polyarthritis
CNS	No symptoms or MRI findings	Multifocal ischemia characterized as SV-cPACNS with hemorrhagic transformation of ischemic stroke (11 years)
Therapy (duration)		
Corticosteroids	Since 6 years continuous PRD 0.2–2.5 mg/kg/day + methylprednisolone	Since 6 years continuous PRD 0.3–2.5 mg/kg/day + methylprednisolone
Other immunosuppression	Azathioprine (3–5 years)	
IVIg	HD-IVIg 2x (7 years) + post rituximab substitution	

TABLE 1 (Continued)

Patient	Patient A	Patient B
Rituximab	5 × 375 mg/m ² (8 years)	
mTOR inhibition	Sirolimus—target levels of 10 µg/L (from 8 years)	
NSAIDs	–	Ibuprofen 1–2x daily (from 10 years)
anti-IL-1	–	Anakinra 100 mg daily (from 9 years)
Methotrexate	–	15 mg s.c. weekly (from 10 years)
Hydroxychloroquine	200 mg daily (from 12 years)	–
Supportive therapy	PPI, vit. D, anti-hypertensive therapy, antihistamines	PPI, TMP/SMX, zoledronate, vit. D, calcium, anti-hypertensive therapy
HSCT	–	MUD-HSCT (11 years)
T-cell clonality (highly abundant clones)		
Effector memory CD4+		CSVDTGTVYNEQFF (32.71%)
Effector memory CD8+	CASRDGKEVELFF (6.25%)	CASSGLNTEAFF (31.85%); CSARDRDTEAFF (6.07%)

Note: Characterization of the newly identified variant with selected annotation by VEP and an overview of the clinical course of the disease in both twins, including the therapies, with their respective start and duration. Expanded T-cell clones exceeding 5% of all sequenced reads in the selected T-cell subpopulations displayed with their AA CDR3 sequence and their relative abundance.

was detected upon 6, 12, 18, and 24 h inhibition w/wo cycloheximide using flow cytometry.

2.9 | Activity of the TLR8^{G572V} variant

Human HEK-Blue Null1 cells (InvivoGen) were cultured in DMEM supplemented with 10% FBS, normocin (50 µg/mL), and zeocin (100 µg/mL) (all from InvivoGen). NF-κB transcriptional activity was tested by the QUANTI-BLUE assay (InvivoGen). The HEK-Blue Null1 cell line was transfected with either TLR8^{WT} or TLR8^{G572V} (or TLR8^{D543A}) plasmids by transient transfection (Lipofectamine; Life Technologies, Thermo Fisher Scientific). Forty-eight hours post-transfection, the cells were seeded in a 96-well plate at a density of 30 000 cells/well and stimulated with 500 ng/mL or 1 µg/mL CL307, 100 ng/mL or 1 µg/mL CL075; 10, 25, 50, 100, or 500 ng/mL TL8-506; 5, 10, or 25 µg/mL imiquimod, 0.1 or 0.5 µg/mL gardiquimod (all from InvivoGen), and 100, 200, or 500 nM GS-9620 (Vesatolimod, Med-ChemExpress, Suite Q, Monmouth Junction, NJ) for 24 h. Then, 50 µL of the supernatant from each well was transferred to a 96-well plate with 150 µL of QUANTI-Blue solution (InvivoGen). The plate was incubated at 37°C for 1 h, and the secreted embryonic alkaline phosphatase (SEAP) levels were determined by reading the plate with a spectrophotometer at 650 nm. Untransfected HEK-Blue Null1 cells served as a negative control for TLR8 activation, as these cells are nonresponsive to TLR8 ligands. Fold-change was calculated by normalizing individual data to the unstimulated O.D. of the untransfected well. Similarly, Human HEK-Blue TLR7 cells (InvivoGen) were cultured in DMEM supplemented with 10% FBS, normocin (50 µg/mL), blasticidin (10 µg/mL), and zeocin (100 µg/mL) (all from InvivoGen). NF-κB transcriptional activity was tested using the QUANTI-BLUE assay (InvivoGen). The HEK-Blue TLR7 cell line was transfected by either TLR8^{WT} or TLR8^{G572V} plasmids, seeded in a 96-well plate 48 h

post-transfection and stimulated with the same ligands and doses as HEK-Blue Null1. The plate was incubated at 37°C for 1 h, and SEAP levels were determined by reading the plate with a spectrophotometer at 650 nm.

2.10 | Western blotting

Cells were lysed for 30 min on ice in lysis buffer (1% lauryl maltoside (Calbiochem, Merck), 20 mM Tris (pH 7.5), 100 mM NaCl, 5 mM iodoacetamide, 50 mM NaF, 1 mM Na₃VO₄, and 2 mM EDTA (all from Sigma-Aldrich, Merck) containing 100x diluted Protease Inhibitor Cocktail Set III (Calbiochem, Merck). The protein concentration was adjusted to a final concentration of 1 mg/mL using a bicinchoninic acid assay kit according to the manufacturer's instructions (Thermo Fisher Scientific). Proteins were separated on SDS-PAGE gels and transferred to nitrocellulose membranes (Bio-Rad, Hercules, CA). Membranes were blocked at 8°C overnight in phosphate buffered saline (PBS) containing 7.5% low fat bovine milk and 0.05% Tween 20. Primary antibodies against TLR8 (clone D3Z6J, Cell Signaling Technologies) and β-actin (clone AC-74, Sigma-Aldrich, Merck) were used with peroxidase-conjugated secondary antibodies (Jackson ImmunoResearch, West Grove, PA) and SuperSignal West Pico/Femto Chemiluminescent Substrates (Thermo Fisher Scientific). Signals were detected using a MINI HD6 scanner (UVITEC, Cambridge, UK) and analyzed with ImageJ software. TLR8 expression levels were normalized to those of β-actin.

2.11 | Immunophenotyping

Immunophenotyping of lymphocyte subpopulations was performed using the following antibody-fluorochrome conjugates: CD4-BV510, IgM-BV510, CD45RA-BV510, CD27-BV421, CD62L-BV421, CD8-FITC,

TABLE 2 Immunological findings

Cell population	Patient A	Patient B	Age-matched reference values
Leukocytes (cells/ μ L)	14 500	20 400	4500–14 500
Lymphocytes (cells/ μ L)	3720	6793	1300–7500
Neutrophils (cells/ μ L)	9490	11 444	1900–9700
Monocytes (cells/ μ L)	980	1958	0–1300
Eosinophils (cells/ μ L)	10	102	0–1000
Erythrocytes (cells/ μ L)	2 660 000	3 600 000	4 000 000–5 200 000
CD3+ T-cells (% lymphocytes; cells/ μ L)	84; 3125	86; 5842	60–76; 1200–2600
CD3+ CD4+ T-cells (% lymphocytes; cells/ μ L)	37; 1376	32; 2174	31–47; 650–1500
CD3+ CD8+ T-cells (% lymphocytes; cells/ μ L)	41; 1525	46; 3125	18–35; 370–1100
NK cells (% lymphocytes; cells/ μ L) (CD3-CD16+56+)	0.8; 29	1.2; 82	4–17; 100–480
Regulatory T-cells (% CD3+ T-cells) (CD4+CD25+CD127dim to –)	2.29	2.35	2.29–6.49
Naïve CD4+ (% CD4+ T-cells) (CD3+CD4+CD45RA+CD27+)	67	66	46–99
Central memory CD4+ (% CD4+ T-cells) (CD3+CD4+CD45RA–CD27+)	31	31	0.35–100
Effector memory CD4+ (% CD4+ T-cells) (CD3+CD4+CD45RA–CD27–)	1.8	1.6	0.27–18
Terminally diff. CD4 (% CD4+ T-cells) CD3+CD4+CD45RA+CD27–	0.2	0.1	0.0031–1.8
Th1 (% CD3+4+ T-cells) (CXCR3+CCR6–)	10.7	16.4	13.4–25.5
Th2 (% CD3+4+ T-cells) (CXCR3-CCR6-CCR4+CRTH2+)	0.23	0.37	0.19–1.33
Th17 (% CD3+4+ T-cells) (CXCR3-CCR6+)	5.82	5.83	3.53–12
Naïve CD8+ (% CD8+ T-cells) (CD3+CD8+CD45RA+CD27+)	80	83	16–100
Central memory CD8+ (% CD8+ T-cells) (CD3+CD8+CD45RA–CD27+)	4.1	3.7	1–6
Effector memory CD8+ (% CD8+ T-cells) (CD3+CD8+CD45RA–CD27–)	3.4	2	5–100
Terminally diff. CD8+ (% CD8+ T-cells) (CD3+CD8+CD45RA+CD27–)	10	9.5	15–41
% HLA-DR/CD3+CD4+ T-cells	3.4	3	N/A
% HLA-DR/CD3+CD8+ T-cells	8	6	N/A
Double negative CD4-CD8-T-cells (% TCR α cells)	3.9	4.3	<3.5
CD19+ B-cells (% lymphocytes; cells/ μ L)	9.6; 357	8.1; 550	13–27; 270–860
Naïve (% B-cells) (CD19+CD27-IgD+)	75	61	47.3–77
Transitionals (% B-cells) (CD19+CD27-CD24+ +CD38++)	19	6.4	4.6–8.3
Switched memory (% B-cells) (CD19+CD27-IgD–)	8.8	15	10.9–30.4
Marginal zone-like (% B-cells) (CD19+CD27+IgD+)	11	19	5.2–20.4
Plasmablasts (% B-cells) (CD19+CD27++CD38++)	0.1	1.1	0.6–5.3
CD21low (% B-cells) (CD19+CD21lowCD38low)	3.6	3.6	2.3–10
pDC (% leukocytes)	0.019	0.012	0.028–0.61
pDC (% DC)	8.18	6.63	9.59–58.8
mDC (% leukocytes)	0.16	0.11	0.057–0.34
mDC (% DC)	69	61.6	8.26–60

TABLE 2 (Continued)

Cell population	Patient A	Patient B	Age-matched reference values
Immunoglobulins			
IgG (g/l)	7.68	8.27	7.05–11.9
IgA (g/l)	2.6	2.84	0.79–1.37
IgM (g/l)	5.3	3.75	0.47–1.73
Autoantibodies			
ANA (IgG, IgM, IgA)	Mildly positive in IgG	Negative	
ENA	Negative	Negative	
ANCA	Negative	Negative	
ds-DNA	Negative	Negative	
RF (IgG) (IU/mL)	<i>31.1</i>	<i>33.6</i>	0–22
RF (IgA) (IU/mL)	6.8	4	0–22
RF (IgM) (IU/mL)	>100	>100	0–22
Anti-tropomyosin	Positive in titer 1:320	Positive in titer 1:160	
Anti-endomysium (IgG, IgA)	Negative	Negative	
ASCA IgG (U/mL)	<i>15.13</i>	<i>17.93</i>	0–10
ASCA IgA (U/mL)	5.21	5.91	0–10
CIC (arb. units)	<i>187</i>	<i>118</i>	10–46
CRP (mg/L)	<i>15.6</i>	1.8	0–8

Note: Peripheral blood analyses from the time of first admission to the hemato-oncologic department (8 years of age). Bold numbers—values below the reference limit; Italics numbers—values above the reference limit.

IgD-FITC, CD5-PE, CD28-PerCP-Cy5.5, IgM-PerCP-Cy5.5, IgD-PerCP-Cy5.5, and HLA-DR-PerCP-Cy5.5 (Biolegend), CD38-FITC, CD16-PE, CD56-PE, CD4-PerCP-Cy5.5, TCR $\gamma\delta$ -PE-Cy7, CD3-APC, CD21-APC, and CD45-APC-H7 (BD), CD19-PE-Cy7, CD24-APC Alexa750, and CD8-APC-Alexa750 (BC), CD45RO-FITC and CD31-PE (Exbio), and CCR7-PE (Miltenyi Biotech, Bergisch Gladbach, Germany). Th1, Th2 and Th17 cells were determined using CD3-Alexa Fluor 700 (Exbio), CD8-V500 and CD45RA-APC-H7 (BD), CD4-BV650, CCR7-APC, CXCR3-PE, CCR6-BV605, CRTH2-FITC, and CCR4-BV421 (BioLegend), and Tregs using CD3-APC-H7, CD25-PE, and CD127-PE-CF594 (BD), CD4-Alexa Fluor 700 and CD19-APC (Exbio), and CD14-PE-Cy7 (BC). The immunophenotype of the DCs was detected using CD45-Pacific Blue (Dako, Glostrup, Denmark), CD3-FITC, CD16-FITC, CD19-FITC, CD20-FITC, CD56-FITC, CD14-PE-Dy594, and CD11c-APC (Exbio), HLA-DR-PE-Cy7 (BD), CD123-PE (Thermo Fisher Scientific), and subpopulations of monocytes with CD66c-FITC, CD13-PE, and CD33-PE-Cy7 (BC), HLA-DR-PerCP-Cy5.5 and CD11b-BV786 (Biolegend), CD45-APC-H7, IREM-2 (CD300e)-APC, CD15-V500 (BD), and CD16-Alexa Fluor 700 and CD14-Pacific Blue (Exbio). Data were collected with Canto II, Lyric, Aria II, or Aria III flow cytometers and analyzed with FlowJo software (BD).

2.12 | Intracellular staining

Whole blood samples or HEK293/T cells were fixed in 4% formaldehyde at room temperature for 10 min, permeabilized in 0.1% Triton X-100 in a water bath (37°C) for 15 min and frozen to -20°C in 10%

glycerol in FBS (all from Thermo Fisher Scientific). After thawing, the samples were washed in PBS. TLR8 expression was detected using TLR8-PE (clone S16018A, Biolegend) and TLR7 expression was detected using TLR7-PE antibody (clone 533 707, R&D Systems, Minneapolis, MN) in lymphocytes, monocytes, or granulocytes (identified by FSC, SSC, CD14-APC-H7 (BD), and CD4-BV421 (Biolegend)) or in HEK293/T cells. PBMC from patients and HCs were isolated using a Ficoll-Paque gradient (GE Healthcare, Chicago, IL), resuspended in RPMI 1640 (Lonza, Basel, Switzerland) complemented with 10% FBS and antibiotics (Thermo Fisher Scientific) and stimulated using gardiquimod (0.5 $\mu\text{g}/\text{mL}$), imiquimod (10 $\mu\text{g}/\text{mL}$), TL8-506 (25 ng/mL), or ssRNA40/LyoVecTM (5 $\mu\text{g}/\text{mL}$, all from InvivoGen). After 5, 15, or 30 min in a water bath (37°C), the cells were fixed in 4% formaldehyde and permeabilized in 0.1% Triton X-100, and intracellular signaling was detected using anti-phospho-NF- κB p65 (Ser536)-Alexa Fluor 647 or PE (93H1, Cell Signaling Technology, Danvers, MA, USA) in CD45+CD14+ monocytes (CD45-APC-H7 from BD and CD14-PB or PE from Exbio). The data were collected with an LSR II or Celesta flow cytometer and analyzed with FlowJo software (BD).

2.13 | Extracellular cytokine production

The Human Inflammatory Cytokine Kit (BD) was used for the detection of IL-1 β , IL-8, IL-6, IL-10, and IL-12p70 in supernatants and patients' and healthy controls' plasma samples according to the manufacturer's instructions. The samples were acquired using a

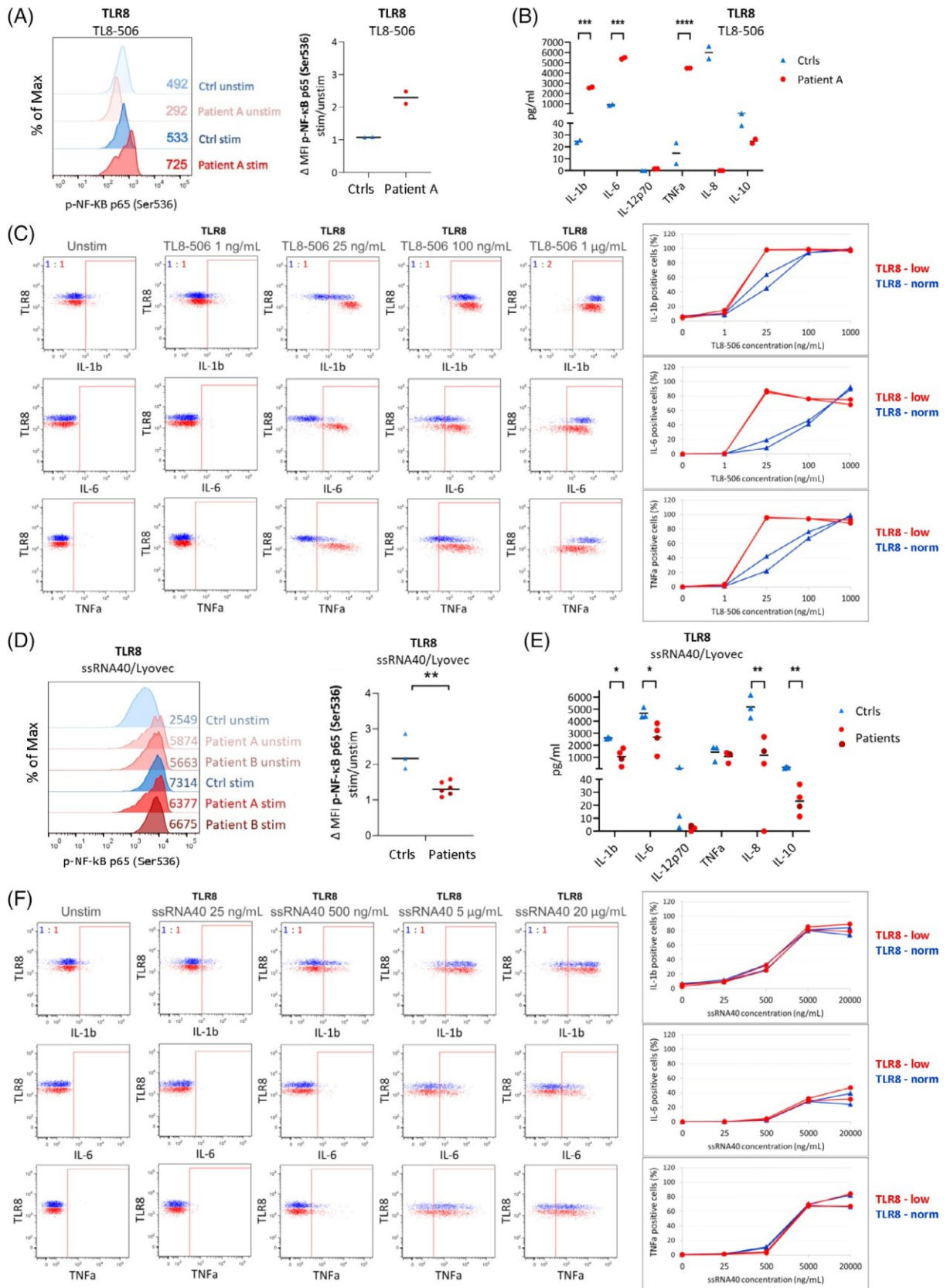


FIGURE 2 Legend on next page.

Celesta flow cytometer and analyzed with FlowJo software (BD). The Human Total IL-18/IL-1F4 Quantikine ELISA Kit (cat. DL180, R&D Systems), Human IFN γ Quantikine ELISA Kit (cat. DIF50, R&D Systems), and IFN Alpha ELISA Kit (cat. 41110-1, PBL Assay Science, Piscataway, NJ) were used for the detection of IL-18, IFN γ and IFN α respectively. The absorbance was measured at 450 nm and analyzed with a VERSAmax Tunable Microplate Reader with the appropriate SoftMaxPro software (Molecular Devices, Sunnyvale, CA).

2.14 | Intracellular cytokine production

Whole blood was withdrawn into ammonium heparin collection tubes and diluted 1:1 with RPMI 1640 (Lonza) complemented with 10% FBS and antibiotics (Thermo Fisher Scientific). To test for cytokine expression in TLR8-positive and TLR8-low monocytes, 100 μ L samples were stimulated using gardiquimod (0.025–0.5 μ g/mL), imiquimod (0.025–10 μ g/mL), GS-9620 (50–1000 nM), ssRNA40/LyoVec™ (0.025–20 μ g/mL), or TL8-506 (1–1000 ng/mL) for 6–8 h in 37°C along with brefeldin A (50 μ g/mL, Sigma Aldrich, Merck). The surface markers were stained with HLA-DR-BV570 (Biolegend) and CD16-FITC (BC), the samples were fixed in 4% formaldehyde, permeabilized in 0.1% Triton X-100 and intracellular markers were detected using CD14-Pacific Blue or CD11c-Pacific Blue, and Lineage (CD3, 19, 20, 56, CCR3)-FITC (Exbio), CD14-BV711, HLA-DR-BV605, TLR8-PE, IL-6-PE-Cy7, and IL-1 β -Alexa Fluor 647 (Biolegend), and TNF α -Alexa Fluor 700, CD123-PE-Cy5.5, and CD45-APC-H7 (BD). Data were collected with an LSR II flow cytometer and Aurora spectral cytometer (Cytek Biosciences, Fremont, CA) and analyzed with FlowJo software (BD).

2.15 | Statistical analysis

Unpaired *t*-test for single comparison was used; *p*-value less than .05 was considered significant.

3 | RESULTS

We report a family with two male monozygotic twins who inherited a novel missense mutation c.1715G>T in the *TLR8* gene located on the X chromosome from their mother (Figure 1A); both siblings developed

severe chronic AIHA with lymphoproliferative and progressive autoimmune-inflammatory disease. Their disease manifested as corticoid-dependent AIHA at the age of 6 and 2.5 years (in twin A and B, respectively), refractory to second (Intravenous Immunoglobulins, IVIG) and third (azathioprine) line of therapeutics. The bouts of AIHA were induced by frequent respiratory and gastrointestinal infections (e.g., salmonellosis) and, eventually, also by fevers of unknown origin with elevated laboratory markers of inflammation. Both twins were referred to hemato-oncologic department at the age of 8 years, presenting with marked hepatosplenomegaly and cervical lymphadenopathy. The AIHA activity was characterized by high titers of anti-erythrocyte antibodies (IgG in twin A; IgM and IgG in twin B), C3d complement fragments and cold agglutinins (genetic characterization, extended clinical features and results of T-cell repertoire sequencing are summarized in Table 1, blood analyses in Table 2). In attempts to control the AIHA, rituximab (4 x 375 mg/m²), followed by sirolimus were used in both patients, which enabled partial steroid detraction. Twin B, however, continued to suffer attacks of fever and developed autoinflammatory organ symptoms (polyarthritis, IBD-like enteropathy, and erythema nodosum). Anti-IL-1 (Anakinra), and eventually, methotrexate were added to his therapy. Despite the combined anti-inflammatory treatment, multifocal CNS vasculitis suddenly manifested with acute hemiparesis and aphasia due to the CNS hemorrhage at the age of 11 years (Figure 1B). This life-threatening event prompted the indication of hematopoietic stem cell transplantation (HSCT) from a matched unrelated donor after a myeloablative conditioning regimen. The post-transplant course was complicated by slow immunological reconstitution, reactivation of cytomegalovirus, adenovirus and EBV requiring prolonged antiviral therapy and thrombocytopenia corrected by eltrombopag. One year after HSCT, complete donor chimerism was achieved and no signs of graft-versus-host disease were present on tapering doses of steroids and cyclosporine A. Twin A continued to experience attacks of fever with panniculitis despite combined corticosteroid and sirolimus treatment. Therefore, hydroxychloroquine was added to the therapeutic regimen, resulting in marked clinical improvement after 1 month, enabling gradual cessation of corticosteroid therapy. Interestingly, the patients' mother has a history of polyarthritis and steroid-sensitive antiphospholipid syndrome.

TLR8 forms a homodimer that undergoes a conformation change upon ligand binding activating its downstream signaling. The c.1715G>T mutation leads to a substitution of glycine with valine at position 572 (p.G572V) in leucine-rich repeat (LRR) 18 in proximity to the first ligand-binding site^{25–27} (Figure 1C,D) and could, therefore, affect the TLR8 activity.

FIGURE 2 The response of patients' cells to diverse TLR8 ligands. Phosphorylation (p-) of NF- κ B p65 (Ser536) in monocytes (A) and production of pro-inflammatory cytokines from PBMCs upon stimulation with chemical TLR8 ligand TL8-506 (25 ng/mL) (B). Production of proinflammatory cytokines from mother's TLR8-low and TLR8-norm (healthy) cells upon stimulation with chemical TLR8 ligand TL8-506 (C). Phosphorylation of NF- κ B p65 (Ser536) in monocytes (D) and production of pro-inflammatory cytokines from PBMC upon stimulation with TLR8 ligand ssRNA40/Lyovec (5 μ g/mL) (E). Production of proinflammatory cytokines from mother's TLR8-low and TLR8-nom (healthy) cells upon stimulation with TLR8 ligand ssRNA40/Lyovec (F). Data acquired in two (A, B, C, F) and three (D, E) independent experiments, mean \pm SEM. Histograms and dot plots show representative data, the gates indicate positivity for respective cytokine according to unstimulated state, MFI in numbers. **p* < .05, ***p* < .005 (unpaired *t*-test) [Color figure can be viewed at wileyonlinelibrary.com]

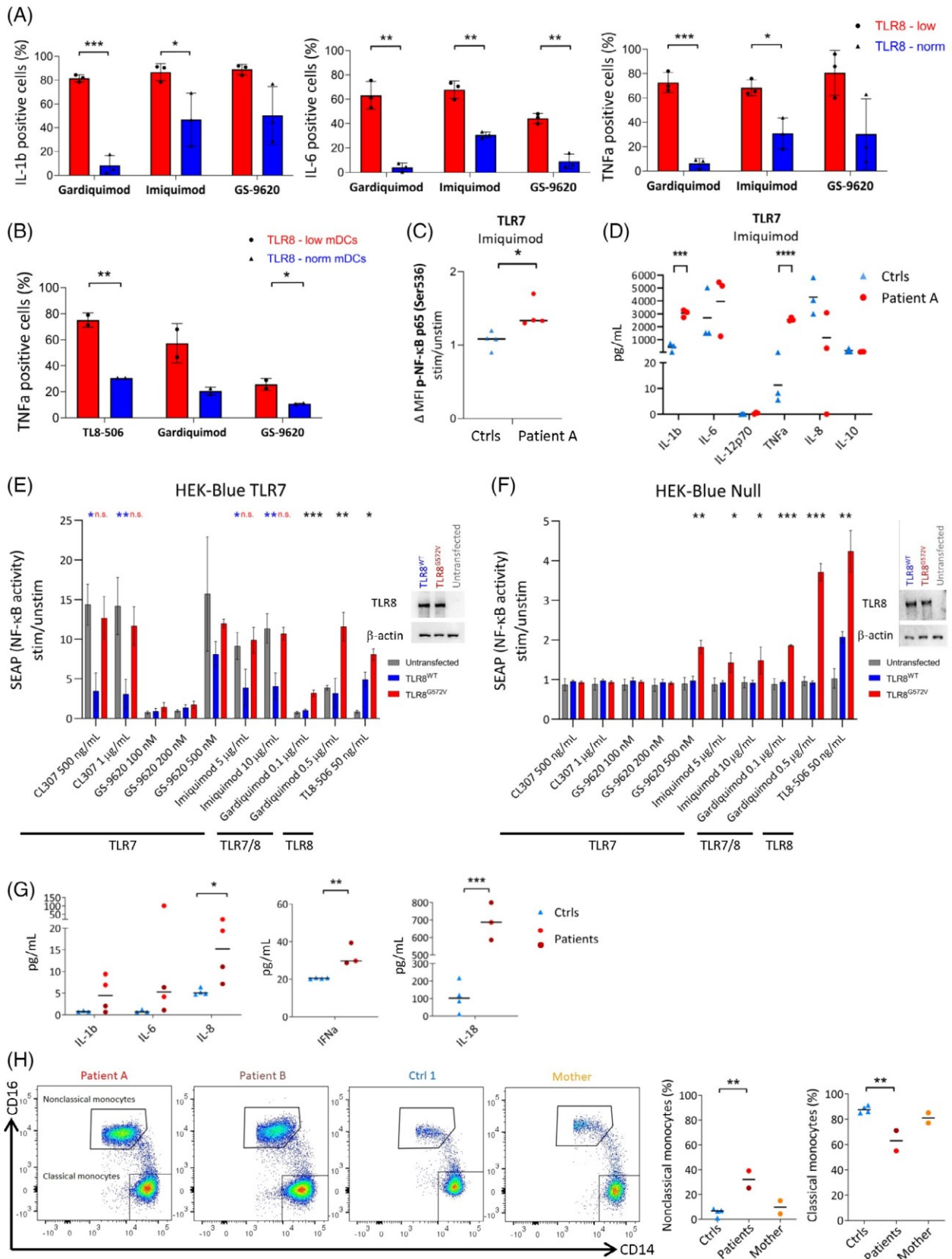


FIGURE 3 Legend on next page.

Once the wild-type TLR8 (TLR8^{WT}) and mutant TLR8 (TLR8^{G572V}) were transiently expressed in HEK-Blue TLR7/8-Null cells and stimulated with base analogs TL8-506 and CL075, TLR8^{G572V} showed increased NF- κ B transcriptional activity compared to TLR8^{WT} (Figure 1E). However, TLR8 protein levels were half that of the healthy controls in the patients' cells (Figure 1F). An unexpected observation was made in the mother, whose cells could be separated into two populations based on TLR8 protein levels; a higher one (as controls) and a lower one (as the patients), due to random inactivation of the X chromosome bearing the c.1715G>T mutation (Figure 1F,G). We speculated that mRNA level or protein stability could be affected by the mutation. The *TLR8* mRNA levels were not significantly different in sorted monocytes of both twins compared to healthy controls (Figure 1H). However, upon transient transfection of TLR8^{WT} and TLR8^{G572V} into HEK293/T cells and stopping the proteosynthesis with cycloheximide, the mutant TLR8^{G572V} protein was degraded more rapidly compared to TLR8^{WT} (Figure 1I). Intriguingly, various TLR8 ligands elicited different responses. Chemical compounds, such as TL8-506 or CL075, bind only at site 1, enabling strong non-physiological TLR8 activation.²⁷ Stimulation with TL8-506 increased phospho- (p-)NF- κ B and proinflammatory cytokine production in the patients' peripheral blood mononuclear cells (PBMCs, Figure 2A,B) and, consistently, in the mother's TLR8-low monocytes compared to her TLR8-norm monocytes (Figure 2C). However, ssRNA40 (which better mimics viral/bacterial RNA and requires two binding sites to physiologically activate TLR8²⁶) did not trigger this hyperactivation (Figure 2D-F). Moreover, both the patients' and the mother's TLR8-low cells responded more to TLR7 ligands. We observed increased production of the proinflammatory cytokines IL-1 β , IL-6, and TNF α by the mother's TLR8-low monocytes (Figure 3A) (similarly by her TLR8-low mDCs, Figure 3B) as well as enhanced p-NF- κ B in the patients' monocytes (Figure 3C) and cytokine production in the patients' PBMCs (Figure 3D). Of note, *TLR7* gene, and basal TLR7 mRNA/protein levels were not affected. This suggests that mutant TLR8^{G572V} could impair the interaction with TLR7^{9,28} and skew the TLR8^{G572V}/TLR7 balance towards TLR7,⁹ manifesting as a TLR7-dependent autoinflammatory phenotype. As expected, transient co-expression of TLR8^{G572V} or TLR8^{WT} with TLR7 in HEK-Blue TLR8-TLR7+ cells led to attenuation of TLR7 signaling in TLR8^{WT}-transfected cells,^{7,9} but not in TLR8^{G572V}-transfected cells (Figure 3E). Moreover, TLR8^{G572V} cross-reacted to diverse TLR7 ligands in comparison to TLR8^{WT} in HEK-Blue TLR8-TLR7- cells (Figure 3F).

The dysregulation of TLR7 and TLR8 is well described in murine models where TLR8 deficiency causes TLR7-driven autoantibody production and glomerulonephritis¹⁶; structural studies also showed that TLR8 mutations near ligand binding site 1 skewed the affinity to TLR7 ligands¹⁰; however, little is known about these phenomena in humans. In this study, the patients presented with a partial TLR8 protein deficiency, with mutant TLR8^{G572V} that did not impair TLR7 signaling and cross-responded to diverse TLR7 ligands. This imbalance between mutant TLR8^{G572V} and TLR7 introduced a bias towards TLR7-dependent pro-inflammatory signaling. The successful use of hydroxychloroquine in twin A indirectly supports our findings.

Since TLR8 and TLR7 act in a balance to recognize ssRNA of external pathogens as well as endogenous ssRNA within immune complexes,^{11,12} their imbalance may lead to pathological responses to microbes and drive autoinflammation. Indeed, both twins suffered from frequent enteritis and fevers and their AIHA worsened with infections. We found increased levels of multiple pro-inflammatory cytokines, type I interferons (Figure 3G), and increased counts of pro-inflammatory nonclassical monocytes²⁹ in their peripheral blood (Figure 3H).

4 | DISCUSSION

The disparity in the disease severity between twin A and B is intriguing. It may be explained by different spectrum of pathogens encountered by the siblings, which may have revealed diverse autoantigens driving the severity of autoinflammatory phenomena. Interestingly, the disturbed recognition of autoantigens (self-nucleic acids) by endosomal TLRs contributes to the pathogenesis of SLE,¹¹ which may present with corresponding clinical features to those of our patients (AIHA, fevers, arthritis, and CNS vasculitis).³⁰ Both twins also had high plasma levels of autoantibodies, and increased double-negative TCR $\alpha\beta$ +CD4-CD8-T-cells (Table 2), which are associated with autoimmunity. The development of autoimmunity can be intrinsic and/or extrinsic. Regulatory T-cells could be affected directly by TLR8 mutation³¹ or indirectly by an inflammatory environment.³² Moreover, dysregulated TLRs can affect the activity of antigen-presenting cells similar to a murine model of SLE with TLR8 deficiency and thus drive T-cell proliferation.³³ Hypothetically, the activated T-cells might also include autoreactive clones, which would subsequently activate autoreactive B-cells. Interestingly, both patients presented with

FIGURE 3 Imbalance in activation induced by TLR7 agonists in patients' cells and cellular models, and inflammatory phenotypes in patients' peripheral blood. Production of proinflammatory cytokines from mother's TLR8-low and TLR8-norm (healthy) monocytes (A) and mDCs (B) upon stimulation with TLR7 ligands Imiquimod (10 μ g/mL) and GS-9620 (Vesatolimod, 500 nM), or TLR7/8 ligand Gardiquimod (0.5 μ g/mL). Phosphorylation of NF- κ B p65 (Ser536) in monocytes (C) and production of pro-inflammatory cytokines from PBMC upon stimulation with TLR7 ligand Imiquimod (10 μ g/mL) (D). Impaired inhibitory effect of mutant TLR8^{G572V} on TLR7 signaling compared to TLR8^{WT}. Black asterisks indicate significance between TLR8^{WT} and mutant TLR8^{G572V}; blue asterisks indicate significance between untransfected cells and TLR8^{WT}-transfected cells; comparison between untransfected cells and TLR8^{G572V}-transfected cells is in red (E). TLR8^{G572V} gain-of-function upon TLR8 stimulation (TL8-506) and upon TLR7 stimulation (GS-9620, Imiquimod) (F). Cytokine levels in patients' and controls' peripheral blood plasmas (G). Enriched nonclassical monocytes (CD45+CD66c-CD13+HLA-DR+IREM-2+CD14dimCD16+) in patients' monocytes pool (H). Data acquired in three (A, C, D, E, F, G) and two (B, H) independent experiments, mean \pm SEM. Histograms, dot plots and WB show representative data. * p < .05, ** p < .005, *** p < .0005, **** p < .0001 (unpaired t -test) [Color figure can be viewed at wileyonlinelibrary.com]

oligoclonality and expanded clonotypes within their effector T-cells subsets (Table 1). In summary, we show the first human partial TLR8 protein deficiency, which manifests as complex autoimmune and autoinflammatory phenotypes. The mutation causes TLR8 cross-reactivity to TLR7 ligands and leads to dysregulation of TLR8 and TLR7 responses. Finally, we propose the inclusion of partial TLR8 protein deficiency with TLR8/TLR7 dysregulation in the classification of Inborn Errors of Immunity.

ACKNOWLEDGMENTS

This study was performed in accordance with the recommendations of the Second Faculty of Medicine Ethics Committee Guidelines and the Declaration of Helsinki. We are especially grateful to the patients and their parents for giving us consent to perform all research activities associated with the disease and to publish the results. We also kindly acknowledge Nermina Saucier, Katerina Rejllova, and Pavel Semerak for their technical assistance.

CONFLICT OF INTEREST

Authors declare that they have no competing interests.

AUTHOR CONTRIBUTIONS

Martina Fejtikova and Veronika Kanderova designed, performed, and analyzed the ex vivo and in vitro experiments and immunophenotyping. Martina Sukova cared for the patients and provided clinical data. Michael Svaton and Eva Fronkova designed, performed, and analyzed the genetic tests. David Jakubec performed structural analyses. Jahnvi Aluri, Katerina Hlozkova, and Karolina Skvarova Kramarzova designed the in vitro cellular model and performed and analyzed the in vitro experiments. Michaela Novakova, Adam Kloperk, Zuzana Parackova, and Anna Sediva contributed to the immunological characterization of the patients and analyzed the ex vivo experiments. Marketa Rackova and Marina Bakardjieva performed in vitro and ex vivo experiments. Tomas Kalina, Marketa Bloomfield, and Ondrej Hrusak supervised the study, reviewed the manuscript and provided comments. Martina Sukova, Petr Sedlacek, Hana Malcova, Zuzana Liba, Martin Kudr, and Jan Stary provided medical care, critically reviewed the manuscript and provided comments. Veronika Kanderova, Michael Svaton, and Megan A. Cooper designed the project and supervised the research. Martina Fejtikova, Veronika Kanderova, and Michael Svaton wrote the manuscript. All of the authors provided critical input and agreed to this publication.

DATA AVAILABILITY STATEMENT

The data that support the findings of this study are available from the corresponding authors upon reasonable request.

ORCID

Martina Fejtikova  <https://orcid.org/0000-0002-6417-4486>

Karolina Skvarova Kramarzova  <https://orcid.org/0000-0003-4860-7453>

Marketa Rackova  <https://orcid.org/0000-0002-2991-8873>

Marina Bakardjieva  <https://orcid.org/0000-0002-5919-6306>

Marketa Bloomfield  <https://orcid.org/0000-0001-5330-9341>

Adam Kloperk  <https://orcid.org/0000-0002-1526-4557>

Zuzana Parackova  <https://orcid.org/0000-0002-2398-532X>

Anna Sediva  <https://orcid.org/0000-0001-7730-2304>

Michaela Novakova  <https://orcid.org/0000-0003-2964-5956>

Tomas Kalina  <https://orcid.org/0000-0003-4475-2872>

Michael Svaton  <https://orcid.org/0000-0003-2966-3687>

Veronika Kanderova  <https://orcid.org/0000-0001-8513-1066>

REFERENCES

- Picard C, von Bernuth H, Chandil P, et al. Clinical features and outcome of patients with Irak-4 and MyD88 deficiency. *Medicine*. 2010; 89(6):403-425. doi:10.1097/MD.0b013e3181fd8ec3
- Aluri J, Bach A, Kaviani S, et al. Immunodeficiency and bone marrow failure with mosaic and germline TLR8 gain of function. *Blood*. 2021; 137(18):2450-2462. doi:10.1182/blood.202009620
- Farrugia M, Baron B. The role of toll-like receptors in autoimmune diseases through failure of the self-recognition mechanism. *Int J Inflam*. 2017;2017:1-12. doi:10.1155/2017/8391230
- Eigenbrod T, Pelka K, Latz E, Kreikemeyer B, Dalpke AH. TLR8 senses bacterial RNA in human monocytes and plays a nonredundant role for recognition of streptococcus pyogenes. *J Immunol*. 2015;195(3):1092-1099. doi:10.4049/jimmunol.1403173
- Bender AT, Tzvetkov E, Pereira A, et al. TLR7 and TLR8 differentially activate the IRF and NF- κ B pathways in specific cell types to promote inflammation. *ImmunoHorizons*. 2020;4(2):93-107. doi:10.4049/immunoHorizons.2000002
- Asano T, Boisson B, Onodi F, et al. X-linked recessive TLR7 deficiency in ~1% of men under 60 years old with life-threatening COVID-19. *Sci Immunol*. 2021;6(62). doi:10.1126/sciimmunol.abl4348
- de Marcken M, Dhaliwal K, Danielsen AC, Gautron AS, Dominguez-Villar M. TLR7 and TLR8 activate distinct pathways in monocytes during RNA virus infection. *Sci Signal*. 2019;12(605):eaaw1347. doi:10.1126/scisignal.aaw1347
- Larange A, Antonios D, Pallardy M, Kerdine-Romer S. TLR7 and TLR8 agonists trigger different signaling pathways for human dendritic cell maturation. *J Leukoc Biol*. 2009;85(4):673-683. doi:10.1189/jlb.08.08504
- Wang J, Shao Y, Bennett TA, Shankar RA, Wightman PD, Reddy LG. The functional effects of physical interactions among toll-like receptors 7, 8, and 9. *J Biol Chem*. 2006;281(49):37427-37434. doi:10.1074/jbc.M605311200
- Zhang Z, Ohto U, Shibata T, et al. Structural analyses of toll-like receptor 7 reveal detailed RNA sequence specificity and recognition mechanism of agonistic ligands. *Cell Rep*. 2018;25(12):3371-3381.e5. doi:10.1016/j.celrep.2018.11.081
- Lee PY, Kumagai Y, Li Y, et al. TLR7-dependent and Fc γ R-independent production of type I interferon in experimental mouse lupus. *J Exp Med*. 2008;205(13):2995-3006. doi:10.1084/jem.20080462
- Hoffmann MH, Skriner K, Herman S, et al. Nucleic acid-stimulated antigen-presenting cells trigger T cells to induce disease in a rat transfer model of inflammatory arthritis. *J Autoimmun*. 2011;36(3-4):288-300. doi:10.1016/j.jaut.2011.02.007
- Guiducci C, Gong M, Cepika A-M, et al. RNA recognition by human TLR8 can lead to autoimmune inflammation. *J Exp Med*. 2013; 210(13):2903-2919. doi:10.1084/jem.20131044
- Deane JA, Pisitkun P, Barrett RS, et al. Control of toll-like receptor 7 expression is essential to restrict autoimmunity and dendritic cell proliferation. *Immunity*. 2007;27(5):801-810. doi:10.1016/j.immuni.2007.09.009
- Fairhurst A, Hwang S, Wang A, et al. Yaa autoimmune phenotypes are conferred by overexpression of TLR7. *Eur J Immunol*. 2008;38(7):1971-1978. doi:10.1002/eji.200838138

16. Demaria O, Pagni PP, Traub S, et al. TLR8 deficiency leads to autoimmunity in mice. *J Clin Invest*. 2010;120(10):3651-3662. doi:10.1172/JCI42081
17. Desnues B, Macedo AB, Roussel-Queval A, et al. TLR8 on dendritic cells and TLR9 on B cells restrain TLR7-mediated spontaneous autoimmunity in C57BL/6 mice. *Proc Natl Acad Sci*. 2014;111(4):1497-1502. doi:10.1073/pnas.1314121111
18. Li H, Durbin R. Fast and accurate short read alignment with Burrows-Wheeler transform. *Bioinformatics*. 2009;25(14):1754-1760. doi:10.1093/bioinformatics/btp324
19. Koboldt DC, Zhang Q, Larson DE, et al. VarScan 2: somatic mutation and copy number alteration discovery in cancer by exome sequencing. *Genome Res*. 2012;22(3):568-576. doi:10.1101/gr.129684.111
20. Li H, Handsaker B, Wysoker A, et al. The sequence alignment/map format and SAMtools. *Bioinformatics*. 2009;25(16):2078-2079. doi:10.1093/bioinformatics/btp352
21. Tangye SG, Al-Herz W, Bousfiha A, et al. Human inborn errors of immunity: 2019 update on the classification from the International Union of Immunological Societies Expert Committee. *J Clin Immunol*. 2020;40(1):24-64. doi:10.1007/s10875-019-00737-x
22. Sobreira N, Schiettecatte F, Valle D, Hamosh A. GeneMatcher: A Matching Tool for Connecting Investigators with an Interest in the Same Gene. *Human Mutation*. 2015;36(10):928-930. doi:10.1002/humu.22844
23. Brüggemann M, Kotrová M, Knecht H, et al. Standardized next-generation sequencing of immunoglobulin and T-cell receptor gene recombinations for MRD marker identification in acute lymphoblastic leukaemia; a EuroClonality-NGS validation study. *Leukemia*. 2019;33(9):2241-2253. doi:10.1038/s41375-019-0496-7
24. Bystry V, Reigl T, Krejci A, et al. ARResT/interrogate: an interactive immunoprofiler for IG/TR NGS data. *Bioinformatics*. 2016;33(3):435-437. doi:10.1093/bioinformatics/btw634
25. Tanji H, Ohto U, Motoi Y, Shibata T, Miyake K, Shimizu T. Autoinhibition and relief mechanism by the proteolytic processing of toll-like receptor 8. *Proc Natl Acad Sci U S A*. 2016;113(11):3012-3017. doi:10.1073/pnas.1516000113
26. Tanji H, Ohto U, Shibata T, et al. Toll-like receptor 8 senses degradation products of single-stranded RNA. *Nat Struct Mol Biol*. 2015;22(2):109-115. doi:10.1038/nsmb.2943
27. Tanji H, Ohto U, Shibata T, Miyake K, Shimizu T. Structural reorganization of the toll-like receptor 8 dimer induced by agonistic ligands. *Science*. 2013;339(6126):1426-1429. doi:10.1126/science.1229159
28. Itoh H, Tatematsu M, Watanabe A, et al. UNC93B1 physically associates with human TLR8 and regulates TLR8-mediated signaling. *PLoS One*. 2011;6(12):e28500. doi:10.1371/journal.pone.0028500
29. Mukherjee R, Kanti Barman P, Kumar Thatoi P, Tripathy R, Kumar Das B, Ravindran B. Non-classical monocytes display inflammatory features: validation in sepsis and systemic lupus erythematosus. *Sci Rep*. 2015;5(July):1-14. doi:10.1038/srep13886
30. Bundhun PK, Kumari A, Huang F. Differences in clinical features observed between childhood-onset versus adult-onset systemic lupus erythematosus. *Medicine*. 2017;96(37):e8086. doi:10.1097/MD.00000000000008086
31. Peng G, Guo Z, Kiniwa Y, et al. Toll-like receptor 8-mediated reversal of CD4+ regulatory T cell function. *Science*. 2005;309(5739):1380-1384. doi:10.1126/science.1113401
32. La Cava A. Tregs are regulated by cytokines: implications for autoimmunity. *Autoimmun Rev*. 2008;8(1):83-87. doi:10.1016/j.autrev.2008.08.002
33. Tran NL, Manzin-Lorenzi C, Santiago-Raber ML. Toll-like receptor 8 deletion accelerates autoimmunity in a mouse model of lupus through a toll-like receptor 7-dependent mechanism. *Immunology*. 2015;145(1):60-70. doi:10.1111/imm.12426

How to cite this article: Fejtkova M, Sukova M, Hlozkova K, et al. TLR8/TLR7 dysregulation due to a novel *TLR8* mutation causes severe autoimmune hemolytic anemia and autoinflammation in identical twins. *Am J Hematol*. 2022;97(3):338-351. doi:10.1002/ajh.26452